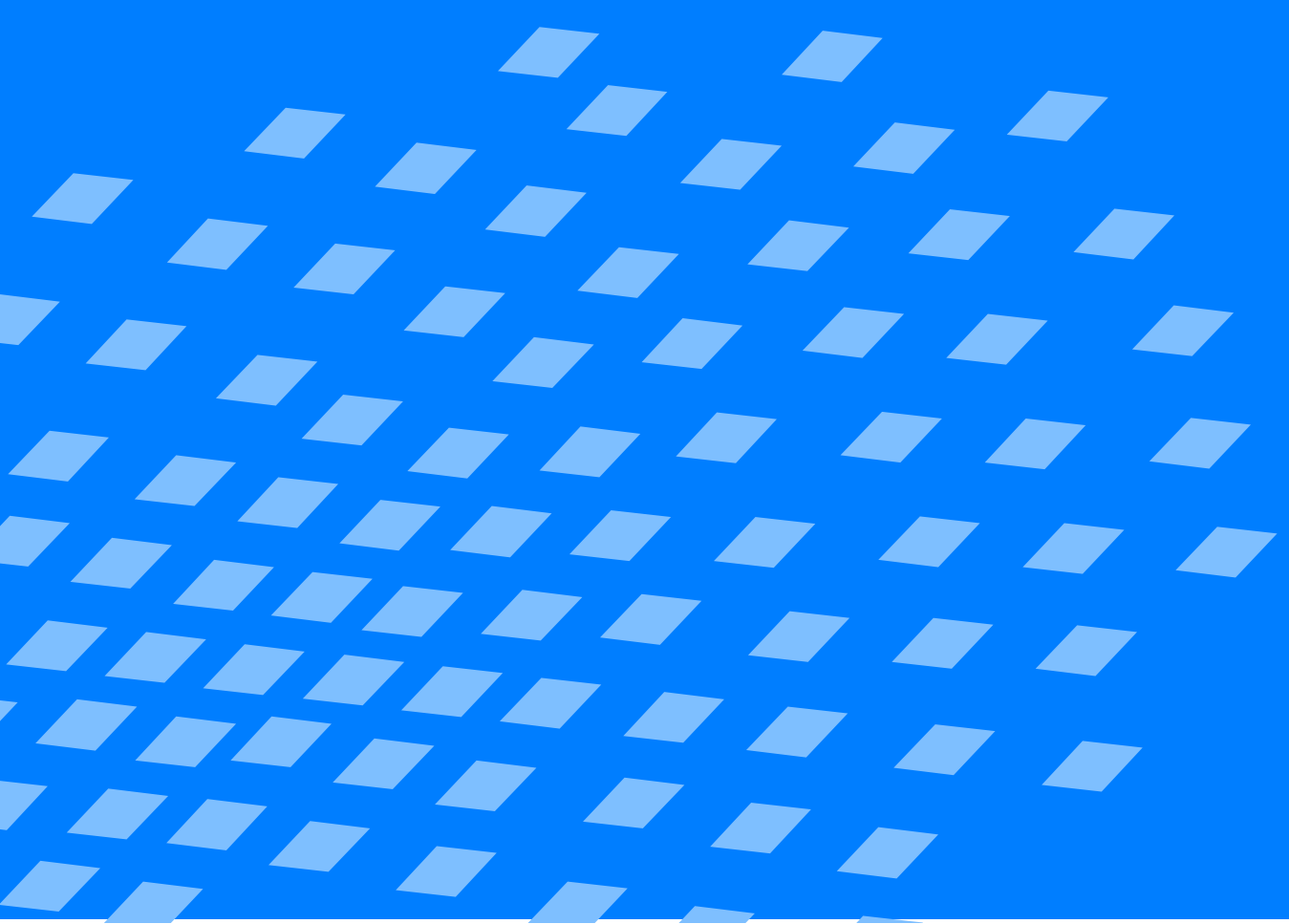




The Variational Multiscale Method for Laminar and Turbulent Incompressible Flow

Volker Gravemeier

Volker Gravemeier



The Variational Multiscale Method for Laminar and Turbulent Incompressible Flow

von

Volker Gravemeier

Bericht Nr. 40 (2003)
Institut für Baustatik der Universität Stuttgart
Professor Dr.-Ing. E. Ramm
Stuttgart 2003



© Volker Gravemeier

Berichte können bezogen werden über:

Institut für Baustatik

Universität Stuttgart

Pfaffenwaldring 7

D-70550 Stuttgart

Tel.: 07 11 / 6 85 61 23

Fax: 07 11 / 6 85 61 30

<http://www.uni-stuttgart.de/ibs/>

Alle Rechte, insbesondere das der Übersetzung in andere Sprachen, vorbehalten. Ohne Genehmigung des Autors ist es nicht gestattet, diesen Bericht ganz oder teilweise auf photomechanischem, elektronischem oder sonstigem Wege zu kommerziellen Zwecken zu vervielfältigen.

ISBN 3-00-013034-9

The Variational Multiscale Method for Laminar and Turbulent Incompressible Flow

Von der Fakultät Bau- und Umweltingenieurwissenschaften
der Universität Stuttgart zur Erlangung der Würde eines Doktors der
Ingenieurwissenschaften (Dr.-Ing.) genehmigte Abhandlung

vorgelegt von

Volker Gravemeier

aus Andernach

Hauptberichter: Prof. Dr.-Ing. Ekkehard Ramm, Stuttgart

Mitberichter: Prof. Dr.-Ing. Wolfgang A. Wall, München

Tag der mündlichen Prüfung: 10. Dezember 2003

Abstract

The present thesis addresses a new approach for solving numerically instationary, incompressible flow governed by the appropriate set of Navier–Stokes equations. This approach named ‘variational multiscale method’ has recently been introduced as a powerful means for problems of computational mechanics having to deal with large ranges of scales. Such notably widened scale ranges emerge in various flow situations. At large, this study aims firstly at the development of a general framework for the numerical solution of the Navier–Stokes equations based on the variational multiscale method. Secondly, a specific implementation within a Galerkin finite method is realized based on this general framework. Finally, an extensive test program for the developed method in form of sample laminar and turbulent flow situations is conducted.

The variational multiscale method enables the separation of the complete scale range into various scale groups. In this work, the distinction of three different scale groups is mainly proposed in view of the underlying fluid flow problems. These are especially large resolved scales, small resolved scales and unresolved scales. The scale separation is initially applied to the linear model problem of a scalar convection–diffusion–reaction equation and some solution strategies are suggested in this context. The transition to the more complicated problem of the nonlinear set of instationary, incompressible Navier–Stokes equations is performed and reasonable solution strategies for this problem are picked up again. Additional considerations have to be taken into account as soon as the challenging phenomenon of turbulent flow regimes is encountered. As a starting point for these particular considerations, two classical procedures for the numerical simulation of turbulent flows, Direct Numerical Simulation (DNS) and Large Eddy Simulation (LES), are adapted to the numerical method of choice in this work, the Galerkin finite element method, in a straightforward manner. It is, in fact, possible to identify these classical approach as special cases of the variational multiscale method employing a separation of two scales. Nevertheless, the variational multiscale method gives rise to further approaches going beyond this, e.g. based on the three–scale separation proposed in this work

As a practical method based on the three–scale separation, a three–level finite element method is developed. A major objective of this practical method has to be on computational efficiency inevitably due to the usual imbalance of necessary and available computer resources in the context of turbulent flow situations. Therefore, a local approximation in form of residual–free bubbles is exploited as a first approach for the three–level method. The name of the method especially accounts for three different types of discretizations linked with the respective levels. Starting with a basic discretization (level 1), submeshes (level 2) are introduced on each element of this basic mesh. These two levels constitute a two–level finite element method for the time being, which is tested in numerical examples. With the help of these submeshes, approximate solutions for residual–free bubbles on these elements are pursued. Particular attention is also paid to the adequate consideration of the continuity equation on level 2. The proposed three–level method is not achieved until a third level is introduced. In particular, a dynamic way of modeling the still unresolved scales of the problem is proposed as the manifestation of third level. According to this, a third type of discretization, namely elementwise sub–submeshes, i.e. slightly refined submeshes with regard to the submeshes on the second level, is employed into the method. The performance of the three–level finite element method is demonstrated for several laminar and turbulent flow examples.

Zusammenfassung

Die vorliegende Arbeit behandelt einen neuen Ansatz für die numerische Lösung instationärer, inkompressibler Strömungen, die mathematisch vom zugehörigen Navier-Stokes'schen Gleichungssystem beschrieben werden. Dieser neue Ansatz, 'variationelle Mehrskalen-Methode' genannt, ist kürzlich als vielversprechendes Mittel zur Lösung von Problemen der Numerischen Mechanik mit sehr breiten Skalenspektren eingeführt worden. Solche deutlich erweiterten Skalenspektren treten in einer Vielzahl von Strömungssituationen auf. In Ihrer Gesamtheit zielt diese Studie zunächst auf die Entwicklung eines allgemeinen Rahmensystems für die numerische Lösung der Navier-Stokes Gleichungen basierend auf der variationellen Mehrskalen-Methode. auf Grundlage dieses allgemeinen Rahmensystems wird hieran anschließend eine spezielle Implementierung innerhalb einer Galerkin Finite Element Methode vollzogen. Zum Schluss dieser Arbeit wird ein umfangreiches Testprogramm für die entwickelte Methode in Form von lamina- ren und turbulenten Beispielströmungen durchgeführt.

Die variationelle Mehrskalen-Methode ermöglicht die Separation des kompletten Skalenspektrums in verschiedene Skalengruppen. In dieser Arbeit wird mit Blick auf die vorliegenden Strömungsprobleme hauptsächlich eine Unterscheidung von drei verschiedenen Skalengruppen vorgeschlagen. Dies sind namentlich grobe aufgelöste Skalen, feine aufgelöste Skalen und unaufgelöste Skalen. Die Skalenseparation wird zunächst auf die lineare Problemstellung einer skalaren Konvektions-Diffusions-Reaktionsgleichung angewendet und es werden einige Lösungsstrategien in diesem Zusammenhang vorgeschlagen. Der Übergang zur komplizierteren Problemstellung des nichtlinearen Systems der instationären, inkompressiblen Navier-Stokes Gleichungen wird vollzogen und sinnvolle Lösungsstrategien hierfür wieder aufgegriffen. Weitere Überlegungen müssen angestellt werden, sobald das herausfordernde Phänomen turbulenter Strömungsbereiche auftritt. Als Ausgangspunkt für diese speziellen Betrachtungen werden zwei klassische Ansätze für die numerische Simulation, die Direkte Numerische Simulation (DNS) und die Large Eddy Simulation (LES), auf einfache Weise in die numerische Methode der Wahl in dieser Arbeit, der Galerkin Finite Element Methode, eingepasst. Es ist in der Tat möglich, diese klassischen Ansätze als Spezialfälle der variationellen Mehrskalen-Methode für eine Zwei-Skalen-Separation zu identifizieren. Die variationelle Mehrskalen-Methode bietet nichtsdestoweniger die Möglichkeit darüber hinausgehender Ansätze, zum Beispiel basierend auf der in dieser Arbeit vorgeschlagenen Drei-Skalen-Separation.

Als praktische Methode basierend auf der Drei-Skalen-Separation wird eine Drei-Ebenen Finite Element Methode entwickelt. Eine Hauptzielsetzung dieser praktischen Methode muss aufgrund des üblichen negativen Ungleichgewichtes zwischen notwendiger und verfügbarer Rechenleistung im Zusammenhang mit turbulenten Strömungen zwangsläufig auf rechenbetonter Effizienz liegen. Zu diesem Zweck wird als ein erster Ansatz eine lokale Approximation in Form von residuenfreien 'bubbles' ausgenutzt. Der Name der Methode weist insbesondere drei verschiedene Arten von Diskretisierungen, die mit den jeweiligen Ebenen verbunden sind, aus. Ausgehend von einer Basisdiskretisierung (Ebene 1) werden Unterdiskretisierungen in jedem Element der Basisdiskretisierung eingeführt. Mit Hilfe der Unterdiskretisierungen werden näherungsweise Lösungen der residuenfreien 'bubbles' in diesen Elementen angestrebt. Besondere Aufmerksamkeit ist einer adäquaten Berücksichtigung der Kontinuitätsgleichung auf Ebene 2 gewidmet. Diese beiden Ebenen konstituieren zunächst eine Zwei-Ebenen Finite Element Methode, die in numerischen Beispielen getestet wird. Die vorgeschlagene Drei-Ebenen Methode

wird erst mit der Einführung einer dritten Ebene vollendet. Eine dynamischer Modellierungsansatz für die immer noch unaufgelösten Skalen des Problems wird hier als dritte Ebene eingeführt. Dementsprechend wird eine dritte Diskretisierungsart, nämlich elementweise Unter-Unterdiskretisierungen, d.h. leicht verfeinerte Unterdiskretisierungen in relation zu den Unterdiskretisierungen auf der zweiten Ebene, in die Methode eingebracht. Das Verhalten der Drei-Ebenen Finite Element Methode wird anhand etlicher laminarer und turbulenter Strömungsbeispiele demonstriert.

Vorwort

Die vorliegende Arbeit entstand während meiner Tätigkeit als wissenschaftlicher Mitarbeiter am Institut für Baustatik der Universität Stuttgart in der Zeit von Januar 2000 bis Dezember 2003.

Mein besonderer Dank gilt Herrn Professor Dr.-Ing. Ekkehard Ramm für die Gewährung der Möglichkeit, diese Arbeit zu erstellen, die sicherlich thematisch weit außerhalb des Kernbereiches der üblichen Forschungsthematik eines Institutes für Baustatik anzuordnen ist. Sie ist somit auch eine Facette des sehr breit gefächerten Forschungsprofils des Institutes, das unter seiner Leitung geschaffen wurde. Sein wissenschaftliches Interesse an den Fragestellungen, denen sich diese Arbeit widmet, war Grundlage für die Initiierung des vorliegenden Promotionsprojektes. Insbesondere habe ich den persönlichen Umgang in den Jahren meiner Tätigkeit am Institut als äußerst angenehm empfunden.

Außerordentlichen Dank über denjenigen für die Übernahme des Mitberichtes hinaus möchte ich Herrn Professor Dr.-Ing. Wolfgang Wall aussprechen. Von Beginn meiner Tätigkeit habe ich ihn als 'zweite treibende Kraft' des Institutes für Baustatik und kongeniale Ergänzung zu Herrn Professor Ramm erlebt. Die zwischenzeitliche Berufung auf einen eigenen Lehrstuhl war für mich eine zwangsläufige Entwicklung. Seine hervorragende Dissertation, die die erste grundlegende Beschäftigung mit der Thematik 'Numerische Fluidmechanik' an diesem Institut darstellt, hat weiteren Arbeiten auf diesem Gebiet wie die vorliegende den Weg geebnet. Darüber hinaus möchte ich auch in Bezug auf Herrn Professor Wall ganz besonders meine große Freude über das von mir als äußerst positiv empfundene persönliche Verhältnis ausdrücken.

Bedauerlicherweise konnte Herr Professor Leopoldo P. Franca, der sich zur Übernahme eines weiteren Mitberichtes bereit erklärt hatte, die Mitgliedschaft in meiner Prüfungskommission aufgrund einer ernsthaften Erkrankung nicht aufrecht erhalten.

Weiterhin möchte ich mich bei all meinen Kolleginnen und Kollegen, die ich während meiner Zeit am Institut erlebt habe, bedanken. Ihre nahezu ausnahmslos offene und freundliche Persönlichkeit stellt die Grundlage für das sehr angenehme Arbeitsklima, das man als Mitarbeiter an diesem Institut antrifft, dar.

Den in diesem Vorwort zwar zuletzt angeordneten, zweifellos aber größten, Dank möchte ich hiermit meinen Eltern aussprechen. In diesem Zusammenhang kann meine allgemeine Dankbarkeit für die weitreichende Unterstützung während meiner Promotionszeit auch insbesondere auf die Tatsache fokussiert werden, dass diese Arbeit ohne die Unterstützung meiner Eltern, insbesondere in finanzieller Hinsicht, niemals von mir hätte erstellt werden können.

Volker Gravemeier

Contents

1	Introduction	1
1.1	Motivation	1
1.2	Ambition of this work	5
1.3	Overview	6
2	Continuum Mechanical Basics of Incompressible Flow	7
2.1	Introduction	7
2.2	Kinematics	7
2.3	Kinetics	9
2.4	Constitutive equation	10
2.5	Integral and differential formulation of conservation principles	11
2.6	The incompressible Navier-Stokes equations	14
2.7	A model problem: scalar convection-diffusion-reaction equation	22
3	Numerical Simulation of Incompressible Flow using a Standard Galerkin Finite Element Method	25
3.1	Introduction	25
3.2	Spatial discretization	26
3.3	Temporal discretization and linearization	31
3.4	Numerical problems with the standard Galerkin finite element method ...	40
4	A Brief Insight into Turbulence	45
4.1	What is so special about turbulent flows?	45
4.2	The Reynolds equation and its closure problem	46
4.3	Spatial and temporal scales based on two-point correlations	50
4.4	Richardson's energy cascade and Kolmogorov energy spectrum	52
5	Alternative Procedures for the Numerical Simulation of Turbulent Flows ..	57
5.1	Introduction	57
5.2	Direct Numerical Simulation (DNS)	57
5.3	Large Eddy Simulation (LES)	59
5.4	Simulation based on the Reynolds Averaged Navier-Stokes equations (RANS)	69
6	Variational multiscale method for scalar convection-diffusion-reaction equations	70
6.1	Separation of two scales	70

6.2	Solving for the small scales	72
6.3	Taking into account locally the effect of unresolved scales onto resolved scales	81
6.4	Separation of three scales	85
6.5	Transient case and the concept of quasi-static small scales	88
7	Variational multiscale method for the Navier-Stokes equations	92
7.1	Separation of two scales	92
7.2	Solving for the small scales	97
7.3	Taking into account locally the effect of unresolved scales onto resolved scales	107
7.4	Separation of three scales	109
7.5	Closure: three-scale separation based on residual-free bubbles and the subgrid viscosity approach	113
8	Practical Implementation: a two- and a three-level finite element method .	114
8.1	A two-level finite element method based on the RFB approach	114
8.2	Introducing a third level	119
8.3	Future topics	127
9	Numerical examples of laminar flow situations	135
9.1	Impinging fluid flow (2-D)	135
9.2	Lid-driven cavity flow (2-D)	142
9.3	Cavity flow with oscillating lid (2-D)	149
9.4	Flow past a circular cylinder (2-D)	153
9.5	Beltrami flow (3-D)	157
10	Numerical examples of turbulent flow situations	162
10.1	The choice of turbulent flow examples	162
10.2	Lid-driven cavity flow (3-D)	163
10.3	Plane mixing layer (2-D)	170
10.4	Remark concerning computational cost of the applied methods	179
11	Summary and Outlook	180
11.1	The past (of this work)	180
11.2	... and the future (beyond this work)?	181
Appendix	183
A	Some measures for the statistical description of turbulence	183
B	A hierarchy of functional spaces	186

C	A brief survey of used computational tools	188
References	190

Abbreviations and Notations

The following abbreviations and notations are used within this work:

Abbreviations

BE	Backward Euler scheme
CDR	Convection-Diffusion-Reaction equation
CFD	Computational Fluid Dynamics
CN	Crank-Nicolson scheme
Da	Damköhler number
DAE	Differential Algebraic Equation system
DNS	Direct Numerical Simulation
FEM	Finite Element Method
IBVP	Initial Boundary Value Problem
LES	Large Eddy Simulation
Ma	Mach number
NS	Navier-Stokes equations
ODE	Ordinary Differential Equation
Pe	Peclet number
PPE	Pressure Poisson Equation
RANS	Reynolds Averaged Navier-Stokes
Re	Reynolds number
RFB	Residual-Free Bubble
USFEM	Unusual Stabilized Finite Element Method

Notations

Bilinear forms

$B_{cdr}(\cdot; \cdot)$	bilinear form (CDR - stationary)
$B_{cdr}^t(\cdot; \cdot)$	bilinear form (CDR - instationary)
$B_{cdr}^{dt}(\cdot; \cdot)$	bilinear form, discrete in time (CDR - instationary)
$B_{NS}(\cdot; \cdot)$	bilinear form (NS)
$B_{NS}^{dt}(\cdot; \cdot)$	bilinear form, discrete in time (NS)
$C(\cdot; \cdot)$	projection of the cross stress tensor
$L(\cdot; \cdot)$	projection of the Leonard stress tensor
$R(\cdot; \cdot)$	projection of the subfilter-scale Reynolds stress tensor

Bubble functions

\mathfrak{B}_1	normalized bubble function
\mathfrak{F}	'right-hand-side' bubble function
\mathfrak{P}	'pressure' bubble function
\mathfrak{U}	velocity bubble function

Domains and boundaries

Γ	domain boundary
Γ'	union of all element boundaries excluding the domain boundary
Γ_e	element boundary
Γ_g	Dirichlet boundary
Γ_h	Neumann boundary
Γ^{st}	space-time domain boundary
Γ_-	inflow boundary
Γ_+	outflow boundary
Ω	domain
Ω'	union of all element interiors
Ω_e	element domain

Finite element matrices and vectors

C	convective matrix
D	diffusive matrix
E	vector containing entries due to Dirichlet boundary conditions (CDR)
E^M	vector containing entries due to Dirichlet boundary conditions (NS - momentum)
E^C	vector containing entries due to Dirichlet boundary conditions (NS - continuity)
F	body force vector
G	gradient matrix
G^T	divergence matrix
K	'stiffness' matrix
M	mass matrix
N	Neumann boundary condition vector
R	right-hand-side vector
T	'time-right-hand-side' vector
V	viscous matrix
b	vector of unknown parameters of normalized bubble function
p	vector of unknown parameters of pressure solution function
u	vector of unknown parameters of velocity solution function
\dot{u}	vector of unknown parameters of acceleration solution function

ϕ vector of unknown parameters of solution function (CDR)

Function spaces and classes

$B(\Omega_e)$ bubble function space for element domain Ω_e
 $C^0(\Omega)$ class of continuous functions
 $H^1(\Omega)$ Sobolev space of square-integrable functions with square-integrable derivatives
 \mathcal{J}^h space of discretely divergence-free functions
 $L_2(\Omega)$ Sobolev space of square-integrable functions
 \mathcal{P}_ϕ solution function space (CDR)
 \mathcal{P}_p solution function space for pressure (NS)
 \mathcal{P}_u solution function space for velocity (NS)
 $\mathcal{P}_{u,p}$ combined solution function space (NS)
 \mathcal{V}_ϕ weighting function space (CDR)
 \mathcal{V}_p weighting function space for pressure (NS)
 \mathcal{V}_u weighting function space for velocity (NS)
 $\mathcal{V}_{u,p}$ combined weighting function space (NS)
 \mathcal{V}_{EGF} weighting function space for element Green's function (CDR)
 \mathcal{V}_{RFB} weighting function space for residual-free bubble function (CDR)

Mathematical symbols

$(\cdot, \cdot)_\Omega$ L_2 -inner product on Ω
 $[\cdot]_\pm^+$ jump operator
 $\|\cdot\|_0$ L_2 -norm on Ω
 $\|\cdot\|_1$ H^1 -norm on Ω
 \otimes tensor product
 \oplus direct sum
 \forall for all; for each
 $meas(\cdot)$ measure symbol
 $O(\cdot)$ order symbol
 \mathbb{R} real numbers
 $\mathbb{R}^{n_{sd}}$ Euclidean n_{sd} -space

Operator symbols

∇ gradient operator
 $\nabla \cdot$ divergence operator
 Δ Laplace operator
 \mathcal{A} finite element assembly operator
 \mathcal{L} differential operator
 \mathcal{L}^* adjoint differential operator

\mathcal{L}^{RFB}	differential operator indicating zero Dirichlet boundary conditions (RFB)
\mathcal{L}_C	differential operator (NS) - continuity equation
\mathcal{L}_M	differential operator (NS) - momentum equation
$\mathcal{L}_M^{dt, lin}$	differential operator (NS) - discrete in time and linearized momentum equation
\mathcal{L}_M^{stat}	differential operator (NS) - stationary momentum equation
\mathcal{L}_c	differential operator (CDR) - convective term
\mathcal{L}_{cdr}	differential operator (CDR) - stationary
$\mathcal{L}_{cdr, t}$	differential operator (CDR) - instationary
\mathcal{L}_{cdr}^{stab}	differential operator (CDR) - stabilizing operator acting on weighting function
\mathcal{L}_{cdr}^{1-D}	one-dimensional differential operator (CDR)
\mathcal{L}_{conv}	differential operator (NS) - convective term
\mathcal{L}_d	differential operator (CDR) - diffusive term
\mathcal{L}_{pres}	differential operator (NS) - pressure term
\mathcal{L}_r	differential operator (CDR) - reactive term
\mathcal{L}_{reac}	differential operator (NS) - reactive term
\mathcal{L}_t	differential operator (NS) - temporal term
\mathcal{L}_{visc}	differential operator (NS) - viscous term
\mathcal{M}	integral operator
\mathcal{P}	general projection operator
\mathcal{P}_G^h	discrete Galerkin projection operator
\mathcal{P}_g^h	projection operator into discretely divergence-free subspace
\mathcal{R}_{cdr}	residual of CDR
$\mathcal{R}_{NS, M}$	residual of NS momentum equation
$\mathcal{R}_{NS, C}$	residual of NS continuity equation

Scalars – Greek symbols

Δ	characteristic filter length
θ	parameter for generalized trapezoidal scheme
$\alpha, \bar{\alpha}$	parameters for nonlinear iteration scheme (NS)
β	parameter for convective term (NS)
γ	parameter for viscous term (NS)
δ	Dirac delta function / vorticity thickness
δ_0	initial vorticity thickness
δ_ν	viscous length
ε	rate of dissipation
η	Kolmogorov length scale
κ	kinematic physical diffusivity / scalar wavenumber

κ_{dyn}	dynamic physical diffusivity
κ_t	temporal artificial kinematic 'diffusivity'
κ^{art}	artificial kinematic diffusivity
κ^{stab}	stabilizing kinematic diffusivity
κ^G	numerical kinematic diffusivity due to Guermond
λ	material constant / Taylor microscale
λ_a	wavelength
μ	dynamic physical viscosity
ν	kinematic physical viscosity
ν^{eff}	effective kinematic viscosity
ν^T	kinematic turbulent (eddy) viscosity
ν^{art}	artificial kinematic viscosity
ν^G	numerical kinematic viscosity due to Guermond
ξ	function for calculation of stabilization parameter
ρ	density / correlation coefficient
σ	reaction coefficient
σ_m	mean normal stress
σ_{mod}	modified reaction coefficient
τ	stabilization parameter
τ_η	Kolmogorov time scale
ϕ	scalar quantity
ϕ_0	continuous initial scalar quantity
ϕ^0	discrete initial scalar quantity
ψ	streamfunction
ψ_{per}	perturbed streamfunction
ω	scalar vorticity
ω_{max}	maximum scalar vorticity

Scalars – Latin symbols

A	convective velocity scale
C_K	Kolmogorov constant
C_S	Smagorinsky constant
C^{art}	constant for calculation of artificial viscosity
C^G	Guermond constant
E	kinetic energy spectrum function
E_{kin}	kinetic energy
G	spatial filter

\hat{G}	sharp cutoff filter
L	integral length scale
L_{\max}	maximum length scale
N	shape function
N_S	number of spatial nodes
N_T	number of 'temporal' nodes
N_{S+T}	number of spatial and 'temporal' nodes
S	surface
St	Strouhal number
T	time period / time scale
T_{cav}	circulation time in cavity
U	velocity scale
V	volume
a_r	projection of convective velocity vector onto direction r
c	speed of sound
d	dimension
e	error / element of discretization
f	scalar right-hand-side (CDR)
f_ϕ	source (or sink) term (CDR)
g	scalar Dirichlet boundary condition / Green's function
h	scalar Neumann boundary condition / characteristic element length
k	turbulent kinetic energy / polynomial order
l	length
l_{mix}	mixing length
l_s	length in streamwise direction
m	mass
m_k	polynomial interpolation parameter for calculation of stabilization parameter
n_{dofs}	number of degrees of freedom
n_{ed}	number of element degrees of freedom
n_{el}	number of elements
n_{RFB}	number of residual-free bubble functions
n_{sd}	number of spatial dimensions
n_{vort}	number of vortices
p	kinematic pressure
p_{dyn}	dynamic pressure
q	scalar weighting (test) function (NS - pressure)
s	temporal separation

t	time
δt	discrete time step
u_η	Kolmogorov velocity scale
Δu_{ml}	velocity jump across mixing layer
v_{mix}	mixing velocity
w	scalar weighting (test) function (CDR)

Tensors and tensor–related notation

C	cross stress tensor
ε	rate-of-velocity tensor
I	identity tensor
L	Leonard stress tensor
L^T	Leonard stress tensor based on Germano’s identity
L_{mod}^T	model expression for Leonard stress tensor based on Germano’s identity
R	two-point correlation tensor / subfilter-scale Reynolds stress tensor
σ	stress tensor
σ_{tot}	’total’ stress tensor
τ	viscous stress tensor
τ^R	Reynolds stress tensor
τ^S	subfilter-scale stress tensor
τ^T	subtest-scale stress tensor
ϕ	velocity spectrum tensor
Ω	spin tensor
$(\cdot)^T$	transpose of tensor
$tr(\cdot)$	trace of tensor
$dev(\cdot)$	deviatoric tensor

Value specifications

$\langle (\cdot) \rangle$	mean value
$\hat{(\cdot)}$	fluctuating value
$\overline{(\cdot)}$	large-scale value
$(\cdot)'$	small-scale value
$\hat{(\cdot)}$	unresolved value
$(\cdot)^h$	discrete value (characteristic length of discretization h)
$(\cdot)^n$	value at time step n
$(\cdot)_i$	value at iteration step i

Vectors

X	material coordinate vector
-----	----------------------------

\mathbf{a}	convective velocity vector
\mathbf{e}_i	unit vector in coordinate direction i
\mathbf{f}	body force vector (NS)
\mathbf{f}_t^n	'time-right-hand-side' vector (NS)
\mathbf{g}	Dirichlet boundary condition vector
\mathbf{h}	Neumann boundary condition vector
\mathbf{h}_{tot}	'total' Neumann boundary condition vector
$\boldsymbol{\kappa}$	wavenumber vector
\mathbf{n}	normal vector
\mathbf{r}	spatial separation vector
\mathbf{t}	stress vector
\mathbf{t}_ϕ	surface vector related to scalar quantity ϕ
\mathbf{u}	velocity vector
\mathbf{u}_0	initial velocity vector
\mathbf{u}_{int}	intermediate velocity vector
\mathbf{u}_g	discretely divergence-free velocity vector
\mathbf{u}^0	discrete initial velocity vector
$\dot{\mathbf{u}}$	acceleration vector
\mathbf{v}	weighting (test) function vector (NS - velocity)
\mathbf{x}	spatial coordinate vector
$\boldsymbol{\omega}$	vorticity vector

1 Introduction

1.1 Motivation

Turbulence is the *"invention of the Devil on the seventh day of creation"*. This is the way Peter Bradshaw expressed his view of this very special flow condition in Bradshaw (1994). Beyond it, the title of this publication asserts his claim to designate turbulence as the chief outstanding difficulty in, at least, fluid mechanics. However, turbulence is only one aspect of the present work and, more precisely, the one at the road's end. Correspondingly, it is advisable to start at the beginning of it all - conspicuously later than the seventh day of creation though, in order not to let this work burst at the seams.

Fluids can be divided into liquids and gases with water and air being the most prominent representatives of these two groups, respectively. In Fig. 1.1, some everyday examples for flows of liquids like the wake of a motorboat, the water flow of an alpine creek, the oil flow in a pipeline, or the blood flow in an artery are displayed.

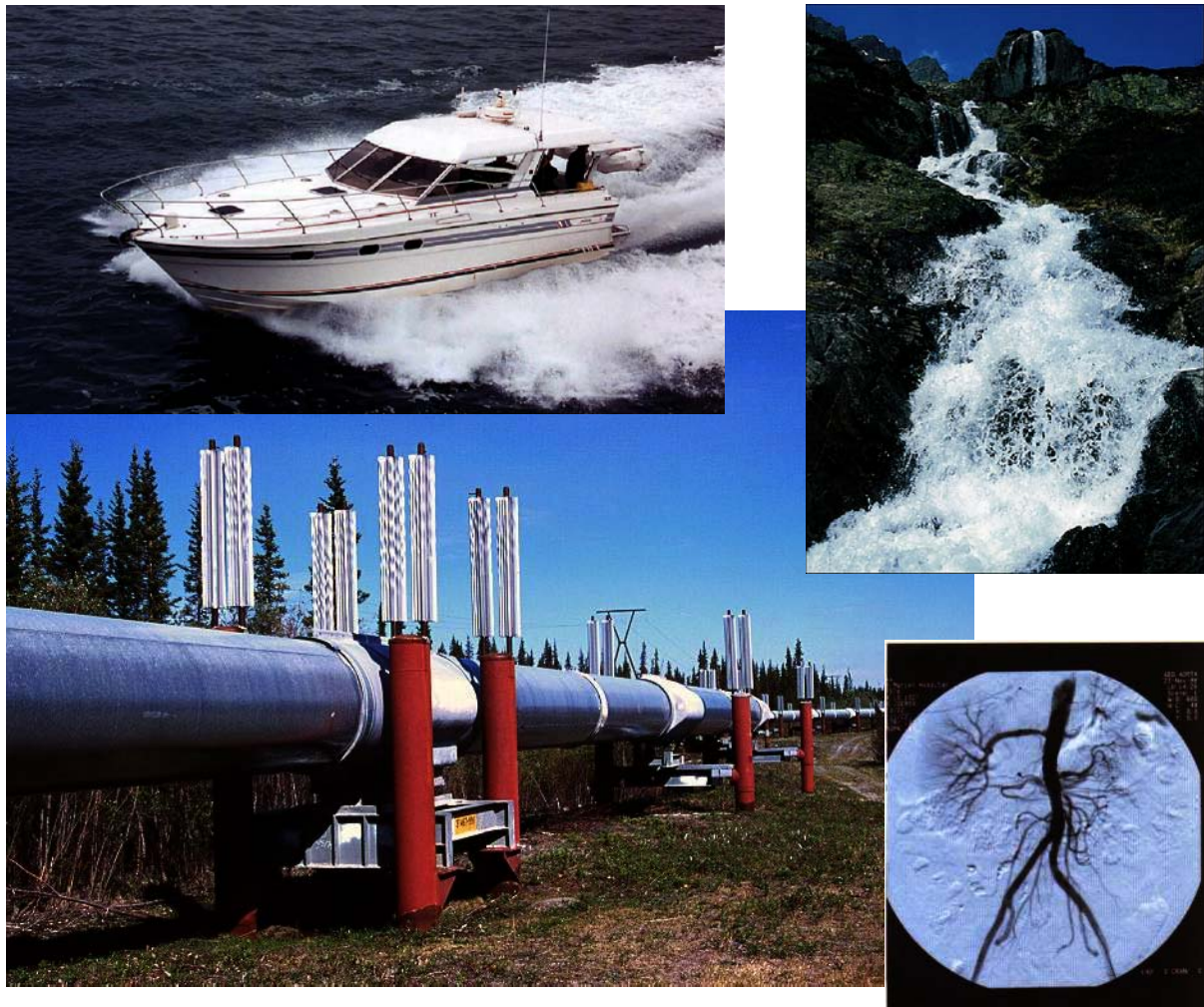


Fig. 1.1: Some common examples for liquid flows

In almost all cases, the flow of liquids like water may be treated as being incompressible. Under certain conditions like, for instance, flow governed by a low Mach number, air and other gases may also be dealt with based on the assumption of incompressibility. Fig 1.2 illustrates some well-known examples for flows of gases like the air flow around a plane, a motorbike, or a bridge. Of course, a flow around an airplane usually has to be viewed as being compressible. However, the respective flow parameters have to be considered in the other two cases, in order to judge the classification of the flow finally.



Fig. 1.2: Some common examples for gas (air) flows

The concept of incompressibility describes a presumed flow performance where the temperature field will exhibit no influence on the velocity and pressure field, if, in addition to the density, all further characteristic material properties like, for example, the viscosity are constant as well. The scope of the incompressibility assumption is broad and, thus, the area of application of the perceptions of this work.

Incompressible flow is specified mathematically by the incompressible version of the set of Navier-Stokes equations. Interestingly, the last proposition is basically valid for two crucial states of flow, laminar flow and turbulent flow, although they are quite different from the physical point of view. The occurrence of one or the other state strongly depends on the so-called Reynolds number associated with the flow. This has already been observed by Osborne Reynolds (1842-1912), the eponym of this dimensionless number, in the later half of the 19th century. In typical enginee-

ring applications, turbulent flows are surely prevalent due to its positive features like a more effective transport and mixing ability with respect to a comparable laminar flow. By dissecting Figs. 1.1 and 1.2, the reader may also verify that most of the depicted common examples represent turbulent flow situations or flow situations which may at least enter the turbulent regime temporarily. According to this, the interest in this flow regime is very high.

The analytical point of view is extremely deficient with regard to the turbulent flow regime in particular. There exist no analytical solutions even to the simplest turbulent flow situations. To that effect, all hope culminates in a numerical way of solving this 'chief outstanding' problem. The straightforward approach, i.e. simply solving the Navier-Stokes equations with appropriate boundary conditions in a numerical manner, discovers its limitations very soon. By the way, this straightforward procedure is called Direct Numerical Simulation (DNS) - and it shall be explained later on. It sounds so easy - what is the trouble? Well, the major problem in solving the Navier-Stokes equations computationally can be assigned to the scales or, more precisely spoken, the broad range of scales. For laminar flows already, a substantial range of scales may be encountered (and will be encountered indeed as the reader may realize below). Dealing with turbulent flows, however, ostensibly means nothing more than dealing with even broader ranges of scales in comparison to laminar flows. A quantitative prediction of this range obeys a simple proportional correlation with the particular Reynolds number. In computational mechanics, severe difficulties emerge as soon as the spectrum of scales to be treated extends beyond the limits of the available computer power - and, still today unfortunately, this is indeed an undisputable actuality for most of the turbulent flows.

Lowering the demands of resolution leads to what is well-established under the name of 'Large Eddy Simulation' (LES) in the meantime. The core of this approach may be expressed verbally as follows: it is aimed at a complete resolution of the large-scale structure of the turbulent flow and the effect of the smaller scales, which are not acquired by this resolution, is modeled. Technically, the unresolved scales are distinguished from the resolved scales by the application of a spatial filter of limited extent. Of course, LES is not the 'miracle cure'. The computational effort required for LES may be less than for DNS, but it is still of substantial complexity. Hence, it is also still not possible to perform LES for most of the turbulent flows arising in characteristic engineering applications. However, it seems to be more auspicious to believe in LES than in DNS for the near future - and there may be some support in improving LES erupting from quite a different field.

This redeemer potentially being instrumental in fighting the devil of turbulence has also a name as a matter of course: the variational multiscale method. This theoretical framework has been established by Hughes (1995) and further developed as a powerful means for problems of computational mechanics having to deal with large scale ranges by Hughes and co-workers in Hughes and Stewart (1996) and Hughes et al. (1998). The basic concept consists in differentiating scale groups, for example large (resolved) and small (resolved) scales or resolved and unresolved scales depending on the resolution requirements. This methodological framework has also been applied to the underlying problem, the incompressible Navier-Stokes equations, in order to facilitate numerical simulations in the sense of LES. You may consult Hughes et al. (2000a) for a theoretical elaboration and Hughes et al. (2001a, 2001b) for results of some early applications. In preference to the usage of a filter in the aforementioned 'classical' way of performing LES, variational projection separates scale ranges within the variational multiscale method. After all, it has to be remarked that the initial concept of the variational multiscale method as Hughes and

co-workers have proposed it in their publications assumes a separation of two scale ranges. Nevertheless, the framework is basically unsealed to arrangements going beyond this two-scale decomposition.

Independent of the author's thoughts in this direction, Collis (2001) has recently broadened the picture of the variational multiscale method in the LES-context by raising the number of separated scale ranges beyond the original twofold separation. This enables a completely different numerical treatment for any of these ranges resulting in a paramountly flexible numerical simulation, e.g. by using the finite element method. The variational multiscale method was basically developed for the application within a Galerkin finite element method and this will, in fact, be the method of choice in this work. It is by no means restricted to this variant of a numerical method though. At this stage, it has to be pointed out that the variational multiscale method is from a practical standpoint 'merely' a theoretical framework for the separation of scales. Corresponding practical methods fitting in this framework on the one hand and enabling an implementation as a computational algorithm on the other hand are still rare. For such practical methods, it is crucial that a clear separation of the different ranges is actually achieved.

The Galerkin finite element method has just been addressed as the numerical method of choice. This represents a hazardous choice for problems of fluid mechanics - and, in this context, the devil actually shows up with two heads. Independent of the effective flow regime, it is, in general, not possible to achieve unspoilt results using the standard form of the Galerkin finite element in case of a dominating convective term, i.e. a very large Reynolds number in fact, without resorting to an extremely fine discretization level. The second problem, which has to be dealt with in the context of the Navier-Stokes equations, is the required fulfillment of the so-called inf-sup condition exhaustively described, for instance, in Brezzi and Fortin (1991). However, there is a cure (considered miraculous or not) effectively addressing these two problems in the meantime: stabilized Galerkin finite element methods. These stabilized methods may be incorporated into the framework of the variational multiscale method though. This leads to the opportunity to proceed an overall conclusion of this short motivation weaving the addressed problems (and, accordingly, the respective methods to tackle these problems later on) into a general problem classification.

In case the very small scales at one end of a scale spectrum represent the essential problem, two classes of problems can be distinguished according to Franco Brezzi, confer e.g. Brezzi (2000). To the first class, all the just mentioned situations may be assigned for which the chosen discretization level does not provide the necessary stability properties. This has to be viewed, in general, as being the result of an improper treatment of the small scales of the problem. An actual physical effect cannot be ascribed to the small scales of these problems though. This is the important difference with respect to problems associated with the second class of problems where this small-scale physics is crucial. Consequently, turbulent flows have to be allocated to the second class of this simplified categorization. The final result, however, appears to be the same for the representatives of both classes in that a questionable solution is achieved in the end due to the disregard of the small scales.

Finally, for this motivation to be what it's name implies, there should be some light visible at the end of the 'tunnel of problems' at least. In treating properly the first kind of problems, a certain amount of experience has been gathered in the meantime, in particular by using the particular procedure of stabilized methods. Moreover, there is a ray of hope that a transfer of the experience to the second problem class may be conceivable. In order to express this hope, Franco Brezzi

(2000) is quoted as follows: *"These two situations are quite different, in nature and scale. Nevertheless it is not unreasonable to hope that some techniques that have been developed for dealing with the former class of phenomena might be adapted to deal with the latter one. In this sense, the most promising technique seems to be the use of Residual-Free Bubbles."*

At this introductory stage already, it has to be emphasized that using residual-free bubbles will provide us with substantial computational savings. The quality of approximation, however, may be qualified as being inadequate, in particular, for turbulent flow applications as will be shown later in this work.

1.2 Ambition of this work

The numerical simulation of problems covering extremely wide ranges of scales like the one considered in this work is certainly a challenging but, at the same time, a highly contemporary topic in computational mechanics as has been pointed out, for instance, by Oden et al. (2003) recently. In order to accomplish this challenge, the following strategy is pursued: Basically, this work tries to range in the paths enlightened by the ray of hope mentioned at the end of the last section. Precisely, this means that the framework of the variational multiscale method shall be exploited, in order to develop a method suitable for problems with wide ranges of scales governed by the incompressible Navier-Stokes equations. Besides the practical implementation of the method, promising alternative approaches within the variational multiscale method should also be pointed out. Initially, there is no special attention to either laminar or turbulent flow situations, respectively. Nevertheless, the ultimate goal is certainly the development of a method which exhibits its particular strengths in the treatment of turbulent flows. The core of this work primarily consists in focussing on the methodological aspects of the method and to a lesser extent on the actual application of the method. After developing the methodological aspects including its practical implementation, various laminar flow situations are shown as examples for the performance of the multi-level finite element methods in this work. Afterwards, two initial turbulent flow applications are executed pointing out the still inherent shortcomings of the methods. Hence, this work leaves room for further improvement of the methods and gives some comments in direction of potential developments.

There is an even higher-ranking target though. This work has been proceeded at an Institute of Structural Mechanics. The reader might have already wondered at the, normally, hardly achievable reconciliation of the topic of this work on the one hand and the scientific environment of its compilation on the other hand. The dawn for the introduction of fluid mechanical topics into the Institute broke with the work of Wall (1999). His work aimed at problems of fluid-structure-interaction and, in consequence, this is actually the aforementioned higher-ranking target. For tackling the fluid part in Wall (1999), stabilized Galerkin finite element methods have been applied limited to purely laminar flow situations though. In a second work at the Institute of Structural Mechanics, Mok (2001) focussed on further developments related to the coupling part of fluid-structure-interaction problems. The present work aims at further developments within the fluid mechanical part of coupled fluid-structure-interaction problems. In particular, it is, on the one hand, the first work dealing with turbulent flows and, on the other hand, also the first work introducing the topic of multiscale methods at this Institute. Due to this reason, the basics of these issues will be presented in a more elaborate manner.

1.3 Overview

At the end of this introduction, the following short overview should procure an impression of what will be dealt with in the respective chapters of this work.

In **chapter 2**, the continuum mechanical basics of fluid mechanics related to kinematical, kinetical and constitutive aspects are presented. From the formulation of the conservation principles, the incompressible Navier–Stokes equations are developed in various forms along with the appropriate initial and boundary conditions as a particular problem of fluid mechanics. At the end of this chapter, the model problem of a scalar convection–diffusion–reaction equation is introduced as another partial differential equation being auxiliary in the subsequent developments.

The necessary foundations for the numerical solution of the scalar convection–diffusion–reaction equation as well as the Navier–Stokes equations are established in **chapter 3** with regard to the spatial and temporal discretization. The numerical problems linked with the standard Galerkin finite element method are addressed in the last section of this chapter.

Chapter 4 provides a brief insight into some issues of turbulent flows. This material represents a succinct selection of topics which are important for the goals of this work. A furthergoing treatment of theoretical aspects related to turbulence is not feasible within the bounds of this work.

In **chapter 5**, the three major approaches used for the numerical simulation of turbulent flows, i.e. DNS, LES and RANS, are presented. After characterizing DNS as the comprehensive procedure, LES will be the main focus of this chapter. On the one hand, the aspect of the ‘classical’ way of performing LES is dealt with and, on the other hand, its incorporation into the framework of a Galerkin finite element method is pushed forward.

Chapter 6 focusses on a comprehensive introduction of the variational multiscale method for the model case of the convection–diffusion–reaction equation. The solution strategies for the small scales are particularly emphasized. Two- and three-scale separations of the basic scalar variable are distinguished explicitly.

The ‘modus operandi’ applied to the convection–diffusion–reaction equation is transferred to the Navier–Stokes equations in **chapter 7**. The interpretation of the perceptions of this chapter in the sense of DNS and LES is enforced. At the end of this chapter, the theoretical basis for the following two- and three-level methods is pointed out.

In **chapter 8**, the practical implementation of the insight from the preceding chapters is realized in the form of a two- and three-level finite element method. Starting with the introduction of the residual-free bubble approach on the second level, an additional third level is presented constituted by the dynamic modeling procedure for the dissipative effect of still unresolved scales. In the last section of this chapter, some furthergoing developments are addressed related, on the one hand, to the presented method and, on the other hand, to potentially alternative strategies.

Chapter 9 contains various numerical examples for laminar flow situations. Afterwards, some initial findings for turbulent flow situations are presented in **chapter 10**.

This work results in a short summary and future prospects in **chapter 11**. In the subsequent **appendix**, some measures for the statistical description of turbulence, a hierarchy of functional spaces in principle as well as some remarks concerning the computational tools used for the compilation of the sample calculations in chapters 9 and 10 may be found as supportive material to the preceding elaboration.

2 Continuum Mechanical Basics of Incompressible Flow

2.1 Introduction

The continuum approach enables the neglect of the molecular structure of solids and fluids rather regarding them as being without empty spaces, i.e. there are always neighbor particles. Mathematically, one is left with continuous functions valid at all points in space and time. This applies to the derivatives of these functions too. The justification for the assumption of a continuous medium in the just described sense may be found by considering the so-called Knudsen number. This dimensionless number relates the mean free path to the smallest length scale probably appearing in the flow. With a mean free path of about 10^{-7} m for e.g. air under atmospheric conditions and an estimated smallest length scale seldomly falling below 10^{-4} m, the Knudsen number is calculated to be 10^{-3} . For this number being notably smaller than 1, it is a justifiable approach to rely on the continuum hypothesis according to e.g. Pope (2000).

Within the wide range of books dealing with continuum mechanics as its main topic, a large number of monographs is encountered dedicating a predominant part the treatment of the mechanics of solids. For the purposes of this work, three books assigning a considerable portion of their content to the field of fluid mechanics may be mentioned: Fung (1977), Lai et al. (1993), and Malvern (1969). Besides the special literature on continuum mechanics, a vast number of monographs on fluid mechanics also touch the basic continuum mechanical topics more or less comprehensive. It should be sufficient to name the classic textbooks of Batchelor (1967) as well as Schlichting (1979) here. Moreover, the multimedia package of Homsy et al. (2000) should be mentioned as a very attractive offer from a didactical point of view. Several visual impressions may also be gained from the famous album of van Dyke (1982).

2.2 Kinematics

2.2.1 Velocity in Lagrangean and Eulerian description

Although there may be a distinction of up to four descriptions (see Malvern (1969)), it will be focussed on the popular twofold classification here. On the one hand, the referential description, called material description by many authors and attributed to Joseph Louis Lagrange (1736-1813), may be applied. Therein, the velocity vector \mathbf{u} of a particle depends here on the material coordinates X_1, X_2 and X_3 , i.e. the coordinates of its position in the reference configuration, and the time t : $\mathbf{u}(X_1, X_2, X_3, t)$.

On the other hand, by fixing the observer's location, \mathbf{u} may be expressed as a function of the spatial coordinates x_1, x_2 and x_3 and the time t . This description is ascribed to Leonard Euler (1707-1783). For historical correctness, it has to be remarked that both Lagrange and Euler have been aware of both descriptions which makes this attribution somehow accidental. The spatial coordinates depend on the material coordinates as

$$\mathbf{x} = \mathbf{x}(\mathbf{X}, t) \tag{2.1}$$

with the essential condition

$$\mathbf{x} = \mathbf{x}(\mathbf{X}, t_0) = \mathbf{X} \quad (2.2)$$

at the reference time t_0 .

2.2.2 Acceleration: Material (Substantial) time derivative

The Eulerian description, which is mostly used in fluid mechanics, will be concentrated on here. The material time derivative, also termed substantial time derivative, expressing the acceleration

$$\dot{\mathbf{u}}(\mathbf{x}, t) = \frac{D\mathbf{u}}{Dt}(\mathbf{X}, t) \quad (2.3)$$

in a Lagrangian description can also be formulated with reference to a spatial description by using the chain rule as follows:

$$\dot{\mathbf{u}}(\mathbf{x}, t) = \frac{D\mathbf{u}}{Dt}(\mathbf{x}, t) = \frac{\partial \mathbf{u}}{\partial t} + \frac{\partial \mathbf{u}}{\partial \mathbf{x}} \frac{\partial \mathbf{x}}{\partial t} = \frac{\partial \mathbf{u}}{\partial t} + \mathbf{u} \cdot \nabla \mathbf{u} \quad (2.4)$$

The acceleration in (2.4) consists of the local time derivative vanishing in a steady flow situation and a convective rate of change.

2.2.3 Rate-of-velocity and spin tensor (spatial gradient)

The unification of the spatial derivatives in the coordinate directions, i.e. the spatial gradient, of the velocity $\nabla \mathbf{u}$ may be decomposed into a symmetric part

$$\boldsymbol{\varepsilon}(\mathbf{u}) = \frac{1}{2}(\nabla \mathbf{u} + (\nabla \mathbf{u})^T) \quad (2.5)$$

and a skew-symmetric part

$$\boldsymbol{\Omega}(\mathbf{u}) = \frac{1}{2}(\nabla \mathbf{u} - (\nabla \mathbf{u})^T) \quad (2.6)$$

The symmetric part $\boldsymbol{\varepsilon}$ is termed 'rate-of-velocity tensor' and the skew-symmetric part $\boldsymbol{\Omega}$ is denoted 'spin tensor'. Since one may encounter different definitions of the spatial gradient in the literature, an explicit definition for this work reading

$$\nabla \mathbf{u} = \begin{pmatrix} \frac{\partial u_1}{\partial x_1} & \frac{\partial u_1}{\partial x_2} & \frac{\partial u_1}{\partial x_3} \\ \frac{\partial u_2}{\partial x_1} & \frac{\partial u_2}{\partial x_2} & \frac{\partial u_2}{\partial x_3} \\ \frac{\partial u_3}{\partial x_1} & \frac{\partial u_3}{\partial x_2} & \frac{\partial u_3}{\partial x_3} \end{pmatrix} = \boldsymbol{\varepsilon}(\mathbf{u}) + \boldsymbol{\Omega}(\mathbf{u}) \quad (2.7)$$

seems to be necessary, with which its transpose is also defined unambiguously. The dual (or axial) vector of the spin tensor is the vorticity vector $\boldsymbol{\omega}$ which is obtained by applying the curl operator to the velocity

$$\boldsymbol{\omega} = \frac{1}{2} \nabla \times \mathbf{u} \quad (2.8)$$

The relation to the nonzero components of $\boldsymbol{\Omega}$ is given by

$$\boldsymbol{\omega} = -(\Omega_{23}\mathbf{e}_1 + \Omega_{31}\mathbf{e}_2 + \Omega_{12}\mathbf{e}_3) \quad (2.9)$$

where \mathbf{e}_i denotes the unit vector in the coordinate direction i . It is clear by definition (2.6) that all diagonal components of $\boldsymbol{\Omega}$ are always zero. If all off-diagonal components of $\boldsymbol{\Omega}$ (and likewise all components of $\boldsymbol{\omega}$) are zero, the velocity field is said to be irrotational.

2.3 Kinetics

2.3.1 Body and surface force vectors

Two types of external forces have to be respected. On the one hand, body forces act on the elements of the volume inside the body, e.g. gravity due to long-range interaction with matter. The body force per unit mass acting on the infinitesimal actual volume dV of the body is denoted by the vector \mathbf{f} . On the other hand, the surface forces (or traction) act on the real or imagined surface separating two parts of the body. The stress vector (or traction vector) named after Augustin Louis Cauchy (1789–1857) is defined as

$$\mathbf{t} = \lim_{\Delta S \rightarrow 0} \frac{\Delta \mathbf{F}}{\Delta S} = \mathbf{t}(\mathbf{x}, t, \mathbf{n}) \quad (2.10)$$

where $\Delta \mathbf{F}$ denotes the resultant force on a small area ΔS on the respective surface. The usual notation 'body' and 'force' stemming from the field of solid mechanics may be viewed as being suboptimal in the field of fluid mechanics. However, it will be stuck to this notation due to its widespread use in continuum mechanics and thought of a volume of liquid or gas and a 'flow', respectively.

2.3.2 Stress tensor

It is indicated in (2.10) that the stress vector is a function of the unit outward normal vector \mathbf{n} of the surface. The vector \mathbf{t} may also be obtained by the transformation

$$\mathbf{t} = \mathbf{n} \cdot \boldsymbol{\sigma} \quad (2.11)$$

where $\boldsymbol{\sigma}$ denotes the Cauchy stress tensor. The components of the stress tensor are

$$\boldsymbol{\sigma} = \begin{pmatrix} \sigma_1 & \tau_{12} & \tau_{13} \\ \tau_{21} & \sigma_2 & \tau_{23} \\ \tau_{31} & \tau_{32} & \sigma_3 \end{pmatrix} \quad (2.12)$$

with σ_i indicating normal stresses and τ_{ij} shear stresses. The principle of conservation of moment of momentum, which will not be mentioned explicitly in section 2.5, tells us that the stress tensor is symmetric, i.e. $\boldsymbol{\sigma} = \boldsymbol{\sigma}^T$. Hence, six independent unknowns remain in (2.12). Like any tensor, the stress tensor exhibits three invariants, of which merely the first one termed the trace of $\boldsymbol{\sigma}$ and reading

$$tr \boldsymbol{\sigma} = \sigma_1 + \sigma_2 + \sigma_3 \quad (2.13)$$

should be mentioned here. This definition leads to the mean normal stress being equivalent to the negative thermodynamic pressure

$$\sigma_m = -p_{dyn} = \frac{1}{3} \text{tr} \boldsymbol{\sigma} = \frac{\sigma_1 + \sigma_2 + \sigma_3}{3} \quad (2.14)$$

Herewith, the stress tensor may be written as the sum of a spherical tensor

$$\sigma_m \mathbf{I} = -p_{dyn} \mathbf{I} = \begin{pmatrix} -p_{dyn} & 0 & 0 \\ 0 & -p_{dyn} & 0 \\ 0 & 0 & -p_{dyn} \end{pmatrix} \quad (2.15)$$

describing a hydrostatic state of stress and a deviatoric tensor

$$\text{dev} \boldsymbol{\sigma} = \boldsymbol{\sigma} - (-p_{dyn} \mathbf{I}) = \begin{pmatrix} \sigma_1 + p_{dyn} & \tau_{12} & \tau_{13} \\ \tau_{21} & \sigma_2 + p_{dyn} & \tau_{23} \\ \tau_{31} & \tau_{32} & \sigma_3 + p_{dyn} \end{pmatrix} \quad (2.16)$$

where \mathbf{I} denotes the identity tensor. (2.16) may be redefined as the viscous stress tensor

$$\boldsymbol{\tau} = \begin{pmatrix} \tau_{11} & \tau_{12} & \tau_{13} \\ \tau_{21} & \tau_{22} & \tau_{23} \\ \tau_{31} & \tau_{32} & \tau_{33} \end{pmatrix} \quad (2.17)$$

with the diagonal components $\tau_{ii} = \sigma_i + p_{dyn}$.

2.4 Constitutive equation

In order to close the 'gap' still being open between kinematics and kinetics, a constitutive equation has to be introduced. As aforementioned, the stress is given by the sum of a purely hydrostatic state of stress represented by the thermodynamic pressure p_{dyn} and the viscous stress tensor in accordance with

$$\boldsymbol{\sigma} = -p_{dyn} \mathbf{I} + \boldsymbol{\tau} \quad (2.18)$$

George Gabriel Stokes (1819-1903) assumed the viscous stress to be a function of the rate-of-velocity tensor, i.e.

$$\boldsymbol{\tau} = \mathcal{F}(\boldsymbol{\varepsilon}(\mathbf{u})) \quad (2.19)$$

If this function \mathcal{F} is linear, the fluid is called a Newtonian fluid (Isaac Newton (1643-1727)), which this work is focussed on. With the additional assumption of isotropy for Newtonian fluids, the general functional connection between the viscous stress tensor and the rate-of-velocity tensor reads

$$\boldsymbol{\tau} = \lambda(\text{tr} \boldsymbol{\varepsilon}) \mathbf{I} + 2\mu \boldsymbol{\varepsilon} \quad (2.20)$$

with the material constants λ and μ . By introducing the so-called Stokes condition assuming the bulk viscosity to be zero subject to

$$\lambda + \frac{2}{3}\mu = 0 \quad (2.21)$$

the final form of the relation between the stress tensor and the rate-of-velocity tensor reads

$$\boldsymbol{\sigma} = -p_{dyn}\mathbf{I} - \frac{2}{3}\mu(tr\boldsymbol{\epsilon})\mathbf{I} + 2\mu\boldsymbol{\epsilon} \quad (2.22)$$

The only remaining material constant is the dynamic viscosity μ with a dimension of stress multiplied by time. For elaboration of the underlying concepts yielding (2.20) and (2.21), it is referred to the literature named within the introduction of this chapter as well as references therein.

In historical view, it has to be remarked that the constitutive equation in the 3-dimensional case was obtained from molecular models by Claude Louis Marie Henri Navier (1785-1836) in 1821 and by Siméon Denis Poisson (1781-1840) in general in 1831. The continuum theory is due to Adhémar Jean Claude Barré de St. Venant (1797-1886) in 1843 and Stokes in 1845. See also Malvern (1969) for this historical perspective.

2.5 Integral and differential formulation of conservation principles

In this section, the principle of conservation of mass leading to the continuity equation and the principle of conservation of momentum resulting in the momentum equation will be introduced. Finally, the principle of conservation of a scalar quantity is described paving the way for the model problem of a convection-diffusion-reaction equation which will be used throughout this work. This will all be done in integral form yielding a global principle which will then be transformed into a differential equation providing us with a local principle valid at every point of the continuous medium. The result of the principle of moment of momentum has already been established in section 2.3 stating that the Cauchy stress tensor $\boldsymbol{\sigma}$ is symmetric. The formulation of these conservation principles together with the assumption of incompressible flow lead to the set of incompressible Navier-Stokes equations which will both be introduced in the next section. The principle of conservation of energy is not an essential part of the set of incompressible Navier-Stokes equations. This principle will not be dealt with explicitly thus. At the beginning, two important theorems have to be established which will be used in the subsequent derivations.

2.5.1 Gauss' theorem and Reynolds transport theorem

First of all, the theorem named after Johann Carl Friedrich Gauss (1777-1855), also termed divergence theorem, states that the integral of the outer normal component of a vector over a closed surface is equal to the integral of the divergence of the vector over the volume bounded by this closed surface. This reads exemplary for any vector function $\mathbf{v}(\mathbf{x}, t)$

$$\int_S \mathbf{n} \cdot \mathbf{v}(\mathbf{x}, t) dS = \int_V \nabla \cdot \mathbf{v}(\mathbf{x}, t) dV \quad (2.23)$$

with the already introduced outward normal vector \mathbf{n} of the surface S .

Any scalar, vector or tensor function $\mathbf{F}(\mathbf{x}, t)$ may be chosen to be the subject of the explanation of the transport theorem introduced by Osborne Reynolds. The theorem predicates that the rate of change of the amount of $\mathbf{F}(\mathbf{x}, t)$ possessed by the material instantaneously inside a control surface S is equal to the rate of change of the total amount of $\mathbf{F}(\mathbf{x}, t)$ inside S plus the net rate of outward flux of $\mathbf{F}(\mathbf{x}, t)$ due to the mass transport with velocity \mathbf{u} through S . This reads

$$\frac{D}{Dt} \int_V \mathbf{F}(\mathbf{x}, t) dV = \int_V \frac{\partial}{\partial t} \mathbf{F}(\mathbf{x}, t) dV + \int_S \mathbf{F}(\mathbf{x}, t)(\mathbf{n} \cdot \mathbf{u}) dS \quad (2.24)$$

2.5.2 Conservation of mass

The principle of conservation of mass declares that the mass contained in a volume V does not change with time, i.e.

$$\frac{Dm}{Dt} = \frac{D}{Dt} \int_V \rho(\mathbf{x}, t) dV = 0 \quad (2.25)$$

with the density $\rho(\mathbf{x}, t)$ of the continuum. Replacing the right hand side according to the Reynolds transport theorem (2.24) for the scalar function $\rho(\mathbf{x}, t)$ results in

$$\int_V \frac{\partial \rho}{\partial t} + \int_S \rho(\mathbf{n} \cdot \mathbf{u}) dS = 0 \quad (2.26)$$

With the help of Gauss' theorem (2.23), the integral form of the principle

$$\int_V \left[\frac{\partial \rho}{\partial t} + \nabla \cdot (\rho \mathbf{u}) \right] dV = 0 \quad (2.27)$$

is obtained. Since (2.27) must be valid for any V , the differential form of the principle of conservation of mass is given by

$$\frac{\partial \rho}{\partial t} + \nabla \cdot (\rho \mathbf{u}) = 0 \quad (2.28)$$

which could have also been derived by assuming that the total mass $dm = \rho dV$ of an infinitesimal volume dV remains constant throughout time.

2.5.3 Conservation of momentum

Newton's laws of motion provide us with the principle that the material rate of change of linear momentum of any fixed part of material is equal to the resultant of applied forces on this part. With the already introduced types of forces, namely body and surface forces, this principle is stated as

$$\frac{D}{Dt} \int_V (\rho \mathbf{u}) dV = \int_S \mathbf{t} dS + \int_V \rho \mathbf{f} dV \quad (2.29)$$

with the material rate of change of linear momentum on the left hand side. Introducing Reynolds transport theorem (2.24) for the vector function $(\rho \mathbf{u})(\mathbf{x}, t)$, i.e. density times velocity, this results in

$$\int_V \frac{\partial (\rho \mathbf{u})}{\partial t} dV + \int_S (\rho \mathbf{u})(\mathbf{n} \cdot \mathbf{u}) dS = \int_S \mathbf{t} dS + \int_V \rho \mathbf{f} dV \quad (2.30)$$

Applying Gauss' theorem (2.23) to the left and right hand side of (2.30) yields

$$\int_V \left[\frac{\partial(\rho \mathbf{u})}{\partial t} + \nabla \cdot ((\rho \mathbf{u}) \otimes \mathbf{u}) \right] dV = \int_V \nabla \cdot \boldsymbol{\sigma} dV + \int_V \rho \mathbf{f} dV \quad (2.31)$$

where the transformation (2.11) has been exploited and \otimes designates a dyadic product. Since (2.31) must be valid for any V , the differential form of the principle of conservation of momentum is given by

$$\frac{\partial(\rho \mathbf{u})}{\partial t} + \nabla \cdot ((\rho \mathbf{u}) \otimes \mathbf{u}) = \nabla \cdot \boldsymbol{\sigma} + \rho \mathbf{f} \quad (2.32)$$

Equation (2.32) is called Cauchy's equation of motion and could have also been derived by satisfying Newton's laws of motion for each point of the continuous medium. An alternative formulation may subsume the Cauchy stress tensor on the right hand side and the convective term, which can also be interpreted as a convective 'stress', on the left hand side of (2.32) yielding

$$\frac{\partial(\rho \mathbf{u})}{\partial t} = \nabla \cdot \boldsymbol{\sigma}_{tot} + \rho \mathbf{f} \quad (2.33)$$

where the 'total stress' is defined to be

$$\boldsymbol{\sigma}_{tot} = - ((\rho \mathbf{u}) \otimes \mathbf{u}) + \boldsymbol{\sigma} \quad (2.34)$$

The differentiation of (2.32) and (2.33) will become crucial for the later introduction of appropriate boundary conditions. Using the differential form of the principle of conservation of mass (2.28), equation (2.32) may be simplified as follows:

$$\rho \left(\frac{\partial \mathbf{u}}{\partial t} + \mathbf{u} \cdot \nabla \mathbf{u} \right) = \nabla \cdot \boldsymbol{\sigma} + \rho \mathbf{f} \quad (2.35)$$

Both forms of the convective term, i.e. the one in (2.32) as well as the one in (2.35), will be investigated in section 2.6.3.

2.5.4 Conservation of a scalar quantity

In view of a convection-diffusion-reaction equation to be introduced as a model problem for the Navier-Stokes equations, it is required to discuss the conservation of a scalar quantity ϕ . This quantity may be specified, for instance, by a temperature which would then be the subject of the following considerations. Analog to the principle of conservation of momentum, a balance for a volume V according to

$$\frac{D}{Dt} \int_V (\rho \phi) dV = \int_S \mathbf{t}_\phi dS + \int_V \rho f_\phi dV \quad (2.36)$$

is established. Applying the Reynolds transport theorem (2.24) transforms (2.36) into

$$\int_V \frac{\partial(\rho \phi)}{\partial t} dV + \int_S (\rho \phi)(\mathbf{n} \cdot \mathbf{a}) dS = \int_S \mathbf{t}_\phi dS + \int_V \rho f_\phi dV \quad (2.37)$$

where \mathbf{a} denotes an independent convective velocity field. In combination with the Navier-Stokes equations, \mathbf{a} may be replaced by the velocity field \mathbf{u} . Fourier's law for heat diffusion is introduced in order to obtain a specification for \mathbf{t}_ϕ as

$$\mathbf{t}_\phi = \mathbf{n} \cdot \kappa_{dyn} \nabla \phi \quad (2.38)$$

where κ_{dyn} denotes the diffusivity for the quantity ϕ . Using Gauss' theorem (2.23) in (2.37) along with (2.38) results in

$$\int_V \left[\frac{\partial \phi}{\partial t} + \nabla \cdot (\mathbf{a}\phi) \right] dV = \int_V \nabla \cdot (\kappa \nabla \phi) dV + \int_V f_\phi dV \quad (2.39)$$

where the diffusivity $\kappa = \kappa_{dyn}/\rho$ is scaled by the density. In case ϕ is indeed a temperature, κ represents the thermal diffusivity. With the same reasoning as for the momentum and mass conservation the differential form may be obtained as

$$\frac{\partial \phi}{\partial t} + \nabla \cdot (\mathbf{a}\phi) - \nabla \cdot (\kappa \nabla \phi) = f_\phi \quad (2.40)$$

where f_ϕ is a source or sink term, respectively. (2.40) represents a convection-diffusion equation for the scalar quantity ϕ .

2.6 The incompressible Navier-Stokes equations

2.6.1 Compressible vs. incompressible flow: basic formulation of the equations

It has to be emphasized in the beginning of this section that the property of incompressibility is **not** a feature of the fluid. It is rather a feature of the flow performed by the fluid. If the two representatives of fluids, liquids and gases are considered, it can be said that most of the time liquids, in particular its main representative water, may be treated as performing an incompressible flow. This is due to the fact that the changes of density are mostly negligible. Even though gases are mostly being viewed as performing compressible flows, sometimes they can also be treated as incompressible. Roughly speaking, this is possible up to a Mach number of 0.3 (see Ferziger and Peric (1999)). This number, named after the physicist Ernst Mach (1838-1916), relates the characteristic velocity u of the flow to the velocity of sound c , i.e.

$$Ma = \frac{u}{c} \quad (2.41)$$

What does $Ma = 0.3$ actually mean? Assuming c to be approximately 340 m/s in air, it means that the conditions of incompressibility can be maintained up to a fluid velocity of about 100 m/s which corresponds to 360 km/h or 220 miles/h. Using an automobile, for example, this velocity is hardly within reach. After all, the scope of incompressible flow situations is pretty large and, thus, the validity of the following elaborations.

The incompressibility assumption, meaning the neglect of density changes, simplifies the resulting equations of sections 2.4 and 2.5. The principle of conservation of mass in differential form (2.28) then reads

$$\nabla \cdot \mathbf{u} = 0 \quad (2.42)$$

The principle of conservation of momentum (2.32) may be simplified to

$$\frac{\partial \mathbf{u}}{\partial t} + \nabla \cdot (\mathbf{u} \otimes \mathbf{u}) = \frac{1}{\rho} \nabla \cdot \boldsymbol{\sigma} + \mathbf{f} \quad (2.43)$$

By inspecting (2.5), one sees that (2.42) corresponds to the trace of the rate-of-velocity tensor $\boldsymbol{\varepsilon}(\mathbf{u})$. Therefore, the constitutive equation (2.22) transfers to

$$\boldsymbol{\sigma} = -p_{dyn}\mathbf{I} + 2\mu\boldsymbol{\varepsilon}(\mathbf{u}) \quad (2.44)$$

where it has to be emphasized that $\boldsymbol{\varepsilon}(\mathbf{u})$ is a traceless tensor. This implies the special role of the pressure as the mean normal compressive stress according to (2.14). Without prescribed boundary conditions for the pressure it is indeterminate in the sense that it can only be determined up to a constant. Combining (2.42)-(2.44) yields the set of incompressible Navier–Stokes equations to be solved in the domain Ω during the time period T subject to

$$\nabla \cdot \mathbf{u} = 0 \quad \text{in } \Omega \times (0, T) \quad (2.45)$$

$$\frac{\partial \mathbf{u}}{\partial t} + \nabla \cdot (\mathbf{u} \otimes \mathbf{u}) + \nabla p - 2\nu \nabla \boldsymbol{\varepsilon}(\mathbf{u}) = \mathbf{f} \quad \text{in } \Omega \times (0, T) \quad (2.46)$$

where $p = p_{dyn}/\rho$ denotes the kinematic pressure. $\nu = \mu/\rho$ designates the kinematic viscosity with a dimension of squared length divide by time, which is assumed to be constant.

The set (2.45)-(2.46) is constituted by a system of nonlinear coupled mixed hyperbolic-parabolic partial differential equations for the vector quantity \mathbf{u} and the scalar quantity p . For a classification of partial differential equations consult e.g. Bronstein and Semendjajew (1996) or Strauss (1992). Existence and uniqueness of solutions for the Navier–Stokes equations are discussed, for instance, by Temam and co-workers in Temam (1979), Marion and Temam (1998) and Dubois et al. (1999). For this initial-boundary value problem (IBVP), initial as well as boundary conditions have to be specified before proceeding towards a solution of (2.45)-(2.46).

2.6.2 Initial and boundary conditions

As an initial condition, a vector field for the velocity \mathbf{u}_0 at time $t = 0$ may be prescribed on the domain Ω as

$$\mathbf{u} = \mathbf{u}_0 \quad \text{in } \Omega \times \{0\} \quad (2.47)$$

which certainly has to fulfill the continuity equation, i.e. $\nabla \cdot \mathbf{u}_0 = 0$, in order to obtain a well-posed problem.

Furthermore, the well-posedness of the IBVP depends on the boundary conditions imposed on the boundary $\Gamma = \partial\Omega$ of the domain. Γ is usually separated into a Dirichlet boundary Γ_g and a Neumann boundary Γ_h with the conditions $\Gamma = \Gamma_g \cup \Gamma_h$ and $\Gamma_g \cap \Gamma_h = \emptyset$. A Dirichlet (or essential) boundary condition in the form of a prescribed velocity \mathbf{g} reads

$$\mathbf{u} = \mathbf{g} \quad \text{on } \Gamma_g \times (0, T) \quad (2.48)$$

whereas a Neumann (or natural) boundary condition \mathbf{h} usually prescribes the normal component of the stress on the boundary, already introduced as the traction \mathbf{t} , as

$$\mathbf{t} = \mathbf{n} \cdot \boldsymbol{\sigma} = \mathbf{n} \cdot \left(-p_{dyn}\mathbf{I} + 2\mu\boldsymbol{\varepsilon}(\mathbf{u}) \right) = \mathbf{h} \quad \text{on } \Gamma_h \times (0, T) \quad (2.49)$$

associated with the usual formulations (2.32) or (2.35), respectively. According to the alternative formulation (2.33) with the total stress in (2.34), the total momentum flux consisting of the convective flux and the traction may be prescribed as

$$\mathbf{n} \cdot \boldsymbol{\sigma}_{tot} = \mathbf{n} \cdot (-\rho \mathbf{u} \otimes \mathbf{u} + \boldsymbol{\sigma}) = \mathbf{n} \cdot (-\rho \mathbf{u} \otimes \mathbf{u} - p_{dyn} \mathbf{I} + 2\mu \boldsymbol{\varepsilon}(\mathbf{u})) = \mathbf{h}_{tot} \quad (2.50)$$

Transforming the integral of the continuity equation (2.45) over the domain Ω in the sense of Gauss' theorem (2.23) yields a constraint for an IBVP with a pure Dirichlet boundary $\Gamma = \Gamma_g$ subject to

$$\int_{\Omega} \nabla \cdot \mathbf{u} \, d\Omega = \int_{\Gamma} \mathbf{n} \cdot \mathbf{u} \, d\Gamma = \int_{\Gamma_g} \mathbf{n} \cdot \mathbf{g} \, d\Gamma = 0 \quad \text{on } \Gamma = \Gamma_g \times (0, T) \quad (2.51)$$

Simply spoken, (2.51) states that everything which flows into the domain has to flow out of the domain somewhere sometime. For this purpose, the inflow part

$$\Gamma_- = \{x \in \Gamma \mid \mathbf{u}(x) \cdot \mathbf{n}(x) < 0\} \quad (2.52)$$

and the respective outflow part

$$\Gamma_+ = \Gamma \setminus \Gamma_- \quad (2.53)$$

of the boundary may be distinguished depending on the velocity field \mathbf{u} which is here part of the solution. The topic of mathematically permissible boundary conditions and, moreover, 'good' boundary conditions providing us with a well-posed IBVP is exhaustively dealt with in Gresho (1991a), Gresho (1991b) and Gresho (1992) as well as in section 3.8 of the book by Gresho and Sani (1998).

The mostly used practical boundary conditions are:

- **no-slip boundary condition:**

This boundary condition describes the adherence of fluid particles at, for example, a solid wall. Therefore, the fluid immediately at the wall has to move with the wall velocity which may be specified as \mathbf{g} in (2.48). In the usual case of a non-moving wall this comes down to

$$\mathbf{u} = \mathbf{0} \quad \text{on } \Gamma_g \times (0, T) \quad (2.54)$$

The no-slip condition prescribes the tangential and the normal component of the velocity at the wall.

- **slip boundary condition:**

In contrast to the former boundary condition, the slip boundary condition merely prescribes the normal component of the velocity at the wall

$$\mathbf{n} \cdot \mathbf{u} = \mathbf{n} \cdot \mathbf{g} \quad \text{on } \Gamma_g \times (0, T) \quad (2.55)$$

incorporating the special case $\mathbf{g} = \mathbf{0}$. A non-zero boundary condition of this type may be realized, for instance, by blowing or suction through a permeable wall. According to (2.55), the fluid particle is allowed to slip at the wall, i.e. at a solid wall, for example, the tangential component of the velocity is not required to be zero. A special case of boundary conditions lying in between slip and no-slip boundary conditions are slip boundary conditions with linear friction and no penetration or slip boundary conditions with linear friction and penetration with resistance. These special boundary conditions have been developed in Galdi and Layton (2000) and are further used e.g. in John (2002a) and John (2002b).

- **inflow boundary condition:**
The examples in the course of this work are without exception subject to inflow boundary conditions in the sense of a Dirichlet boundary condition with a prescribed velocity \mathbf{g} at the inflow part of the boundary Γ_- . This means that the inflow boundary is completely covered by the Dirichlet part of the boundary: $\Gamma_- \subseteq \Gamma_g$.
- **outflow boundary condition:**
The topic of outflow boundary conditions is definitely a challenging one and actually far from being completely resolved. For elaboration of this, it is referred to Gresho (1992), Heywood et al. (1996) and section 3.8f of Gresho and Sani (1998). The frequently (not always) successful simple version of a 'do nothing' boundary condition should just be mentioned here. Lack of successful numerical simulation with this type of boundary condition may be traced back to a disturbance in form of a wrongly implied Neumann boundary condition by the numerical method.
- **pressure boundary condition:**
The special role of the pressure resulting in the fact that it can only be determined up to a constant has already been identified. Pressure boundary conditions fixing this constant merely appear as a part of the Neumann boundary condition in (2.49) or (2.50), respectively. If $\Gamma = \Gamma_g$, i.e. there is no Neumann boundary, two practical ways of fixing the constant consist in either prescribing a mean value with respect to the complete domain reading

$$\int_{\Omega} p \, d\Omega = 0 \quad (2.56)$$

or prescribing discrete value(s) of the pressure at individual node(s) of a discretization. The last procedure will be the foremost choice in this work.

- **periodic boundary condition:**
This boundary condition does not have a physical meaning. It may rather be introduced for computational reasons with the objective of reducing the extent of the computational domain. This becomes crucial in numerical simulations of turbulent flows in order to reduce the enormous effort of the computation. The assumption of periodic conditions determines the simulation to be one period of an infinite number of such realizations in the periodic direction(s).

2.6.3 Alternative formulations

Alternative formulations being able to replace the Navier-Stokes equations in the form (2.45)-(2.46) partly or completely will be discussed now. This means a replacement of parts of the momentum equation (2.46), the complete continuity equation (2.45) or the complete set of Navier-Stokes equations. Before starting with a partial replacement of the momentum equation, a dissection has to be performed. Using differential operators, (2.45)-(2.46) may be written as

$$\mathcal{L}_C[\mathbf{u}] = \mathcal{L}_{cont}\mathbf{u} = 0 \quad (2.57)$$

$$\mathcal{L}_M[\mathbf{u}, p] = \mathcal{L}_t\mathbf{u} + \mathcal{L}_{conv}(\mathbf{u})\mathbf{u} + \mathcal{L}_{pres}p + \mathcal{L}_{visc}\mathbf{u} = \mathbf{f} \quad (2.58)$$

The continuity equation is represented by the operator

$$\mathcal{L}_{cont}\mathbf{u} = \nabla \cdot \mathbf{u} \quad (2.59)$$

The momentum equation consists of 4 operators, namely the differential operator in time

$$\mathcal{L}_t\mathbf{u} = \frac{\partial \mathbf{u}}{\partial t} \quad (2.60)$$

the nonlinear convective operator

$$\mathcal{L}_{conv}(\mathbf{u})\mathbf{u} = \nabla \cdot (\mathbf{u} \otimes \mathbf{u}) \quad (2.61)$$

the operator acting on the pressure

$$\mathcal{L}_{pres}p = \nabla p \quad (2.62)$$

and the viscous operator

$$\mathcal{L}_{visc}\mathbf{u} = -2\nu\nabla \cdot \boldsymbol{\varepsilon}(\mathbf{u}) \quad (2.63)$$

The time-dependent operator and the operator acting on the pressure cannot be altered. However, variations of the convective and the viscous operator are possible.

Alternative formulations of the viscous term

According to the notation in Gresho and Sani (1998) the viscous term may be expanded as

$$-2\nu\nabla \cdot \boldsymbol{\varepsilon}(\mathbf{u}) = -\nu\Delta\mathbf{u} - \gamma[\nu\nabla(\nabla \cdot \mathbf{u})] \quad (2.64)$$

introducing the factor γ . Setting $\gamma = 1$ recovers the stress-divergence form on the left hand side and ensures (2.64) to be a valid equation. Setting $\gamma = 0$ yields the simpler conventional form $-\nu\Delta\mathbf{u}$. As can be seen by inspecting the dropped out second part of (2.64), this is justified in the continuous case by the continuity equation (2.45) and yields an equivalent result. However, in the discrete case this may not be true and, thus, both the stress-divergence form and the conventional form of the viscous term governed by the factor γ have to be kept in mind. Regarding the boundary conditions, it has to be respected that using the conventional form of the viscous term alters the Neumann boundary condition (2.49) to

$$\mathbf{n} \cdot \left(-p_{dyn}\mathbf{I} + \mu(\nabla\mathbf{u}) \right) = \mathbf{h} \quad (2.65)$$

and (2.50) to

$$\mathbf{n} \cdot \left(-\rho\mathbf{u} \otimes \mathbf{u} - p_{dyn}\mathbf{I} + \mu(\nabla\mathbf{u}) \right) = \mathbf{h}_{tot} \quad (2.66)$$

respectively. (2.65) may be described as a 'pseudo-traction' bearing severe difficulties concerning their physical interpretation. In passing, further forms of the viscous term, the div-curl form and the curl form, both playing no role in the following, are noted.

Alternative formulations of the convective term

The convective term may be expanded as

$$\nabla \cdot (\mathbf{u} \otimes \mathbf{u}) = \mathbf{u} \cdot \nabla\mathbf{u} + \beta\mathbf{u}(\nabla \cdot \mathbf{u}) \quad (2.67)$$

with the introduction of $\beta = 1$ for recovering the divergence form on the left hand side of (2.67) and ensuring it to be a valid equation. Setting $\beta = 0$ provides us with the simpler conventional form $\mathbf{u} \cdot \nabla \mathbf{u}$. As for the conventional form of the viscous term, there is no difference in the continuous case due to the continuity equation. Differences may, however, appear in the discrete case. Besides these two values of β , the important case of $\beta = 1/2$, called skew-symmetric form, guaranteeing conservation of kinetic energy in the discrete case has to be considered, confer e.g. Temam (1979) as well as Quarteroni and Valli (1994). Moin (2002) emphasizes the necessity to conserve energy in discrete methods for large eddy simulation of turbulent flows. The simultaneous conservation of momentum and energy in the discrete case is, in general, not possible. In order to guarantee stability, conservation of energy is actually more important than conservation of momentum. In passing again, further possibilities, namely the rotational form and a symmetric form by Gellert and Harbord (1987) as well as Harbord and Gellert (1990) both playing no role in the following, are noted.

The pressure Poisson equation

Equal replacement of the continuity equation (2.45) may be executed via a pressure Poisson equation. The pressure Poisson equation is obtained by applying the divergence operator to the momentum equation as a whole. For (2.46), this reads

$$\Delta p = \nabla \cdot \left[-\frac{\partial \mathbf{u}}{\partial t} - \nabla \cdot (\mathbf{u} \otimes \mathbf{u}) + 2\nu \nabla \cdot \boldsymbol{\varepsilon}(\mathbf{u}) + \mathbf{f} \right] \quad \text{in } \Omega \times (0, T) \quad (2.68)$$

In order to obtain a useful 'working version' of the pressure Poisson equation, Gresho and Sani (1998) suggest at least to neglect the time-dependent term by invoking the continuity condition. Using the conventional form of the convective as well as the viscous term, i.e. $\beta = \gamma = 0$, leaves us with the so-called consistent pressure Poisson equation reading

$$\Delta p = \nabla \cdot [-\mathbf{u} \cdot \nabla \mathbf{u} + \nu \Delta \mathbf{u} + \mathbf{f}] \quad \text{in } \Omega \times (0, T) \quad (2.69)$$

which 'works best' according to Gresho and Sani (1998). The introduction of the pressure Poisson equation bears two important features of the incompressible Navier-Stokes equations. Firstly, the pressure is governed by an elliptic equation enforcing an immediate transfer of a pressure signal over the complete domain Ω . This is based on an infinitely high velocity of sound in this medium. Secondly, in the basic form of the Navier-Stokes equations (2.45)-(2.46) the pressure equation is 'camouflaged', i.e. the pressure is indeed governed by the continuity equation, although it does not appear within this equation. For brevity reasons, the answer to the question of boundary conditions for the pressure Poisson equation is omitted and it is rather referred to e.g. Gresho and Sani (1998) for a discussion of this.

Streamfunction-vorticity formulation

Equally replacing the momentum equation is possible by referring to the vorticity defined in (2.8). Applying the curl-operator to the momentum equation (using the conventional form of the convective and the viscous term and no body force here) yields after some analysis

$$\frac{\partial \boldsymbol{\omega}}{\partial t} + \mathbf{u} \cdot \nabla \boldsymbol{\omega} - \boldsymbol{\omega} \cdot \nabla \mathbf{u} - \nu \Delta \boldsymbol{\omega} = \mathbf{0} \quad \text{in } \Omega \times (0, T) \quad (2.70)$$

constituting together with the continuity equation (2.45) and the definition of the vorticity (2.8) an equal representation of the Navier-Stokes equations. In the two-dimensional case, (2.70) simplifies to

$$\frac{\partial \omega}{\partial t} + \mathbf{u} \cdot \nabla \omega - \nu \Delta \omega = \mathbf{0} \quad \text{in } \Omega \times (0, T) \quad (2.71)$$

with ω being a scalar. With the streamfunction ψ defined as

$$u_1 = \frac{\partial \psi}{\partial x_2}, \quad u_2 = \frac{\partial \psi}{\partial x_1} \quad (2.72)$$

a complete replacement of the set of Navier-Stokes equations by adding to (2.71)-(2.72) the Poisson equation

$$\Delta \psi = -\omega \quad (2.73)$$

is achieved. This completely equivalent set (2.71)-(2.73) incorporating not any one of the original equations is called streamfunction-vorticity formulation and it is, however, practically possible only in the two-dimensional case. The much more complicated three-dimensional analogon can be found e.g. in Gunzburger (1989). The major advantage of the streamfunction-vorticity formulation may be attributed to the 'loss' of the continuity equation. For this, one has to pay with physically more difficult definitions of the boundary conditions for the streamfunction and the vorticity. In view of problems of fluid-structure-interaction, a long-term goal of the efforts in this work, these difficulties become crucial. Therefore, this last alternative formulation partially leaving the ground of the primitive variables velocity \mathbf{u} and pressure p will be neglected below.

2.6.4 The Reynolds number rules

The most important non-dimensional number characterising a specific flow situation bears the name of Osborne Reynolds (1842-1912). It quantifies the relation between the convective term and the viscous term in the set of Navier-Stokes equations and is defined as

$$\text{Re} = \frac{UL}{\nu} \quad (2.74)$$

where U is a measure of the velocity, L a characteristic length scale and ν the kinematic viscosity of the respective flow. The associated 'similarity rule' states that two flows described by the same Reynolds number will show similar flow features, even if the individual constituents of the Reynolds number definition are found to be in quite different ranges. Some examples for 'real-life' Reynolds numbers may be gathered from Table 2.1.

Two crucial features of fluid flows strongly depend on the value of the Reynolds number. On the one hand, a critical Reynolds number (or a critical Reynolds number range) distinguishes the laminar flow regime from the turbulent flow regime. This distinction is a crucial aspect of this work and will be elaborated in chapter 4. On the other hand, one may observe an asymptotic behaviour of the flow for extreme Reynolds numbers in the sense of $\text{Re} \rightarrow 0$ and $\text{Re} \rightarrow \infty$.

Re $\rightarrow 0$: Stokes equations

A preponderant viscous term with respect to the convective term forces the Reynolds number to decrease. As may be observed by inspecting (2.74), this may be associated with low velocities, small length scales and/or large viscosities. It is usually termed 'creeping flow'. For $\text{Re} \rightarrow 0$, the Navier-Stokes equations (2.45)-(2.46) pass over to the Stokes equations by neglecting the convective term in order to yield the IBVP

$$\frac{\partial \mathbf{u}}{\partial t} + \nabla p - 2\nu \nabla \cdot \boldsymbol{\varepsilon}(\mathbf{u}) = \mathbf{f} \quad \text{in } \Omega \times (0, T) \quad (2.75)$$

in combination with (2.45) prescribing the same kind of initial and boundary conditions as in the case of the Navier-Stokes equations.

Description	Re
Spermatozoon (L=0.07 mm) swimming at max. speed	6×10^{-3}
Water droplet (D=0.07 mm) falling through air	6.4×10^{-1}
Blood flow (U=13.5 cm/s) in a circular artery (r=0.2 cm)	1.35×10^2
Wind blowing (10 m/s) over telegraph wires	1×10^3
Cricket or baseball propelled at 35 m/s	2×10^5
Car (L=4.5 m) at U=15 m/s (i.e. 54 km/h)	4×10^6
Shark (L=1.5 m) swimming at max. speed	8×10^6
Large jet transport aircraft (747) at cruise altitude	7×10^7
Ocean liner (Q.E. II, L=324 m) at U=15 m/s	4.5×10^9
Planetary boundary layer (L=1000 km, U=20 m/s)	18×10^{12}

Table 2.1 Some 'typical' Reynolds numbers (Fletcher (1991) and Wall (1999))

Re $\rightarrow \infty$: Euler equations and boundary layer theory

The more interesting case in the course of this work and in practice appears to be in the range of high Reynolds numbers. For Re $\rightarrow \infty$, another asymptotic behaviour may be observed. Here, the convective term shows a substantial preponderance with regard to the viscous term. For the 'final' case of $\nu = 0$, the set of Euler equations consisting of (2.45) and

$$\frac{\partial \mathbf{u}}{\partial t} + \nabla \cdot (\mathbf{u} \otimes \mathbf{u}) + \nabla p = \mathbf{f} \quad \text{in } \Omega \times (0, T) \quad (2.76)$$

is encountered describing a system of nonlinear first-order partial differential equations which leads to necessary deviations from the boundary conditions formulated for the Navier-Stokes equations. For instance, the no-slip boundary condition at solid walls is no longer capable of being fulfilled. At this point, the boundary layer theory developed by Ludwig Prandtl (1875-1953) which initially appeared before the public in his lecture in the year 1904 (Prandtl (1904)) comes into play. The theory is exhaustively described in the book of Schlichting (1979). Based on the Euler equations, a flow governed by a finite but very high Reynolds number may be dealt with as a singular disturbance of the Euler equations. The singular disturbance is exclusively related to the necessary fulfillment of the boundary condition at, for example, a solid wall. The finite velocity value in the vicinity of the wall resulting from a solution of Euler's equations is transferred to a vanishing value directly at the wall within a boundary layer by this procedure. The higher the Reynolds number the smaller is the thickness of the boundary layer.

Practically, the solution procedure of a wall-bounded flow goes as follows: In the overwhelming inner part of the domain the solution may be found utilizing Euler's equations (or even the Laplace equation for the scalar velocity potential in the case of irrotational flow). The remaining, usually very thin, boundary layer has to be resolved by respecting the finite viscosity. However, the Navier-Stokes equations can be simplified substantially due to some reasonable assumptions valid within the boundary layer. As a result, one encounters the so-called boundary equations going back to Prandtl's work. As an important last fact with regard to the next chapter, it has to be emphasized that the boundary layer concept describes laminar as well as turbulent boundary layers. Thus, it cannot be stated that every boundary layer has to be either laminar or turbulent. Frequently, an initially laminar boundary layer undergoes a transition to a turbulent boundary layer during its course.

2.7 A model problem: scalar convection-diffusion-reaction equation

2.7.1 Problem formulation

In contrast to the set of Navier-Stokes equations (2.45)-(2.46), one merely has to deal with **one** scalar equation here. However, this single equation may act as a model problem for the Navier-Stokes equations on the one hand and will be an essential part of the later described multiscale strategy on the other hand. By splitting the right hand side of (2.40) as

$$f_\phi = f - \sigma\phi \quad (2.77)$$

a reactive term specified by the reaction coefficient σ is introduced. σ is assumed to be positive and constant. Thus, the case of productive terms (negative σ) is neglected throughout this work. The conservation form of the convection-diffusion-reaction equation then reads

$$\frac{\partial\phi}{\partial t} + \nabla \cdot (\mathbf{a}\phi) - \nabla \cdot (\kappa\nabla\phi) + \sigma\phi = f \quad \text{in } \Omega \times (0, T) \quad (2.78)$$

Assuming a constant diffusivity κ throughout the domain and a divergence-free velocity field subject to

$$\nabla \cdot \mathbf{a} = 0 \quad (2.79)$$

the conservation form switches over to the convective form

$$\frac{\partial\phi}{\partial t} + \mathbf{a} \cdot \nabla\phi - \kappa\Delta\phi + \sigma\phi = f \quad \text{in } \Omega \times (0, T) \quad (2.80)$$

which will be used later on. In case the velocity field is not divergence-free, the additional part of the convective term may be incorporated into the reactive term by defining a modified reaction coefficient

$$\sigma_{\text{mod}} = \sigma + \nabla \cdot \mathbf{a} \quad (2.81)$$

Analog to the Navier-Stokes equations, a dissection may be performed using differential operators. The complete differential operator is put together by a convective, a diffusive and a reactive as well as a time-dependent operator subject to

$$\mathcal{L}_{cdr,t}\phi = \frac{\partial\phi}{\partial t} + \mathcal{L}_{cdr}\phi = \frac{\partial\phi}{\partial t} + \mathcal{L}_c\phi + \mathcal{L}_d\phi + \mathcal{L}_r\phi \quad (2.82)$$

The operators may easily be identified by comparing (2.80) and (2.82). The respective adjoint differential operator of the stationary problem reads

$$\mathcal{L}_{cdr}^* \phi = \mathcal{L}_c^* \phi + \mathcal{L}_d^* \phi + \mathcal{L}_r^* \phi = -\mathbf{a} \cdot \nabla \phi - \kappa \Delta \phi + \sigma_{(mod)} \phi \quad (2.83)$$

The parentheses in the subscript of $\sigma_{(mod)}$ indicate here and below that either the 'pure' reaction coefficient or the modified reaction coefficient subject to (2.81) may appear in the respective equations.

2.7.2 Initial and boundary conditions

As an initial condition, a scalar field ϕ_0 at $t = 0$ may be prescribed on the domain Ω as

$$\phi = \phi_0 \quad \text{in } \Omega \times \{0\} \quad (2.84)$$

As for the Navier-Stokes equations, the boundary $\Gamma = \partial\Omega$ is usually separated into a Dirichlet boundary Γ_g and a Neumann boundary Γ_h with the conditions $\Gamma = \Gamma_g \cup \Gamma_h$ and $\Gamma_g \cap \Gamma_h = \emptyset$. The Dirichlet boundary condition reads

$$\phi = g \quad \text{on } \Gamma_g \times (0, T) \quad (2.85)$$

with the prescribed scalar g . The Neumann boundary condition for the convective form (2.80) is defined as

$$\mathbf{n} \cdot \kappa \nabla \phi = h \quad \text{on } \Gamma_h \times (0, T) \quad (2.86)$$

with h being prescribed. If the convective flux on the Neumann boundary is also known and required to be specified (e.g. for the conservative form (2.78)), the Neumann boundary condition reads

$$\mathbf{n} \cdot (-\mathbf{a}\phi + \kappa \nabla \phi) = h \quad \text{on } \Gamma_h \times (0, T) \quad (2.87)$$

Furthermore, the inflow part

$$\Gamma_- = \{\mathbf{x} \in \Gamma \mid \mathbf{a}(\mathbf{x}) \cdot \mathbf{n}(\mathbf{x}) < 0\} \quad (2.88)$$

and the respective outflow part

$$\Gamma_+ = \Gamma \setminus \Gamma_- \quad (2.89)$$

of the boundary may be distinguished.

2.7.3 The Peclet number rules

Comparable with the importance of the Reynolds number for the Navier-Stokes equations, a non-dimensional number bearing the name of Eugene Peclet (1793-1857) is defined as

$$Pe = \frac{AL}{\kappa} \quad (2.90)$$

where A is a measure of the convective velocity, L a length scale and κ the kinematic diffusivity. (2.90) quantifies the relation between the convective term and the diffusive term. Usually, one may denote the flow as being convection-dominated for $Pe > 1$ and diffusion-dominated for $Pe < 1$. As in the case of the Navier-Stokes equations, an asymptotic behaviour is observed for

extreme Peclet numbers in the sense of $Pe \rightarrow 0$ and $Pe \rightarrow \infty$. For $Pe \rightarrow 0$, the elliptic character of the equation emerges being very comfortable from the numerical point of view. In contrast to this, the case $Pe \rightarrow \infty$ is extremely challenging for computational purposes, as will be seen later on. Here again, very thin boundary layers have to be dealt with. An analogon of the Euler equations is the hyperbolic limit of the convection-diffusion equation appearing for $\kappa = 0$ as

$$\frac{\partial \phi}{\partial t} + \mathbf{a} \cdot \nabla \phi = f \quad \text{in } \Omega \times (0, T) \quad (2.91)$$

with similar consequences for an admissible formulation of boundary conditions. In an artificial 1-D case, for instance, it is not allowed to prescribe a value of ϕ at the outflow boundary.

For the sake of completeness, the Damköhler number should be mentioned governing quantitatively the relationship of the convective term and the reactive term. It is defined as

$$Da = \frac{\sigma L}{A} \quad (2.92)$$

Finally, the Peclet number and the Damköhler number may be combined multiplicatively in order to get a dimensionless number describing the quantitative relation of the reactive and the diffusive term reading

$$Pe \cdot Da = \frac{\sigma L^2}{\kappa} \quad (2.93)$$

3 Numerical Simulation of Incompressible Flow using a Standard Galerkin Finite Element Method

3.1 Introduction

In this chapter, the Galerkin finite element method in its standard form is introduced as the numerical method of choice for solving the equations of incompressible flow. Strategically, the developments in the course of this chapter will be applied to the scalar convection-diffusion-reaction equation first and, afterwards, transferred to the more challenging vectorial set of Navier-Stokes equations. This twofold procedure is necessary, since both will play a major role in the later to be introduced two- and three-level finite element method. Thus, the description of the variational multiscale method will also be carried out for both types of equations in chapters 6 and 7, respectively.

Starting point and, likewise, core of this chapter is the spatial discretization of the partial differential equations. Hughes (2000) summarized the procedure of spatial discretization schematically in four steps:

$$(S) \Leftrightarrow (W) \approx (G) \Leftrightarrow (M) \tag{3.1}$$

Starting with the strong form (S) of the problem represented by the partial differential equation(s) having been developed in chapter 2 and to be repeated in section 3.2.1, a weak form (W) based on the method of weighted residuals will be derived in section 3.2.2. The only approximation in (3.1) consisting in the introduction of Galerkin finite element functions (G) into the weak form will be presented in section 3.2.3 based on two different function types. The result of the preceding efforts and subject of section 3.2.4 will be the semi-discrete matrix system of algebraic equations (M).

The strategy of semi-discretization in time will be followed allowing to separate the temporal discretization from the spatial discretization. Two different schemes of time integration, a fully implicit one and a semi-implicit one, will be presented. The crucial advantage of the semi-implicit scheme may be ascribed to the fact that it exhibits a linearization of the originally nonlinear set of Navier-Stokes equations implicitly integrated into the time integration scheme. This obviates an additional linearization scheme which is, however, necessary for the fully implicit scheme and will be presented within the respective section 3.3.2 thus. The part devoted to the discretization in time will end up with the final matrix system. It is stopped there and the undoubtedly important topic of solvers for this matrix system will not be discussed. For this, it is referred to special literature on this issue and the literature on the finite element method to be mentioned at the end of this introduction which also partly deals with solution strategies.

This chapter will be concluded by pointing out the two major problems linked with numerical solution attempts using the standard Galerkin finite element method. The first problem, an explicit preponderance of the convective term with respect to the viscous or diffusive term, respectively, may be gathered quantitatively by the respective Reynolds or Peclet number of the flow situation. This problem can definitely occur for both the convection-diffusion-reaction equation and the Navier-Stokes equations. The second problem may merely be encountered in the context

of the Navier–Stokes equations, since it is actually set up by the relationship between the approximations of the velocity and the pressure. The name of this ‘devil’ reads inf-sup-condition. LBB (Ladyzhenskaya–Babuska–Brezzi)- or, shorter, BB-condition are alternative names of the same ‘fate’ which will be the subject of section 3.4.2. Both problems are viewed as a matter of ‘missing’ scales which leads to the assumption that both problems may also be overcome by the strategy of including more scales.

This introduction is concluded by providing the reader with some references. Some classic text books on the finite element method in general are Bathe (1996), Hughes (2000), Szabo and Babuska (1991), as well as Zienkiewicz and Taylor (2000a) aiming more at the engineering point of view and Brenner and Scott (1994), Eriksson et al. (1996), Johnson (1987), as well as Strang and Fix (1973) aiming more at the mathematical point of view. The finite element method for incompressible flow is dealt with in the more engineering-related books of Cuvelier et al. (1986), Donea and Huerta (2003), Gresho and Sani (1998), Löhner (2001), Reddy and Gartling (2001), as well as Zienkiewicz and Taylor (2000b) and the more mathematically oriented books like Girault and Raviart (1986), Gunzburger (1989), as well as Pironneau (1989). The classification separating into mathematical and engineering books carried out here merely relies on a subjective impression of the author concerning the general tendency of the respective book. The frontiers are surely ‘fluid’. The book of Brezzi and Fortin (1991) should be mentioned explicitly, since this is (at least one of) the standard text(s) on mixed methods and the inf-sup-condition related to these methods. Gresho and Sani (1998), for instance, appeal to it as the ‘authority’.

Despite its immense popularity for problems of structural mechanics, the finite element method is far from being the most popular numerical method in fluid mechanics as well. This may, among others, be ascribed to the fact that the finite element method exhibits the feature of so-called ‘best approximation’ for elliptic problems with self-adjoint differential operators mostly found in structural mechanics. In fluid mechanics, non-self-adjoint differential operators usually have to be faced and the ‘best approximation’ is lost thus. Confer e.g. Hughes (2000), section 4.1, for elaboration of this. In the end, this leads to the numerical problems to be described in section 3.4.

More widespread reputation within the field of computational fluid dynamics (CFD) has to be ascribed to the finite difference method and, in particular, the finite volume method described, for example, in Ferziger and Peric (1999), Hirsch (1988), Hirsch (1990), and Wesseling (2001). Especially for turbulent flow applications in relatively simple domains, spectral methods still enjoy an overwhelming prestige. See e.g. Canuto et al. (1988) for elaboration of spectral methods for problems of fluid mechanics. Overcoming the problems of the standard Galerkin finite element, for instance, by way of the variational multiscale method described in this work may pave the way for a growing popularity of the finite element method for problems of CFD, in particular for turbulent flow problems.

3.2 Spatial discretization

3.2.1 Systems of partial differential equations (strong form)

The systems of partial differential equations developed in chapter 2 from continuum mechanical considerations are restated here in compact form for convenience.

Convection-diffusion-reaction equation

The convection-diffusion-reaction problem with a potentially modified reaction coefficient on the space-time domain $\Omega \times (0, T)$ including an open, bounded domain $\Omega \subset \mathbb{R}^d$ ($d = 2, 3$) with sufficiently smooth boundary $\Gamma = \partial\Omega$ is considered, i.e. it is searched for the scalar quantity $\phi : \Omega \times (0, T) \rightarrow \mathbb{R}$ such that

$$\frac{\partial \phi}{\partial t} + \mathbf{a} \cdot \nabla \phi - \kappa \Delta \phi + \sigma_{(\text{mod})} \phi = f \quad \text{in } \Omega \times (0, T) \quad (3.2)$$

with the boundary conditions

$$\phi = g \quad \text{on } \Gamma_g \times (0, T) \quad (3.3)$$

$$\mathbf{n} \cdot \kappa \nabla \phi = h \quad \text{on } \Gamma_h \times (0, T) \quad (3.4)$$

and the initial condition

$$\phi = \phi_0 \quad \text{in } \Omega \times \{0\} \quad (3.5)$$

Navier-Stokes equations

Here, the object of consideration is the set of instationary incompressible Navier-Stokes equations phrased in the primitive variables velocity \mathbf{u} and kinematic pressure p , i.e. pressure divided by density. Accordingly, it is searched for $\mathbf{u} : \Omega \times (0, T) \rightarrow \mathbb{R}^d$ and $p : \Omega \times (0, T) \rightarrow \mathbb{R}$ on the space-time domain specified above such that

$$\frac{\partial \mathbf{u}}{\partial t} + \mathbf{u} \cdot \nabla \mathbf{u} + \beta \mathbf{u} (\nabla \cdot \mathbf{u}) + \nabla p - 2\nu \nabla \cdot \boldsymbol{\varepsilon}(\mathbf{u}) = \mathbf{f} \quad \text{in } \Omega \times (0, T) \quad (3.6)$$

$$\nabla \cdot \mathbf{u} = 0 \quad \text{in } \Omega \times (0, T) \quad (3.7)$$

with the boundary conditions

$$\mathbf{u} = \mathbf{g} \quad \text{on } \Gamma_g \times (0, T) \quad (3.8)$$

$$\mathbf{n} \cdot \boldsymbol{\sigma} = \mathbf{n} \cdot (-p\mathbf{I} + 2\nu \boldsymbol{\varepsilon}(\mathbf{u})) = \mathbf{h} \quad \text{on } \Gamma_h \times (0, T) \quad (3.9)$$

and the initial condition

$$\mathbf{u} = \mathbf{u}_0 \quad \text{in } \Omega \times \{0\} \quad (3.10)$$

where the initial velocity field \mathbf{u}_0 has to be divergence-free. The expanded form (2.67) of the convective term has been chosen here in view of the crucial choice of the parameter β for discrete methods (see also the respective discussion in section 2.6.3).

3.2.2 Variational formulation (weak form)

By introducing the weak form of the problem, the condition of fulfillment of the sets of equations (3.2)-(3.5) and (3.6)-(3.10), respectively, at every single point of the domain Ω is weakened to a desired fulfillment in an integral sense over the complete domain Ω . This procedure termed weighted residual method consists of two steps. Firstly, the residual of the respective equation is weighted by a test function and, secondly, integrated over the domain Ω .

For the convection-diffusion-reaction equation this reads

$$\int_{\Omega} w \mathfrak{R}_{cdr} d\Omega = 0 \quad (3.11)$$

where w is the scalar test function and \mathfrak{R}_{cdr} denotes the residual of the convection-diffusion-reaction equation. With the usual notation for the L_2 -inner product in the domain Ω (see Appendix B) subject to

$$(a, b)_{\Omega} = \int_{\Omega} ab d\Omega \quad (3.12)$$

(3.11) may be expanded as

$$\left(w, \frac{\partial \phi}{\partial t} \right)_{\Omega} + (w, \mathbf{a} \cdot \nabla \phi)_{\Omega} + (w, \kappa \Delta \phi)_{\Omega} + (w, \sigma_{(\text{mod})} \phi)_{\Omega} = (w, f)_{\Omega} \quad (3.13)$$

After integration-by-parts of the diffusive term, a bilinear form $B_{cdr}^t(w, \phi)$ may be defined according to

$$B_{cdr}^t(w, \phi) = \left(w, \frac{\partial \phi}{\partial t} \right)_{\Omega} + (w, \mathbf{a} \cdot \nabla \phi)_{\Omega} + (\nabla w, \kappa \nabla \phi)_{\Omega} + (w, \sigma_{(\text{mod})} \phi)_{\Omega} \quad (3.14)$$

and (3.13) can be restated as

$$B_{cdr}^t(w, \phi) = (w, f)_{\Omega} + (w, h)_{\Gamma_h} \quad (3.15)$$

where the second term on the right hand side denotes an L_2 -inner product in the sense of (3.12) on the Neumann boundary Γ_h arising 'naturally' from the integration-by-parts of the diffusive term. This represents the Neumann boundary condition (3.4) within the integral formulation. A weak form with lower demands of differentiability (first derivative instead of second derivative) is obtained in the wake of the integration-by-parts procedure. It remains to choose the solution and weighting function space wherein the problem of finding ϕ is defined such that (3.15) is fulfilled. The solution function space reads

$$\mathfrak{S}_{\phi} = \left\{ \phi \in H^1(\Omega) \mid \phi = g \text{ on } \Gamma_g \right\} \quad (3.16)$$

and the weighting function space

$$\mathcal{W}_{\phi} = \left\{ w \in H^1(\Omega) \mid w = 0 \text{ on } \Gamma_g \right\} \quad (3.17)$$

where $H^1(\Omega)$ denotes the Sobolev space of square-integrable functions and square-integrable first derivatives. For some further remarks concerning this Sobolev space as well as a classification of this space within a hierarchy of spaces, please consult appendix B.

Navier-Stokes equations

The weighted integral statements of (3.6) and (3.7) are given by

$$\int_{\Omega} \mathbf{v} \mathfrak{R}_{NS,M} d\Omega = 0 \quad (3.18)$$

and

$$\int_{\Omega} q \mathfrak{R}_{NS,C} d\Omega = 0 \quad (3.19)$$

respectively, where \mathbf{v} is the vectorial test function applied to the residual of the momentum equation $\mathfrak{R}_{NS,M}$ and q indicates the scalar test function applied to the residual of the continuity equation $\mathfrak{R}_{NS,C}$. (3.18) and (3.19) are combined by a minus sign as

$$\int_{\Omega} \mathbf{v} \mathfrak{R}_{NS,M} d\Omega - \int_{\Omega} q \mathfrak{R}_{NS,C} d\Omega = 0 \quad (3.20)$$

in order to get one integral formulation bearing a symmetric matrix system in the end. Applying the notation (3.12), the weak form of the Navier-Stokes equations reads

$$B_{NS}(\mathbf{v}, q; \mathbf{u}, p) = (\mathbf{v}, \mathbf{f})_{\Omega} + (\mathbf{v}, \mathbf{h})_{\Gamma_h} \quad (3.21)$$

where the bilinear form $B_{NS}(\mathbf{v}, q; \mathbf{u}, p)$ on the left hand side is obtained after integration-by-parts of the viscous term as well as the pressure term according to

$$\begin{aligned} B_{NS}(\mathbf{v}, q; \mathbf{u}, p) &= \left(\mathbf{v}, \frac{\partial \mathbf{u}}{\partial t} \right)_{\Omega} + (\mathbf{v}, \mathbf{u} \cdot \nabla \mathbf{u} + \beta \mathbf{u} (\nabla \cdot \mathbf{u}))_{\Omega} - (\nabla \cdot \mathbf{v}, p)_{\Omega} \\ &\quad + (\boldsymbol{\varepsilon}(\mathbf{v}), 2\nu \boldsymbol{\varepsilon}(\mathbf{u}))_{\Omega} - (q, \nabla \cdot \mathbf{u})_{\Omega} \end{aligned} \quad (3.22)$$

The Neumann boundary term on the right hand side again comes into play 'naturally' from the integration-by-parts of the viscous and the pressure term. The highest derivative appearing in (3.21) is of first order. Thus, similar function spaces with respect to the case of the convection-diffusion-reaction equation can be chosen. The vectorial solution function space for the velocity is defined as

$$\mathcal{S}_{\mathbf{u}} = \left\{ \mathbf{u} \in (H^1(\Omega))^d \mid \mathbf{u} = \mathbf{g} \text{ on } \Gamma_g \right\} \quad (3.23)$$

and the weighting function space as

$$\mathcal{V}_{\mathbf{u}} = \left\{ \mathbf{v} \in (H^1(\Omega))^d \mid \mathbf{v} = \mathbf{0} \text{ on } \Gamma_g \right\} \quad (3.24)$$

The respective scalar function spaces for the pressure read

$$\mathcal{S}_p = \mathcal{V}_p = \{(p, q) \in L_2(\Omega)\} \quad (3.25)$$

Applying e.g. the pressure constraint (2.56), the solution function space would have to be expanded as

$$\mathcal{S}_p = \left\{ p \in L_2(\Omega) \mid \int_{\Omega} p d\Omega = 0 \right\} \quad (3.26)$$

The solution and weighting function spaces may be written in combined form as

$$\mathcal{Y}_{up} := \mathcal{Y}_u \times \mathcal{Y}_p; \quad \mathcal{V}_{up} := \mathcal{V}_u \times \mathcal{V}_p \quad (3.27)$$

3.2.3 Galerkin finite element functions

The presupposition for the application of the finite element method is a discretization of the domain Ω into n_{el} element subdomains Ω_e ($e = 1, \dots, n_{el}$) with element boundaries Γ_e where

$$\Omega' = \bigcup_{e=1}^{n_{el}} \Omega_e \quad (3.28)$$

denotes the union of all element interiors and

$$\Gamma' = \bigcup_{e=1}^{n_{el}} \Gamma_e \setminus \Gamma \quad (3.29)$$

denotes the union of all element boundaries excluding the domain boundary Γ .

The solution and weighting functions may now be replaced by standard Galerkin finite element functions in (3.15) and (3.21) yielding the problem of finding $\phi^h \in \mathcal{Y}_\phi^h$ such that

$$B_{CDR}^t(w^h, \phi^h) = (w^h, f)_\Omega + (w^h, h)_{\Gamma_h} \quad \forall w^h \in \mathcal{V}_\phi^h \quad (3.30)$$

as well as the problem of finding $\{\mathbf{u}^h, p^h\} \in \mathcal{Y}_{up}^h$ such that

$$B_{NS}(\mathbf{v}^h, q^h; \mathbf{u}^h, p^h) = (\mathbf{v}^h, \mathbf{f})_\Omega + (\mathbf{v}^h, \mathbf{h})_{\Gamma_h} \quad \forall \{\mathbf{v}^h, q^h\} \in \mathcal{V}_{up}^h \quad (3.31)$$

In (3.30) and (3.31), the finite-dimensional subspaces \mathcal{Y}_ϕ^h , \mathcal{V}_ϕ^h , \mathcal{Y}_{up}^h and \mathcal{V}_{up}^h replace their basically infinite-dimensional counterparts \mathcal{Y}_ϕ , \mathcal{V}_ϕ , \mathcal{Y}_{up} and \mathcal{V}_{up} . Within these finite-dimensional subspaces, the solution functions ϕ^h , \mathbf{u}^h and p^h as well as the weighting functions w^h , \mathbf{v}^h and q^h are chosen to replace the respective original functions without superscript h . The usual finite element functions are constituted by unknown parameters ϕ_B , \mathbf{u}_B and p_B which will have to be determined and shape functions N_B , mostly represented by polynomial functions, subject to

$$\phi^h = \sum_{B=1}^{n_{dofs}} N_B \phi_B, \quad \mathbf{u}^h = \sum_{B=1}^{n_{dofs}} N_B \mathbf{u}_B, \quad p^h = \sum_{B=1}^{n_{dofs}} N_B p_B \quad (3.32)$$

where n_{dofs} indicates the number of degrees of freedom of the problem. Choosing the same functions for the approximation of the weighting functions subject to

$$w^h = \sum_{A=1}^{n_{dofs}} N_A w_A, \quad \mathbf{v}^h = \sum_{A=1}^{n_{dofs}} N_A \mathbf{v}_A, \quad q^h = \sum_{A=1}^{n_{dofs}} N_A q_A \quad (3.33)$$

leaves us behind with a standard Galerkin method which is also termed Bubnov-Galerkin method sometimes. Different choices for the solution and the weighting functions are usually categorized under the label of Petrov-Galerkin methods.

Two different concepts for (3.32) and (3.33) are possible on principle: standard Lagrange-based shape functions and hierarchical shape functions. Within the standard Lagrangean concept, the parameters, for example ϕ_B , are entirely assigned to nodal values whereas in the hierarchical concept this is not the case in general. The crucial second difference lies in the generation of the

polynomial shape functions N_B . In the standard concept every polynomial order k is associated with a completely different set of shape functions entirely built by functions of this order k whereas the hierarchical shape functions of a particular order k are made up of functions of order k and lower order. This constitutes the basic reason for the suitability of the hierarchical concept for the variational multiscale method as a whole. That is to say that the hierarchical basis of order $k - 1$ is a subset of the one of order k which amounts to a natural scale separation. This point will be picked up again within the context of the variational multiscale method. Whereas the standard Lagrange-based concept may be found in every referenced book on the finite element method mentioned in the introduction of this chapter the hierarchical concept is more rarely included. Elementary descriptions of the hierarchical concept can be found in Szabo and Babuska (1991), Zienkiewicz et al. (1983), and Zienkiewicz and Taylor (2000a).

3.2.4 Semi-discrete matrix systems

The matrix systems follow from the introduction of the functions (3.32) and (3.33) into the variational formulations (3.30) and (3.31). After all, it has to be solved for the unknown parameters of the solution functions ϕ_B and \mathbf{u}_B as well as p_B , respectively. The linear matrix system for the convection-diffusion-reaction equation reads after assembly of the element matrices

$$\mathbf{M}\dot{\phi} + \left[\mathbf{C}(\mathbf{a}) + \mathbf{D} + \sigma_{(mod)}\mathbf{M} \right] \phi = \mathbf{F} + \mathbf{N} - \mathbf{E} \quad (3.34)$$

The nonlinear matrix system for the Navier-Stokes equations reads

$$\mathbf{M}\dot{\mathbf{u}} + \left[\mathbf{C}(\mathbf{u}) + \mathbf{V} + \beta(\nabla \cdot \mathbf{u})\mathbf{M} \right] \mathbf{u} + \mathbf{G}\mathbf{p} = \mathbf{F} + \mathbf{N} - \mathbf{E}^M \quad (3.35)$$

$$\mathbf{G}^T \mathbf{u} = -\mathbf{E}^C \quad (3.36)$$

Please observe that the notation \mathbf{u} and $\dot{\mathbf{u}}$ already introduced as the velocity and accelerations vector, respectively, is used here and in the following also for denoting the vector containing the respective unknown parameters of the solution function. This is a widespread way of marking. Hopefully, there will be no chance of confusion due to this double notation. Accordingly, ϕ and $\dot{\phi}$ represent the vectors incorporating the unknown parameters ϕ_B and its first time derivative, respectively. The same applies to \mathbf{p} . In (3.34)-(3.36), \mathbf{M} , \mathbf{C} , \mathbf{D} , \mathbf{V} , \mathbf{G} and \mathbf{G}^T denote the mass, convective, diffusive, viscous, gradient, and transposed gradient, i.e. divergence, matrix, respectively. \mathbf{F} and \mathbf{N} indicate the right hand side vectors due to the body force term and the Neumann boundary conditions (3.4) and (3.9), respectively. \mathbf{E} , \mathbf{E}^M and \mathbf{E}^C denote the vectors on the right hand side with entries due to the essential Dirichlet boundary conditions (3.3) and (3.8), respectively, whereby the influence is splitted for the momentum and the continuity equation within the set of Navier-Stokes equations. The structure of the respective matrices and vectors or, more precisely spoken, the respective element matrices and vectors which they are composed of will be explained for the final matrix system to be presented in section 3.3.4 after the introduction of the temporal discretization.

3.3 Temporal discretization and linearization

3.3.1 Introduction

The matrix systems (3.34) and (3.35)-(3.36), respectively, now have to undergo a discretization in time after the just described discretization in space. In particular, the matrix system

(3.35)-(3.36) for the Navier-Stokes equations is extremely challenging concerning its temporal discretization. (3.35)-(3.36) represents a differential-algebraic equation (DAE), i.e. an ordinary differential equation (ODE) represented by (3.35) subject to an algebraic constraint represented by (3.36). There is no intent here to discuss the difficult topic of solving DAE's efficiently. Elaboration of this may be found, for instance, in Gresho and Sani (1998) or Wall (1999). The particular choice of time integration schemes is just described here and, moreover, this introduction is utilized in order to motivate this particular choice.

First of all, the path of semi-discretization in time is followed as a sequential way of discretizing in space and time. A potential alternative consists in a simultaneous way of discretizing in space and time, i.e. applying finite element functions in space and time $N(\mathbf{x}, t)$ acting on so-called space-time elements. These would replace the ones in section 3.2.3 which only depend on the spatial coordinates $N(\mathbf{x})$. This is usually practised with discontinuous Galerkin methods for the discretization in time, see e.g. Johnson and Saranen (1986), Shakib (1988) or Hughes et al. (1989). The most important disadvantage of simultaneous methods shows up in substantially larger systems of equations. This disadvantage lets the alternative of simultaneous methods become unattractive, since it already has to be dealt with extremely large systems of equations in turbulent flow applications.

Another alternative, namely decoupled solution methods in the sense of pressure projection methods, has also not been established within this work. The advantage consisting in the fact that one is allowed to deal with smaller equation systems in the respective fractional steps is overshadowed by the drawbacks in the behaviour at the boundaries yet (see also the discussion in Wall (1999)). Nevertheless, a first implementation of a pressure projection-based solver at the Institute of Structural Mechanics has been carried out in Basol (2003) and is about to be used for comparison with the coupled methods favoured herein.

Following the strategy of using a coupled and sequential method, a fully implicit scheme, namely the implicit variants of the generalized trapezoidal method, will be described. This constitutes the 'workhorse' for the applications. It will be introduced for the linear convection-diffusion-reaction equation and then transferred to the nonlinear Navier-Stokes equations, for which a linearization step is necessary. In addition to this, a semi-implicit scheme is introduced for the Navier-Stokes equations making the linearization unnecessary. This scheme may potentially act as an alternative to the semi-implicit schemes mostly used for turbulent flow simulations consisting in an implicit variant of the generalized trapezoidal scheme, e.g. the Crank-Nicolson scheme, for the linear terms and an explicit method, e.g. a variant of the Adams-Bashfort schemes, for the nonlinear convective term. Another interesting alternative is the generalized α -method. This method, well-established in computational solid mechanics, has recently been applied by Jansen et al. (2000) to the compressible Navier-Stokes equations in the context of a stabilized finite element method.

The procedure of section 3.3 is as follows. The temporal discretization with the generalized trapezoidal method (and, additionally, the linearization in the case of the Navier-Stokes equations) is carried out in section 3.3.2. Both, the temporal discretization and the linearization, is firstly executed for the strong as well as for the weak form of the problem, in order to exemplify the procedure in these stages. Subsequently, a semi-implicit scheme is pointed out as a potential alternative. Hereafter, the fully discrete matrix systems are shown in section 3.3.4 as a result of the application of the temporal discretization (and linearization) to the semi-discrete matrix systems which have been obtained from the spatial discretization and displayed in section 3.2.4.

Due to this modus operandi, the follower of both strategies, i.e. 'spatial discretization first, temporal discretization after' and 'temporal discretization first, spatial discretization after', respectively, will hopefully find everything they need for their individual way of proceeding within this chapter 3.

3.3.2 Fully implicit scheme

Temporal discretization of the convection-diffusion-reaction equation

Starting with a discrete initial field ϕ^0 according to (3.5), the application of the generalized trapezoidal scheme to the convection-diffusion-reaction equation yields for the scalar field ϕ^{n+1} at time level $n + 1$ the formula

$$\frac{\phi^{n+1} - \phi^n}{\delta t} + \theta(\mathcal{L}_{cdr}\phi^{n+1}) + (1 - \theta)(\mathcal{L}_{cdr}\phi^n) = \theta f^{n+1} + (1 - \theta)f^n \quad (3.37)$$

subject to the discrete Dirichlet boundary condition

$$\phi^{n+1} = g^{n+1} \quad (3.38)$$

and the discrete Neumann boundary condition

$$\mathbf{n} \cdot \kappa \nabla \phi^{n+1} = h^{n+1} \quad (3.39)$$

where δt denotes the chosen time step, n the previous time level subject to $n = 0, \dots, (T/\delta t) - 1$, T the simulation time and θ the parameter of the method, taken to be in the interval $[0, 1]$. Here and below, the concise notation for the values depending on the parameter θ subject to

$$(\cdot)^{n+\theta} = \theta(\cdot) + (1 - \theta)(\cdot) \quad (3.40)$$

is used. Herewith, (3.37) is transferred to

$$\frac{\phi^{n+1} - \phi^n}{\delta t} + \mathbf{a} \cdot \nabla \phi^{n+\theta} - \kappa \Delta \phi^{n+\theta} + \sigma_{(\text{mod})} \phi^{n+\theta} = f^{n+\theta} \quad (3.41)$$

The variational formulation analog to (3.15) for the now discrete-in-time problem reads

$$B_{cdr}^{dt}(w, \phi) = \left(w, \frac{\phi^n}{\delta t} \right)_{\Omega} + (w, f^{n+\theta})_{\Omega} + (w, h^{n+\theta})_{\Gamma_h} \quad (3.42)$$

where

$$\begin{aligned} B_{cdr}^{dt}(w, \phi) &= \left(w, \frac{\phi^{n+1}}{\delta t} \right)_{\Omega} + (w, \mathbf{a} \cdot \nabla \phi^{n+\theta})_{\Omega} + (\nabla w, \kappa \nabla \phi^{n+\theta})_{\Omega} \\ &\quad + (w, \sigma_{(\text{mod})} \phi^{n+\theta})_{\Omega} \end{aligned} \quad (3.43)$$

After the introduction of the respective finite element functions in (3.32) and (3.33), the fully discrete matrix system for the convection-diffusion-reaction equation is obtained reading

$$\left\{ \mathbf{M} + \theta \delta t \left[\mathbf{C}(\mathbf{a}) + \mathbf{D} + \sigma_{(\text{mod})} \mathbf{M} \right] \right\} \boldsymbol{\phi}^{n+1}$$

$$\begin{aligned}
&= \left\{ \mathbf{M} - (1 - \theta)\delta t \left[\mathbf{C}(\mathbf{a}) + \mathbf{D} + \sigma_{(mod)}\mathbf{M} \right] \right\} \boldsymbol{\phi}^n \\
&\quad + \theta\delta t(\mathbf{F} + \mathbf{N} - \mathbf{E})^{n+1} + (1 - \theta)\delta t(\mathbf{F} + \mathbf{N})^n
\end{aligned} \tag{3.44}$$

(3.44) may also be achieved as a continuation of the semi-discrete matrix system (3.34) after temporal discretization.

Temporal discretization of the Navier-Stokes equation

The realization for the convection-diffusion-reaction equation may now be transferred to the set of Navier-Stokes equations with some modifications. The discrete initial (divergence-free) velocity field \mathbf{u}^0 according to (3.10) constitutes the start of the algorithm which reads for time level $n + 1$ in concise notation

$$\frac{\mathbf{u}^{n+1} - \mathbf{u}^n}{\delta t} + \mathbf{u}^{n+\theta} \cdot \nabla \mathbf{u}^{n+\theta} + \beta \mathbf{u}^{n+\theta} (\nabla \cdot \mathbf{u}^{n+\theta}) + \nabla p^{n+\theta} - 2\nu \boldsymbol{\varepsilon}(\mathbf{u}^{n+\theta}) = \mathbf{f}^{n+\theta} \tag{3.45}$$

$$\nabla \cdot \mathbf{u}^{n+\theta} = 0 \tag{3.46}$$

where again the expanded form (2.67) of the convective term has been used. The discrete-in-time boundary conditions are

$$\mathbf{u}^{n+1} = \mathbf{g}^{n+1} \tag{3.47}$$

$$\mathbf{n} \cdot \left(-p^{n+1} \mathbf{I} + 2\nu \boldsymbol{\varepsilon}(\mathbf{u}^{n+1}) \right) = \mathbf{h}^{n+1} \tag{3.48}$$

As aforementioned, a pressure Poisson equation may replace the continuity equation. The PPE is discretized in time subject to

$$\Delta p^{n+\theta} = \nabla \cdot \left(-\mathbf{u}^{n+\theta} \cdot \nabla \mathbf{u}^{n+\theta} + \nu \Delta \mathbf{u}^{n+\theta} + \mathbf{f}^{n+\theta} \right) \tag{3.49}$$

The variational formulation analog to (3.21) for the temporally discretized Navier-Stokes equations reads

$$B_{NS}^{dt}(\mathbf{v}, q; \mathbf{u}, p) = \left(\mathbf{v}, \frac{\mathbf{u}^n}{\delta t} \right)_{\Omega} + \left(\mathbf{v}, \mathbf{f}^{n+\theta} \right)_{\Omega} + \left(\mathbf{v}, \mathbf{h}^{n+\theta} \right)_{\Gamma_h} \tag{3.50}$$

where

$$\begin{aligned}
B_{NS}^{dt}(\mathbf{v}, q; \mathbf{u}, p) &= \left(\mathbf{v}, \frac{\mathbf{u}^{n+1}}{\delta t} \right)_{\Omega} + \left(\mathbf{v}, \mathbf{u}^{n+\theta} \cdot \nabla \mathbf{u}^{n+\theta} + \beta \mathbf{u}^{n+\theta} (\nabla \cdot \mathbf{u}^{n+\theta}) \right)_{\Omega} \\
&\quad - \left(\nabla \cdot \mathbf{v}, p^{n+\theta} \right)_{\Omega} + \left(\boldsymbol{\varepsilon}(\mathbf{v}), 2\nu \boldsymbol{\varepsilon}(\mathbf{u}^{n+\theta}) \right)_{\Omega} - \left(q, \nabla \cdot \mathbf{u}^{n+\theta} \right)_{\Omega}
\end{aligned} \tag{3.51}$$

After the introduction of the respective finite element functions in (3.32) and (3.33), the fully discrete matrix system for the Navier-Stokes equations is obtained reading

$$\begin{aligned}
&\left\{ \mathbf{M} + \theta\delta t \left[\mathbf{C}(\mathbf{u}^{n+1}) + \mathbf{V} + \beta(\nabla \cdot \mathbf{u}^{n+1})\mathbf{M} \right] \right\} \mathbf{u}^{n+1} + \theta\delta t \mathbf{G} \mathbf{p}^{n+1} \\
&= \left\{ \mathbf{M} - (1 - \theta)\delta t \left[\mathbf{C}(\mathbf{u}^n) + \mathbf{V} + \beta(\nabla \cdot \mathbf{u}^n)\mathbf{M} \right] \right\} \mathbf{u}^n - (1 - \theta)\delta t \mathbf{G} \mathbf{p}^n
\end{aligned}$$

$$+ \theta \delta t (\mathbf{F} + \mathbf{N} - \mathbf{E}^M)^{n+1} + (1 - \theta) \delta t (\mathbf{F} + \mathbf{N})^n \quad (3.52)$$

$$\theta \delta t \mathbf{G}^T \mathbf{u}^{n+1} = - (1 - \theta) \delta t \mathbf{G}^T \mathbf{u}^n + \theta \delta t (-\mathbf{E}^C)^{n+1} \quad (3.53)$$

(3.52)-(3.53) may also be achieved as a continuation of the semi-discrete matrix system (3.35)-(3.36) after temporal discretization.

Analysis of the generalized trapezoidal method

Famous representatives of the generalized trapezoidal method are the explicit forward Euler method ($\theta = 0$), the implicit backward Euler method ($\theta = 1$) and the implicit Crank-Nicolson scheme ($\theta = 1/2$). Furthermore, the schemes with $\theta = 1/3$ and $\theta = 2/3$ are sometimes termed 'Galerkin schemes'. Particular attention has to be paid to the Crank-Nicolson scheme, since it is the only scheme bearing second-order accuracy. The other schemes exclusively show up with first-order accuracy. However, there are some significant drawbacks associated with the Crank-Nicolson scheme. The crucial disadvantage surely lies in the potential occurrence of oscillations during the development of the solution. This is usually blamed to be due to a chosen time step being too large for the underlying problem. Using, for example, the backward Euler scheme such an 'incorrect' time step may be overcome by the strong damping feature of the scheme. This damping feature comes into play by choosing $\theta > 1/2$ and is, hence, not inherent, in the Crank-Nicolson scheme. For a general analysis of the generalized trapezoidal method with regard to these damping features, one may consult e.g. Hughes (2000). For a furthergoing analysis of this method, among others, particularly aiming at stabilized methods for the Navier-Stokes equations, it is referred to the recent publication of Dettmer and Peric (2003).

The explicit forward Euler method is subject to the so-called CFL(Courant-Friedrich-Levy)-condition governing the size of the time step depending on the velocity and the chosen spatial discretization. The CFL-condition may become very restrictive resulting in extremely small time steps. Despite the still enjoyed popularity of explicit time stepping schemes (which may surely be justified for a vast number of problems), implicit schemes whose parameter θ lies between $1/2$ and 1 are favoured here. In order to overcome the oscillations associated with the Crank-Nicolson scheme, Heywood and Rannacher (1990) suggest a slight increase of θ beyond $\theta = 1/2$ if necessary. It has to be remarked, however, that this also reduces the order of accuracy losing the second-order accuracy of the Crank-Nicolson scheme.

Two potential simplifications of (3.45)-(3.46) and (3.49), respectively, should be remarked. Firstly, it is a widespread used option to set $\theta = 1$ in (3.46) or (3.49), respectively, although this may be, in general, algorithmically inconsistent with the chosen parameter θ for the momentum equation (3.45). The 'dangerous' aspect of this choice results in some kind of 'damping-out' process of ill-posed initial conditions. Secondly, the pressure in (3.45) may be evaluated at time level $n + 1$, independent of the choice of θ . Although this results in a similar 'danger' with respect to the first simplification, this second assumption avoids the necessity of determining an initial pressure field p^0 required to be compatible with the initial velocity field \mathbf{u}^0 . It is obvious that both simplifications are inherently employed by choosing the backward Euler scheme.

Finally, the question why multistep methods are not considered as an alternative probably has to be answered. This is definitely a subjective choice driven by the smaller complexity and storage requirements posed by the one-step schemes yet. However, multistep methods may become

an attractive alternative which have to be investigated more thoroughly for the methods presented in this work.

Linearization of the Navier-Stokes equations

At the end of the description of the fully implicit schemes the necessity still remains to linearize the nonlinear matrix system for the set of Navier-Stokes equations. Within the standard Galerkin method the only nonlinear term is the convective term expanded in (2.67). A linearization applying the Gateaux-derivative is performed in Wall (1999) and details may be found therein. In consequence, the discussion will be started with a global linearization equation for the convective term in the expanded form of (2.67) reading

$$\begin{aligned} \mathbf{u}_{i+1} \cdot \nabla \mathbf{u}_{i+1} + \beta \mathbf{u}_{i+1} (\nabla \cdot \mathbf{u}_{i+1}) &= \bar{\alpha} [\mathbf{u}_i \cdot \nabla \mathbf{u}_{i+1} + \beta \mathbf{u}_{i+1} (\nabla \cdot \mathbf{u}_i)] \\ &+ \bar{\alpha} \alpha [\mathbf{u}_{i+1} \cdot \nabla \mathbf{u}_i + \beta \mathbf{u}_i (\nabla \cdot \mathbf{u}_{i+1})] - \alpha [(\mathbf{u}_i \cdot \nabla \mathbf{u}_i + \beta \mathbf{u}_i (\nabla \cdot \mathbf{u}_i))] \end{aligned} \quad (3.54)$$

with the current iteration step indicated by the subscript $i + 1$. By altering the pair of parameters $[\bar{\alpha}, \alpha]$ one encounters various ways of linearizing the convective term. For $[0, -1]$, a fixed point iteration, for $[1, 1]$, a Newton(-Raphson) iteration and, for $[1, 0]$, a fixed point like iteration is obtained according to the notation in Wall (1999). There is undoubtedly some confusion in literature concerning the correct denotation of the respective methods. Due to its good numerical features the fixed point like iteration is the method of choice throughout this work. In order to explain some of the confusion, it may be alluded to the fact that this method is termed, for instance, Picard iteration in Codina (2000a). The linearized convective term to be worked within the framework of the generalized trapezoidal method is $\mathbf{u}_i^{n+\theta} \cdot \nabla \mathbf{u}_{i+1}^{n+\theta} + \beta \mathbf{u}_{i+1}^{n+\theta} (\nabla \cdot \mathbf{u}_i^{n+\theta})$ thus.

In view of the introduction of the variational multiscale method for the Navier-Stokes equations in chapter 7, it is helpful to define formally the underlying differential operator for the temporally semi-discrete momentum equation (3.45) along with the just described linearization in form of a fixed point like iteration. First of all, (3.45) after introducing the linearization is rearranged as

$$\begin{aligned} \frac{1}{\theta \delta t} \mathbf{u}_{i+1}^{n+1} + \mathbf{u}_i^{n+1} \cdot \nabla \mathbf{u}_{i+1}^{n+1} + \beta \mathbf{u}_{i+1}^{n+1} (\nabla \cdot \mathbf{u}_i^{n+1}) + \nabla p_{i+1}^{n+1} - 2\nu \nabla \cdot \boldsymbol{\varepsilon}(\mathbf{u}_{i+1}^{n+1}) \\ = \mathbf{f}^{n+1} + \mathbf{f}_t^n \end{aligned} \quad (3.55)$$

where a 'time-rhs' \mathbf{f}_t^n containing all known values of time level n has been introduced in (3.55) being defined as

$$\mathbf{f}_t^n = \frac{1}{\theta \delta t} \mathbf{u}^n - \frac{(1 - \theta)}{\theta} [\mathbf{u}^n \cdot \nabla \mathbf{u}^n + \beta \mathbf{u}^n (\nabla \cdot \mathbf{u}^n) + \nabla p^n - 2\nu \nabla \cdot \boldsymbol{\varepsilon}(\mathbf{u}^n) - \mathbf{f}^n] \quad (3.56)$$

Analogously to what has been carried out in the continuous case (confer section 2.6.3), the complete differential operator of the momentum equation (3.55) can be split into a convective, diffusive and reactive differential operator plus a differential operator acting on the pressure subject to

$$\begin{aligned} \mathcal{L}_M^{dt, lin}[\mathbf{u}, p] &= \mathcal{L}_{conv}(\mathbf{u}_i) \mathbf{u} + \mathcal{L}_{visc} \mathbf{u} + \mathcal{L}_{reac} \mathbf{u} + \mathcal{L}_{pres} p \\ &= \mathbf{u}_i \cdot \nabla \mathbf{u} - 2\nu \nabla \cdot \boldsymbol{\varepsilon}(\mathbf{u}) + \left(\frac{1}{\theta \delta t} + \beta (\nabla \cdot \mathbf{u}_i) \right) \mathbf{u} + \nabla p \end{aligned} \quad (3.57)$$

The respective adjoint differential operator reads

$$\begin{aligned}\mathcal{L}_M^{* dt, lin}[\mathbf{u}, p] &= \mathcal{L}_{conv}^*(\mathbf{u}_i)\mathbf{u} + \mathcal{L}_{visc}^*\mathbf{u} + \mathcal{L}_{reac}^*\mathbf{u} + \mathcal{L}_{pres}^*p \\ &= -\mathbf{u}_i \cdot \nabla \mathbf{u} - 2\nu \nabla \cdot \boldsymbol{\varepsilon}(\mathbf{u}) + \left(\frac{1}{\theta \delta t} + \beta(\nabla \cdot \mathbf{u}_i) \right) \mathbf{u} - \nabla p\end{aligned}\quad (3.58)$$

A stationary version of (3.57) is defined as

$$\begin{aligned}\mathcal{L}_M^{stat}[\mathbf{u}, p] &= \mathcal{L}_{conv}(\mathbf{u}_i)\mathbf{u} + \mathcal{L}_{visc}\mathbf{u} + \mathcal{L}_{reac}^{stat}\mathbf{u} + \mathcal{L}_{pres}p \\ &= \mathbf{u}_i \cdot \nabla \mathbf{u} - 2\nu \nabla \cdot \boldsymbol{\varepsilon}(\mathbf{u}) + \beta(\nabla \cdot \mathbf{u}_i)\mathbf{u} + \nabla p\end{aligned}\quad (3.59)$$

with its adjoint counterpart

$$\begin{aligned}\mathcal{L}_M^{* stat}[\mathbf{u}, p] &= \mathcal{L}_{conv}^*(\mathbf{u}_i)\mathbf{u} + \mathcal{L}_{visc}^*\mathbf{u} + \mathcal{L}_{reac}^{* stat}\mathbf{u} + \mathcal{L}_{pres}p \\ &= -\mathbf{u}_i \cdot \nabla \mathbf{u} - 2\nu \nabla \cdot \boldsymbol{\varepsilon}(\mathbf{u}) + \beta(\nabla \cdot \mathbf{u}_i)\mathbf{u} - \nabla p\end{aligned}\quad (3.60)$$

which both will be used later on.

3.3.3 Semi-implicit scheme

Although the idea for this method probably goes back to work of Temam in the 1960's, this group of methods was particularly proposed by Simo and co-workers, see e.g. Simo and Armero (1994) and Simo et al. (1995). The crucial aspect of the semi-implicit scheme is the treatment of the nonlinear convective term. Aside from this, the remaining terms may be dealt with by the generalized trapezoidal method with any choice for the parameter θ .

For the derivation of the scheme, the just obtained final form of the convective term may be modified after applying the generalized trapezoidal method and the fixed point like iteration scheme as $\mathbf{u}^{n+\gamma} \cdot \nabla \mathbf{u}^{n+\theta} + \beta \mathbf{u}^{n+\theta} (\nabla \cdot \mathbf{u}^{n+\gamma})$. This means that the values from the last iteration step $\mathbf{u}_i^{n+\theta}$ have been replaced by the value $\mathbf{u}^{n+\gamma}$ which is defined as

$$\mathbf{u}^{n+\gamma} = \begin{cases} \gamma \mathbf{u}^{n+1} + (1 - \gamma) \mathbf{u}^n; & \gamma > 0 \\ \gamma \mathbf{u}^{n-1} + (1 - \gamma) \mathbf{u}^n; & \gamma \leq 0 \end{cases}\quad (3.61)$$

Certainly, a nonlinear scheme is still encountered for $\gamma > 0$. Hence, it has to be focussed on methods with $\gamma \leq 0$ in order to achieve the premier goal, a linear scheme. Such a linearization may be interpreted as an extrapolation in time. Obviously, choosing γ to be zero is equal to one fixed point like iteration if \mathbf{u}_0^{n+1} at time level $n + 1$ is taken to be the converged velocity from the previous time level n . It has to be remarked, however, that the combination of $\gamma = 0$ and a Crank-Nicolson scheme is an overall method of first order. The most attractive scheme seems to be the two-step scheme $\gamma = -1/2$ and $\theta = 1/2$ which keeps up second-order accuracy. A high price has to be paid for this, however, in form of the necessity to store the results of an additional time level. The drawback of this necessity for large systems has already been pointed out. Practically, this two-step scheme has to be initiated utilizing a starting algorithm in form of a one-step method, for instance, with a backward Euler scheme using $\gamma = 0$ and $\theta = 1$. An important remark aims at the form of the convective term. Simo and Armero (1994) have shown

a favourable stability behaviour of the linear schemes with good accuracy. The presupposition for this, however, is a strictly skew-symmetric form of the convective term achieved by setting $\beta = 1/2$ in (2.67). Since this is the foremost choice herein due to similar reasoning for other methods as well (see also the discussion in section 2.6.3), this constraint poses no additional problem. Due to the extended storage requirements of the aforementioned most attractive scheme, this method will not be used for the numerical examples within this work. It offers itself as a potential alternative in the future however.

3.3.4 Final matrix systems

The final matrix system for the convection-diffusion-reaction equation (3.44) reads in short form

$$\mathbf{K}_{cdr,t} \boldsymbol{\phi}^{n+1} = \theta \delta t (\mathbf{F} + \mathbf{N} - \mathbf{E})^{n+1} + \mathbf{T}_{cdr} \quad (3.62)$$

where the 'stiffness' matrix is composed as

$$\mathbf{K}_{cdr,t} = \mathbf{M} + \theta \delta t [\mathbf{C}(\mathbf{a}) + \mathbf{D} + \sigma_{(mod)} \mathbf{M}] \quad (3.63)$$

and the 'time-rhs' as

$$\mathbf{T}_{cdr} = \left\{ \mathbf{M} - (1 - \theta) \delta t [\mathbf{C}(\mathbf{a}) + \mathbf{D} + \sigma_{(mod)} \mathbf{M}] \right\} \boldsymbol{\phi}^n + (1 - \theta) \delta t (\mathbf{F} + \mathbf{N})^n \quad (3.64)$$

Sample components of the respective element matrices based on the discretization subject to (3.28) and (3.29) read

$$M_{ab}^e = \int_{\Omega_e} N_a N_b d\Omega \quad (3.65)$$

$$C_{ab}^e(\mathbf{a}) = \int_{\Omega_e} N_a \mathbf{a} \cdot \nabla N_b d\Omega \quad (3.66)$$

$$D_{ab}^e = \kappa \int_{\Omega_e} \nabla N_a \cdot \nabla N_b d\Omega \quad (3.67)$$

Sample components of the element vectors on the right hand side are defined as

$$F_a^e = \int_{\Omega_e} N_a f d\Omega \quad (3.68)$$

$$N_a^e = \int_{\Gamma_{h,e}} N_a h d\Gamma \quad (3.69)$$

The element matrices (3.65)-(3.67) as well as the element vectors (3.68)-(3.69) are then assembled in order to get the global matrices and vectors in (3.62). This assembly operation may be expressed by the assembly operator \mathcal{A} , for instance, for the mass matrix (3.65) subject to

$$\mathbf{M} = \mathcal{A}_{e=1}^{n_{el}} (\mathbf{M}^e) \quad (3.70)$$

The entry \mathbf{E} on the right hand side of (3.62) is due to a potential Dirichlet boundary condition and arises from the assembly operation. Please consult the general references considering the finite element method mentioned in the introduction for details of this operation.

For the Navier-Stokes equations, the final matrix system (3.52)-(3.53) reads in short form after applying the fixed point like iteration scheme

$$\begin{bmatrix} \mathbf{K}_{NS}(\mathbf{u}_i^{n+1}) & \theta \delta t \mathbf{G} \\ \theta \delta t \mathbf{G}^T & \mathbf{0} \end{bmatrix} \cdot \begin{bmatrix} \mathbf{u}_{i+1}^{n+1} \\ \mathbf{p}_{i+1}^{n+1} \end{bmatrix} = \begin{bmatrix} \theta \delta t (\mathbf{F} + \mathbf{N} - \mathbf{E}^M)^{n+1} + \mathbf{T}_{NS, M} \\ \theta \delta t (-\mathbf{E}^C)^{n+1} + \mathbf{T}_{NS, C} \end{bmatrix} \quad (3.71)$$

where the 'stiffness' matrix is put together as

$$\mathbf{K}_{NS}(\mathbf{u}_i^{n+1}) = \mathbf{M} + \theta \delta t \left[\mathbf{C}(\mathbf{u}_i^{n+1}) + \mathbf{V} + \beta (\nabla \cdot \mathbf{u}_i^{n+1}) \mathbf{M} \right] \quad (3.72)$$

and the 'time-rhs' for the momentum equation as

$$\begin{aligned} \mathbf{T}_{NS, M} = & \left\{ \mathbf{M} - (1 - \theta) \delta t \left[\mathbf{C}(\mathbf{u}^n) + \mathbf{V} + \beta (\nabla \cdot \mathbf{u}^n) \mathbf{M} \right] \right\} \mathbf{u}^n - (1 - \theta) \delta t \mathbf{G} \mathbf{p}^n \\ & + (1 - \theta) \delta t (\mathbf{F} + \mathbf{N})^n \end{aligned} \quad (3.73)$$

as well as the 'time-rhs' for the continuity equation as

$$\mathbf{T}_{NS, C} = - (1 - \theta) \delta t \mathbf{G}^T \mathbf{u}^n \quad (3.74)$$

Applying the semi-implicit scheme, the iteration counter may be omitted and the velocities \mathbf{u}_i^{n+1} as well as \mathbf{u}^n have to be replaced by $\mathbf{u}^{n+\gamma}$.

The definitions of the sample components of the element matrices M_{ab}^e and C_{ab}^e as well as the element vectors F_{ab}^e and N_{ab}^e may easily be transferred to the case of the Navier Stokes equations. Sample components of the viscous element matrix and the gradient element matrix are defined as

$$V_{ab}^e = 2\nu \int_{\Omega_e} \boldsymbol{\varepsilon}(N_a) : \boldsymbol{\varepsilon}(N_b) d\Omega \quad (3.75)$$

$$G_{ab}^e = - \int_{\Omega_e} \nabla \cdot N_a N_b d\Omega \quad (3.76)$$

respectively. For choosing the conventional form of the viscous term in (2.64), the form of the diffusive matrix (3.67) may be adopted with ν replacing κ for the Navier-Stokes equations. The element matrices and vectors are then subject to the same assembly process symbolically indicated in (3.70). As before, the entries \mathbf{E}^M and \mathbf{E}^C on the right hand side of (3.71) are due to a potential Dirichlet boundary condition and arise from the assembly operation.

3.4 Numerical problems with the standard Galerkin finite element method

3.4.1 Velocity oscillations for high Reynolds and Peclet number flow

Problem demonstration for a model case

This problem is usually demonstrated for the model case of a one-dimensional stationary convection-diffusion equation, i.e. (3.2) with the just named simplifications, reading

$$a \frac{d\phi}{dx} - \kappa \frac{d^2\phi}{dx^2} = 0 \quad \text{in } \Omega \quad (3.77)$$

where, additionally, the right hand side is set to zero for convenience. For instance, this model case is used as an initial example in the didactically oriented lecture notes of Hughes et al. (1994a). (3.77) is confined to the domain $\Omega = [0, L]$ with Dirichlet boundary conditions at the the inflow boundary $\phi(x = 0) = 0$ and at the outflow boundary $\phi(x = L) = 1$. For a constant convective velocity a being defined positive in positive x -direction and a constant diffusive coefficient κ , the analytical solution of (3.77) reads with the Peclet number defined in (2.90)

$$\phi(x) = \frac{e^{Pe^x} - 1}{e^{Pe} - 1} \quad (3.78)$$

The flow is assumed to be convection-dominated for $Pe > 1$ and diffusion-dominated for $Pe < 1$ with a quite different behaviour for extreme values of the Peclet number, see Fig. 3.1. For $Pe \rightarrow \infty$, Fig. 3.1 displays the thin boundary layer which has to be resolved at the outflow boundary $x = L$. The application of the standard Galerkin finite element method in the sense of section 3.2 with piecewise linear elements, for example, leads to equations similar to the ones achieved with a central difference approximation in a finite difference method, confer e.g. Donea and Huerta (2003). After all, the solution of the approximate problem at some discrete node A ($A = 0, \dots, N$) reads

$$\phi_A = \phi(x_A = Ah) = \frac{\left(\frac{1+Pe^e}{1-Pe^e}\right)^A - 1}{\left(\frac{1+Pe^e}{1-Pe^e}\right)^N - 1} \quad (3.79)$$

where a uniform discretization with N elements of length h has been applied. Pe^e denotes the element-based Peclet number subject to

$$Pe^e = \frac{ah}{2\kappa} \quad (3.80)$$

By inspecting (3.79), one may observe that the numerical solution oscillates for $Pe^e > 1$. This situation is sketched in Fig. 3.2. Please compare the numerical solutions to the situation in Fig. 3.1 above and note, in particular, the obvious corruption in the convection-dominated case.

The only way to solve this problem with the standard Galerkin finite element method lies in an adequate choice of the element lengths such that $Pe^e < 1$ for every element. This, however, will in almost every case result in an enormous computational effort which is not feasible in general. Therefore, the scales not resolved will be incorporated by a multiscale approach below.

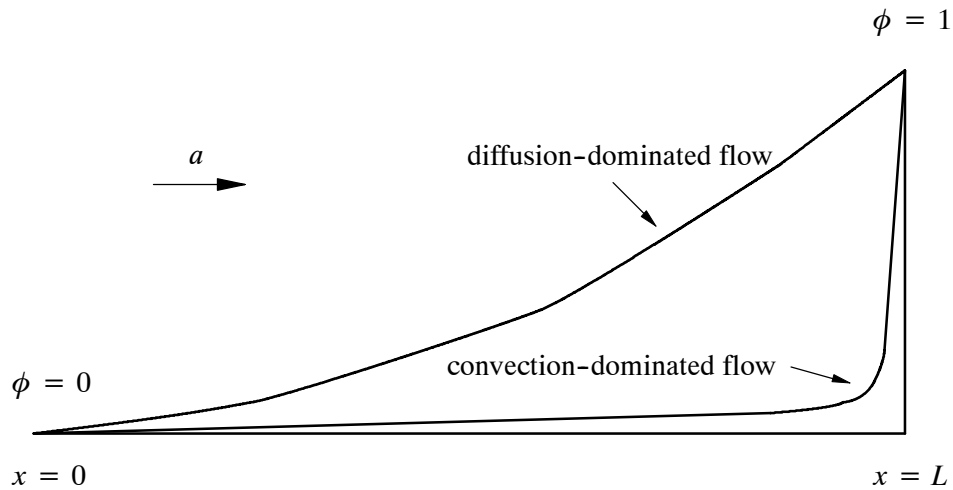


Fig. 3.1: Sketch of analytical solutions in convection- and diffusion-dominated case

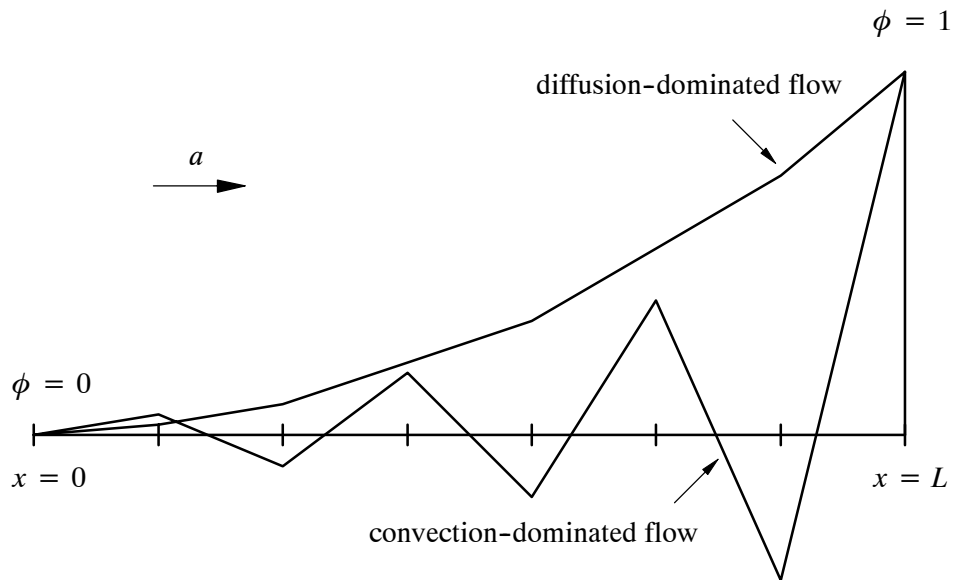


Fig. 3.2: Sketch of numerical solutions in convection- and diffusion-dominated case

Mathematical analysis of the problem

The focus is still leveled at the model case of a stationary convection-diffusion equation. In variational formulation after the introduction of the finite element functions, it looks like

$$\left(w^h, a \frac{d\phi^h}{dx} \right)_{\Omega} + \left(\frac{dw^h}{dx}, \kappa \frac{d\phi^h}{dx} \right)_{\Omega} = (w^h, f)_{\Omega} \quad (3.81)$$

with the right hand side f being introduced again. This model case reduces the convection-diffusion-reaction equation in general form to a crucial balance of a convective and a diffusive term quantitatively expressed by the element Peclet number (3.80) for a discretization with characteristic element length h . Two properties for a bilinear form like (3.81) which is expressed more generally as

$$B(w^h, \phi^h) = (w^h, f)_\Omega \quad (3.82)$$

have to be established in order to prove that a method converges: consistency and stability. Additionally, interpolation estimates for the finite element functions of the standard Galerkin finite element method have to be carried out, but they will be omitted here. It is straightforward to prove the consistency of the bilinear form of (3.81), since (3.81) has been achieved by applying a weighted residual method. Subtracting the general bilinear form for the exact solution

$$B(w^h, \phi) = (w^h, f)_\Omega \quad (3.83)$$

from (3.82) results in

$$B(w^h, \phi^h - \phi) = 0 \quad (3.84)$$

due to the conditions of bilinearity of B . (3.84) establishes that the error $e = \phi^h - \phi$ is orthogonal to all test functions $w^h \in \mathcal{V}_\phi^h$ with respect to the bilinear form B (Galerkin orthogonality). The problem is to be found within the proof of the stability condition, also termed condition of V-ellipticity, requiring

$$B(w^h, w^h) \geq c \|w^h\|^2 \quad (3.85)$$

with c being a constant and $\|\cdot\|$ some norm defined on \mathcal{V}_ϕ^h . For (3.81), this results in

$$B(w^h, w^h) = \kappa \|\nabla w^h\|_0^2 \quad \forall w^h \in \mathcal{V}_\phi^h \quad (3.86)$$

For $Pe \rightarrow \infty$, κ may become very small revealing a serious deficiency of the standard Galerkin finite element method. An estimate of the error e in Hughes (1987) reading

$$\|\nabla e\| = o((1 + Pe^e)h) \quad (3.87)$$

shows the definite dependency of the error e on the element Peclet number Pe^e yielding an optimal error bound for diffusion-dominated flows with small Pe^e and the loss of it for Pe^e increasing.

3.4.2 Pressure oscillations and the role of the inf-sup-condition

Mathematical analysis of the problem

In order to explain the problem of potential pressure oscillations it is sufficient to concentrate on the stationary Stokes equations, i.e. (2.75) without the time-dependent term along with the continuity equation (2.42), reading

$$\nabla p - 2\nu\nabla \cdot \varepsilon(\mathbf{u}) = \mathbf{f} \quad \text{in } \Omega \times (0, T) \quad (3.88)$$

$$\nabla \cdot \mathbf{u} = 0 \quad \text{in } \Omega \times (0, T) \quad (3.89)$$

The omitted time-dependent and nonlinear convective terms do not have a direct influence on the core of the problem. The variational formulation of (3.88)-(3.89) reads

$$-(\nabla \cdot \mathbf{v}, p)_\Omega + (\varepsilon(\mathbf{v}), 2\nu\varepsilon(\mathbf{u}))_\Omega - (q, \nabla \cdot \mathbf{u})_\Omega = (\mathbf{v}, \mathbf{f})_\Omega \quad (3.90)$$

with homogeneous Dirichlet boundary conditions assumed on the complete boundary for simplicity. The theory of mixed finite element methods governing (3.90) is explicitly described in Brezzi and Fortin (1991). As a result, it bears a constraint alternatively called inf-sup-condition, LBB-condition or BB-condition. The condition, howsoever named, demands the existence of a constant c such that

$$\inf_{0 \neq q^h \in \mathcal{Q}_p^h} \sup_{0 \neq \mathbf{v}^h \in \mathcal{Q}_u^h} \frac{(\nabla \cdot \mathbf{v}^h, q^h)}{\|\mathbf{v}^h\|_1 \|q^h\|_0} \geq c \quad (3.91)$$

for any characteristic length h . After all, (3.91) determines the relationship between function spaces for the velocity and pressure approximation. In particular, the convenient choice of equal-order interpolations for velocity and pressure is ruled out to be a stable method by condition (3.91).

Alternatively, the problem may be observed by inspecting the matrix system resulting from (3.90) by following the usual steps. In the end, it looks like

$$\begin{bmatrix} \mathbf{V} & \mathbf{G} \\ \mathbf{G}^T & \mathbf{0} \end{bmatrix} \cdot \begin{bmatrix} \mathbf{u} \\ \mathbf{p} \end{bmatrix} = \begin{bmatrix} \mathbf{F} \\ \mathbf{0} \end{bmatrix} \quad (3.92)$$

with the matrix and vector definitions of section 3.3.4. It is evident that the matrix system (3.92) is singular, if the kernel of \mathbf{G} is not equal to zero, i.e.

$$\text{Ker } \mathbf{G} \neq \{0\} \quad (3.93)$$

This means that pressure solutions $\mathbf{p} \neq \mathbf{0}$ appear belonging to the zero eigenvalues of matrix \mathbf{G} and, hence, resulting in $\mathbf{G}\mathbf{p} = \mathbf{0}$ for these non-zero pressure solutions. This fatal result may be blamed on the fact that the only term testing the pressure in (3.90), namely $-(\nabla \cdot \mathbf{v}^h, p^h)_{\Omega}$ after the introduction of the finite element functions, is not equipped with a sufficient number of weighting functions for \mathbf{v}^h to 'rule out' all artificial pressure modes. In consequence, the weighting function space \mathcal{Q}_u^h is definitely too small in this case.

Satisfying the inf-sup-condition by a proper choice of interpolation functions

Two procedures may be distinguished to solve the problem, confer Franca and Hughes (1988). On the one hand, the variational formulation (3.90) may be enhanced by introducing additional terms which will also weight and potentially 'rule out' artificial pressure modes. This concept named 'Circumventing Babuska-Brezzi' (CBB) will be inherent for the multiscale methods to be presented in the following. However, the alternative concept of 'Satisfying Babuska-Brezzi' (SBB) should at least be addressed briefly for one explicit example of choosing the interpolation functions. Simply spoken, SBB means increasing the number of velocity functions with respect to the number of pressure functions. In the end, the interpolation for the pressure must be at least one order lower than the one for the velocity.

One element satisfying the inf-sup-condition is the so-called Taylor-Hood quadrilateral element (Taylor and Hood (1973)). In its original version in the two-dimensional case, it is constituted by a serendipity-type quadratic interpolation with 8 degrees of freedom for each spatial direction of the velocity and a bilinear interpolation with 4 degrees of freedom for the pressure ($\mathcal{Q}_2^{(8)}\mathcal{Q}_1$). The slightly different element with a biquadratic velocity interpolation with 9 degrees

of freedom (Q_2Q_1) is also often termed to be a Taylor-Hood element. Concerning these and a tabulation of other elements in 2-D and 3-D satisfying the inf-sup-condition please consult, for instance, Gresho and Sani (1998) or Gunzburger (1989).

4 A Brief Insight into Turbulence

This chapter aims at providing the reader with a short introduction into some characteristics of turbulent flows. The bounds of this work allow no exhaustive description of all aspects of turbulence. For example, everything but the famous Kolmogorov energy spectrum which is related to a spectral description will be omitted, since numerical methods 'living' in the physical space are merely considered afterwards. Due to this necessary lack of completeness, the reader will now be given a longer list of references dealing with the topics of turbulence for consultation. Proceeding in chronological order of their first appearance, it is started with the classic monographs of Batchelor (1953), Townsend (1956), and Hinze (1959). At the beginning of the 1970's, a large number of books were published, e.g. Bradshaw (1971), Panchev (1971), the exhaustive two-volume work of Monin and Yaglom (1971/1975), Tennekes and Lumley (1972), Rotta (1972), Launder and Spalding (1972), as well as Leslie (1973). More recent works are the ones of Landahl and Mollo-Christensen (1986), Lesieur (1990), McComb (1990), and Frisch (1995). About three years ago, the books of Mathieu and Scott (2000) as well as Pope (2000) have been published.

4.1 What is so special about turbulent flows ?

4.1.1 Laminar vs. turbulent flow

For 'low enough' Reynolds number, flows can be described as 'well-behaved', largely controlled by viscous diffusion. Such flow regimes are called laminar due to an idea of fluid motion within orderly 'laminae'. With increasing Reynolds number, laminar flow regimes become unstable. Passing a transitional stage, the range of turbulent flow regimes is entered¹. In the turbulent regime, the main velocity field is superimposed by random velocity fluctuations making a comprehensive theoretical solution approach hopeless. However, nearly all flows of practical engineering interest are in fact turbulent. This indicates its importance and, thus, the need of finding adequate solution methods. Depending on one's personal point of view, dealing with turbulent flows may be described as being attractive by an optimist, challenging by a neutral person or terrible by a pessimist. Please remember the quoting of Peter Bradshaw given at the beginning of the general introduction classifying turbulence as "*the invention of the devil on the seventh day of creation*". The two major problems in solving the Navier-Stokes equations within turbulent flow regimes will now be addressed within the following two sections.

4.1.2 Random feature of turbulent flows

The usual approach to a description of turbulence is based on methods of statistics. The necessity to fall back on this way of describing is due to the appearance of the random velocity fluctuations forcing us to leave the 'safe ground' of deterministic methods. Although it sounds hardly believa-

1. The perception of the existence of two quite different flow regimes goes back to Osborne Reynolds proving this in his famous experiment where he injected a dye streak into a pipe flow and observed its behaviour.

ble on first sight that deterministic equations are the source of random solutions, this may be explained precisely by the existence of the nonlinear convective term. The basic reason for the causalness of the solutions lies, on the one hand, in unavoidable perturbations e.g. in initial conditions, boundary conditions and material parameters and, on the other hand, in the high sensitivity of instantaneous values of turbulent flows to all these perturbations. However, the statistical averages do not show this sensitivity predestinating this approach for use in the analysis of turbulent flows. Some measures for the statistical description of turbulence may be found in appendix A.

4.1.3 Wide range of scales

The second important problem related to turbulent flows besides its random feature is the wide range of scales usually linked with such a flow. For instance, a crude measure for the range of length scales depending on the Reynolds number reads

$$\frac{L}{\eta} \sim \text{Re}_L^{\frac{3}{4}} \quad (4.1)$$

with L denoting a measure of the largest scales, the smallest so-called Kolmogorov scale η and the Reynolds number Re_L based on L and a related velocity measure U . For instance, a flow with a thoroughly usual Re_L of about 10^6 bears a smallest scale η being about 32,000 times smaller than the largest scales in this flow. There is also a chance besides the burden. In particular, this wide range of scales also opens a wide field for the application of multiscale methods for reasonable numerical solutions of such problems. In fact, it may be viewed as a challenging 'playground' for multiscale methods offering the opportunity to show their qualities.

4.2 The Reynolds equation and its closure problem

4.2.1 Reynolds decomposition

Based on, for instance, time or ensemble averaging (see appendix A), the velocity $\mathbf{u}(\mathbf{x}, t)$ may be decomposed into a mean value $\langle \mathbf{u}(\mathbf{x}, t) \rangle$ and a fluctuating part $\tilde{\mathbf{u}}(\mathbf{x}, t)$ such that

$$\mathbf{u}(\mathbf{x}, t) = \langle \mathbf{u}(\mathbf{x}, t) \rangle + \tilde{\mathbf{u}}(\mathbf{x}, t) \quad (4.2)$$

and, accordingly, the pressure such that

$$p(\mathbf{x}, t) = \langle p(\mathbf{x}, t) \rangle + \tilde{p}(\mathbf{x}, t) \quad (4.3)$$

Spatial and temporal differentiation commute with averaging revealing

$$\left\langle \frac{\partial \mathbf{u}}{\partial t} \right\rangle = \frac{\partial \langle \mathbf{u} \rangle}{\partial t}, \quad \langle \nabla \mathbf{u} \rangle = \nabla \langle \mathbf{u} \rangle \quad (4.4)$$

The continuity equation (2.45) formulated for the mean flow with the help of (4.4) reads

$$\nabla \cdot \langle \mathbf{u} \rangle = 0 \quad (4.5)$$

By the way, subtracting (4.5) from (2.45) shows that the fluctuations are also divergence-free:

$$\nabla \cdot \tilde{\mathbf{u}} = 0 \quad (4.6)$$

The introduction of (4.2), (4.3) and (4.4) into the momentum equation (2.46) leads to the momentum equation for the mean flow reading

$$\frac{\partial \langle \mathbf{u} \rangle}{\partial t} + \nabla \cdot (\langle \mathbf{u} \otimes \mathbf{u} \rangle) + \nabla \langle p \rangle - 2\nu \nabla \cdot \varepsilon (\langle \mathbf{u} \rangle) = \mathbf{0} \quad (4.7)$$

where the right hand side \mathbf{f} is omitted for simplicity.

4.2.2 Reynolds stress tensor

The problematic aspect of (4.7) is the averaging of the nonlinear convective term. Using (4.2), it may be expanded as

$$\begin{aligned} \langle \mathbf{u} \otimes \mathbf{u} \rangle &= \langle (\langle \mathbf{u} \rangle + \tilde{\mathbf{u}}) \otimes (\langle \mathbf{u} \rangle + \tilde{\mathbf{u}}) \rangle \\ &= \langle (\langle \mathbf{u} \rangle \otimes \langle \mathbf{u} \rangle + \langle \mathbf{u} \rangle \otimes \tilde{\mathbf{u}} + \tilde{\mathbf{u}} \otimes \langle \mathbf{u} \rangle + \tilde{\mathbf{u}} \otimes \tilde{\mathbf{u}}) \rangle \\ &= \langle \mathbf{u} \rangle \otimes \langle \mathbf{u} \rangle + \langle \tilde{\mathbf{u}} \otimes \tilde{\mathbf{u}} \rangle \end{aligned} \quad (4.8)$$

where it has been taken advantage of

$$\langle \langle \mathbf{u} \rangle \rangle = \langle \mathbf{u} \rangle, \quad \langle \tilde{\mathbf{u}} \rangle = \mathbf{0} \quad (4.9)$$

and

$$\langle (\langle \mathbf{u} \rangle \otimes \tilde{\mathbf{u}}) \rangle = \mathbf{0} \quad (4.10)$$

As a result, the so-called Reynolds equation reading

$$\begin{aligned} \frac{\partial \langle \mathbf{u} \rangle}{\partial t} + \nabla \cdot (\langle \mathbf{u} \rangle \otimes \langle \mathbf{u} \rangle) + \nabla \langle p \rangle \\ - \nabla \cdot (2\nu \varepsilon (\langle \mathbf{u} \rangle) - \langle \tilde{\mathbf{u}} \otimes \tilde{\mathbf{u}} \rangle) = \mathbf{0} \end{aligned} \quad (4.11)$$

is obtained where the last term on the left hand side is constituted by the so-called Reynolds stress tensor². It has been arranged within (4.11) according to its physical interpretation as stress in order to get an overall stress term constituted by the viscous stress and the Reynolds stress. The Reynolds stress tensor is the only component of (4.11) distinguishing it from a momentum equation like (2.46) formulated for the mean values $\langle \mathbf{u} \rangle$ and $\langle p \rangle$. However, it is the crucial component of (4.11), since it 'brings the turbulence into this equation'.

The analogy to the viscous stress lies in the fact that both stem from momentum transfer. The viscous stress results from momentum transfer at the molecular level whereas the Reynolds stress results from momentum transfer by the fluctuating velocity field. Therefore, a Reynolds stress tensor may be built up analog to the viscous stress tensor (2.17) as

$$\boldsymbol{\tau}^R = \begin{pmatrix} \langle \tilde{u}_1 \tilde{u}_1 \rangle & \langle \tilde{u}_1 \tilde{u}_2 \rangle & \langle \tilde{u}_1 \tilde{u}_3 \rangle \\ \langle \tilde{u}_2 \tilde{u}_1 \rangle & \langle \tilde{u}_2 \tilde{u}_2 \rangle & \langle \tilde{u}_2 \tilde{u}_3 \rangle \\ \langle \tilde{u}_3 \tilde{u}_1 \rangle & \langle \tilde{u}_3 \tilde{u}_2 \rangle & \langle \tilde{u}_3 \tilde{u}_3 \rangle \end{pmatrix} \quad (4.12)$$

(4.12) is symmetric with $\langle \tilde{u}_i \tilde{u}_i \rangle$ indicating normal stresses and $\langle \tilde{u}_i \tilde{u}_j \rangle (i \neq j)$ indicating shear stresses. Half the trace of the Reynolds stress tensor in the form (4.12) is defined to be the turbulent kinetic energy, i.e.

2. More precisely, the stress tensor is usually termed to be the respective term multiplied by the density.

$$k(\mathbf{x}, t) = \frac{1}{2} \langle \tilde{\mathbf{u}}(\mathbf{x}, t) \cdot \tilde{\mathbf{u}}(\mathbf{x}, t) \rangle \quad (4.13)$$

Analog to the viscous tensor, $\boldsymbol{\tau}^R$ may be written as the sum of a spherical tensor depending on the turbulent kinetic energy k subject to

$$\frac{2}{3}k\mathbf{I} = \begin{bmatrix} \frac{2}{3}k & 0 & 0 \\ 0 & \frac{2}{3}k & 0 \\ 0 & 0 & \frac{2}{3}k \end{bmatrix} \quad (4.14)$$

and a deviatoric tensor $dev \boldsymbol{\tau}^R$ being defined as

$$dev \boldsymbol{\tau}^R = \boldsymbol{\tau}^R - \frac{2}{3}k\mathbf{I} = \begin{bmatrix} \langle \tilde{u}_1 \tilde{u}_1 \rangle - \frac{2}{3}k & \langle \tilde{u}_1 \tilde{u}_2 \rangle & \langle \tilde{u}_1 \tilde{u}_3 \rangle \\ \langle \tilde{u}_2 \tilde{u}_1 \rangle & \langle \tilde{u}_2 \tilde{u}_2 \rangle - \frac{2}{3}k & \langle \tilde{u}_2 \tilde{u}_3 \rangle \\ \langle \tilde{u}_3 \tilde{u}_1 \rangle & \langle \tilde{u}_3 \tilde{u}_2 \rangle & \langle \tilde{u}_3 \tilde{u}_3 \rangle - \frac{2}{3}k \end{bmatrix} \quad (4.15)$$

Transferring this decomposition to (4.11) yields

$$\begin{aligned} \frac{\partial \langle \mathbf{u} \rangle}{\partial t} + \nabla \cdot (\langle \mathbf{u} \rangle \otimes \langle \mathbf{u} \rangle) + \nabla \left(\langle p \rangle + \frac{2}{3}k \right) \\ - \nabla \cdot (2\nu\varepsilon \langle \mathbf{u} \rangle - dev \boldsymbol{\tau}^R) = \mathbf{0} \end{aligned} \quad (4.16)$$

demonstrating that the spherical part of $\boldsymbol{\tau}^R$ may be subsumed in a modified term for the mean pressure and the deviatoric part of $\boldsymbol{\tau}^R$ is the part being more effective in momentum transport than the spherical part.

4.2.3 Closure problem

Unfortunately, a severe imbalance between the number of equations and the number of unknowns has occurred. Starting from the initial position with four equations, i.e. 3 components of the momentum equation and the continuity equation, for four unknowns u_1 , u_2 , u_3 and p , the introduction of the symmetric Reynolds stress tensor bears six additional unknowns with no additional equation for their solution. By multiplying the momentum component equations with a fluctuating value and averaging the product afterwards, differential equations for the components of the Reynolds stress tensor can be derived. This makes the problem worse though. It brings up 6 new equations (one for each independent component of $\boldsymbol{\tau}^R$), but also 22 additional new unknowns of the form $\langle \tilde{\mathbf{u}} \otimes \tilde{\mathbf{u}} \otimes \tilde{\mathbf{u}} \rangle$. With every higher and higher moment applied to the momentum equation it becomes even worse in bearing more and more unknowns with no chance of reaching a balance between equations and unknowns - a situation typical for all nonlinear stochastic systems. During the averaging process, information is removed from the Navier-Stokes equations which cannot return. This describes the closure problem which has to be overcome by a modeling process in practice.

4.2.4 Boussinesq's turbulent (eddy) viscosity assumption

The basic modeling hypothesis consists in the introduction of a (here kinematic) turbulent viscosity (also named eddy viscosity) ν^T . This simple ansatz goes back to work of Valentin Joseph

Boussinesq (1842–1929) in the year 1877 (see Boussinesq (1877)). The hypothesis exploits the aforementioned analogy of momentum transfer at the molecular level and by the fluctuating velocity field. Despite its (in the meantime well-known) limitations it is still a widespread used modeling procedure and, moreover, the basis for more sophisticated models. For elaboration of the analogy of the molecular and turbulent transport of momentum the Boussinesq hypothesis relies on and its limitations, the reader may consult the literature mentioned in the introductory part of this chapter and e.g. Wilcox (1998).

Analog to Stokes' hypothesis (2.22) governing the relation between the viscous stress and the rate-of-velocity tensor for a Newtonian fluid, Boussinesq assumes a linear connection between the deviatoric part of the Reynolds stress tensor and the rate-of-velocity tensor for the mean flow reading

$$- \text{dev } \boldsymbol{\tau}^R = 2\nu^T \boldsymbol{\varepsilon}(\langle \mathbf{u} \rangle) \quad (4.17)$$

Incorporating (4.17) into the Reynolds equation (4.16) yields

$$\begin{aligned} \frac{\partial \langle \mathbf{u} \rangle}{\partial t} + \nabla \cdot (\langle \mathbf{u} \rangle \otimes \langle \mathbf{u} \rangle) + \nabla \left(\langle p \rangle + \frac{2}{3} k \mathbf{I} \right) \\ - 2\nabla \cdot ((\nu + \nu^T) \boldsymbol{\varepsilon}(\langle \mathbf{u} \rangle)) = \mathbf{0} \end{aligned} \quad (4.18)$$

In consequence, one ends up with the original momentum equation (2.46) formulated for the mean flow with a modified mean pressure and an effective kinematic viscosity

$$\nu^{eff}(\mathbf{x}, t) = \nu + \nu^T(\mathbf{x}, t) \quad (4.19)$$

replacing the kinematic physical viscosity alone. With the Boussinesq hypothesis being introduced, the closure problem has been overcome and the Navier-Stokes equations for the mean flow (4.5) and (4.18) can be solved provided that the turbulent viscosity ν^T can be specified.

4.2.5 Prandtl's mixing-length hypothesis

By exclusively arguing on dimensional grounds, one may state that the kinematic turbulent viscosity ν^T must be put together by some velocity ν and some length l in the sense that

$$\nu^T \sim \nu l \quad (4.20)$$

Prandtl (1925) specified this initial guess physically by introducing the mixing-length hypothesis which further exploits the analogy of momentum transfer on the molecular level and by turbulent fluctuating velocities. According to this, the mixing length l_{mix} is the analogon to the mean free path on the molecular level within the kinetic theory of gases. A mixing velocity ν_{mix} is then based on this mixing length and a measure of the rate-of-velocity tensor of the mean flow subject to

$$\nu_{mix} = \text{const } l_{mix} \text{ meas}(\boldsymbol{\varepsilon}(\langle \mathbf{u} \rangle)) \quad (4.21)$$

with some constant factor. Absorbing the constant in (4.21) and the proportionality constant leading to an equation in (4.20) in the mixing length l_{mix} , one obtains Prandtl's definition of the turbulent viscosity as

$$\nu^T = l_{mix}^2 \text{ meas}(\boldsymbol{\varepsilon}(\langle \mathbf{u} \rangle)) \quad (4.22)$$

Admittedly, Prandtl has merely shifted the crucial problem from finding a specification for Boussinesq's turbulent viscosity ν^T to finding a specification for the mixing length l_{mix} . However, he has gone a substantial step further, since the mixing length is more open to physical reasoning. Within the scope of numerical methods, a length definition being characteristic for the respective discretization replacing in somehow modified form l_{mix} is appropriate in order to close the overall problem. This idea will be picked up again below.

4.3 Spatial and temporal scales based on two-point correlations

4.3.1 The benefit and burden of two-point correlation

Up to now, a one-point correlation in form of the Reynolds stress has already been considered as a way to describe the effect of turbulence within the resulting momentum equation. Here, one-point means that the velocity at one particular point in space and time is viewed as a measure for the turbulent flow. However, this is not a sufficient proceeding in general. Due to the presence of the pressure, the motion at one point is rather affected by the motion at other points separated from the original point both in space and time. Generally, a correlation between the velocity fluctuations at two points being separated spatially and temporally can be defined as

$$\mathbf{R}^{ST}(\mathbf{x}_1, \mathbf{x}_2, t_1, t_2) = \langle \tilde{\mathbf{u}}(\mathbf{x}_1, t_1) \otimes \tilde{\mathbf{u}}(\mathbf{x}_2, t_2) \rangle \quad (4.23)$$

The bulk of information contained in a two-point correlation like (4.23) may easily be imagined. By introducing some restrictions in (4.23), it is possible to identify some relevant scales yet. Basically, the correlation in space and time will be clearly distinguished in order to obtain spatial and temporal scales describing the respective correlations.

4.3.2 Spatial scales

The two-point correlation tensor based on a spatial separation assumes homogeneous turbulence and is defined as

$$\mathbf{R}^S(\mathbf{x}, t; \mathbf{r}) = \langle \tilde{\mathbf{u}}(\mathbf{x}, t) \otimes \tilde{\mathbf{u}}(\mathbf{x} + \mathbf{r}, t) \rangle = \mathbf{R}^S(t; \mathbf{r}) \quad (4.24)$$

where \mathbf{r} denotes the vector specifying the geometrical distance between the two points in space. (4.24) does obviously not depend on the location \mathbf{x} due to the assumption of homogeneity. The Reynolds stress tensor is recovered by setting $\mathbf{r} = \mathbf{0}$ in (4.24) revealing

$$\boldsymbol{\tau}^R(\mathbf{x}, t) = \mathbf{R}^S(\mathbf{x}, t; \mathbf{0}) = \langle \tilde{\mathbf{u}}(\mathbf{x}, t) \otimes \tilde{\mathbf{u}}(\mathbf{x}, t) \rangle \quad (4.25)$$

The most important aspect to be observed is the tendency of decorrelation with the spatial separation \mathbf{r} increasing. This may be analyzed, for example, for the first diagonal element of (4.24) at some point in time $R_{11}^S(\mathbf{r})$ with $\mathbf{r} = (r_1, 0, 0)$ being representative in its qualitative progress for other elements of \mathbf{R}^S and other directions of \mathbf{r} . Scaling $R_{11}^S(r_1, 0, 0)$ by the one-point correlation $R_{11}^S(0, 0, 0) = \langle \tilde{u}_1 \tilde{u}_1 \rangle$, the resulting spatial correlation coefficient reads

$$\rho_{11}^S(r_1, 0, 0) = \frac{R_{11}^S(r_1, 0, 0)}{\langle \tilde{u}_1 \tilde{u}_1 \rangle} \quad (4.26)$$

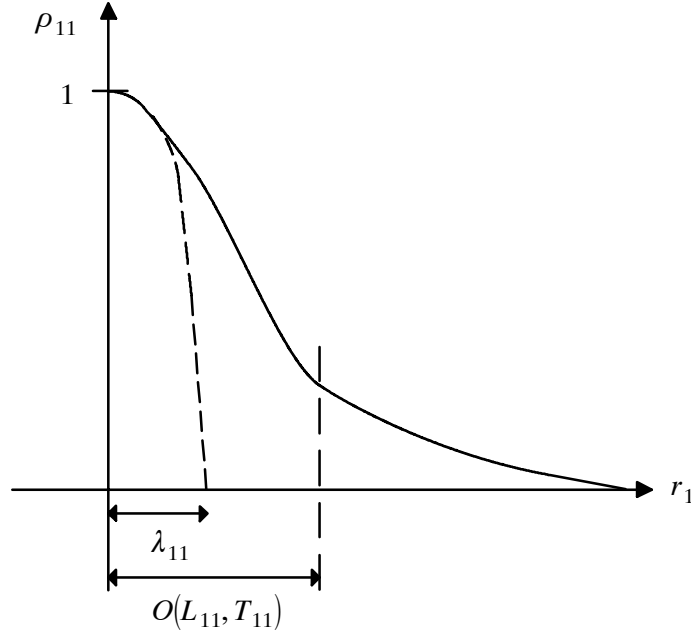


Fig. 4.1: Principal sketch of spatial (temporal) correlation coefficient

The course of $\rho_{11}^S(r_1, 0, 0)$ depending on the separation r_1 is sketched in Fig. 4.1 in principal. It is to be observed that ρ_{11} is a symmetric function starting at $r_1 = 0$ with unit value and decreasing to zero for $|r_1| \rightarrow \infty$. As a measure of the length over which the order of separation is significantly nonzero, the integral length scale $L_{11}^{[1]}$ is introduced with its definition

$$L_{11}^{[1]} = \int_0^{\infty} \rho_{11}^S(r_1, 0, 0) dr_1 \quad (4.27)$$

The second measure displayed in Fig. 4.1 is the Taylor microscale $\lambda_{11}^{[1]}$ defined as

$$\lambda_{11}^{[1]} = \sqrt{-\frac{2}{\left(\frac{\partial^2 \rho_{11}^S}{\partial r_1^2}\right)_{r_1=0}}} \quad (4.28)$$

which hopefully becomes somewhat more distinct by its geometric interpretation. Creating a parabola which osculates, i.e. matches the curvature of, $\rho_{11}^S(r_1, 0, 0)$ at $r_1 = 0$ (indicated in Fig. 4.1 as a dashed line), the Taylor microscale $\lambda_{11}^{[1]}$ may be interpreted as the intersection of the osculating parabola with the r_1 -axis. Although both spatial scales, the integral scale and the Taylor microscale, have been defined here for a particular component of \mathbf{R}^S in a particular direction, the definition can be transferred to other components and other directions in a straightforward manner.

4.3.3 Temporal scales

Analog to the procedure for a spatial separation, a two-point correlation tensor based on a temporal separation, also named auto-correlation tensor, is defined by assuming a steady flow as

$$\mathbf{R}^T(\mathbf{x}, t; s) = \langle \tilde{\mathbf{u}}(\mathbf{x}, t) \otimes \tilde{\mathbf{u}}(\mathbf{x}, t + s) \rangle = \mathbf{R}^T(\mathbf{x}; s) \quad (4.29)$$

where s denotes the time of separation at one point in space. (4.29) does obviously not depend on the point in time t due to the steadiness assumption. Again, the Reynolds stress tensor is recovered by setting $s = 0$ in (4.29) yielding

$$\boldsymbol{\tau}^R(\mathbf{x}, t) = \mathbf{R}^T(\mathbf{x}, t; 0) = \langle \tilde{\mathbf{u}}(\mathbf{x}, t) \otimes \tilde{\mathbf{u}}(\mathbf{x}, t) \rangle \quad (4.30)$$

With the time delay s increasing, a tendency of decorrelation will be observed. Analyzing this again for the first diagonal element of (4.29) at some point in space $R_{11}^T(s)$, a temporal (or auto-) correlation coefficient

$$\rho_{11}^T(s) = \frac{R_{11}^S(s)}{\langle \tilde{u}_1 \tilde{u}_1 \rangle} \quad (4.31)$$

may be defined with the one-point scaling factor $R_{11}^T(0)$ being equivalent to $R_{11}^S(0, 0, 0)$ in (4.26). Displaying the course of $\rho_{11}^T(0)$ now depending on the time separation s instead of the spatial separation r_1 yields a very similar picture as can be seen in Fig. 4.1. The integral time scale T_{11} replacing $L_{11}^{[1]}$ reads

$$T_{11} = \int_0^{\infty} \rho_{11}^T(s) ds \quad (4.32)$$

and the micro-time scale λ_{11}^T replacing $\lambda_{11}^{[1]}$ reads

$$\lambda_{11}^T = \sqrt{-\frac{2}{\left(\frac{\partial^2 \rho_{11}^T}{\partial s^2}\right)_{s=0}}} \quad (4.33)$$

Again, the analysis for this particular component of \mathbf{R}^T bears representative temporal scales also for other components.

4.4 Richardson's energy cascade and Kolmogorov energy spectrum

The turbulent kinetic energy or, more precisely, its distribution among the scales of various size is the topic of this section. Two concepts are helpful in understanding the physical processes involved. Firstly, the idea of an energy cascade introduced by Lewis Fry Richardson (1881-1953) in Richardson (1922) qualifies the process. Secondly, the later introduced hypotheses of Andrei Nikolaevich Kolmogorov (1903-1987) in Kolmogorov (1941) (republished in an English translation in Kolmogorov (1991) on the occasion of the fiftieth anniversary of the original publication) quantify this view. These two concepts are, for instance, described in Pope (2000), section 6.1, which the following short summary is mostly relied on.

4.4.1 Richardson's energy cascade

At the outset of Richardson's energy cascade, the kinetic energy is introduced by productive mechanisms at the largest scales. Following the picture of a cascade, the energy is then transmitted to smaller and smaller scales by processes not depending on the molecular viscosity ν . The visco-

sity merely acts at the end of the process enforcing dissipation of the energy. The end of the cascade is characterized by the smallest scales of motion. The basic constituents of turbulence are eddies of various scale sizes ranging from very large to very small ones. The energy cascade proceeds due to a breaking up of larger eddies which transfers the energy formerly attributed to these larger scales to smaller eddies. This goes on until a finally stable eddy motion is reached and dissipation of kinetic energy can take place. Hence, the rate of dissipation ε is actually caused by the transfer of energy from the largest eddies subject to

$$\varepsilon = - \frac{dk}{dt} \quad (4.34)$$

which is independent of the molecular viscosity ν . It scales as

$$\varepsilon \sim \frac{U^3}{L} \quad (4.35)$$

with U and L being a typical velocity and length scale of the largest eddies, respectively. As a measure for L , it may be fallen back upon the integral length scale $L_{11}^{[1]}$ introduced in section 4.3.2.

4.4.2 Kolmogorov's hypotheses and Kolmogorov scales

Kolmogorov quantified Richardson's picture of an energy cascade. In particular, he identified the smallest scales in this energetic process which are named in his honour thus. He formulated 3 hypotheses all being valid only for a flow with a sufficiently high Reynolds number. The first one is his **hypothesis of local isotropy** stating that the small-scale turbulent motions, i.e. the ones with a characteristic length scale $l \ll L$, are statistically isotropic. Pope (2000) introduces a length scale $l_{EI} \approx (1/6)L$ denoting the limit between the anisotropic larger eddies and the isotropic smaller eddies. Using this definition, Kolmogorov's **first similarity hypothesis** is formulated as follows: For all scales $l < l_{EI}$, the statistics has a universal form uniquely determined by the rate of dissipation ε and the viscosity ν . Hence, the range $l < l_{EI}$ may be named the universal equilibrium range. Using only the two values ε and ν , a length scale

$$\eta = \left(\frac{\nu^3}{\varepsilon} \right)^{\frac{1}{4}} \quad (4.36)$$

a velocity scale

$$u_\eta = \sqrt[4]{\varepsilon \nu} \quad (4.37)$$

and a time scale

$$\tau_\eta = \sqrt{\frac{\nu}{\varepsilon}} \quad (4.38)$$

can be created. These so-called Kolmogorov scales assemble a Reynolds number

$$\text{Re}_\eta = \frac{\eta u_\eta}{\nu} = 1 \quad (4.39)$$

marking the lower end of the scale range. These smallest scales can now be related to the largest scales using the scaling law (4.35) and the concept of the energy cascade stating that we encounter a constant rate of dissipation throughout the complete transfer process. This results in a length scale ratio

$$\frac{\eta}{L} \sim \text{Re}_L^{-\frac{3}{4}} \quad (4.40)$$

a velocity scale ratio

$$\frac{u_\eta}{U} \sim \text{Re}_L^{-\frac{1}{4}} \quad (4.41)$$

and a time scale ratio

$$\frac{\tau_\eta}{T} \sim \text{Re}_L^{-\frac{1}{2}} \quad (4.42)$$

(4.40)-(4.42) show the unique dependence of the scale range width on the Reynolds number Re_L .

Kolmogorov's **second similarity hypothesis** further distinguishes an inertial subrange within the universal equilibrium range. The lower limit of this inertial subrange is indicated by the length scale l_{DI} . Beyond l_{DI} , the dissipation range is encountered. The crucial feature of the inertial subrange is its sole dependence on ε . Fig. 4.2 summarizes the just introduced ranges and length scales between the (problem dependent) maximum flow scale L_{\max} and the Kolmogorov length scale η for a flow at very high Reynolds number.

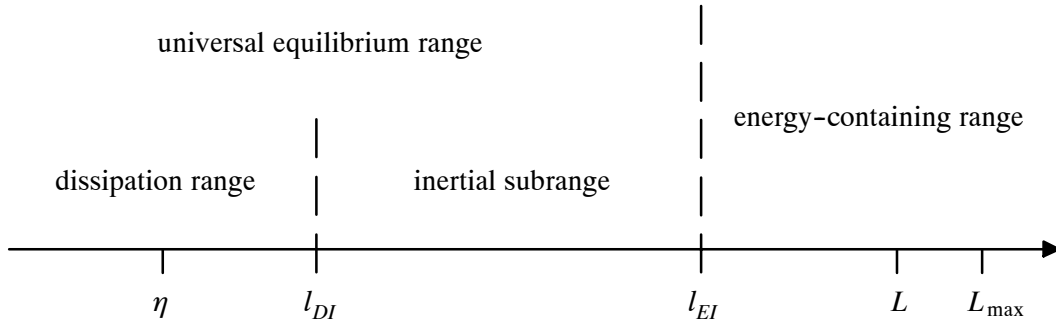


Fig. 4.2: Various length scales and ranges on a logarithmic scale (Pope 2000)

The last length scale of section 4.3.2 remaining to be categorized is the Taylor microscale λ . Based on an analysis of Taylor (1935), it may be assumed that for homogeneous isotropic turbulence

$$\frac{\lambda}{\eta} \approx 7 \left(\frac{L}{\eta} \right)^{\frac{1}{3}} \quad (4.43)$$

λ will usually lie within the inertial subrange and, hence, in a medium range between the largest and the smallest scales.

4.4.3 Kolmogorov energy spectrum

Starting point of the considerations in this section is the two-point correlation tensor based on a spatial separation \mathbf{R}^S defined in (4.24). Transferring this correlation into the spectral space by a Fourier transform yields the velocity spectrum tensor

$$\Phi(\boldsymbol{\kappa}, t) = \frac{1}{(2\pi)^3} \int_{-\infty}^{\infty} \int_{-\infty}^{\infty} \int_{-\infty}^{\infty} e^{-i\boldsymbol{\kappa}\mathbf{r}} \mathbf{R}^S(t; \mathbf{r}) d\mathbf{r} \quad (4.44)$$

with the usual relation between the wavenumber vector $\boldsymbol{\kappa}$ and the corresponding wavelength l subject to

$$l = \frac{2\pi}{|\boldsymbol{\kappa}|} \quad (4.45)$$

If all directional information is removed from (4.44), the energy spectrum function

$$E(\kappa, t) = \frac{1}{2} \int_{-\infty}^{\infty} \int_{-\infty}^{\infty} \int_{-\infty}^{\infty} \text{tr} \Phi(\boldsymbol{\kappa}, t) \delta(|\boldsymbol{\kappa}| - \kappa) d\boldsymbol{\kappa} \quad (4.46)$$

is obtained which depends on the scalar wavenumber κ . Summing over the complete range of scalar wavenumbers reveals the kinetic energy

$$\int_0^{\infty} E(\kappa, t) d\kappa = k(\mathbf{x}, t) \quad (4.47)$$

already introduced in (4.13) as half the trace of the Reynolds stress tensor. According to this, $E(\kappa, t) d\kappa$ denotes the contribution to $k(\mathbf{x}, t)$ contained in the modes between κ and $\kappa + d\kappa$. Certainly, both Kolmogorov's first and second similarity hypothesis also transfer to the spectral space. This means that there exists an inertial subrange $\kappa_{EI} < \kappa < \kappa_{DI}$ and a dissipation range $\kappa > \kappa_{DI}$. Kolmogorov's famous $-5/3$ -law was developed by a dimensional analysis and is valid within the inertial subrange. It reads

$$E(\kappa) = C_K \varepsilon^{\frac{2}{3}} \kappa^{-\frac{5}{3}}; \quad \kappa_{EI} < \kappa < \kappa_{DI} \quad (4.48)$$

where C_K denotes the Kolmogorov constant. The functional dependencies $E(\kappa)$ valid within the energy-containing range $\kappa < \kappa_{EI}$ and within the dissipation range $\kappa > \kappa_{DI}$ as well as the subsequent matching process yielding (4.48) will not be developed here. For this purpose, it is referred to the literature mentioned in the introduction of this chapter. However, the famous graphical display of the Kolmogorov energy spectrum is obligatory and, thus, shown in Fig. 4.3. The spectrum in Fig. 4.3 is typical for any turbulent flow. It is well established and confirmed in the meantime.

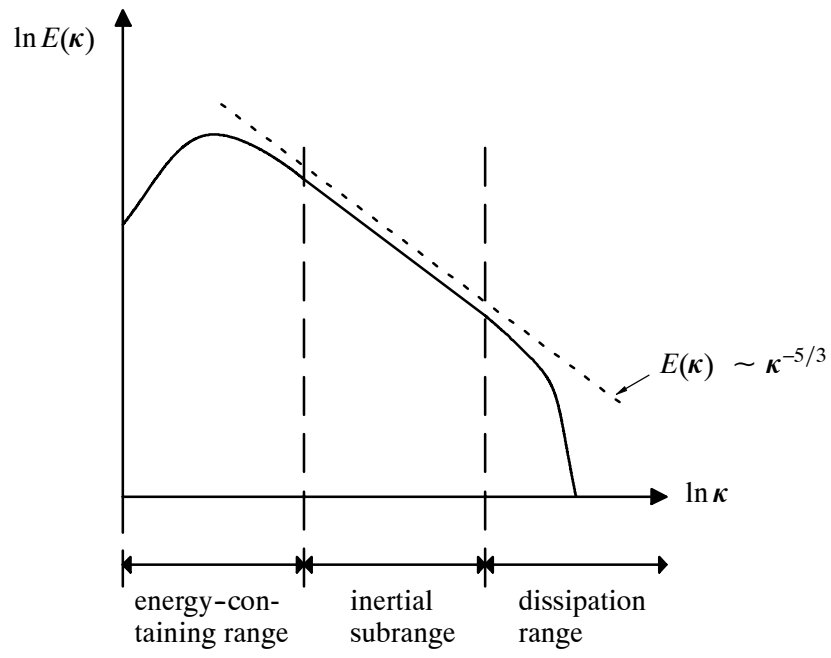


Fig. 4.3: Kolmogorov energy spectrum

5 Alternative Procedures for the Numerical Simulation of Turbulent Flows

5.1 Introduction

The standard Galerkin finite element method for the incompressible Navier–Stokes equations has been developed in the preceding chapter. By taking additional measures to overcome the numerical problems described in section 3.4, this method may be utilized to simulate laminar flow situations. However, new challenges have to be faced as soon as a turbulent flow regime is reached. This chapter is devoted to the introduction of three alternative procedures to adapt the standard Galerkin finite element method also to simulations of turbulent flow regimes. The first one, named Direct Numerical Simulation (DNS), does not need an adaption in principle. Thus, the respective section of this chapter is basically a statement of the unfeasibility of a DNS in general. In the author’s view, the most promising ‘tool’ for the numerical simulation of turbulent flows seems to be within the basic concept of Large Eddy Simulation (LES). It is intermediate in its requirement of computational effort between DNS and the simulation utilizing the Reynolds Averaged Navier–Stokes equations (RANS) which will be briefly introduced in the last section of this chapter. In Fig. 5.1, a comparison of the three procedures concerning the respective degree of modeling and resolution inherent in the method is displayed.

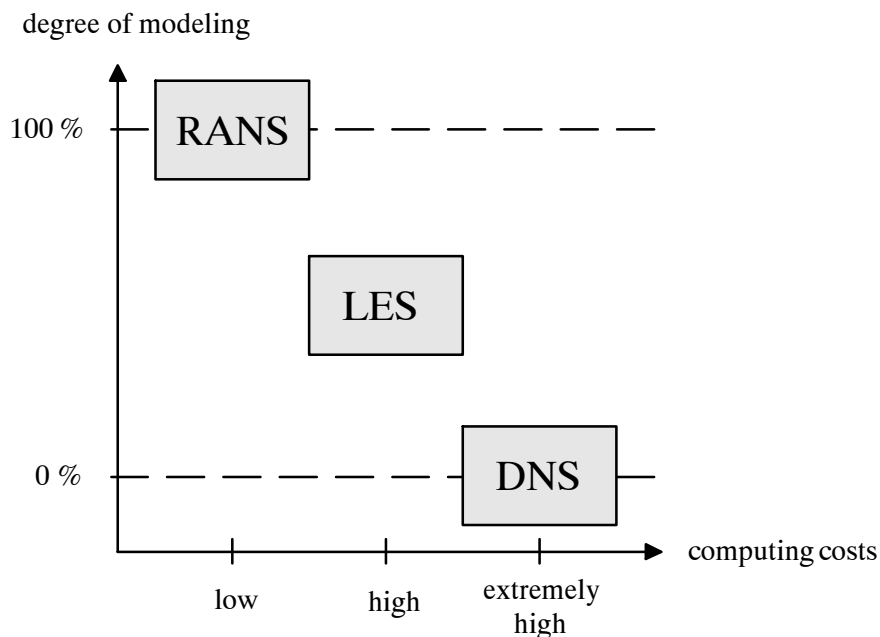


Fig. 5.1: Schematic classification of the alternative procedures (Breuer (2000))

5.2 Direct Numerical Simulation (DNS)

The basics of a Direct Numerical Simulation and its impact on the numerical simulation of turbulence including a historical review are provided by Moin and Mahesh (1998). The books of Ferziger and Peric (1999), Pope (2000), and Wilcox (1998), for instance, also devote a section to DNS.

Basically, it can be stated that DNS is conceptually the most straightforward approach of all three. In the present case, DNS exclusively relies on the standard Galerkin finite element method introduced in the preceding chapter, since it is widely accepted in the meantime that the Navier-Stokes equations in its basic form describe the turbulent flow regime as well. Thus, the finite element formulation (3.31) which is repeated here in symbolically modified form as

$$B_{NS}(\mathbf{v}^h, q^h; \mathbf{u}^h, p^h) = (\mathbf{v}^h, \mathbf{f})_{\Omega} + (\mathbf{v}^h, \mathbf{h})_{\Gamma_h} + [\textit{unresolved scales}] \quad (5.1)$$

may be applied. The symbolical modification consists in the addition of a term representing the effect of the unresolved scales onto the scales resolved by the standard Galerkin FEM. A short remark concerning (5.1) is perhaps necessary. It goes without saying that the Galerkin method with the characteristic element length $h \rightarrow 0$ is basically able to resolve all scales. However, (5.1) addresses the usual situation that refinement of the discretization beyond a certain (mostly low) level is not feasible. Aside from this, the formulation (5.1) is already an anticipation in view of the later multiscale formulation. In fact, DNS aims at a complete resolution of all scales linked with the respective flow situation. Hence, there would not be any unresolved scales. The problem lies in the extremely wide range of length and time scales appearing in a turbulent flow. A widely used measure for the necessary computational effort is based on the estimation (4.1) quantifying the ratio of the largest and the smallest scale. Assuming the computational domain to be at least as large as the largest eddy along with the necessity to resolve the Kolmogorov scale η at the other end of the scale spectrum, a three-dimensional spatial resolution approximately requires

$$N_S \approx \left(\frac{L}{\eta}\right)^3 \sim \left(\text{Re}_L^{\frac{3}{4}}\right)^3 = \text{Re}_L^{\frac{9}{4}} \quad (5.2)$$

degrees of freedom to be made available. Furthermore, assuming a time step of the same order as the characteristic length scale, the sum of 'temporal' and spatial degrees of freedom is approximately

$$N_{S+T} \approx \left(\frac{L}{\eta}\right)^4 \sim \left(\text{Re}_L^{\frac{3}{4}}\right)^4 = \text{Re}_L^3 \quad (5.3)$$

i.e. the number of degrees of freedom scales with Re^3 . Due to this reason, DNS is still unfeasible to simulate high Reynolds number flows of engineering interest with the currently existing computer hardware. Even for the lower Reynolds number flows which have been simulated in a DNS manner, the Kolmogorov scale is indeed seldomly resolved. The smallest resolved scale usually appears to be merely of $O(\eta)$, confer Moin and Mahesh (1998). Collis (2001) even claims that the smallest resolved scale in a DNS is often up to four times the size of the Kolmogorov scale. Thus, there are still unresolved scales in a DNS. The crucial modeling approach for a DNS assumes

$$[\textit{unresolved scales}] = 0 \quad (5.4)$$

in (5.1) according to this. More precisely spoken, (5.4) does not suppose the unresolved scales itself being zero. It rather states that the Galerkin projection of the unresolved scales onto the Galerkin finite element space is zero. This way of thinking will hopefully become clear with the introduction of the Galerkin method as a projection method in section 5.2.2 and, finally, with the multiscale interpretation in chapters 6 and 7.

5.3 Large Eddy Simulation (LES)

5.3.1 'Classical' Large Eddy Simulation based on explicit spatial filtering

Basic concept and literature

Usually, a situation will have to be faced in that adequate computational power to execute a DNS of a turbulent flow is (by far) not available. In this case, a promising approach commending itself for this purpose is Large Eddy Simulation (LES). The basic idea of LES consists in the strategy of resolving the larger eddies and modeling the effect of the smaller eddies onto the larger eddies. Since it has been learned from Kolmogorov's hypotheses in section 4.4 that the smaller scales exhibit a more universal character in general, this seems to be a promising approach in two respects. On the one hand, a (sometimes very much) coarser discretization is sufficient for resolving the larger scales and, on the other hand, the universal character of the smaller scales potentially simplifies the modeling process. The 'classical' way of performing LES is described, for instance, in the comprehensive articles of Fröhlich and Rodi (2000), Lesieur and Metais (1996), Piomelli (1994), Piomelli (1999), Rogallo and Moin (1984), and, in particular, in the book of Sagaut (2002), which has appeared in its second edition in 2002 after the first edition was being released in 2001. Massimo Germano values this within the foreword to the second edition as an indicator for the strong interest in the topic. Some recent advances in LES for complex flows are reported in Moin (2002) and steps towards a mathematical analysis are carried out in Guermond et al. (2002) and Layton (2003).

Explicit spatial filtering

The first step in a 'classical' LES consist in applying a spatial filter G to the unknown velocity \mathbf{u} resulting in

$$\bar{\mathbf{u}}(\mathbf{x}, t) = \int_{-\infty}^{+\infty} \int_{-\infty}^{+\infty} \int_{-\infty}^{+\infty} G(\mathbf{x} - \boldsymbol{\xi}) \mathbf{u}(\boldsymbol{\xi}, t) d^3\xi \quad (5.5)$$

This procedure was first proposed by Leonard (1974). The three most commonly used filters for LES are the box filter, the Gaussian filter and the sharp or spectral cutoff filter. These filters are displayed in physical space as well as their associated version in the spectral space, for instance, in Sagaut (2002), Figs. 2.1-2.6, and it is referred to this reference for an extensive discussion of these types of filters and some other ways of filtering. It should be remarked that only the sharp cutoff filter has the property of a projector for the multiple application of the operator, i.e.

$$\hat{G}^n = \hat{G} \circ \hat{G} \circ \dots \circ \hat{G} = \hat{G} \quad (5.6)$$

and is idempotent in the spectral space thus. The problems associated with the extension of these homogeneous filters to the inhomogenous case which have to be taken into account, in particular, as soon as a domain boundary is approached should just be mentioned here. For proposals in this context, consult e.g. Ghosal and Moin (1995) for second order and Vasilyev et al. (1998) for higher order commuting filters, respectively. This strategy has been extended to the case of unstructured meshes in Marsden et al. (2002).

After applying a filter to (2.45)-(2.46), the Navier–Stokes equations for the filtered velocity $\bar{\mathbf{u}}$ and the filtered pressure \bar{p} reading

$$\nabla \cdot \bar{\mathbf{u}} = 0 \quad \text{in } \Omega \times (0, T) \quad (5.7)$$

$$\frac{\partial \bar{\mathbf{u}}}{\partial t} + \nabla \cdot (\overline{\mathbf{u} \otimes \mathbf{u}}) + \nabla \bar{p} - 2\nu \nabla \cdot \varepsilon(\bar{\mathbf{u}}) = \mathbf{0} \quad \text{in } \Omega \times (0, T) \quad (5.8)$$

are obtained where the right hand side \mathbf{f} has been omitted for simplicity. The difference between the original unknown velocity and the new filtered unknown velocity

$$\mathbf{u}' = \mathbf{u} - \bar{\mathbf{u}} \quad (5.9)$$

represents the subgrid-scale or, more precisely, the subfilter-scale velocity in 'classical' filter-based LES. The term 'subgrid scale' is certainly established, but in order to distinguish it from following approaches the term 'subfilter scale' is introduced.

A very illuminating impression of the different scale ranges and the effects of filtering can be achieved by considering the Kolmogorov energy spectrum in Fig. 4.3. After applying the filtering procedure, the spectral amplitude of the kinetic energy $E(\kappa)$ may look as displayed in Fig. 5.2. The area under the curve still illustrates the turbulent kinetic energy. Using the box or Gaussian filter results in the deviating line, see e.g. Fröhlich and Rodi (2000). Of course, the progression still obeys the Kolmogorov $-5/3$ -law in the inertial range.

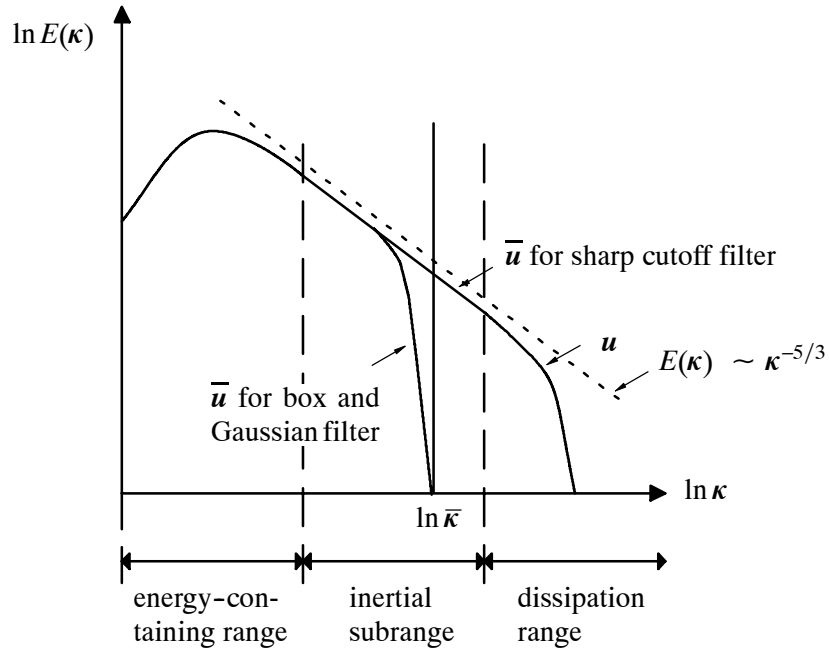


Fig. 5.2: Kolmogorov energy spectrum for LES with different types of spatial filters

The nonlinear term incorporates the effects of the subfilter scales onto the resolved scales. Since one is only able to compute $\bar{\mathbf{u}} \otimes \bar{\mathbf{u}}$, the difference between the nonlinear term in (5.8) and the computable nonlinear term has to be modeled. This describes the **closure problem** of LES exhibiting a similar character with respect to the famous closure problem of turbulence pointed out in section 4.2. The only difference consists in the fact that the closure problem in chapter 4 has been encountered after a process of Reynolds averaging, usually in time, and here it has risen due to a process of spatial filtering. Both procedures show basic similarities though. The tensor

comparable to the Reynolds stress tensor (4.12) which may be termed subfilter-scale stress tensor is defined as

$$\boldsymbol{\tau}^S = \overline{\mathbf{u} \otimes \mathbf{u}} - \bar{\mathbf{u}} \otimes \bar{\mathbf{u}} \quad (5.10)$$

and the 'new' momentum equation including $\boldsymbol{\tau}^S$ can be written as

$$\frac{\partial \bar{\mathbf{u}}}{\partial t} + \nabla \cdot (\bar{\mathbf{u}} \otimes \bar{\mathbf{u}}) + \nabla \bar{p} - \nabla \cdot (2\nu \nabla \varepsilon(\bar{\mathbf{u}}) - \boldsymbol{\tau}^S) = \mathbf{0} \quad \text{in } \Omega \times (0, T) \quad (5.11)$$

Double and triple (Leonard) decomposition

The unknown nonlinear term in (5.8) may be extended analog to what has been done in (4.8) as

$$\overline{\mathbf{u} \otimes \mathbf{u}} = \overline{(\bar{\mathbf{u}} + \mathbf{u}') \otimes (\bar{\mathbf{u}} + \mathbf{u}')} = \overline{\bar{\mathbf{u}} \otimes \bar{\mathbf{u}}} + \overline{\bar{\mathbf{u}} \otimes \mathbf{u}'} + \overline{\mathbf{u}' \otimes \bar{\mathbf{u}}} + \overline{\mathbf{u}' \otimes \mathbf{u}'} \quad (5.12)$$

Starting from (5.12), a double or a triple decomposition may be developed, see Winckelmans et al. (1996). The more popular triple decomposition was first proposed by Leonard (1974) and is named Leonard decomposition thus. It expands the subfilter-scale stress tensor according to

$$\boldsymbol{\tau}^S = \mathbf{L} + \mathbf{C} + \mathbf{R} \quad (5.13)$$

where \mathbf{L} is the Leonard stress tensor reading

$$\mathbf{L} = \overline{\bar{\mathbf{u}} \otimes \bar{\mathbf{u}}} - \bar{\mathbf{u}} \otimes \bar{\mathbf{u}} \quad (5.14)$$

\mathbf{C} denotes the cross stress tensor reading

$$\mathbf{C} = \overline{\bar{\mathbf{u}} \otimes \mathbf{u}'} + \overline{\mathbf{u}' \otimes \bar{\mathbf{u}}} \quad (5.15)$$

and \mathbf{R} is called the subfilter-scale Reynolds stress tensor reading

$$\mathbf{R} = \overline{\mathbf{u}' \otimes \mathbf{u}'} \quad (5.16)$$

It is obvious that the Leonard stress tensor represents interactions among resolved scales, the cross stress tensor interactions between resolved and unresolved scales and the subfilter-scale Reynolds stress tensor is restricted to interactions among unresolved scales.

The double decomposition assuming

$$\boldsymbol{\tau}^S = \mathbf{C} + \mathbf{R} \quad (5.17)$$

considers all terms including the nonlinear term in (5.11) to be filtered quantities, i.e. the nonlinear term $\nabla \cdot (\bar{\mathbf{u}} \otimes \bar{\mathbf{u}})$ in (5.11) is altered to be $\nabla \cdot (\overline{\bar{\mathbf{u}} \otimes \bar{\mathbf{u}}})$. This, however, requires a second application of the filter in contrast to the triple decomposition where the Leonard stress tensor represents the result of this process and has to be modeled thus.

If the applied filter fulfills the requirements of a Reynolds operator, i.e. the filtering process may be viewed as a projection, then $\mathbf{L} = \mathbf{C} = \mathbf{0}$ and

$$\boldsymbol{\tau}^S = \mathbf{R} = \overline{\mathbf{u}' \otimes \mathbf{u}'} \quad (5.18)$$

which is obviously the same for the double and triple decomposition. As aforementioned, the sharp cutoff filter exhibits this property in the spectral space. A generalization of the Leonard decomposition was developed by Germano as a consistent decomposition defining generalized central moments with the filter G , see e.g. Germano (1986) and Germano (1992).

Implicit and effective filtering

According to Sagaut (2002), four different types of filters in a LES may be identified:

- an explicit analytical filter G represented by a convolution product as in (5.5)
- an implicit filter induced by the numerical scheme applied to the underlying problem which may be, for instance, ascribed to the approximation of continuous differential operators by discrete operators (The introduction of an implicit filter due to the use of artificial dissipation, for example, in the context of an upwinding scheme should also been mentioned here in the author's point of view, although this filtering is very similar to the filtering introduced by a subgrid viscosity model stated below.)
- an implicit filter linked to the chosen discretization (It is obvious that no frequency higher than the Nyquist frequency associated with this computational grid can be resolved.)
- an implicit filter associated with a potentially applied subgrid-scale model due to the inherent length scale of the model (In the context of a subgrid viscosity model, this may, for instance, be interpreted as the mixing length.)

It is a difficult but crucial question how the effective filter built up by all or some of the filters just mentioned looks like. It is referred to the exhaustive discussion of this important question carried out in Sagaut (2002). One way of clearly identifying the effective filter is by letting one of the filters become predominant over the other filters. This may be done by the so-called pre-filtering technique actually using the explicit filter and, hence, allowing strict control of the form of the filter and the cutoff length. The drawback of this procedure lies in the fact that subfilter scales appear which are resolved by the computational grid but are not resolved scales in the sense of LES and useless therefore. This may increase computational demands substantially without increasing the amount of resolved scales. Thus, an explicit filter actually does not appear in virtually all LES codes, if it is not necessary, for example, to carry out a dynamic modeling process for the unresolved scales as will be presented below, confer e.g. Fröhlich and Rodi (2000). Some explicit discrete filters for this purpose are described in Sagaut (2002), section 12.2.

As a consequence, the usual way of filtering is an implicit one mainly based on the chosen discretization with the other implicit filters mentioned above potentially having an impact. This may be viewed, in principle, as a variant of the 'volume-balance' approach of Schumann (1975) where the respective cells of a finite volume method are utilized as a 'filter' very similar to a box filter. The problem with this filtering approach has to be ascribed to the a priori unknown cutoff length. However, the problems associated with necessary modifications of explicit filters in wall-bounded flows also become obsolete with this purely implicit filtering technique. This strategy will now be extended and adapted to finite element methods by identifying the variational projection within the Galerkin method as a 'filter' for the Navier-Stokes equations.

5.3.2 Large Eddy Simulation based on the Galerkin projection

Some reported applications of the finite element method for LES

As already pointed out, the finite element method is not the numerical method mostly used in CFD and, in particular, scarcely applied for LES or even DNS of turbulent flows yet. Neverthe-

less, some early developments may be found in literature. Firstly, the work of Kenneth Jansen should be mentioned here. He used a stabilized finite element method (variants of this will be developed in chapter 7) on unstructured grids for LES of the flow over an airfoil and published it in a series of Annual Research Briefs of the Center for Turbulence Research (CTR) (see e.g. Jansen (1993, 1994, 1995, 1996)). A summary of the method and the results achieved with it was then reported in Jansen (1999). Secondly, the work of Giovanni P. Galdi, Traian Iliescu, Volker John, and William Layton as well as their co-workers has resulted in a number of publications, of which only a selection are named here: Galdi and Layton (2000), Iliescu et al. (2002), John (2002a), John and Layton (2002), as well as Iliescu et al. (2003). Coming from a mathematical background, the authors particularly approach the topics of filtering and numerical errors in LES as well as some new boundary conditions and subgrid(filter)-scale models.

Besides the aforementioned publications, some more will now be named in their chronological appearance: Chalot et al. (1998), Rollet-Miet et al. (1999), Ding and Tsang (2001), Kollmann et al. (2002), Camarri et al. (2002). For example, Chalot et al. (1998) use a stabilized finite element method similar to Jansen which is implemented into an industrial code. In Ding and Tsang (2001), a least-squares finite element method is utilized for LES. Camarri et al. (2002) use a mixed finite volume / finite element solver on coarse unstructured grids for LES of a flow past a square cylinder.

A common procedure in some of the work named here is an implicit approach to filtering the variables. Nevertheless, some explicit filters particularly suited for the finite element method are described in Jansen (1999), Tejada-Martinez and Jansen (2003), as well as Kollmann et al. (2002), in the two former references exclusively devoted to an employment in a dynamic modeling procedure. The problem of using finite elements satisfying the inf-sup condition by a proper choice of the interpolation functions is pointed out in Rollet-Miet et al. (1999). Since these elements usually go along with a higher-order interpolation for the velocity with respect to the pressure, a larger implicit 'filter width' for the pressure has to be expected according to this.

Galerkin projection acting as an implicit filter

Before using the Galerkin projection as a way of implicit filtering or, more precisely, as a way of separating resolved scales from unresolved scales, it has to be clarified that the Galerkin finite element method is indeed a projection. This question is discussed and, in fact, answered in Gresho and Sani (1998), appendix 3, in exhaustive form. They investigate L_2 - and H^1 -projections both in scalar and vector form. The most important results for the considerations of this section will be summarized here briefly.

Basically, the scalar H^1 -projection both in infinite-dimensional and finite-dimensional form are proven to be projections. The case of primary interest is the projection from an infinite-dimensional original space, e.g. $H^1(\Omega)$ (or its vectorial counterpart $H^1(\Omega)^d$) to a finite-dimensional subspace. Here, one may state that the approximate solution of the underlying problem is actually identical to the H^1 -projection of that solution onto the subspace spanned by the basis functions of the Galerkin finite element method. Denoting the Galerkin projection by \mathcal{P}_G^h , it fulfills the necessary property for the multiple application reading

$$\left(\mathcal{P}_G^h\right)^n = \mathcal{P}_G^h \circ \mathcal{P}_G^h \circ \dots \circ \mathcal{P}_G^h = \mathcal{P}_G^h \quad (5.19)$$

However, the important property of the projection being orthogonal can only be proven for the rather academic cases of a pure Neumann boundary, i.e. $\Gamma = \Gamma_h$, or vanishing Dirichlet boun-

dary conditions like e.g. $\phi = g = 0$ on Γ_g in (3.3) for the convection-diffusion-reaction equation. In contrast to this, inhomogeneous Dirichlet boundary conditions cause the appearance of a non-linear subspace of $H^1(\Omega)$ containing the admissible functions for the problem. Therefore, the Galerkin projection is non-orthogonal in general and projects into a non-linear subspace.

In view of the actual problem, the incompressible Navier-Stokes equations, the step to vector projections has to be taken. Grounding on the findings for the scalar case and its straightforward transformation to the vector space, an additional projection has to be introduced, that is the projection to the (discretely) divergence-free subspace. Denoting by \mathcal{J}^h the discretely divergence-free subspace and by $\mathcal{P}_\mathcal{J}^h$ the respective projection, it was shown by Gresho and Sani (1998) that either applying the projection $\mathcal{P}_\mathcal{J}^h$ directly or applying the non-divergence-free projection operator \mathcal{P}_G^h first and then $\mathcal{P}_\mathcal{J}^h$ yields the same result, i.e.

$$\mathbf{u}_\mathcal{J} = \mathcal{P}_\mathcal{J}^h \mathbf{u} = \mathcal{P}_\mathcal{J}^h \mathcal{P}_G^h \mathbf{u} \quad (5.20)$$

In (5.20), \mathbf{u} denotes the solution vector and $\mathbf{u}_\mathcal{J}$ its discretely divergence-free H^1 -projection. For elaboration of this, it is referred to Gresho and Sani (1998).

After clarifying the role of the Galerkin finite element method as a projection, it may now be applied in the sense of LES. For this purpose, an intuitive procedure will be followed here by adopting the separation of the velocity and the pressure from 'classical' LES and incorporating them into the finite element framework as

$$\mathbf{u} = \bar{\mathbf{u}}^h + \mathbf{u}', \quad p = \bar{p}^h + p' \quad (5.21)$$

The decompositions (5.21) are then introduced into (3.31) yielding

$$B_{NS}(\mathbf{v}^h, q^h; \bar{\mathbf{u}}^h + \mathbf{u}', \bar{p}^h + p') = (\mathbf{v}^h, \mathbf{f})_\Omega + (\mathbf{v}^h, \mathbf{h})_{\Gamma_h} \quad \forall \{\mathbf{v}^h, q^h\} \in \mathcal{V}_{up}^h \quad (5.22)$$

What is done here intuitively will be arranged in the more general framework of the variational multiscale method in chapter 7 and justified yet. The procedure is continued here in a straightforward manner however. For this purpose, the bilinear form B_{NS} is linearized according to Hughes et al. (2000a) by expanding it as

$$\begin{aligned} B_{NS}(\mathbf{v}^h, q^h; \bar{\mathbf{u}}^h + \mathbf{u}', \bar{p}^h + p') &= B_{NS}(\mathbf{v}^h, q^h; \bar{\mathbf{u}}^h, \bar{p}^h) \\ &+ \frac{d}{d\epsilon} B_{NS}(\mathbf{v}^h, q^h; \bar{\mathbf{u}}^h + \epsilon \mathbf{u}', \bar{p}^h + \epsilon p')|_{\epsilon=0} + \frac{d^2}{d\epsilon^2} B_{NS}(\mathbf{v}^h, q^h; \bar{\mathbf{u}}^h + \epsilon \mathbf{u}', \bar{p}^h + \epsilon p')|_{\epsilon=0} \\ &= B_{NS}(\mathbf{v}^h, q^h; \bar{\mathbf{u}}^h, \bar{p}^h) + B_{NS}^1(\mathbf{v}^h, q^h; \bar{\mathbf{u}}^h, \mathbf{u}', p') + B_{NS}^2(\mathbf{v}^h; \mathbf{u}') \end{aligned} \quad (5.23)$$

where $B_{NS}(\mathbf{v}^h, q^h; \bar{\mathbf{u}}^h, \bar{p}^h)$ is given according to (3.22),

$$\begin{aligned} &\frac{d}{d\epsilon} B_{NS}(\mathbf{v}^h, q^h; \bar{\mathbf{u}}^h + \epsilon \mathbf{u}', \bar{p}^h + \epsilon p')|_{\epsilon=0} \\ &= \left(\mathbf{v}^h, \frac{\partial \mathbf{u}'}{\partial t} \right)_\Omega + \left(\mathbf{v}^h, \bar{\mathbf{u}}^h \cdot \nabla \mathbf{u}' + \beta \mathbf{u}' (\nabla \cdot \bar{\mathbf{u}}^h) + \mathbf{u}' \cdot \nabla \bar{\mathbf{u}}^h + \beta \bar{\mathbf{u}}^h (\nabla \cdot \mathbf{u}') \right)_\Omega \\ &\quad - \left(\nabla \cdot \mathbf{v}^h, p' \right)_\Omega + \left(\varepsilon(\mathbf{v}^h), 2\nu \varepsilon(\mathbf{u}') \right)_\Omega - \left(q^h, \nabla \cdot \mathbf{u}' \right)_\Omega \end{aligned} \quad (5.24)$$

and

$$\frac{d^2}{d\epsilon^2} B_{NS}(\mathbf{v}^h, q^h; \bar{\mathbf{u}}^h + \epsilon \mathbf{u}', \bar{p}^h + \epsilon p')|_{\epsilon=0} = \left(\mathbf{v}^h, \mathbf{u}' \cdot \nabla \mathbf{u}' + \beta \mathbf{u}' (\nabla \cdot \mathbf{u}') \right)_{\Omega} \quad (5.25)$$

Rearranging (5.22) with the help of (5.23) yields

$$\begin{aligned} B_{NS}(\mathbf{v}^h, q^h; \bar{\mathbf{u}}^h, \bar{p}^h) &= \left(\mathbf{v}^h, \mathbf{f} \right)_{\Omega} + \left(\mathbf{v}^h, \mathbf{h} \right)_{\Gamma_h} \\ &\quad - B_{NS}^1(\mathbf{v}^h, q^h; \bar{\mathbf{u}}^h, \mathbf{u}', p') - B_{NS}^2(\mathbf{v}^h; \mathbf{u}') \quad \forall \{ \mathbf{v}^h, q^h \} \in \mathcal{V}_{up}^h \end{aligned} \quad (5.26)$$

The last two terms on the right hand side of (5.26) may now be identified as the influence of the unresolved scales onto the resolved scales. In terms of the interpretation of the Galerkin FEM as a projection, these two terms can be viewed as the projection of the unresolved scales into the subspace of the resolved scales - and, hence, it is only this projection that has to be represented by a subgrid-scale model in this context, confer Collis (2001). With this knowledge at hand, the DNS-equation (5.1) may also be re-interpreted in that the symbolic term on the right hand side merely has to be replaced by the two terms on the right hand side of (5.26). Moreover, these two terms, i.e. the projection of the unresolved scales onto the resolved scales, are assumed to be zero in a DNS-FEM as already indicated in (5.4).

Double and triple (Leonard) decomposition

Analog to what is usually done in 'classical' LES, the triple summation according to Leonard (1974) may be adopted to this case. However, the identification of the projection of the Leonard stress tensor \mathbf{L} has to be postponed until the complete multiscale framework will have been developed in chapter 7. Therefore, the analogon of the double decomposition is identified first. The projection of the cross stress tensor \mathbf{C} reads

$$C(\mathbf{v}^h; \bar{\mathbf{u}}^h, \mathbf{u}') = - \left(\mathbf{v}^h, \bar{\mathbf{u}}^h \cdot \nabla \mathbf{u}' + \beta \mathbf{u}' (\nabla \cdot \bar{\mathbf{u}}^h) + \mathbf{u}' \cdot \nabla \bar{\mathbf{u}}^h + \beta \bar{\mathbf{u}}^h (\nabla \cdot \mathbf{u}') \right)_{\Omega} \quad (5.27)$$

where the cross stress tensor can be easily isolated by setting $\beta = 1$ and shifting the differential operator to the test function through integration-by-parts which results in

$$C(\mathbf{v}^h; \bar{\mathbf{u}}^h, \mathbf{u}') = \left(\nabla \mathbf{v}^h, \bar{\mathbf{u}} \otimes \mathbf{u}' + \mathbf{u}' \otimes \bar{\mathbf{u}} \right)_{\Omega} \quad (5.28)$$

Of course, an additional Neumann boundary term will appear in the wake of the integration-by-parts. The projection of the Reynolds stress tensor \mathbf{R} may be defined as

$$R(\mathbf{v}^h; \mathbf{u}') = - \left(\mathbf{v}^h, \mathbf{u}' \cdot \nabla \mathbf{u}' + \beta \mathbf{u}' (\nabla \cdot \mathbf{u}') \right)_{\Omega} \quad (5.29)$$

With the same rationale and, as a matter of course, the same consequence as before, the Reynolds stress tensor can be isolated within the bilinear form as

$$R(\mathbf{v}^h; \mathbf{u}') = \left(\nabla \mathbf{v}^h, \mathbf{u}' \otimes \mathbf{u}' \right)_{\Omega} \quad (5.30)$$

Collis (2001) suggests assuming an orthonormal basis which modifies (5.26) to

$$B_{NS}(\mathbf{v}^h, q^h; \mathbf{u}^h, p^h) = \left(\mathbf{v}^h, \mathbf{f} \right)_{\Omega} + \left(\mathbf{v}^h, \mathbf{h} \right)_{\Gamma_h} + C(\mathbf{v}^h; \bar{\mathbf{u}}^h, \mathbf{u}') + R(\mathbf{v}^h; \mathbf{u}') \quad (5.31)$$

With (5.31) at hand, a simple comparison with the equations (5.7) and (5.11) of 'classical' LES including the double decomposition (5.17) of the subfilter-scale stress tensor is enabled. As a

result, the only major difference lies in the use of Galerkin variational projection in lieu of explicit (or implicit) spatial filtering.

5.3.3 Subgrid(filter)-scale modeling

Functional vs. structural modeling and the subgrid viscosity concept

As a matter of principle, two different modeling strategies of 'classical' LES may be distinguished according to Sagaut (2002). On the one hand, it is intended to approximate the subgrid(filter)-scale stress tensor τ^S itself. Thus, a relation

$$\tau^S = \mathcal{F}(\bar{\mathbf{u}}) \quad (5.32)$$

is assumed. This first strategy is called **structural modeling**. Perhaps the most famous structural modeling approach is the Bardina model (see Bardina et al. (1980), Bardina et al. (1983)) or its improved version, the filtered Bardina model (see Horiuti (1997), Layton (2000)), respectively. The basic idea behind these models is the hypothesis of a similarity between the subgrid(filter) scales which have to be modeled and the smallest resolved scales which are available for modeling purposes. This basic idea is also picked up beyond the borders of the Bardina models and will, for instance, be instrumental to the dynamic modeling procedure to be presented below. The drawback of the Bardina models lies in its only slightly dissipative character and its herewith linked underestimation of the energy cascade. In order to remedy this problem, the Bardina model is often used in a mixed form along with a functional (and usually more dissipative) model like e.g. the Smagorinsky model to be presented in the next section. See, for example, Sarghini et al. (1999) for applications of mixed models. For an exhaustive list of structural models, it is referred to Sagaut (2002), chapter 6.

The second strategy aims at modeling the action of the subgrid scales onto the resolved scales and not the tensor τ^S itself. This assumption may look like

$$\nabla \tau^S = \mathcal{F}(\bar{\mathbf{u}}) \quad (5.33)$$

In the following, this second assumption called **functional modeling** will be focussed on. A very popular and widespread way of functional modeling relies on the **subgrid (or eddy) viscosity concept** which is based on the Boussinesq turbulent (or eddy) viscosity assumption explained in section 4.2.4. Here, it is assumed that the energy transfer mechanism from the resolved to the unresolved scales is similar to the molecular mechanism based on the physical viscosity of the respective fluid. Analog to (4.17) thus, the tensor τ^S or, more precisely expressed, the deviatoric part of it is calculated as a product of a subgrid viscosity ν^T and the rate-of-velocity tensor of the resolved scales $\varepsilon(\bar{\mathbf{u}})$ such that

$$- \text{dev } \tau^S = 2\nu^T \varepsilon(\bar{\mathbf{u}}) \quad (5.34)$$

The reason for constricting the modeling efforts to the deviatoric part of the subgrid(filter)-scale stress tensor is justified by the concept. For incompressible flows, $\varepsilon(\bar{\mathbf{u}})$ has a zero trace which results in an identity between the tensor and its deviatoric part. Depending on such a deviatoric tensor, one is only able to model a deviatoric tensor as well. The complementary spherical tensor is usually added to the pressure term which then reads in modified form

$$\bar{P}_{\text{mod}} = \bar{P} + \frac{1}{3} \text{tr } \tau^S \quad (5.35)$$

and, hence, requires no modeling. However, the picture would not be complete without describing what should be modelled by ν^T . There are two main phenomena in the interaction between the resolved scales, particularly the small resolved scales, and the unresolved scales. The main process is generated by a drainage of energy from the resolved scales to the unresolved scales. Aside of this, a weak backscatter occurs in the opposite direction. All functional modeling efforts are based on the hypothesis that the action of the unresolved scales onto the resolved scales can be viewed as an energetic action whose respective energy transfer balance should be sufficient for its description.

There is another interesting functional modeling strategy called **implicit diffusion** which is solely based on the numerical scheme used and the hypothesis that the aforementioned subgrid scale action is strictly dissipative. Here, the associated truncation error is asked to create the desired effects. The most popular examples for this strategy are constituted by the variety of upwind schemes. The later to be presented stabilized finite element methods may also be ranged into this class, although they have not been designed for this purpose initially. In Donea and Huerta (2003), it is depicted that all three approaches, i.e. the direct introduction of numerical diffusion (or viscosity), the use of an upwinding scheme or a stabilized method, may basically viewed as equivalent methodologies in that all of them introduce some kind of numerical diffusion (or viscosity) finally. However, the different approach of stabilized methods with respect to the other two techniques is slight but crucial as will be seen later on.

Please consult Sagaut (2002), chapters 4 and 5, for a comprehensive description of functional models basically developed for an isotropic case and their adjustment to anisotropic cases. An investigation of the emphasized subgrid-scale models, i.e. the Smagorinsky model, the dynamic modeling procedure and further models based on the scale similarity hypothesis may be found in Meneveau and Katz (2000).

'Static' modeling using Smagorinsky's model

The Smagorinsky (1963) model was the first subgrid-scale model and is still a commonly used one due to its attractive simplicity. Its basic idea falls back upon Prandtl's mixing length hypothesis (see section 4.2.5). The mixing length l_{mix} is replaced by, for example, the filter size Δ in 'classical' filter-based LES scaled by the so-called Smagorinsky constant C_S . The norm of the rate-of-velocity tensor based on the mean velocity is replaced by the rate-of-velocity tensor $\epsilon(\bar{\mathbf{u}})$ based on the resolved velocity. Herewith, the Smagorinsky model reads

$$\nu^T = (C_S \Delta)^2 |\epsilon(\bar{\mathbf{u}})| \quad (5.36)$$

The obvious analog would be to replace Δ by a characteristic element length h in LES based on the Galerkin projection. The weak point of the Smagorinsky model is represented by the constant in (5.36). Due to investigations of isotropic turbulence, a value of $C_S = 0.18$ (see e.g. Lilly (1967)) had been proposed which proved to be too large for most flows yet. Hence, a lower value should be employed usually. Furthermore, the value has to be reduced artificially in the vicinity of walls, mostly with the aid of van Driest damping, see e.g. Fröhlich and Rodi (2001). Since it does not vanish in laminar regimes, it is not useful for the simulation of transition. A last problem with the Smagorinsky model concerns the exclusion of the mechanism of backscatter due to the strictly dissipative character of the model resulting in $\nu^T \geq 0$ for all time.

Dynamic modeling using Smagorinsky's model

All of the aforementioned negative features of the Smagorinsky model somehow trace back to the preliminary fixing of the constant C_S . Therefore, the idea of Germano et al. (1991) was to unfix the constant and permit it to change in space and time, i.e. $C_S = C_S(\mathbf{x}, t)$, by way of a dynamic algorithm. The original idea was slightly modified by Lilly (1992) and generalized to inhomogeneous cases in Ghosal et al. (1995). According to the scale similarity hypothesis, the basic intention of the dynamic procedure consists in exploiting the resolved scales, particularly the ones in the vicinity of the filter scale, to get information for the modeling. A test filter with a filter size $\hat{\Delta}$ larger than the basic LES filter (often twice as large) is introduced. Thus, a subtest-scale stress tensor

$$\boldsymbol{\tau}^T = \overline{\hat{\mathbf{u}} \otimes \hat{\mathbf{u}}} - \hat{\mathbf{u}} \otimes \hat{\mathbf{u}} \quad (5.37)$$

appears besides the subfilter-scale stress tensor $\boldsymbol{\tau}^S$. Germano's identity provides us with the tensor

$$\mathbf{L}^T = \boldsymbol{\tau}^T - \boldsymbol{\tau}^S = \overline{\hat{\mathbf{u}} \otimes \hat{\mathbf{u}}} - \hat{\mathbf{u}} \otimes \hat{\mathbf{u}} \quad (5.38)$$

which can actually be calculated. On the other hand, a model expression $\mathbf{L}_{\text{mod}}^T$ which should fulfill the condition

$$\mathbf{L}^T - \mathbf{L}_{\text{mod}}^T = \mathbf{0} \quad (5.39)$$

has to be established. This gives rise to a tensor equation which can only be solved in some average sense in order to get **one** value for C_S which may then be used for the subgrid-scale modeling with, for example, the Smagorinsky model. However, it has to be emphasized that the dynamic procedure is not restricted to being based on the Smagorinsky model. In principle, it is rather open to any modeling ansatz including an a priori undertermined constant. Fig. 5.3 depicts the dynamic procedure against the background of the Kolmogorov energy spectrum, solely for a sharp or spectral cutoff filter here. A furthergoing development of the dynamic procedure for more complex configurations is the so-called Lagrangean Dynamic Procedure, see Meneveau et al. (1996). Further details of the dynamic procedure are left out here and it is referred to the literature on LES alluded in the beginning of section 5.2 besides the original references mentioned above.

Finally, it should be noted that all the problems associated with the constant-coefficient Smagorinsky model may be addressed adequately by this procedure. Admittedly, some potential numerical difficulties have to be faced related to either unbounded or negative (and, thus, anti-dissipative) values of C_S jeopardizing the stability of the simulation. On the one hand, appropriate measures may be taken to overcome these problems, see e.g. Sagaut (2002). For example, an artificial condition may be introduced as

$$\nu + \nu^T \geq 0 \quad (5.40)$$

On the other hand, negative values of C_S and, consequently, of the subgrid viscosity may be interpreted physically as modeling the process of backscattering. The problem becomes critical when the dynamically calculated constant remains too long in the negative range. This corresponds to a too high transfer of kinetic energy to the resolved scales, see Carati et al. (1995). Within the localized dynamic model in Ghosal et al. (1995), an energy equation is included preventing the simulation from becoming unstable.

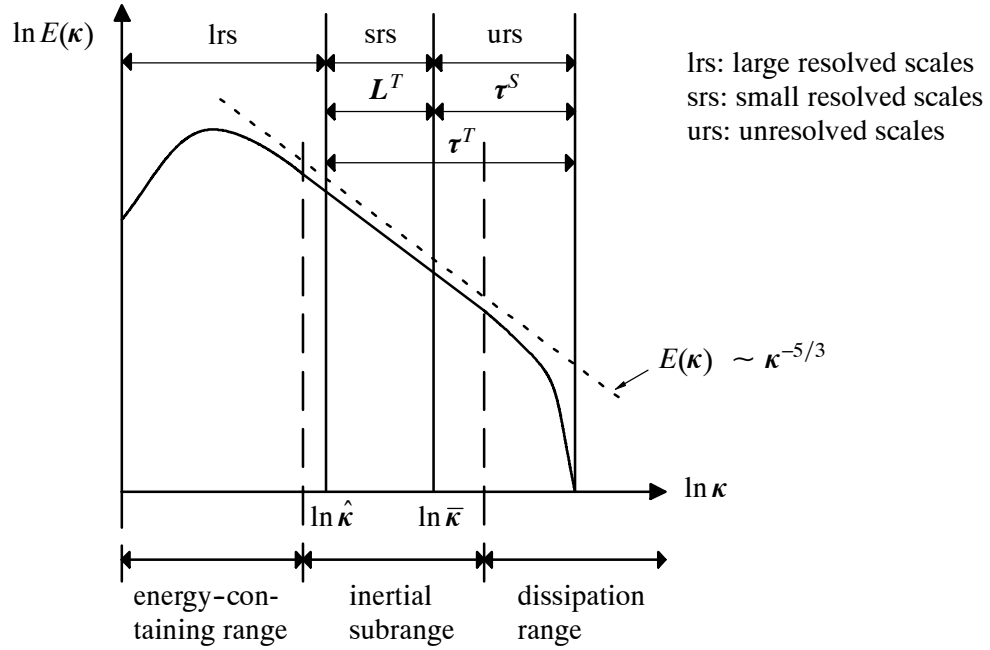


Fig. 5.3: Kolmogorov energy spectrum for dynamic procedure of Germano et al. (1991)

5.4 Simulation based on the Reynolds Averaged Navier-Stokes equations (RANS)

Since this simulation technique is not an essential part of this work, it will be mentioned here merely for reasons of completeness. It basically relies on the explanations and results of section 4.2, i.e. Reynolds averaging (see appendix A.1) is used instead of spatial filtering in form of (5.5). As a result, the decompositions (4.2) and (4.3) are obtained instead of (5.21). According to this, the complete fluctuations or, more precisely, the complete Reynolds stress tensor have to be modeled. Turbulence models have to be used for this purpose which are, however, lacking generality, since they have to model an extremely wide range of scales. The principal advantage of LES in that only the small scales with their more universal character have to be modeled is lost within the RANS technique. A large number of turbulence modeling approaches have been developed ranging from simple algebraic models to a full Reynolds stress closure. For an exhaustive description of RANS and related modeling approaches, it is referred to Wilcox (1998).

An interesting aspect with respect to LES is the potential application of RANS and LES in combined form which may reduce the computational effort necessary for the numerical simulation. Such hybrid RANS/LES approaches are described in Sagaut (2002), chapter 11. Representatives of this method are, for example, the so-called Detached Eddy Simulation (DES) proposed by Philippe Spalart and co-workers (see e.g. Spalart et al. (1997), Travin et al. (1999), Strelets (2001), and Spalart (2002)) and the zonal multi-domain RANS/LES simulation proposed by Quéméré and Sagaut (2002). Among other attempts in this direction, a universal modeling approach for hybrid RANS/LES models that should 'throw a bridge from RANS to DNS' has been proposed by Germano (1999).

6 Variational multiscale method for scalar convection-diffusion-reaction equations

The current and the subsequent chapter are devoted to the application of the variational multiscale method to the convection-diffusion-reaction equation and the Navier-Stokes equations, respectively. Two versions of the variational multiscale method will be presented bearing a separation of two and three scales. Further applications of a two-scale separation in fields of activity besides the ones addressed here have been reported, for example, by Garikipati and Hughes (1998, 2000a, 2000b) for problems of strain localization with an extension to the case of strong discontinuities.

6.1 Separation of two scales

The first attempt of separation distinguishes two scale ranges of the problem variable that is to say the solution function $\phi \in \mathcal{Y}$ is decomposed as

$$\phi = \bar{\phi}^{\bar{h}} + \phi' \quad (6.1)$$

and the weighting function $w \in \mathcal{V}$ as

$$w = \bar{w}^{\bar{h}} + w' \quad (6.2)$$

The characteristic element length \bar{h} is introduced here in the context of the variational multiscale method in view of a later to be introduced characteristic element length h' . In the following, $\bar{\phi}^{\bar{h}}$ and $\bar{w}^{\bar{h}}$ will be denoted $\bar{\phi}$ and \bar{w} , respectively, for convenience. Accordingly, a direct sum decomposition of the solution and weighting function spaces is performed reading

$$\mathcal{Y}_\phi = \bar{\mathcal{Y}}_\phi \oplus \mathcal{Y}'_\phi \quad (6.3)$$

$$\mathcal{V}_\phi = \bar{\mathcal{V}}_\phi \oplus \mathcal{V}'_\phi \quad (6.4)$$

Here, $\bar{\mathcal{Y}}_\phi$ may be thought of as, for instance, a standard finite element space analog to \mathcal{Y}_ϕ^h associated with a discretization characterized by \bar{h} and, for the time being, \mathcal{Y}'_ϕ as an infinite-dimensional space. That applies to the decomposed weighting function spaces too. $\bar{\phi}$ is required to fulfill the essential Dirichlet boundary condition (3.3) exclusively, i.e.

$$\bar{\phi} = g \quad \text{on } \Gamma_g \quad \forall \bar{\phi} \in \bar{\mathcal{Y}}_\phi \quad (6.5)$$

All other function variables, namely ϕ' , \bar{w} and w' , face zero Dirichlet boundary conditions. The first application will now be done to the stationary convection-diffusion-reaction equation, i.e. (3.2) without the transient term $\partial\phi/\partial t$. In section 6.5, the procedure will be extended to the instationary case. The variational form of the stationary problem reads according to (3.15) with $B_{cdr}^t(w, \phi)$ being replaced by $B_{cdr}(w, \phi)$ which is defined as

$$B_{cdr}(w, \phi) = (w, \mathbf{a} \cdot \nabla \phi)_\Omega + (\nabla w, \kappa \nabla \phi)_\Omega + (w, \sigma_{(\text{mod})} \phi)_\Omega \quad (6.6)$$

Inserting (6.1) and (6.2) into (3.15) leads to

$$B_{cdr}(\bar{w} + w', \bar{\phi} + \phi') = (\bar{w} + w', f)_{\Omega} + (\bar{w} + w', h)_{\Gamma_h} \quad (6.7)$$

from which the two subproblems

$$B_{cdr}(\bar{w}, \bar{\phi}) + B_{cdr}(\bar{w}, \phi') = (\bar{w}, f)_{\Omega} + (\bar{w}, h)_{\Gamma_h} \quad \forall \bar{w} \in \bar{\mathcal{V}}_{\phi} \quad (6.8)$$

$$B_{cdr}(w', \bar{\phi}) + B_{cdr}(w', \phi') = (w', f)_{\Omega} + (w', h)_{\Gamma_h} \quad \forall w' \in \mathcal{V}'_{\phi} \quad (6.9)$$

can be derived due to the linearity of the problem. Since it is intended to solve the $(\cdot)'$ -scales somehow in the following, it will be deviated from a usual way of naming $(\bar{\cdot})$ -scales resolved scales and $(\cdot)'$ -scales unresolved or subgrid scales with one important exception described in section 6.3. With regard to the later separation of three scales, they are named large and small (resolved) scales. Accordingly, (6.8) is called 'large-scale equation' and (6.9) is called 'small-scale equation' below.

In the context of the finite element method with the usual choice of C^0 -elements for problems described by second-order differential operators, the problem of 'loosing' continuity of the first derivatives on the element boundaries is encountered. The second derivatives even cause Dirac delta functions at the element boundaries. Hence, some terms showing up due to integration-by-parts have to be understood in a distributional sense. For a description of the theory of distributions, confer e.g. Stakgold (1998), chapter 2. In the current context, this topic is dealt with exhaustively in the publication of Hughes et al. (1998). Thus, it is referred to it for further elaboration. In order to demonstrate the procedure, the attention is concentrated on the general integrated-by-parts term $B_{cdr}(w, \phi)_{\Omega_e}$ on one element domain Ω_e without any particular reference to large or small scales. The integration-by parts procedure will be carried in two directions, i.e., on the one hand, the weighting function w will be 'isolated' in the variational formulation and, on the other hand, this 'isolation' process will be applied to the solution function ϕ . The results of these two procedures will then be applied to various terms in the two subproblems (6.8)-(6.9).

$B_{cdr}(w, \phi)_{\Omega_e}$ differs from (6.6) due to the presence of the Dirac delta functions on the element boundary Γ_e which give rise to an additional boundary integral such that

$$\begin{aligned} B_{cdr}(w, \phi)_{\Omega_e} &= (w, \mathcal{L}_{cdr}\phi)_{\Omega_e} + (w, \mathbf{n} \cdot \kappa \nabla \phi)_{\Gamma_e} \\ &= \int_{\Omega_e} w \left(\mathbf{a} \cdot \nabla \phi - \kappa \Delta \phi + \sigma_{(\text{mod})} \phi \right) d\Omega + \int_{\Gamma_e} w (\mathbf{n} \cdot \kappa \nabla \phi) d\Gamma \end{aligned} \quad (6.10)$$

Here, \mathbf{n} indicates the outward unit normal vector on the element boundary of Ω_e . Integrating (6.10) by parts in the other direction by 'shifting' derivative operators on the weighting function w reveals

$$\begin{aligned} B_{cdr}(w, \phi)_{\Omega_e} &= (\mathcal{L}_{cdr}^* w, \phi)_{\Omega_e} + (\mathbf{n} \cdot \mathbf{a} w, \phi)_{\Gamma_e} + (\mathbf{n} \cdot \kappa \nabla w, \phi)_{\Gamma_e} \\ &= \int_{\Omega_e} \left(-\mathbf{a} \cdot \nabla w - \kappa \Delta w + \sigma_{(\text{mod})} w \right) \phi d\Omega \end{aligned}$$

$$+ \int_{\Gamma_e} (\mathbf{n} \cdot \mathbf{a}w) \phi \, d\Gamma + \int_{\Gamma_e} (\mathbf{n} \cdot \kappa \nabla w) \phi \, d\Gamma \quad (6.11)$$

The boundary terms in (6.10) and (6.11) have ambiguous meaning in this respect, since they belong to two elements. Due to the opposite direction of \mathbf{n} from the neighbour element's point of view, the difference of the boundary value from both elements merely has to be taken into account. This is indicated by the jump operator $[\cdot]_{-}^{+}$. Hence, by summing (6.11) over all elements and adding the Neumann and Dirichlet boundary terms,

$$\begin{aligned} B_{cdr}(w, \phi) &= (\mathcal{L}_{cdr}^* w, \phi)_{\Omega'} + ([\mathbf{n} \cdot \kappa \nabla w]_{-}^{+}, \phi)_{\Gamma'} + (\mathbf{n} \cdot (\mathbf{a}w + \kappa \nabla w), \phi)_{\Gamma_h} \\ &\quad + (\mathbf{n} \cdot \kappa \nabla w, \phi)_{\Gamma_g} \\ &= (\mathcal{L}_{cdr}^* w, \phi)_{\Omega} + (\mathbf{n} \cdot (\mathbf{a}w + \kappa \nabla w), \phi)_{\Gamma_h} + (\mathbf{n} \cdot \kappa \nabla w, \phi)_{\Gamma_g} \end{aligned} \quad (6.12)$$

is obtained where the third line of (6.12) has to be understood as an integral on the global domain Ω in a distributional sense plus a Neumann and a Dirichlet boundary term. Please note that the first boundary term in (6.11) drops out at the interelement boundaries in the summing-up of all elements due to the continuity of the functions and at the Dirichlet boundary due to the zero boundary condition for the large- and small-scale weighting functions. By doing the same in (6.10), one obtains

$$\begin{aligned} B_{cdr}(w, \phi) &= (w, \mathcal{L}_{cdr} \phi)_{\Omega'} + \left(w, [\mathbf{n} \cdot \kappa \nabla \phi]_{-}^{+} \right)_{\Gamma'} + (w, \mathbf{n} \cdot \kappa \nabla \phi)_{\Gamma_h} \\ &= (w, \mathcal{L}_{cdr} \phi)_{\Omega} + (w, \mathbf{n} \cdot \kappa \nabla \phi)_{\Gamma_h} \end{aligned} \quad (6.13)$$

where the Dirichlet boundary term has been omitted due to the zero boundary conditions for the large- and small-scale weighting functions.

As a result, the final form of the large- and small-scale equation in (6.8)-(6.9) is achieved after integrating by parts $B_{cdr}(\bar{w}, \phi')$ according to (6.12) as well as $B_{cdr}(w', \bar{\phi})$ and $B_{cdr}(w', \phi')$ according to (6.13) as

$$B_{cdr}(\bar{w}, \bar{\phi}) + (\mathcal{L}_{cdr}^* \bar{w}, \phi')_{\Omega} + (\mathbf{n} \cdot (\mathbf{a}\bar{w} + \kappa \nabla \bar{w}), \phi')_{\Gamma_h} = (\bar{w}, f)_{\Omega} + (\bar{w}, h)_{\Gamma_h} \quad (6.14)$$

$$(w', \mathcal{L}_{cdr} \bar{\phi} + \mathcal{L}_{cdr} \phi')_{\Omega} + (w', \mathbf{n} \cdot (\kappa \nabla \bar{\phi} + \kappa \nabla \phi'))_{\Gamma_h} = (w', f)_{\Omega} + (w', h)_{\Gamma_h} \quad (6.15)$$

where the third term in the third line of (6.12) drops out in the large-scale equation (6.14) due to the zero Dirichlet boundary condition for ϕ' . This system of two coupled variational equations will now be the subject of different solution strategies whereby the main focus will be on the small-scale equation in the form of (6.9) or (6.15), respectively.

6.2 Solving for the small scales

The first imaginable (and perhaps most obvious) solution strategy for the coupled system of large- and small-scale equation consists in solving the monolithic matrix scheme resulting from

the application of the usual finite element methodology to (6.8)–(6.9). The scale separation in this context can be done, for example, by using hierarchical shape functions. One might ask here why the scale separation has been performed, although the complete matrix is solved in the usual way. The reason for this distinction lies in the opportunity to treat the large and the small scales in a different way by, for instance, applying different (Petrov-)Galerkin methods to them or adding additional terms only to one of the two scale groups. The motive for proceeding this way will hopefully become clear during the course of this work.

On the other hand, explicitly solving for the small scales will provide the opportunity to eliminate them from the large-scale equation in the form (6.14). The related global strategy may be based on the use of Green's function. Restricting this function to individual elements of the original discretization named element Green's function offers the possibility to localize the small-scale solution. Such a localization has the benefit of drastically reducing the necessary computational effort along with the drawback of diverging from the real, in general globally affected, solution to a greater or lesser extent. With regard to the handled problem, one will have to judge, if this 'approximation by localization' seems to be reasonable. The interrelation between element Green's function and elementwise residual-free bubbles, which will be presented finally, is described in Brezzi et al. (1997), Hughes (1995) and Hughes et al. (1998).

6.2.1 Global monolithic solution using hierarchical shape functions

The hierarchical concept has been briefly explained in section 3.2.3. Picking up the essential feature of a natural scale separation within the set of shape functions of order k , a certain polynomial order \bar{k} for the large-scale space and a, necessarily higher, complete order k may now be chosen. The order(s) k' subject to

$$\bar{k} < k' \leq k; \quad [\bar{k}, k', k] \in \mathbb{N} \quad (6.16)$$

are then assigned to the small-scale space. Adjusting (6.3) and (6.4) to this approach yields

$$\mathcal{P}_\phi = \bar{\mathcal{P}}_\phi \oplus \mathcal{P}'_\phi \approx \bar{\mathcal{P}}_{\phi, \bar{k}} \oplus \mathcal{P}'_{\phi, k-\bar{k}} \quad (6.17)$$

$$\mathcal{Q}_\phi = \bar{\mathcal{Q}}_\phi \oplus \mathcal{Q}'_\phi \approx \bar{\mathcal{Q}}_{\phi, \bar{k}} \oplus \mathcal{Q}'_{\phi, k-\bar{k}} \quad (6.18)$$

where $\mathcal{P}'_{\phi, k-\bar{k}}$ indicates the finite-dimensional space approximating \mathcal{P}'_ϕ . Of course, the same applies to \mathcal{Q}'_ϕ in (6.18). Accordingly, large- and small-scale shape functions may be distinguished so as to get the large-scale approximations

$$\bar{w} = \sum_{\bar{A}=1}^{\bar{n}_{dofs}} \bar{N}_{\bar{A}} \bar{w}_{\bar{A}}, \quad \bar{\phi} = \sum_{\bar{B}=1}^{\bar{n}_{dofs}} \bar{N}_{\bar{B}} \bar{\phi}_{\bar{B}} \quad (6.19)$$

and the small-scale approximations

$$w' = \sum_{A'=1}^{n'_{dofs}} N'_{A'} w'_{A'}, \quad \phi' = \sum_{B'=1}^{n'_{dofs}} N'_{B'} \phi'_{B'} \quad (6.20)$$

with the respective number of degrees of freedoms \bar{n}_{dofs} and n'_{dofs} for the two approximation spaces. To be sure, both the large- and the small-scale approximations are subject to the same discretization characterized by an element length h . The only distinction lies in the different assign-

ment of shape functions of certain polynomial orders to either the large- or the small-scale approximation. Feeding these shape functions into (6.8)-(6.9) yields the matrix equivalent of the Galerkin problem reading

$$\begin{bmatrix} \mathbf{K}_{cdr}^- & \mathbf{K}_{cdr}^{-'} \\ \mathbf{K}'_{cdr} & \mathbf{K}_{cdr} \end{bmatrix} \cdot \begin{bmatrix} \bar{\phi} \\ \phi' \end{bmatrix} = \begin{bmatrix} \bar{\mathbf{F}} + \bar{\mathbf{N}} - \bar{\mathbf{E}} \\ \mathbf{F}' + \mathbf{N}' \end{bmatrix} \quad (6.21)$$

where $\mathbf{K}_{cdr} = \mathbf{C}(\mathbf{a}) + \mathbf{D} + \sigma_{(mod)}\mathbf{M}$ indicates the respective submatrices for the left hand sides and \mathbf{F} as well as \mathbf{N} the respective subvectors for the right hand sides of (6.8)-(6.9). $\bar{\mathbf{E}}$ denotes the entries due to the Dirichlet boundary conditions subject to (6.5). Please consult section 3.3.4 for elaboration of the respective matrices and vectors.

An important remark concerns the stability of this Galerkin approximation. It is well known that the standard Galerkin method irrespective of the use of hierarchical or standard Lagrange shape functions yields an unstable formulation for convection-dominated problems. Therefore, stabilizing terms have to be added to the matrix, for instance in the fashion of what will be proposed in section 6.3.1, resulting in additional stabilizing matrices $\mathbf{K}_{cdr,stab}$ in the scheme (6.21). Please keep in mind that scale separation is the only target of this global strategy. Thus, there is no 'help' in stabilizing the problem unless all scales of the problem are captured by the chosen discretization and polynomial order k - an unlikely case in general. The situation will, however, change substantially for all other concepts below with regard to the stability of the final problem to be solved.

Closing the description of this global solution concept, the merits and troubles of the hierarchic concept are emphasized, see e.g. Whiting and Jansen (2001) and Zienkiewicz et al. (1983). One may benefit from an improved conditioning of the matrix (6.21) with respect to matrices stemming from standard concepts. Furthermore, the special structure of the matrix consisting of submatrices which may be preserved allows for some potential computational savings as well as assistance in case of mesh refinement. Some problems associated with the hierarchic concept should be remarked as well. Difficulties arise with the coverage of initial and boundary conditions as well as with the post-processing of the solutions which do not occur in the standard concept.

6.2.2 Global solution by Green's function

The alternative global concept may be introduced by starting from the matrix form (6.21) and applying the process of static condensation. Thus, the description will go the other way round in comparison with Hughes (1995) and Hughes et al. (1998). According to the notation in Hughes (2000) (see (3.1)), the usual way consists in starting with the strong form of the problem and resulting in the matrix form in the long run passing the weak (or variational) form and the Galerkin equation. Starting here with the static condensation procedure for (6.21), the analogon in the variational form (6.15) of the small-scale equation will then be identified.

Solving the second line of (6.21) for ϕ' yields

$$\phi' = \left(\mathbf{K}'_{cdr}\right)^{-1} (\mathbf{F}' + \mathbf{N}') - \left(\mathbf{K}'_{cdr}\right)^{-1} \mathbf{K}'_{cdr} \bar{\phi} \quad (6.22)$$

which by inserting in the first line of (6.21) results in the matrix equation for $\bar{\phi}$ reading

$$\mathbf{K}_{cdr}^* \bar{\phi} = \mathbf{R}_{cdr}^* \quad (6.23)$$

where

$$\mathbf{K}_{cdr}^* = \mathbf{K}_{cdr}^{--} - \mathbf{K}_{cdr}^{-'} (\mathbf{K}_{cdr}^{\prime\prime})^{-1} \mathbf{K}_{cdr}^{-'} \quad (6.24)$$

and

$$\mathbf{R}_{cdr}^* = (\bar{\mathbf{F}} + \bar{\mathbf{N}}) - \mathbf{K}_{cdr}^{-'} (\mathbf{K}_{cdr}^{\prime\prime})^{-1} (\mathbf{F}' + \mathbf{N}') - \bar{\mathbf{E}} \quad (6.25)$$

The attention is now turned to the corresponding continuous problem of (6.14)-(6.15) where (6.15) may be rearranged as an Euler-Lagrange equation with the help of the projection operator \mathcal{P}' projecting onto the small-scale function space \mathcal{V}'_{ϕ} as follows

$$\mathcal{P}' \mathcal{L}_{cdr} \phi' = - \mathcal{P}' (\mathcal{L}_{cdr} \bar{\phi} - f) \quad \text{in } \Omega \quad (6.26)$$

$$\phi' = 0 \quad \text{on } \Gamma_g \quad (6.27)$$

$$\mathbf{n} \cdot \kappa \nabla \phi' = - (\mathbf{n} \cdot \kappa \nabla \bar{\phi} - h) \quad \text{on } \Gamma_h \quad (6.28)$$

Please note that the right hand side of (6.26) is exclusively governed by the residual of the large scales projected on the small-scale space. This assures the consistency of the method, since a function completely resolved by the large-scale approximation leaves nothing for the small scales to be done. Accordingly, they are equal to zero all over the domain Ω . One potential way of solving partial differential equations consists in the use of Green's function whereby one has to deal with a slightly different Green's function due to the fact that it is operated with the projection \mathcal{P}' of a strong form of a partial differential equation. The adjoint problem for the small-scale Green's function $g'(\mathbf{x}, \mathbf{x}_0)$ corresponding to (6.26)-(6.28) reads

$$\mathcal{P}' \mathcal{L}_{cdr}^* g'(\mathbf{x}, \mathbf{x}_0) = \mathcal{P}' \delta(\mathbf{x} - \mathbf{x}_0) \quad \text{in } \Omega \quad (6.29)$$

$$g'(\mathbf{x}, \mathbf{x}_0) = 0 \quad \text{on } \Gamma_g \quad (6.30)$$

$$\mathbf{n} \cdot \kappa \nabla_x g'(\mathbf{x}, \mathbf{x}_0) = 0 \quad \text{on } \Gamma_h \quad (6.31)$$

where \mathbf{x} denotes a general location vector, \mathbf{x}_0 a specific location vector and $\delta(\mathbf{x} - \mathbf{x}_0)$ the Dirac delta function at the specific location \mathbf{x}_0 . With the help of the solution of the adjoint Green's function problem, the small-scale solution at \mathbf{x}_0 may be determined exactly as

$$\begin{aligned} \phi'(\mathbf{x}_0) &= - \int_{\Omega} g'(\mathbf{x}, \mathbf{x}_0) (\mathcal{L}_{cdr} \bar{\phi} - f)(\mathbf{x}) d\Omega_x - \int_{\Gamma_h} g'(\mathbf{x}, \mathbf{x}_0) (\mathbf{n} \cdot \kappa \nabla \bar{\phi} - h)(\mathbf{x}) d\Gamma_x \\ &= - \int_{\Omega'} g'(\mathbf{x}, \mathbf{x}_0) (\mathcal{L}_{cdr} \bar{\phi} - f)(\mathbf{x}) d\Omega_x - \int_{\Gamma'} g'(\mathbf{x}, \mathbf{x}_0) [\mathbf{n} \cdot \kappa \nabla \phi]_+^+(\mathbf{x}) d\Gamma_x \\ &\quad - \int_{\Gamma_h} g'(\mathbf{x}, \mathbf{x}_0) (\mathbf{n} \cdot \kappa \nabla \bar{\phi} - h)(\mathbf{x}) d\Gamma_x \end{aligned} \quad (6.32)$$

which is written in shorthand with the help of a small-scale integral operator \mathcal{M}' as

$$\phi' = \mathcal{M}'(\mathcal{L}_{cdr}\bar{\phi} - f) \quad (6.33)$$

The fact that one is indeed able to recover an explicit result for the small scales on the entire domain Ω is the cause for refusing to designate the small scales as unresolved scales - a 'modus operandi' becoming crucial below. With (6.33) at hand, the small-scale part in the large-scale equation (6.14) may now be eliminated in order to get the one and only (large-scale) equation to be solved reading

$$\begin{aligned} B_{cdr}(\bar{w}, \bar{\phi}) + \left(\mathcal{L}_{cdr}^* \bar{w}, \mathcal{M}'(\mathcal{L}_{cdr}\bar{\phi} - f) \right)_{\Omega} + \left(\mathbf{n} \cdot (\mathbf{a}\bar{w} + \kappa \nabla \bar{w}), \mathcal{M}'(\mathcal{L}_{cdr}\bar{\phi} - f) \right)_{\Gamma_h} \\ = (\bar{w}, f)_{\Omega} + (\bar{w}, h)_{\Gamma_h} \quad \forall \bar{w} \in \bar{\mathcal{V}}_{\phi} \end{aligned} \quad (6.34)$$

with the integral operator $\mathcal{M}'(\mathcal{L}_{cdr}\bar{\phi} - f)$ being defined by the right hand side of (6.32). The process of eliminating the small scales from the large-scale equation may be called static condensation in an infinite-dimensional sense in comparison with what has been done before in a discrete sense, confer Brezzi (2000).

Since the achievement of the exact small-scale solution in (6.32), which implies the exact solution of the small-scale Green's function problem (6.29)-(6.31), will be impossible in almost all cases of interest, it has to be thought of good approximate solutions. What does this mean in this context? With respect to the function spaces, a good approximate, necessarily finite-dimensional, small-scale solution has to be found associated with function spaces $\mathcal{Y}'_{\phi, h'}$ and $\mathcal{V}'_{\phi, h'}$ such that

$$\mathcal{Y}_{\phi} = \bar{\mathcal{Y}}_{\phi} \oplus \mathcal{Y}'_{\phi} \approx \bar{\mathcal{Y}}_{\phi} \oplus \mathcal{Y}'_{\phi, h'} \quad (6.35)$$

$$\mathcal{V}_{\phi} = \bar{\mathcal{V}}_{\phi} \oplus \mathcal{V}'_{\phi} \approx \bar{\mathcal{V}}_{\phi} \oplus \mathcal{V}'_{\phi, h'} \quad (6.36)$$

is reasonable. This goes along with a good approximation of the small-scale Green's function formally expressed as

$$g'(\mathbf{x}, \mathbf{x}_0) \approx g'_{h'}(\mathbf{x}, \mathbf{x}_0) \quad (6.37)$$

replacing the exact analogon on the right hand side of (6.32). The subscript h' should act here as a symbol for any kind of discrete procedure for the small scales. Now the first circle can be closed, since the use of hierarchical bases in the sense of (6.17)-(6.18) has already been the first attempt in doing this approximation. According to this, (6.22) is the discrete analogon of (6.32) and the part in (6.22) that constitutes the approximate small-scale Green's function may formally be identified as containing the inverse of the matrix \mathbf{K}'_{cdr} . If the polynomial order in (6.16) is chosen to be going to infinity as $k \rightarrow \infty$, the exact small-scale Green's function would truly be encountered.

However, one is still left with the problem of huge demands on computational power by this global ansatz. Therefore, it is helpful to get deeper into the topic of coming up to a more localized approach for the small-scale solution in the following.

6.2.3 Local solution by element Green's function

As aforementioned, the localization approach as an assumption for the small scales will be confined by the borders of individual elements of the original discretization used to obtain the large-

scale solution. The underlying separation of function spaces (here only executed for the weighting function space for brevity reasons) for this purpose reads

$$\mathcal{V}_\phi \approx \overline{\mathcal{V}}_\phi \oplus \mathcal{V}'_{EGF} = \overline{\mathcal{V}}_\phi \oplus_{\Omega_e} H_0^1(\Omega_e); \quad e = 1, \dots, n_{el} \quad (6.38)$$

where $H_0^1(\Omega_e)$ is the infinite-dimensional space having its support in the respective element Ω_e and n_{el} the number of elements subject to the discretization. \oplus_{Ω_e} indicates that the small-scale space \mathcal{V}'_{EGF} is made up of a sum of n_{el} independent partial spaces. This is accomplished by introducing zero Dirichlet boundary conditions on the borders of every element as

$$\phi' = 0 \quad \text{on } \Gamma' \cup \Gamma \quad (6.39)$$

$$w' = 0 \quad \text{on } \Gamma' \cup \Gamma \quad (6.40)$$

Here, one can see the crucial assumption of this (and likewise the later to be addressed residual-free bubble) approach, i.e. only those scales are taken into account that do not cross the element boundaries. Please note that any Neumann boundary for the small scales is replaced by a homogeneous Dirichlet boundary herewith, which means that Neumann boundary conditions can only be represented by the large-scale solution $\overline{\phi}$. Hence, (6.37) is specified to be

$$g'(\mathbf{x}, \mathbf{x}_0) \approx g'_e(\mathbf{x}, \mathbf{x}_0); \quad e = 1, \dots, n_{el} \quad (6.41)$$

Assumptions (6.39)-(6.40) give rise to a simplified version of (6.32) reading

$$\phi'(\mathbf{x}_0) = - \sum_{e=1}^{n_{el}} \int_{\Omega_e} g'_e(\mathbf{x}, \mathbf{x}_0) (\mathcal{L}_{cdr} \overline{\phi} - f)(\mathbf{x}) d\Omega_x \quad (6.42)$$

which goes along with an approximate small-scale integral operator \mathcal{M}'_e in (6.33). The large- and small-scale equations (6.14)-(6.15) simplify to

$$B_{cdr}(\overline{w}, \overline{\phi}) + (\mathcal{L}_{cdr}^* \overline{w}, \phi')_{\Omega} = (\overline{w}, f)_{\Omega} + (\overline{w}, h)_{\Gamma_h} \quad \forall \overline{w} \in \overline{\mathcal{V}}_\phi \quad (6.43)$$

$$(w', \mathcal{L}_{cdr} \overline{\phi})_{\Omega} + (w', \mathcal{L}_{cdr} \phi')_{\Omega} = (w', f)_{\Omega} + (w', h)_{\Gamma_h} \quad \forall w' \in \mathcal{V}'_{EGF} \quad (6.44)$$

as well as the final equation (6.34) to be solved to

$$B_{cdr}(\overline{w}, \overline{\phi}) + \sum_{e=1}^{n_{el}} (\mathcal{L}_{cdr}^* \overline{w}, \mathcal{M}'_e(\mathcal{L}_{cdr} \overline{\phi} - f))_{\Omega_e} = (\overline{w}, f)_{\Omega} + (\overline{w}, h)_{\Gamma_h} \quad \forall \overline{w} \in \overline{\mathcal{V}}_\phi \quad (6.45)$$

At this point, the only thing remaining to be done is to solve the element Green's function problem in every element e subject to

$$\mathcal{P}' \mathcal{L}_{cdr}^* g'_e(\mathbf{x}, \mathbf{x}_0) = \mathcal{P}' \delta(\mathbf{x} - \mathbf{x}_0) \quad \text{in } \Omega_e \quad (6.46)$$

$$g'_e(\mathbf{x}, \mathbf{x}_0) = 0 \quad \text{on } \Gamma_e \quad (6.47)$$

An important question is linked with the projection operator \mathcal{P}' concerning the cases which allow us to omit the projection onto the small-scale space. By doing this, one is in the position of 'merely' solving a small-scale equation in strong form on each element domain Ω_e which is then again open to any discrete method on this level. This is the strategy to be followed in a subsequent part of this work. The answer to this question is postponed until the end of the discussion of residual-free bubbles in the next section.

An analytic solution for (6.46)-(6.47) may hardly be found, although the equation is, in general, put on a simpler domain from now on with respect to the global equation system (6.29)-(6.31). For a few situations, solutions are available, see e.g. Duffy (2001) and Stakgold (1998). For the underlying problem of convection-diffusion-reaction equations, Hauke and Garcia-Olivares (2001) give a solution for the one-dimensional version of this equation which they use to develop a stabilization parameter on this ground. This will be picked up again below in the context of stabilized methods. Beyond the one-dimensional case however, the limitations of solving this local approach in analytic form are encountered. Thus, it is now turned to a closely related local strategy paving the way to practical use.

6.2.4 Local solution by residual-free bubbles

Residual-free bubbles represent a very similar strategy in comparison to what has just been introduced as element Green's functions. According to this, using residual-free bubbles means obeying two basic rules:

- The governing differential equation has to be satisfied by the complete solution function in strong form on every individual element domain Ω_e of the basic discretization.
- Zero Dirichlet boundary conditions in the sense of (6.39)-(6.40) have to be assumed for the small-scale part of the solution function on the boundary of every individual element domain Ω_e .

For the underlying case of a separation of the solution function into a large- and a small-scale part, following the above rules amounts to selecting the small-scale bubble part of the solution function such that the governing equation is solved in every individual element up to the large-scale part of the solution function. Correspondingly, the residual of the large-scale part of the solution function appears on the right hand side of the residual-free bubble equation representing the 'driving force' of this equation. This equation is subject to homogeneous Dirichlet boundary conditions as aforementioned. The major distinction to what has been done in the previous section is found in the fact that no Green's functions are exploited for this solution procedure and it is rather reverted to the original strong form of the underlying differential equation.

Before shortly describing the details of the solution strategy employing residual-free bubbles for a convection-diffusion-reaction equation, a selection of the respective literature addressing residual-free bubbles in general as well as for other types of equations authored by Brezzi, Farhat, Franca, Hughes, Russo and co-workers is named: Brezzi and Russo (1994), Brezzi et al. (1997), Brezzi et al. (1998a), Brezzi et al. (1998b), Brezzi (2000), Franca and Farhat (1995) as well as Franca et al. (1998a). In Brezzi et al. (2003), a new idea is developed for the case of a dominating reactive term. The discussion in this paper is confined to the one-dimensional case though. The reader should consult some of these publications for further elaboration.

The derivations of the preceding section may be adopted almost completely. The separation of function spaces reads similar to (6.38)

$$\mathcal{V}_\phi \approx \overline{\mathcal{V}}_\phi \oplus \mathcal{V}'_{RFB} = \overline{\mathcal{V}}_\phi \oplus_{\Omega_e} B(\Omega_e); \quad e = 1, \dots, n_{el} \quad (6.48)$$

where $B(\Omega_e)$ is the infinite-dimensional bubble space in the element Ω_e . It is a usual assumption that $B(\Omega_e) = H_0^1(\Omega_e)$. The crucial difference refers to the small-scale Green's function problem

(6.46)-(6.47) now being replaced by the underlying strong form of the small-scale equation projected onto the small-scale space which has to be solved in each individual element subject to

$$\mathcal{P}' \mathcal{L}_{cdr} \phi' = - \mathcal{P}' (\mathcal{L}_{cdr} \bar{\phi} - f) \quad \text{in } \Omega_e \quad (6.49)$$

$$\phi' = 0 \quad \text{on } \Gamma_e \quad (6.50)$$

At the end of the preceding section, the question of leaving out the projection operator \mathcal{P}' in the element-based small-scale equations has already been raised. In order to answer this question it has to be stated that one is required to avoid any linear dependencies between the large- and small-scale spaces, since they are separated by the direct sum decomposition (6.3)-(6.4). Taking into account the zero Dirichlet boundary conditions on element boundaries, \mathcal{P}' may be left out anyway in case of exclusive use of piecewise linear shape functions for the large-scale space, e.g. for triangular as well as quadrilateral elements in the two-dimensional case. For quadrilateral elements, this can, for instance, be extended to piecewise quadratic and cubic elements of serendipity type. Since Lagrange elements of quadratic (cubic) and higher order for quadrilaterals (triangles) as well as serendipity elements of quartic and higher order possess at least one bubble function, they cannot be applied without potentially violating the direct sum decomposition (6.3)-(6.4). The same applies to three-dimensional elements featuring at least one bubble function. In the following, the focus will be on the unprojected equation, namely

$$\mathcal{L}_{cdr} \phi' = - (\mathcal{L}_{cdr} \bar{\phi} - f) \quad \text{in } \Omega_e \quad (6.51)$$

in conjunction with (6.50) and replacing (6.49). This may be done, since the focus will be on rectangular serendipity elements in the applications below and it is not intended to exceed cubic polynomial shape functions. However, the necessity to switch over to (6.49) otherwise has to be kept in mind.

If one were able to solve these element-based problems, the overall solution

$$\phi' = - \sum_{e=1}^{n_{el}} \left\{ \left(\mathcal{L}_{cdr, \Omega_e}^{RFB} \right)^{-1} (\mathcal{L}_{cdr} \bar{\phi} - f) \right\} \quad (6.52)$$

would be encountered where the inverse of the differential operator $\mathcal{L}_{cdr, \Omega_e}^{RFB}$ may, in general, vary from one element domain Ω_e to another, and the superscript *RFB* shall symbolize here and below the zero Dirichlet boundary condition. (6.52) can now be integrated into the simplified variational equation for the large scales (6.43) so as to get

$$B_{cdr}(\bar{w}, \bar{\phi}) - \sum_{e=1}^{n_{el}} \left(\mathcal{L}_{cdr}^* \bar{w}, \left(\mathcal{L}_{cdr, \Omega_e}^{RFB} \right)^{-1} (\mathcal{L}_{cdr} \bar{\phi} - f) \right)_{\Omega_e} = (\bar{w}, f)_{\Omega} + (\bar{w}, h)_{\Gamma_h} \quad (6.53)$$

As already mentioned in the context of the element Green's function problems, it will hardly be possible to solve these element problems, but it may be tried to solve them by using a discretization on a second level compared to the initial coarse grid. This 'modus operandi' is named 'two-level finite element method' and will be presented in chapter 8.

Comparing (6.53) with (6.45) in conjunction with (6.42), the formal relationship between the element Green's function and the residual-free bubble may easily be recognized to correspond with well-known facts from the theory of Green's function (see e.g. Stakgold (1998)) reading

$$\left(\mathcal{L}_{cdr, \Omega_e}^{RFB}\right)^{-1}(\mathbf{x}_0) = -\mathcal{M}_e' = \int_{\Omega_e} g_e'(\mathbf{x}, \mathbf{x}_0) d\Omega_x \quad (6.54)$$

This result has been pointed out by Brezzi et al. (1997) where it can already be learned from the title of the publication.

Linear finite element methods using shape functions in the sense of (3.32) and (3.33) provide the opportunity to solve directly for the shape function components of the small-scale solution ϕ' , i.e. the expansion in any element e for the large-scale solution function is presumed to be

$$\bar{\phi}_e = \sum_{b=1}^{n_{ed}} \bar{N}_b \phi_b \quad (6.55)$$

and the corresponding small-scale solution function

$$\phi_e' = \sum_{b=1}^{n_{ed}} N_b' \phi_b \quad (6.56)$$

where n_{ed} denotes the number of degrees of freedom associated with element e . The crucial fact to be observed is the difference of (6.55)-(6.56) with respect to (6.19)-(6.20). In (6.19)-(6.20), different numbers of degrees of freedom for the large- and the small-scale approximations have been introduced. This describes an approach suited, for instance, for polynomial bubbles. In the context of residual-free bubbles, only one (large-scale) number of degrees of freedom is encountered indicated in (6.55)-(6.56) on the element level with n_{ed} . According to this, a pair of corresponding large- and small-scale shape functions is found linked with one degree of freedom in each case. The advantage of this may be seen by introducing (6.55)-(6.56) in (6.51) such that

$$\mathcal{L}_{cdr} \sum_{b=1}^{n_{ed}} N_b' \phi_b = - \left[\mathcal{L}_{cdr} \sum_{b=1}^{n_{ed}} \bar{N}_b \phi_b - f \right] \quad \text{in } \Omega_e \quad (6.57)$$

Due to the linearity of the differential operator \mathcal{L}_{cdr} , (6.57) can be decomposed into its basic components so to get

$$\sum_{b=1}^{n_{ed}} \mathcal{L}_{cdr} N_b' \phi_b = - \sum_{b=1}^{n_{ed}} \mathcal{L}_{cdr} \bar{N}_b \phi_b \quad \text{in } \Omega_e \quad (6.58)$$

The degrees of freedom ϕ_b can be omitted on both sides. As a result, n_{ed} equations for the convection-diffusion- reaction problem of the form

$$\mathbf{a} \cdot \nabla N_b' - \kappa \Delta N_b' + \sigma_{(\text{mod})} N_b' = - \left(\mathbf{a} \cdot \nabla \bar{N}_b - \kappa \Delta \bar{N}_b + \sigma_{(\text{mod})} \bar{N}_b \right) \quad \text{in } \Omega_e \quad (6.59)$$

have to be solved in each element e . Completing the solution, an additional small-scale shape function N_f' has to be introduced in order to pick up the effect of f on the right hand side of (6.57) subject to

$$\mathbf{a} \cdot \nabla N_f' - \kappa \Delta N_f' + \sigma_{(\text{mod})} N_f' = f \quad \text{in } \Omega_e \quad (6.60)$$

A number of $n_{RFB} = n_{el}(n_{ed} + 1)$ entirely independent residual-free bubble equations have to be solved in order to feed the final equation with the small-scale information before solving it.

Alternatively, one may think of restricting the approximation of f to the large-scale space (see Codina and Blasco (2002)) resulting in the possibility to omit (6.60) which reduces the overall number of residual-free bubble equations to $n_{RFB} = n_{el}n_{ed}$. For example, a bilinear rectangle gives rise to 5 or 4 equations per element, respectively.

6.3 Taking into account locally the effect of unresolved scales onto resolved scales

6.3.1 Stabilized methods

The interrelation between element Green's function, elementwise residual-free bubbles and stabilized methods has been described e.g. in Hughes (1995) and Hughes et al. (1998) as well as particularly the link between elementwise residual-free bubble and stabilized methods e.g. in Franca and Farhat (1995) and Franca et al. (1998a). Further literature will be mentioned during the course of this section. Despite this connection, it is intended to draw a clear line between stabilized methods and the aforementioned local solution strategies, since stabilized methods in the following form indeed only make available the effect of unresolved scales onto resolved scales in a localized manner. Therefore, it will also be gone back to the terms 'resolved scales' and 'unresolved scales' in this section. Referring to the function space separation in (6.3)-(6.4), it may be stated that this still holds, since no finite-dimensional approximation to \mathcal{P}'_ϕ and \mathcal{V}'_ϕ , respectively, will be introduced like in section 6.2. However, \mathcal{P}'_ϕ and \mathcal{V}'_ϕ are replaced by \mathcal{P}_ϕ and \mathcal{V}_ϕ , respectively, due to the fact that $(\hat{\cdot})$ should indicate unresolved scales here and later in the context of a separation of three scales. Hence, (6.3)-(6.4) now read

$$\mathcal{P}_\phi = \overline{\mathcal{P}}_\phi \oplus \hat{\mathcal{P}}_\phi \quad (6.61)$$

$$\mathcal{V}_\phi = \overline{\mathcal{V}}_\phi \oplus \hat{\mathcal{V}}_\phi \quad (6.62)$$

There is a vast number of literature on the theory and applications of stabilized finite element methods in different fields in the meantime. A brief selection of publications entirely or partly dedicated to the convection-diffusion-reaction equation will be given in the following and, thereafter, the attention will be concentrated on the version intimately linked with the two aforementioned approaches termed 'unusual stabilized finite element method' (USFEM) in Franca and Farhat (1995).

Before getting deeper into different forms of stabilized methods, the general formulation valid for all of them should be stated reading

$$B_{cdr}(\overline{w}, \overline{\phi}) + \sum_{e=1}^{n_{el}} \left(\mathcal{L}_{cdr}^{stab} \overline{w}, \tau_e (\mathcal{L}_{cdr} \overline{\phi} - f) \right)_{\Omega_e} = (\overline{w}, f)_\Omega + (\overline{w}, h)_{\Gamma_h} \quad \forall \overline{w} \in \overline{\mathcal{V}}_\phi \quad (6.63)$$

where the differential operator \mathcal{L}_{cdr}^{stab} acting on the weighting function \overline{w} depends on the respective type of method. Some of the most important ones will be described succinctly. The other aspect of (6.63) distinguishing it from (6.45) and (6.53), respectively, is the elementwise algebraic parameter τ_e which may in some cases vary inside the element. However, the focus will be on the usual way of assuming a constant τ_e in each element of the discretization. Instructions for calculating τ_e will be given later.

Overviews describing the evolution of stabilized finite element methods may be found in Brezzi et al. (1996), Donea and Huerta (2003), Hughes et al. (1994b) and Wall (1999). At the beginning of the 1980's, the triumphal procession of stabilized methods for convection-diffusion equations started with the 'Streamline-Upwind/Petrov-Galerkin' (SUPG) method developed by Hughes and co-workers (see e.g. Brooks and Hughes (1982)), analyzed and used by Johnson and co-workers under the name 'Streamline-Diffusion' method (see e.g. Johnson et al. (1984), Johnson and Saranen (1986) as well as Johnson (1987)). Here, the differential operator acting on the weighting function \bar{w} corresponds to the convective part of the original operator $\mathcal{L}_{cdr}^{stab} = \mathcal{L}_c$. The use of the complete differential operator $\mathcal{L}_{cdr}^{stab} = \mathcal{L}_{cdr}$ is the feature of the 'Galerkin/Least-Squares' (GLS) method of Hughes et al. (1989). Franca et al. (1992) proposed at first to include the negative adjoint differential operator $\mathcal{L}_{cdr}^{stab} = -\mathcal{L}_{cdr}^*$ which was later identified to correspond with the element Green's function method and the residual-free bubble method. At the same time, the close relationship between stabilized methods and bubble methods was elaborated by Brezzi et al. (1992). This has been continued by Brezzi and co-workers, for example, in Baiocchi et al. (1993) as well as in Brezzi and Russo (1994). The method employing the negative adjoint differential operator has been termed as an 'unusual stabilized finite element method' (USFEM) by Franca and co-workers in Franca and Farhat (1995), Franca et al. (1998a) as well as Franca and Valentin (2000), in the latest with the inclusion of a reactive term.

A comparison of different stabilized finite element methods for the convection-diffusion-reaction equation is provided by Codina (1998) and some further applications of the stabilization technique in Codina (2000b). A special design of the stabilization parameter incorporating the flow direction is proposed in Harari et al. (2001). Further recent approaches are the finite increment calculus (FIC) leading to very similar stabilization techniques as could be proven by Oñate and co-workers, for example, in Oñate et al. (1997) and Oñate (1998), and the nearly-optimal Petrov-Galerkin (NOPG) method described e.g. in Barbone and Harari (2001) as well as Nesli-turk and Harari (2003).

Extending the formal relationship between element Green's function and the residual-free bubbles in (6.54) by taking into account the USFEM-version of (6.63), τ_e is obtained to be the mean value of the element Green's function, i.e.

$$\tau_e = \frac{1}{|\Omega_e|} \int_{\Omega_e} \int_{\Omega_e} g_e'(\mathbf{x}, \mathbf{x}_0) d\Omega_x d\Omega_{x_0} \quad (6.64)$$

as well as (formally) the mean value of the residual-free bubble, i.e.

$$\tau_e = \frac{1}{|\Omega_e|} \int_{\Omega_e} \left(\mathcal{L}_{cdr, \Omega_e}^{RFB} \right)^{-1} (\mathbf{x}_0) d\Omega_{x_0} \quad (6.65)$$

by inserting (6.54) into (6.64). In order to restrict the discussion for brevity reasons, a few steps in the derivation of (6.65) have been omitted, and it is referred to Hughes et al. (1998) for this.

At this point, the calculation of the stabilization parameter has to be specified. From the variety of proposals in the literature, it will be focussed on three, listed here in chronologic order of their appearance: the one of Codina (1998), the one of Franca and Valentin (2000), and the one of Codina in Codina and Blasco (2002) and Codina (2002a), respectively. Codina derived his version in Codina (1998) from the maximum principle which reads

$$\tau_e^{Co98} = \frac{1}{\frac{4\kappa}{h^2} + \frac{2|a|}{h} + \sigma_{(\text{mod})}} \quad (6.66)$$

Franca and Valentin (2000) introduced an improved parameter for their USFEM based on convergence theory as follows:

$$\tau_e^{FV} = \frac{1}{\frac{2\kappa}{m_k h^2} \xi(Pe_2) + \sigma_{(\text{mod})} \xi(Pe_1)} \quad (6.67)$$

where

$$\xi(x) = \begin{cases} 1, & 0 \leq x < 1 \\ x, & x \geq 1 \end{cases} \quad (6.68)$$

$$Pe_1 = \frac{2\kappa}{m_k \sigma_{(\text{mod})} h^2} \quad (6.69)$$

$$Pe_2 = \frac{m_k |a| h}{\kappa} \quad (6.70)$$

and the parameter m_k depending on the polynomial order of interpolation in the respective element may be chosen as 1/3 for linear and bilinear as well as 1/12 for quadratic and biquadratic elements. Confer Harari and Hughes (1992) for an exploration of the theory behind this. In (6.67), switches between the different regimes are incorporated. Without these switches (6.66) is similar to (6.67) up to the parameter m_k for a diffusion-dominated regime. In Codina and Blasco (2002) and Codina (2002a), a more general derivation based on a Fourier analysis with the help of the mean value theorem is given in order to identify

$$\tau_e^{Co02} = \frac{1}{\left[\left(c_1 \frac{\kappa}{h^2} + \sigma_{(\text{mod})} \right)^2 + \left(c_2 \frac{|a|}{h} \right)^2 \right]^{\frac{1}{2}}} \quad (6.71)$$

leaving out a precise definition of the constants c_1 and c_2 for the time being. As a first regulation, the relationship between the two constants is given as follows:

$$c_1 \geq c_2^2 \quad (6.72)$$

The reader may easily confirm that both (6.66) and (6.67) implicitly satisfy this inequality.

Hauke and Garcia-Olivares (2001) derived a stabilization parameter τ_e from the already presented element Green's function with the help of (6.64) and were able to show that it provides very similar results for one-dimensional applications in comparison with (6.66) and (6.67). In Hauke (2002), different stabilization parameters are analyzed for the multidimensional case, and the parameter of Franca and Valentin (6.67) is recognized to be the most appropriate with respect to certain requisites. In particular, going beyond the scope of the assumption of keeping the reaction coefficient σ positive, Hauke (2002) also considered a production regime governed by a negative σ . According to this results, the stabilization parameter τ_e will be chosen subject to (6.67) whenever there is a need to employ stabilizing terms.

Concluding this section about stabilization methods as a way of 'solving' for the small scales, the most important point in the author's view should be reiterated. Compared with all the alternative ways of solving for the small scales, may they be globally or locally approximated, this is the only one precluding us from any opportunity to explicitly calculate the global or local distribution of the small scales, at least in a post-processed manner. They are named 'unresolved' in the context of stabilized methods thus. Placing emphasis on this point again, it does not make any difference whether these small scales are confined within individual elements or globally distributed over the whole domain. All the previous solution methods offer a more or less accurate possibility of collecting the small scales. If one thinks of a variation of τ_e over the element domain in the form $\tau_e = \tau_e(\mathbf{x}, \mathbf{x}_0)$ according to the element Green's function in the sense of a generalized stabilized method, some knowledge of the element Green's function will have to be presumed in general. Confer Oberai and Pinsky (1998) for an example with regard to the solution of the Helmholtz equation. As aforementioned, this knowledge is hardly available and, moreover, the 'ring' of solution methods would then be entered again.

6.3.2 Dissipative effect of unresolved scales: artificial diffusion methods

Although artificial diffusion methods are, in general, not used for multidimensional applications mainly due to the inherent crosswind diffusion of this approach, the reason for mentioning this method here at all is twofold. On the one hand, this approach will be used in the following three-scale separation in order to account for the (then introduced) third level with more promising prospects of success in this context. On the other hand, the similar approach in form of the sub-grid viscosity concept has already been presented in section 5.2.3 as a well-established concept in large eddy simulation of turbulent flows. The reason for mentioning artificial diffusion method here is justified by the analogy to the just discussed stabilized methods.

The introduction of an elementwise artificial diffusion κ_e^{art} results in the elementwise addition of a diffusive term replacing the small-scale term in the large-scale equation (6.8) such that it reads

$$B_{cdr}(\bar{w}, \bar{\phi}) + \sum_{e=1}^{n_{el}} (\nabla \bar{w}, \kappa_e^{art} \nabla \bar{\phi})_{\Omega_e} = (\bar{w}, f)_{\Omega} + (\bar{w}, h)_{\Gamma_h} \quad \forall \bar{w} \in \bar{\mathcal{T}}_{\phi} \quad (6.73)$$

where a simplified formula may be used for the calculation of κ_e^{art} as follows:

$$\kappa_e^{art} = \begin{cases} \frac{|a|\bar{h}}{2} \frac{Pe^e}{3}, & \text{for } Pe^e < 3 \\ \frac{|a|\bar{h}}{2}, & \text{for } Pe^e \geq 3 \end{cases} \quad (6.74)$$

with the definition of the element Peclet number

$$Pe^e = \frac{|a|\bar{h}}{2\kappa} \quad (6.75)$$

It may easily be observed that, for instance, the artificial diffusion obtained by using the stabilization parameter of Franca and Valentin (6.67) for a zero reactive term, i.e. $\sigma_{(mod)} = 0$, subject to

$$\kappa_e^{stab} = \tau_e^{FV}(\sigma_{(mod)} = 0) \cdot |\mathbf{a}|^2 = \frac{|\mathbf{a}|^2}{\frac{2\kappa}{m_k \bar{h}^2} \xi(\mathbf{P}e_2) + \frac{2\kappa}{m_k \bar{h}^2}} \quad (6.76)$$

in combination with (6.70) is (exactly for the diffusion-dominated regime and almost exactly for the convection-dominated regime) equal to the artificial diffusion in (6.74) for linear and bilinear elements. Therefore, the major differences of the artificial diffusion method in comparison to the stabilized methods for the convection-diffusion-reaction equation may be pointed out in the following remarks:

- There is no adequate stabilization of the reactive term without taking into account an additional term. (Since 'pure' convection-diffusion equations will also be considered in the following, this is no reason for ceasing from paying attention to this approach at all however.)
- Stabilized methods for linear and bilinear elements (SUPG, GLS and USFEM) introduce artificial diffusion only in the streamline direction whereas artificial diffusion will be introduced in all directions by the artificial diffusion method (This is a well-known and crucial fact, confer e.g. Brooks and Hughes (1982) for further elaboration.)
- Stabilized methods provide a different weighting of the right hand side f (This guarantees the method to be stable and accurate.)
- For higher-order elements, GLS and USFEM introduce additional terms not present in the artificial diffusion method. (This guarantees the method to be consistent for higher-order elements.)

Despite all the drawbacks of the artificial diffusion method, it will be kept in mind due to the reasons accomplished at the beginning of this section as well as its obvious simplicity.

6.4 Separation of three scales

The complete spectrum of scales is now separated into large (resolved) scales, small (resolved) scales and unresolved scales. The idea of distinguishing three such scale ranges for the Navier-Stokes equations with respect to turbulence modeling was introduced by Collis (2001) and further investigated for the specific example of a turbulent channel flow in Ramakrishnan and Collis (2002). This concept will be generalized here and applied to the convection-diffusion-reaction equation. Furthermore, different strategies for treating the effect of the unresolved scales constituting the third level of the scale spectrum will be considered. To be sure, furthergoing separations bearing four, five or more levels are conceivable so that the advantage of being able to treat every level differently with regard to the methods or modeling assumptions, respectively, would be encountered. At first, however, it is not necessary to go beyond a three-scale separation.

The function space separation may be extended in (6.3)-(6.4) or in (6.35)-(6.36), respectively, in order to get

$$\mathcal{Y}_\phi = \bar{\mathcal{Y}}_\phi \oplus \mathcal{Y}'_\phi = \bar{\mathcal{Y}}_\phi \oplus \mathcal{Y}'_{\phi, h'} \oplus \hat{\mathcal{Y}}_\phi \quad (6.77)$$

$$\mathcal{V}_\phi = \bar{\mathcal{V}}_\phi \oplus \mathcal{V}'_\phi = \bar{\mathcal{V}}_\phi \oplus \mathcal{V}'_{\phi, h'} \oplus \hat{\mathcal{V}}_\phi \quad (6.78)$$

where the originally infinite-dimensional space \mathcal{S}'_ϕ is now separated into the already introduced finite-dimensional approximation characterized by h' and the necessarily infinite-dimensional space $\hat{\mathcal{S}}_\phi$ representing the space of unresolved scales. The same applies to the weighting function space \mathcal{V}'_ϕ . The extended equation system reads

$$\mathfrak{B}_{cdr}(\bar{w}, \bar{\phi}) + B_{cdr}(\bar{w}, \phi') + B_{cdr}(\bar{w}, \hat{\phi}) = (\bar{w}, f)_\Omega + (\bar{w}, h)_{\Gamma_h} \quad \forall \bar{w} \in \bar{\mathcal{V}}_\phi \quad (6.79)$$

$$B_{cdr}(w', \bar{\phi}) + B_{cdr}(w', \phi') + B_{cdr}(w', \hat{\phi}) = (w', f)_\Omega + (w', h)_{\Gamma_h} \quad \forall w' \in \mathcal{V}'_{\phi, h'} \quad (6.80)$$

$$B_{cdr}(\hat{w}, \bar{\phi}) + B_{cdr}(\hat{w}, \phi') + B_{cdr}(\hat{w}, \hat{\phi}) = (\hat{w}, f)_\Omega + (\hat{w}, h)_{\Gamma_h} \quad \forall \hat{w} \in \hat{\mathcal{V}}_\phi \quad (6.81)$$

Now, it is assumed that

$$B_{cdr}(\bar{w}, \hat{\phi}) \approx 0 \quad (6.82)$$

i.e. the projection of the unresolved scales onto the large-scale space is approximately zero. This is a reasonable approximation as long as there is a clear scale separation between the large and the unresolved scales. Alternatively expressed, it has to be ensured that the small-scale space is large enough. To be sure, the large scales are still influenced by the unresolved scales. For this purpose however, they need the small scales as a kind of 'medium'. Later on in the context of the Navier-Stokes equations, this assumption will play a major role for turbulent flows and may be proved to make sense. Accordingly, it may be thought of the opposite projection of (2.95) likewise to be

$$B_{cdr}(\hat{w}, \bar{\phi}) \approx 0 \quad (6.83)$$

This leads to a simplified system of equations:

$$B_{cdr}(\bar{w}, \bar{\phi}) + B_{cdr}(\bar{w}, \phi') = (\bar{w}, f)_\Omega + (\bar{w}, h)_{\Gamma_h} \quad \forall \bar{w} \in \bar{\mathcal{V}}_\phi \quad (6.84)$$

$$B_{cdr}(w', \bar{\phi}) + B_{cdr}(w', \phi') + B_{cdr}(w', \hat{\phi}) = (w', f)_\Omega + (w', h)_{\Gamma_h} \quad \forall w' \in \mathcal{V}'_{\phi, h'} \quad (6.85)$$

$$B_{cdr}(\hat{w}, \phi') + B_{cdr}(\hat{w}, \hat{\phi}) = (\hat{w}, f)_\Omega + (\hat{w}, h)_{\Gamma_h} \quad \forall \hat{w} \in \hat{\mathcal{V}}_\phi \quad (6.86)$$

The equations may certainly be formulated for the unresolved scales similar to (6.26)-(6.28) as well as the adjoint Green's function problem (6.29)-(6.31) in global form or the respective localized problems (6.49)-(6.50) as well as (6.46)-(6.47). The $(\cdot)'$ -scales would just have to be replaced by the (\cdot) -scales and the $(\bar{\cdot})$ -scales by the $(\cdot)'$ -scales in the equations, respectively. It has to be kept in mind, however, that one is talking about unresolved scales. Consequently, it is not intended to solve them. Only their effect onto the small scales is rather taken into account. At any rate, the large-scale equation in case of a monolithic solution approach as well as the final enhanced (large-scale) equation resulting from the global or local Green's function or the residual-free bubble approach will not be modified. In the case of the enhanced equations, the modification due to the incorporation of the effect of the unresolved scales enters this equation through an altered small-scale integral operator \mathcal{M}' in (6.34) or \mathcal{M}'_e in (6.45) due to a mutated (element) Green's function or an altered inverse differential operator in (6.53), respectively. In section 6.3, one already got used to two potential ways of accounting for the effect of unresolved scales. They

will be demonstrated using residual-free bubbles on the second level in the course of chapter 8. The transfer to the global monolithic solution strategy is straightforward in that the third-level terms just have to be added to the small-scale equation similar to what has been done in section 6.3.

At first, stabilized methods are presented with the aim of incorporating the complete effect of the unresolved scales onto the small scales. Please keep in mind that this implies the introduction of artificial diffusion only in the streamline direction as stated in the last section. The new enhanced small-scale equation extending (6.9) and replacing (6.85) reads

$$\begin{aligned} & B_{cdr}(w', \bar{\phi}) + B_{cdr}(w', \phi') + \sum_{e=1}^{n_{el}} \left(\mathcal{L}_{cdr}^{stab} w', \tau'_e (\mathcal{L}_{cdr} \phi' - f) \right)_{\Omega_e} \\ & = (w', f)_{\Omega} + (w', h)_{\Gamma_h} \quad \forall w' \in \mathcal{V}'_{\phi, k-\bar{k}} \end{aligned} \quad (6.87)$$

where τ'_e may differ from e.g. the definition in (6.67)-(6.70) in the parameter m_k which should be matched to the emerging polynomial orders or by using a modified \bar{h} . Another opportunity consists in the exclusive comprehension of the dissipative effect as in section 6.3.2. For this purpose, the small-scale equation reads

$$B_{cdr}(w', \bar{\phi}) + B_{cdr}(w', \phi') + \sum_{e=1}^{n_{el}} \left(\nabla w', \kappa_e^{art} \nabla \phi' \right)_{\Omega_e} \quad (6.88)$$

$$= (w', f)_{\Omega} + (w', h)_{\Gamma_h} \quad \forall w' \in \mathcal{V}'_{\phi, k-\bar{k}} \quad (6.89)$$

with the artificial diffusion κ_e^{art} of (6.74)-(6.75) using a modified \bar{h} in case the classical way of artificial diffusion methods is followed. Aside from this, the basic idea of adding such an artificial diffusion term for stability reasons on the second level of a two-level decomposition goes back to Guermond, see e.g. Guermond (1999) and Guermond (2001). You may also consult Layton (2002) (further analyzed in Kaya and Layton (2003) as well as Kaya (2003)) for an interesting, more general, variant of this idea. Accordingly, the guidelines of Guermond are followed here for evaluating an artificial diffusion κ_e^G reading

$$\kappa_e^G = C_e^G h \quad (6.90)$$

with an unspecified h (possibly replaced by the aforementioned modified \bar{h}) and a bounded constant C_e^G having the dimension of a velocity for consistency of (6.90). Comparing (6.90) with the definition of κ_e^{art} in (6.74), it may be detected that C_e^G , for instance, amounts $|a|/2$ in the convection-dominated regime. The relative fuzziness of the constant for the time being is certainly the weak point of this ansatz.

Closing the discussion of these approaches, two important facts have to be remarked. For the artificial diffusion approach, an additional consideration related to the reactive term is necessary, confer section 6.3.2. Moreover, it remains an open question, if there is the necessity to add stability, probably in the form of additional stabilizing terms, to the large-scale equation.

At the end of this section, an interesting alternative approach of Codina described in Codina (2000c), Codina and Blasco (2002), Codina (2002a) as well as Codina (2002b) and well-suited for using a stabilized method on the second level should be addressed. The basic idea explained with the help of the residual-free bubble equation (6.51) is as follows. For this equation to belong

to the complete small-scale solution function space \mathcal{Y}'_ϕ , something has to be added which Codina calls 'orthogonal subscales' subject to

$$\mathcal{L}_{cdr}\phi' = -(\mathcal{L}_{cdr}\bar{\phi} - f) + w_{ort} \quad \text{in } \Omega_e \quad (6.91)$$

The crucial point now is how the function spaces are chosen. \mathcal{Y}'_ϕ is considered to be taken as

$$\mathcal{Y}'_\phi = \bar{\mathcal{Y}}_\phi^\perp \cap \mathcal{Y}_\phi \quad (6.92)$$

where $\bar{\mathcal{Y}}_\phi^\perp$ is the function space orthogonal to the large-scale space $\bar{\mathcal{Y}}_\phi$ which is not closed in \mathcal{Y}_ϕ . The important assumption is

$$\mathcal{Y}'_\phi \approx \bar{\mathcal{Y}}_\phi^\perp \quad (6.93)$$

i.e. the small scales are allowed to be non-conforming and, therefore, potentially going beyond the limits of the basic function space \mathcal{Y}_ϕ defined in (3.16). Furthermore, the orthogonal subscales are assumed to be orthogonal to the small scales such that

$$w_{ort} \in (\mathcal{Y}'_\phi)^\perp \approx (\bar{\mathcal{Y}}_\phi^\perp)^\perp \approx \bar{\mathcal{Y}}_\phi \quad (6.94)$$

i.e. w_{ort} is a standard finite element function and numerically computable thus. In the end, using a stabilized method on the second level, the basic elementwise approximation of the unresolved scales in (6.63) as

$$\phi' \approx -\tau_e(\mathcal{L}_{cdr}\bar{\phi} - f) \quad \text{in } \Omega_e \quad (6.95)$$

will be enhanced by incorporating an approximation for w_{ort} in order to obtain

$$\phi' \approx -\tau_e[(\mathcal{L}_{cdr}\bar{\phi} - f) + \mathcal{P}_\tau(\mathcal{L}_{cdr}\bar{\phi} - f)] \quad \text{in } \Omega_e \quad (6.96)$$

where \mathcal{P}_τ is the projection operator associated with the weighted inner product

$$(x, y)_\tau := \sum_{e=1}^{n_{el}} \tau_e(x, y)_{\Omega_e} \quad (6.97)$$

For further elaboration of this approach, the consultation of the quoted original publications of Codina is advised.

6.5 Transient case and the concept of quasi-static small scales

Finally, the transition to the original, transient problem of the convection-diffusion-reaction equation is made. This may be done in a straightforward manner. Thus, only crucial differences and potential problems will be addressed in this section.

Although the focus is on semi-discretization in time below, a problem possibly arising in the case of using fully discrete space-time methods will be addressed first. The (unprojected) elementwise residual-free bubble equation reads

$$\mathcal{L}_{cdr,t}\phi' = -(\mathcal{L}_{cdr,t}\bar{\phi} - f) \quad \text{in } \Omega_e^{st} \quad (6.98)$$

$$\phi' = 0 \quad \text{on } \Gamma_e^{st} \quad (6.99)$$

where the superscript st indicates space-time element domains and boundaries, respectively. If it is intended to solve what may be called a 'consistent space-time bubble', the problem of ill-posedness of (6.98)-(6.99) will have to be faced. In order to explain this more thoroughly, a split of the space-time element boundary Γ_e^{st} is performed subject to

$$\Gamma_e^{st} = \Gamma_e^{s-} \cup \Gamma_e^{s+} \cup \Gamma_e^{t-} \cup \Gamma_e^{t+} \quad (6.100)$$

where Γ_e^{s-} denotes the spatial inflow boundary and Γ_e^{s+} the spatial outflow boundary of the element e according to the global definitions (2.88)-(2.89). In a formal manner, a temporal 'inflow' boundary Γ_e^{t-} as well as an 'outflow' boundary Γ_e^{t+} may likewise be defined where the 'flow' direction is indicated by the positive direction of the time axis. It is a well-known fact that it is not permitted to prescribe a Dirichlet boundary condition at an 'outflow' boundary for the temporal variable subject to a first-order differential operator in time here. Therefore, (6.98)-(6.99) with Γ_e^{st} defined as in (6.100) is an ill-posed problem and cannot be solved. Hughes and Stewart (1996) suggest to introduce an elliptic regularization in time, i.e. the differential operator is enlarged such that

$$\mathcal{L}_{cdr,t}^{\kappa_t} = \frac{\partial}{\partial t} - \kappa_t \frac{\partial^2}{\partial t^2} + \mathcal{L}_{cdr} = \frac{\partial}{\partial t} - \kappa_t \frac{\partial^2}{\partial t^2} + \mathbf{a} \cdot \nabla - \kappa \Delta + \sigma_{(\text{mod})} \quad (6.101)$$

where κ_t indicates an artificial 'diffusion' in time which helps to fulfill the Dirichlet boundary condition on Γ_e^{t+} . In order to get the result for the original equation (6.98)-(6.99), the limit $\kappa_t \rightarrow 0$ in (6.101) is enforced. In Hughes and Stewart (1996), this is done for the element Green's function problem for the adjoint differential operator of (6.101) and the limit $\kappa_t \rightarrow 0$ for the obtained Green's function is taken afterwards. Apart from this, it may be thought of the possibility to solve (6.98)-(6.99) by leaving out the prescription of the boundary condition at Γ_e^{t+} , i.e. (6.99) is only valid for a reduced element boundary subject to

$$\Gamma_e^{st, \text{red}} = \Gamma_e^{s-} \cup \Gamma_e^{s+} \cup \Gamma_e^{t-} \quad (6.102)$$

However, it is not intended to pursue this topic further, since the focus of this work is on semi-discrete methods in time. Applying the generalized trapezoidal rule to the convection-diffusion-reaction equation results in (3.37). The same what has been done in section 3.3.2 for the Navier-Stokes equations may now be carried out for the convection-diffusion-reaction equation. By rearranging and introducing a 'time-rhs' f_t^n containing all known values of time level n as well as a furthergoing modified reaction coefficient $\sigma_{(\text{mod}),t}$, (3.37) looks like

$$\mathbf{a} \cdot \nabla \phi^{n+1} - \kappa \Delta \phi^{n+1} + \sigma_{(\text{mod}),t} \phi^{n+1} = f^{n+1} + f_t^n \quad \text{in } \Omega \times (0, T) \quad (6.103)$$

with

$$\sigma_{(\text{mod}),t} = \sigma_{(\text{mod})} + \frac{1}{\theta \delta t} \quad (6.104)$$

and

$$f_t^n = \frac{\phi^n}{\theta \delta t} - \frac{(1-\theta)}{\theta} \left[\mathbf{a} \cdot \nabla \phi^n - \kappa \Delta \phi^n + \sigma_{(\text{mod})} \phi^n - f^n \right] \quad (6.105)$$

showing an identical structure with respect to the stationary convection-diffusion-reaction equation. The same applies to the semi-discrete (unprojected) residual-free bubble equation reading

$$\begin{aligned}
& \mathbf{a} \cdot \nabla \phi'^{n+1} - \kappa \Delta \phi'^{n+1} + \sigma_{(\text{mod}),t} \phi'^{n+1} \\
& = - \left(\mathbf{a} \cdot \nabla \bar{\phi}^{n+1} - \kappa \Delta \bar{\phi}^{n+1} + \sigma_{(\text{mod}),t} \bar{\phi}^{n+1} - f^{n+1} \right) + f_t^n \text{ in } \Omega_e \times (0, T) \quad (6.106)
\end{aligned}$$

with the zero Dirichlet boundary condition

$$\phi'^{n+1} = 0 \quad \text{on } \Gamma_e \times (0, T) \quad (6.107)$$

and the initial condition

$$\phi'^0 = 0 \quad \text{on } \Gamma_e \times \{0\} \quad (6.108)$$

Please note that in (6.108) the initial condition (3.5) is assumed to be captured entirely by the large-scale part of the solution completely similar to the treatment of Dirichlet boundary conditions subject to (6.5). Contrary to the space-time method, it is not required to prescribe an illegal condition at some temporal 'outflow' boundary. (6.106) may subsequently be split analog to the stationary case (6.55)-(6.60) in order to obtain finally

$$\begin{aligned}
& \mathbf{a} \cdot \nabla N_b'^{n+1} - \kappa \Delta N_b'^{n+1} + \sigma_{(\text{mod}),t} N_b'^{n+1} \\
& = - \left(\mathbf{a} \cdot \nabla \bar{N}_b^{n+1} - \kappa \Delta \bar{N}_b^{n+1} + \sigma_{(\text{mod}),t} \bar{N}_b^{n+1} \right) \quad (6.109)
\end{aligned}$$

and

$$\mathbf{a} \cdot \nabla N_f'^{n+1} - \kappa \Delta N_f'^{n+1} + \sigma_{(\text{mod}),t} N_f'^{n+1} = f^{n+1} + f_t^n \quad (6.110)$$

which have to be solved in each element e with the appropriate zero Dirichlet boundary and initial conditions. Differences to the stationary case (6.59)-(6.60) only arise due to the furthergoing modified reaction coefficient (6.104) and the additional 'time-rhs' (6.105) occurring in (6.109)-(6.110).

Closing the discussion of the transient residual-free bubble equation, the concept of quasi-static residual-free bubbles, in short quasi-static bubbles (QSB), is introduced. The basic idea has been picked up by Codina and Blasco (2002) for their stabilized methods including orthogonal subscales for convection-diffusion-reaction equations. It will be presented here as a basic concept being particularly attractive from the computational point of view, since one is no longer forced to store the values of the previous time step for all small scales. In the context of the Navier-Stokes equations, it is, on the one hand, referred to some analytical evidence for this approximation being reasonable and, on the other hand, it is shown with the help of some numerical examples in chapter 9 that it yields good results. Assuming the small scales quasi-static means assuming

$$\phi'^{n+1} \approx \phi'^n \quad (6.111)$$

at any time level which allows to replace $\sigma_{(\text{mod}),t}$ again by $\sigma_{(\text{mod})}$ in (6.106), (6.109) and (6.110) on the left hand side. Furthermore, the 'time-rhs' (6.105) has to be adapted to the quasi-static case subject to (6.111). As a result, one arrives exactly at the left-hand-side structure of the stationary residual-free bubble equations (6.59)-(6.60) with slightly modified right hand sides.

At the end of this section, the consequences of the transient case for the approaches of section 6.3 have to be pointed out. Since the artificial diffusion method simply takes into account an additional diffusive term independent of time, there will be no change in the transient case. Please

observe that the first remark at the end of section 6.3.2 still holds, even in a more important sense. For the QSB-case, no more has to be said concerning this method than already done in section 6.3.2.

The final equation including stabilizing terms (6.63) now reads for the transient case

$$B_{cdr}(\bar{w}, \bar{\phi}) + \sum_{e=1}^{n_{el}} \left(\mathcal{L}_{cdr}^{stab} \bar{w}, \tau_e (\mathcal{L}_{cdr,t} \bar{\phi} - f) \right)_{\Omega_e} = (\bar{w}, f)_{\Omega} + (\bar{w}, h)_{\Gamma_h} \quad \forall \bar{w} \in \bar{\mathcal{V}}_{\phi} \quad (6.112)$$

or is not modified at all for the QSB case, respectively. The definitions for the calculation of the elementwise stability parameter in (6.66)-(6.72) will have to be modified in replacing $\sigma_{(mod)}$ by $\sigma_{(mod),t}$ if the QSB assumption is not used. Concerning space-time methods, it has to be remarked that the differential operator \mathcal{L}_{cdr}^{stab} acting on the weighting function \bar{w} has to be replaced by a differential operator including the time derivative, i.e. for SUPG $\mathcal{L}_{cdr}^{stab} = \mathcal{L}_{cdr,t} - \mathcal{L}_d - \mathcal{L}_r$ for GLS $\mathcal{L}_{cdr}^{stab} = \mathcal{L}_{cdr,t}$ and for USFEM

$$\mathcal{L}_{cdr}^{stab} = - \left(\frac{\partial}{\partial t} \right)^* - \mathcal{L}_{cdr}^* = \frac{\partial}{\partial t} - \mathcal{L}_{cdr}^* \quad (6.113)$$

confer e.g. Codina (1998). An inclusion of the time derivative in semi-discrete methods is certainly reasonable as well. This is carried out, for instance, by Huerta and Donea (2002) for higher-order time-stepping schemes. Please observe that the time derivative has to be considered as a reactive term and, thus, may simply be represented by using $\sigma_{(mod),t}$ instead of $\sigma_{(mod)}$. The use of stabilizing terms without the time derivative acting on the weighting function \bar{w} is common practice for semi-discrete methods in time however (see the remark at the end of section 5 in Huerta and Donea (2002)). Finally, it has to be mentioned that all the considerations for the transient case may be transferred in a straightforward manner to the separation of three scales presented in section 6.4.

7 Variational multiscale method for the Navier-Stokes equations

At the beginning of this chapter, the additional difficulties being encountered in the context of the Navier-Stokes equations with respect to the preceding chapter dealing with the convection-diffusion-reaction equation should be named briefly. First of all, the scalar quantity ϕ is replaced by the vector-valued velocity \mathbf{u} . Furthermore, an additional scalar variable comes into play, the pressure p , going along with an additional equation in form of the continuity equation (2.42) or the pressure Poisson equation (2.69), respectively. Last but not least, the convective term in the momentum equation has become nonlinear raising substantial requirements for the solution process.

It is concentrated here on the variational multiscale method, although there exist further methods exploiting the multiscale structure of the problem. Just to name a few aiming at LES of turbulent flows, it is referred to recent work of Dubois, Temam and co-workers using the nonlinear Galerkin method and the incremental unknowns technique (see e.g. Chen and Temam (1991), Debusche et al. (1995), Dubois and Bouchon (1998), Marion and Temam (1990), Temam (1991), and, in particular, Dubois et al. (1998, 1999)) and the multilevel algorithm of Terracol et al. (2001, 2003). Further interesting approaches are the subgrid-scale estimation model of Domaradzki and co-workers (see e.g. Domaradzki and Loh (1999), Domaradzki and Yee (2000), as well as Domaradzki et al. (2002)) and the Local Galerkin Approach (LGA) of McDonough and co-workers (see e.g. McDonough et al. (1984) as well as McDonough and Bywater (1985)). Finally, the Spectral Vanishing Viscosity (SVV) method used by Karamanos and Karniadakis (2000) and the Reproducing Kernel Particle Method (RKPM) of Wagner and Liu (2000) are named. Without naming the aim 'LES' explicitly, the two-grid scheme of Girault and Lions (2001) and the two-level method of Layton (1993), which is, among others, analyzed in John (2001), should be mentioned here nonetheless. In most of these approaches, obvious similarities with the variational multiscale method may be found.

7.1 Separation of two scales

7.1.1 Basic concept

Analog to the preceding chapter, two scale ranges for the velocity and pressure solution functions subject to

$$\mathbf{u} = \bar{\mathbf{u}}^h + \mathbf{u}' , \quad p = \bar{p}^h + p' \quad (7.1)$$

as well as the respective weighting functions subject to

$$\mathbf{v} = \bar{\mathbf{v}}^h + \mathbf{v}' , \quad q = \bar{q}^h + q' \quad (7.2)$$

are distinguished and a direct sum decomposition of the solution and weighting function spaces

$$\mathcal{J}_{\mathbf{u}p} = \bar{\mathcal{J}}_{\mathbf{u}p} \oplus \mathcal{J}'_{\mathbf{u}p} \quad (7.3)$$

$$\mathcal{V}_{\mathbf{u}p} = \overline{\mathcal{V}}_{\mathbf{u}p} \oplus \mathcal{V}'_{\mathbf{u}p} \quad (7.4)$$

with analog considerations as for (6.3)-(6.4) is performed. For convenience, $\overline{\mathbf{u}}^h$, \overline{p}^h , $\overline{\mathbf{w}}^h$ and \overline{q}^h are denoted $\overline{\mathbf{u}}$, \overline{p} , $\overline{\mathbf{w}}$ and \overline{q} , respectively, below. The large-scale velocity $\overline{\mathbf{u}}$ is required to fulfill the essential Dirichlet boundary condition (3.8) exclusively, i.e.

$$\overline{\mathbf{u}} = \mathbf{g} \quad \text{on } \Gamma_g \quad \forall \overline{\mathbf{u}} \in \overline{\mathcal{F}}_{\mathbf{u}} \quad (7.5)$$

\mathbf{u}' , $\overline{\mathbf{w}}$ and \mathbf{w}' face zero Dirichlet boundary conditions. Exploiting the decomposition, two sub-problems, namely a large- and a small-scale equation, are achieved reading

$$B_{NS}(\overline{\mathbf{v}}, \overline{q}; \overline{\mathbf{u}} + \mathbf{u}', \overline{p} + p') = (\overline{\mathbf{v}}, \mathbf{f})_{\Omega} + (\overline{\mathbf{v}}, \mathbf{h})_{\Gamma_h} \quad \forall \{\overline{\mathbf{v}}, \overline{q}\} \in \overline{\mathcal{V}}_{\mathbf{u}p} \quad (7.6)$$

$$B_{NS}(\mathbf{v}', q'; \overline{\mathbf{u}} + \mathbf{u}', \overline{p} + p') = (\mathbf{v}', \mathbf{f})_{\Omega} + (\mathbf{v}', \mathbf{h})_{\Gamma_h} \quad \forall \{\mathbf{v}', q'\} \in \mathcal{V}'_{\mathbf{u}p} \quad (7.7)$$

Due to the nonlinearity of the Navier-Stokes equations, the identification of the large- and the small-scale part in (7.6) and (7.7) is somewhat challenging. Applying the procedure carried out in (5.23)-(5.26) to both the large- and the small-scale equation yields

$$B_{NS}(\overline{\mathbf{v}}, \overline{q}; \overline{\mathbf{u}}, \overline{p}) + B_{NS}^1(\overline{\mathbf{v}}, \overline{q}; \overline{\mathbf{u}}, \mathbf{u}', p') + B_{NS}^2(\overline{\mathbf{v}}; \mathbf{u}') = (\overline{\mathbf{v}}, \mathbf{f})_{\Omega} + (\overline{\mathbf{v}}, \mathbf{h})_{\Gamma_h} \quad (7.8)$$

$$B_{NS}(\mathbf{v}', q'; \overline{\mathbf{u}}, \overline{p}) + B_{NS}^1(\mathbf{v}', q'; \overline{\mathbf{u}}, \mathbf{u}', p') + B_{NS}^2(\mathbf{v}'; \mathbf{u}') = (\mathbf{v}', \mathbf{f})_{\Omega} + (\mathbf{v}', \mathbf{h})_{\Gamma_h} \quad (7.9)$$

After all, it has to be dealt with a nonlinear system of two coupled variational equations (7.8)-(7.9). In view of subsequent practical implementations, the analog system of equations after a discretization process in time as well as a linearization procedure according to section 3.3.2 reads

$$B_{NS}^{dt, lin}(\overline{\mathbf{v}}, \overline{q}; \overline{\mathbf{u}}, \overline{p}) + B_{NS}^{dt, lin}(\overline{\mathbf{v}}, \overline{q}; \mathbf{u}', p') = \left(\overline{\mathbf{v}}, \frac{\mathbf{u}^n}{\delta t} \right)_{\Omega} + (\overline{\mathbf{v}}, \mathbf{f}^{n+\theta})_{\Omega} + (\overline{\mathbf{v}}, \mathbf{h}^{n+\theta})_{\Gamma_h} \quad (7.10)$$

$$\begin{aligned} B_{NS}^{dt, lin}(\mathbf{v}', q'; \overline{\mathbf{u}}, \overline{p}) + B_{NS}^{dt, lin}(\mathbf{v}', q'; \mathbf{u}', p') \\ = \left(\mathbf{v}', \frac{\mathbf{u}^n}{\delta t} \right)_{\Omega} + (\mathbf{v}', \mathbf{f}^{n+\theta})_{\Omega} + (\mathbf{v}', \mathbf{h}^{n+\theta})_{\Gamma_h} \end{aligned} \quad (7.11)$$

where the discrete-in-time (dt) and linearized bilinear form $B_{NS}^{dt, lin}(\mathbf{v}, q; \mathbf{u}, p)$ is obtained from (3.51) after the application of the fixed point like iteration yielding e.g.

$$\begin{aligned} B_{NS}^{dt, lin}(\mathbf{v}, q; \overline{\mathbf{u}}, \overline{p}) = & \left(\mathbf{v}, \frac{\overline{\mathbf{u}}_{i+1}^{n+1}}{\delta t} \right)_{\Omega} + \left(\mathbf{v}, \mathbf{u}_i^{n+\theta} \cdot \nabla \overline{\mathbf{u}}_{i+1}^{n+\theta} + \beta \overline{\mathbf{u}}_{i+1}^{n+\theta} (\nabla \cdot \mathbf{u}_i^{n+\theta}) \right)_{\Omega} \\ & - (\nabla \cdot \mathbf{v}, \overline{p}_{i+1}^{n+\theta})_{\Omega} + (\varepsilon(\mathbf{v}), 2\nu \varepsilon(\overline{\mathbf{u}}_{i+1}^{n+\theta}))_{\Omega} - (q, \nabla \cdot \overline{\mathbf{u}}_{i+1}^{n+\theta})_{\Omega} \end{aligned} \quad (7.12)$$

The derivation of $B_{NS}^{dt, lin}(\mathbf{v}, q; \mathbf{u}', p')$ appears to be straightforward with regard to (7.12). The linearity of (7.10)-(7.11) allows to address the problem already carried into execution in the context of the convection-diffusion-reaction equation at the end of section 6.1: potential appearance of Dirac delta functions at the element boundaries for C^0 -elements. Due to the presence of the Dirac delta functions on the element boundary Γ_e giving rise to an additional boundary integral, the integrated-by-parts term of the sample bilinear form $B_{NS}^{dt, lin}(\mathbf{v}, q; \mathbf{u}, p)_{\Omega_e}$ on one element domain Ω_e looks like

$$\begin{aligned}
B_{NS}^{dt, lin}(\mathbf{v}, q; \mathbf{u}, p)_{\Omega_e} &= \left(\mathbf{v}, \frac{\mathbf{u}^{n+1}}{\delta t} \right)_{\Omega_e} + \left(\mathbf{v}, \mathcal{L}_M^{stat}[\mathbf{u}^{n+\theta}, p^{n+\theta}] \right)_{\Omega_e} - (q, \nabla \cdot \mathbf{u}^{n+\theta})_{\Omega_e} \\
&+ \left(\mathbf{v}, \mathbf{n} \cdot \left(-p^{n+\theta} \mathbf{I} + 2\nu \boldsymbol{\varepsilon}(\mathbf{u}^{n+\theta}) \right) \right)_{\Gamma_e}
\end{aligned} \tag{7.13}$$

where the iteration counter has been omitted for convenience. \mathbf{n} indicates the outward unit normal vector on the element boundary of Ω_e . Integrating (7.13) by parts in the other direction by 'shifting' derivative operators on the weighting functions \mathbf{v} and q reveals

$$\begin{aligned}
B_{NS}^{dt, lin}(\mathbf{v}, q; \mathbf{u}, p)_{\Omega_e} &= \left(\mathbf{v}, \frac{\mathbf{u}^{n+1}}{\delta t} \right)_{\Omega_e} + \left(\mathcal{L}_M^{*stat}[\mathbf{v}, q], \mathbf{u}^{n+\theta} \right)_{\Omega_e} - (\nabla \cdot \mathbf{v}, p^{n+\theta})_{\Omega_e} \\
&+ \left(\mathbf{n} \cdot \left(\mathbf{u}_i^{n+\theta} \mathbf{v} - q \mathbf{I} + 2\nu \boldsymbol{\varepsilon}(\mathbf{v}) \right), \mathbf{u}^{n+\theta} \right)_{\Gamma_e}
\end{aligned} \tag{7.14}$$

where $\mathbf{u}_i^{n+\theta}$ denotes the velocity from the last iteration step for the current time step $n + 1$. As before, the jump operator $[\cdot]_{-}^{+}$ may be used for summing (7.14) over all elements

$$\begin{aligned}
B_{NS}^{dt, lin}(\mathbf{v}, q; \mathbf{u}, p) &= \left(\mathbf{v}, \frac{\mathbf{u}^{n+1}}{\delta t} \right)_{\Omega'} + \left(\mathcal{L}_M^{*stat}[\mathbf{v}, q], \mathbf{u}^{n+\theta} \right)_{\Omega'} - (\nabla \cdot \mathbf{v}, p^{n+\theta})_{\Omega'} \\
&+ \left([\mathbf{n} \cdot (-q \mathbf{I} + 2\nu \boldsymbol{\varepsilon}(\mathbf{v}))]_{-}^{+}, \mathbf{u}^{n+\theta} \right)_{\Gamma'} \\
&+ \left(\mathbf{n} \cdot \left(\mathbf{u}_i^{n+\theta} \mathbf{v} - q \mathbf{I} + 2\nu \boldsymbol{\varepsilon}(\mathbf{v}) \right), \mathbf{u}^{n+\theta} \right)_{\Gamma_h} \\
&+ \left(\mathbf{n} \cdot (-q \mathbf{I} + 2\nu \boldsymbol{\varepsilon}(\mathbf{v})), \mathbf{u}^{n+\theta} \right)_{\Gamma_g} \\
&= \left(\mathbf{v}, \frac{\mathbf{u}^{n+1}}{\delta t} \right)_{\Omega} + \left(\mathcal{L}_M^{*stat}[\mathbf{v}, q], \mathbf{u}^{n+\theta} \right)_{\Omega} - (\nabla \cdot \mathbf{v}, p^{n+\theta})_{\Omega} \\
&+ \left(\mathbf{n} \cdot \left(\mathbf{u}_i^{n+\theta} \mathbf{v} - q \mathbf{I} + 2\nu \boldsymbol{\varepsilon}(\mathbf{v}) \right), \mathbf{u}^{n+\theta} \right)_{\Gamma_h} \\
&+ \left(\mathbf{n} \cdot (-q \mathbf{I} + 2\nu \boldsymbol{\varepsilon}(\mathbf{v})), \mathbf{u}^{n+\theta} \right)_{\Gamma_g}
\end{aligned} \tag{7.15}$$

where the fifth line of (7.15) has to be understood as an integral on the global domain Ω in a distributional sense and the sixth as well as the seventh line contains a Neumann and a Dirichlet boundary term, respectively. The first (convective) part of the boundary term in the second line of (7.14) drops out at the interelement boundaries in the summing-up of all elements due to the continuity of the functions for the velocity approximation whereas the second (pressure) part will only be kept in the case of using elementwise discontinuous pressure approximations, a strategy not intended to be followed in the course of this work. Hence, this term will not be retained as well in general. By doing the same in (7.13),

$$\begin{aligned}
B_{NS}^{dt, lin}(\mathbf{v}, q; \mathbf{u}, p) &= \left(\mathbf{v}, \frac{\mathbf{u}^{n+1}}{\delta t} \right)_{\Omega'} + \left(\mathbf{v}, \mathcal{L}_M^{stat}[\mathbf{u}^{n+\theta}, p^{n+\theta}] \right)_{\Omega'} - (q, \nabla \cdot \mathbf{u}^{n+\theta})_{\Omega'} \\
&+ \left(\mathbf{v}, \left[\mathbf{n} \cdot \left(-p^{n+\theta} \mathbf{I} + 2\nu \boldsymbol{\varepsilon}(\mathbf{u}^{n+\theta}) \right) \right]_{-}^{+} \right)_{\Gamma'}
\end{aligned}$$

$$\begin{aligned}
& + \left(\mathbf{v}, \mathbf{n} \cdot \left(-p^{n+\theta} \mathbf{I} + 2\nu \boldsymbol{\varepsilon}(\mathbf{u}^{n+\theta}) \right) \right)_{\Gamma_h} \\
& = \left(\mathbf{v}, \frac{\mathbf{u}^{n+1}}{\delta t} \right)_{\Omega} + \left(\mathbf{v}, \mathcal{L}_M^{stat}[\mathbf{u}^{n+\theta}, p^{n+\theta}] \right)_{\Omega} - (q, \nabla \cdot \mathbf{u}^{n+\theta})_{\Omega} \\
& + \left(\mathbf{v}, \mathbf{n} \cdot \left(-p^{n+\theta} \mathbf{I} + 2\nu \boldsymbol{\varepsilon}(\mathbf{u}^{n+\theta}) \right) \right)_{\Gamma_h} \tag{7.16}
\end{aligned}$$

is obtained, where the Dirichlet boundary term can be omitted due to the zero boundary conditions for the large- and small-scale weighting functions. Furthermore, what has already been stated for the pressure part in the interelement boundary integral in the wake of (7.15) applies here in similar fashion.

As a result, the final form of the large- and small-scale equation in (7.10)-(7.11) after integrating by parts $B_{NS}^{dt, lin}(\bar{\mathbf{v}}, \bar{q}; \mathbf{u}', p')$ as in (7.15) as well as $B_{NS}^{dt, lin}(\mathbf{v}', q'; \bar{\mathbf{u}}, \bar{p})$ and $B_{NS}^{dt, lin}(\mathbf{v}', q'; \mathbf{u}', p')$ according to (7.16) reads

$$\begin{aligned}
& B_{NS}^{dt, lin}(\bar{\mathbf{v}}, \bar{q}; \bar{\mathbf{u}}, \bar{p}) + \left(\bar{\mathbf{v}}, \frac{\mathbf{u}'^{n+1}}{\delta t} \right)_{\Omega} + \left(\mathcal{L}_M^{*stat}[\bar{\mathbf{v}}, \bar{q}], \mathbf{u}'^{n+\theta} \right)_{\Omega} - (\nabla \cdot \bar{\mathbf{v}}, p'^{n+\theta})_{\Omega} \\
& + \left(\mathbf{n} \cdot \left(\mathbf{u}'_i^{n+\theta} \bar{\mathbf{v}} - \bar{q} \mathbf{I} + 2\nu \boldsymbol{\varepsilon}(\bar{\mathbf{v}}) \right), \mathbf{u}'^{n+\theta} \right)_{\Gamma_h} \\
& = \left(\bar{\mathbf{v}}, \frac{\mathbf{u}'^n}{\delta t} \right)_{\Omega} + (\bar{\mathbf{v}}, \mathbf{f}^{n+\theta})_{\Omega} + (\bar{\mathbf{v}}, \mathbf{h}^{n+\theta})_{\Gamma_h} \quad \forall \{\bar{\mathbf{v}}, \bar{q}\} \in \bar{\mathcal{V}}_{\mathbf{u}p} \tag{7.17}
\end{aligned}$$

$$\begin{aligned}
& \left(\mathbf{v}', \frac{\bar{\mathbf{u}}^{n+1}}{\delta t} \right)_{\Omega} + \left(\mathbf{v}', \mathcal{L}_M^{stat}[\bar{\mathbf{u}}^{n+\theta}, \bar{p}^{n+\theta}] \right)_{\Omega} - (q', \nabla \cdot \bar{\mathbf{u}}^{n+\theta})_{\Omega} \\
& + \left(\mathbf{v}', \mathbf{n} \cdot \left(-\bar{p}^{n+\theta} \mathbf{I} + 2\nu \boldsymbol{\varepsilon}(\bar{\mathbf{u}}^{n+\theta}) \right) \right)_{\Gamma_h} \\
& + \left(\mathbf{v}', \frac{\mathbf{u}'^{n+1}}{\delta t} \right)_{\Omega} + \left(\mathbf{v}', \mathcal{L}_M^{stat}[\mathbf{u}'^{n+\theta}, p'^{n+\theta}] \right)_{\Omega} - (q', \nabla \cdot \mathbf{u}'^{n+\theta})_{\Omega} \\
& + \left(\mathbf{v}', \mathbf{n} \cdot \left(-p'^{n+\theta} \mathbf{I} + 2\nu \boldsymbol{\varepsilon}(\mathbf{u}'^{n+\theta}) \right) \right)_{\Gamma_h} \\
& = \left(\mathbf{v}', \frac{\mathbf{u}'^n}{\delta t} \right)_{\Omega} + (\mathbf{v}', \mathbf{f}^{n+\theta})_{\Omega} + (\mathbf{v}', \mathbf{h}^{n+\theta})_{\Gamma_h} \quad \forall \{\mathbf{v}', q'\} \in \mathcal{V}'_{\mathbf{u}p} \tag{7.18}
\end{aligned}$$

where the term in the seventh line of (7.15) drops out in the large-scale equation (7.17) due to the zero Dirichlet boundary condition for $\mathbf{u}'^{n+\theta}$. After all, a system of two coupled linear variational equations arisen from the primarily nonlinear Navier-Stokes equations through a linearization process may be stated.

7.1.2 Interpretation of the two-scale separation in the sense of a DNS/LES

At this stage, the results of the intuitive procedure in section 5.3.2 may now be interpreted in retrospect with the framework of the variational multiscale method for a two-scale separation

at hand. Equation (5.22) corresponds exactly to the large-scale equation (7.6) with the weighting functions \mathbf{v} and q being replaced by their large-scale part $\bar{\mathbf{v}}$ and \bar{q} , respectively. The small-scale equation (7.7) has not been paid attention to in section 5.2.2 - and it was indeed not necessary to think of such a small-scale equation from the point of view of 'classical' LES. Henceforth, one may recognize that this equation represents the 'natural counterpart' of the large-scale equation, obtained as the result from the two-scale separation. Moreover, equations (5.26) and (5.31) may be identified as the linearized version of the large-scale equation (7.8) by replacing the weighting functions with their large-scale part, the last one with the additional assumption of an orthonormal basis.

The DNS-equation (5.1) along with the assumption (5.4) arises from the large-scale equation by assuming the projection of the small (or, in this case, the actually not resolved) scales to be zero, i.e.

$$B_{NS}^1(\bar{\mathbf{v}}, \bar{q}; \bar{\mathbf{u}}, \mathbf{u}', p') + B_{NS}^2(\bar{\mathbf{v}}; \mathbf{u}') = 0 \quad (7.19)$$

in (5.26) or

$$C(\bar{\mathbf{v}}; \bar{\mathbf{u}}, \mathbf{u}') + R(\bar{\mathbf{v}}; \mathbf{u}') = 0 \quad (7.20)$$

for an orthonormal basis in (5.31), respectively. In order to complete the Leonard decomposition already started in section 5.3.2, the two-scale separation enables the identification of the analog of the Leonard stress within an LES based on a Galerkin projection. It reads

$$\begin{aligned} L(\mathbf{v}'; \bar{\mathbf{u}}) &= - (\mathbf{v}', \bar{\mathbf{u}} \cdot \nabla \bar{\mathbf{u}} + \beta \bar{\mathbf{u}} (\nabla \cdot \bar{\mathbf{u}}))_{\Omega} \\ &= (\bar{\mathbf{v}}, \bar{\mathbf{u}} \cdot \nabla \bar{\mathbf{u}} + \beta \bar{\mathbf{u}} (\nabla \cdot \bar{\mathbf{u}}))_{\Omega} - (\mathbf{v}, \bar{\mathbf{u}} \cdot \nabla \bar{\mathbf{u}} + \beta \bar{\mathbf{u}} (\nabla \cdot \bar{\mathbf{u}}))_{\Omega} \end{aligned} \quad (7.21)$$

confer Hughes et al. (2000a). The isolation of the Leonard stress tensor \mathbf{L} may be performed in the same way as it has been done in section 5.3.2 for the cross stress tensor and the Reynolds stress tensor. (7.21) actually appears within the small-scale equation. Therefore, it was not possible to identify it before the introduction of the small-scale equation.

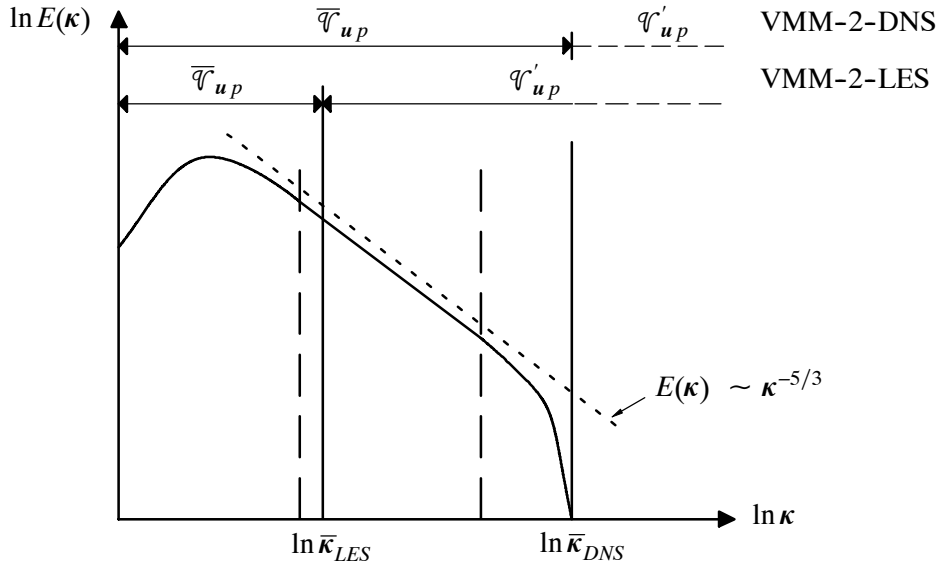


Fig. 7.1: Kolmogorov energy spectrum for 2-scale separation of VMM

Finally, the just accomplished interpretation of the two-scale separation is displayed with the help of the Kolmogorov energy spectrum in Fig. 7.1. The situation is depicted in a symbolic way by indicating the range of scales 'captured' by the respective (weighting) function space. If the large-scale space is extended beyond (or at least close enough to) the Kolmogorov scale, a DNS is actually performed. Otherwise, unresolved scales appear within a 2-scale LES which have to be modeled.

7.2 Solving for the small scales

With respect to the presentation of solution strategies for the convection-diffusion-reaction equation, it is focussed here on two methods. On the one hand, the global strategy of applying hierarchical shape functions to the coupled system of large- and small-scale equation after temporal discretization and linearization (7.10)-(7.11) will be described. On the other hand, the foremost strategy of this work will be emphasized: the use of residual-free bubbles on individual elements. Admittedly, searching for an analytically determined residual-free bubble is practically hopeless. However, this search for a solution will be executed with the aid of a discrete method in chapter 8. What will be left out becomes clear herewith: the use of Green's function, may it be in global or local form. To the author's knowledge, it is definitely impossible to determine anything which looks, at least approximately, like the Green's function for the multidimensional Navier-Stokes problem. Therefore, this is not a reasonable strategy to follow any longer.

7.2.1 Global monolithic solution using hierarchical shape functions

This global approach has been applied with success in the framework of a stabilized method to incompressible and compressible laminar flows and for a DNS of a turbulent channel flow by Whiting and Jansen in Jansen (2001a), Whiting (1999), Whiting et al. (2000), and Whiting and Jansen (2001). Furthermore, Jansen and Tejada-Martinez have also recently proven the suitability of the hierarchical approach for LES in Jansen (2001b) and Jansen and Tejada-Martinez (2002). The hierarchical basis Jansen and co-workers use is provided by the mesh-entity based construction of shape functions proposed by Shephard et al. (1997) relying, among others, on special functions created by Carnevali et al. (1993).

Following the concept presented in section 6.2.1, the function space decomposition (6.17)-(6.18) may be adjusted to this approach as

$$\mathcal{S}_{u p} = \bar{\mathcal{P}}_{u p} \oplus \mathcal{S}'_{u p} \approx \bar{\mathcal{P}}_{u p, \bar{k}} \oplus \mathcal{S}'_{u p, k-\bar{k}} \quad (7.22)$$

$$\mathcal{V}_{u p} = \bar{\mathcal{V}}_{u p} \oplus \mathcal{V}'_{u p} \approx \bar{\mathcal{V}}_{u p, \bar{k}} \oplus \mathcal{V}'_{u p, k-\bar{k}} \quad (7.23)$$

where k and \bar{k} are chosen according to (6.16). Similar to (6.19)-(6.20), the large- and small-scale solution and weighting function shape functions for the approximation of velocity and pressure may be determined. The focus is on equal-order interpolations for velocity and pressure, i.e. the large- and small-scale number of degrees of freedom (\bar{n}_{dofs} and n'_{dofs}) are equal for velocity and pressure interpolation. Inserting the shape functions into (7.10)-(7.11), the matrix equivalent of the Galerkin problem

$$\begin{aligned}
& \begin{bmatrix} \mathbf{K}_{NS}^{\bar{\bar{}}}(\mathbf{u}_i^{n+1}) & \theta \delta t \mathbf{G}^{\bar{\bar{}}} & \mathbf{K}_{NS}^{\bar{\prime}}(\mathbf{u}_i^{n+1}) & \theta \delta t \mathbf{G}^{\bar{\prime}} \\ \theta \delta t \mathbf{G}^{T\bar{\bar{}}} & \mathbf{0} & \theta \delta t \mathbf{G}^{T\bar{\prime}} & \mathbf{0} \\ \mathbf{K}_{NS}^{\bar{}}(\mathbf{u}_i^{n+1}) & \theta \delta t \mathbf{G}^{\bar{\prime}} & \mathbf{K}_{NS}^{\prime}(\mathbf{u}_i^{n+1}) & \theta \delta t \mathbf{G}^{\prime\prime} \\ \theta \delta t \mathbf{G}^{T\bar{\prime}} & \mathbf{0} & \theta \delta t \mathbf{G}^{\prime\prime} & \mathbf{0} \end{bmatrix} \cdot \begin{bmatrix} \bar{\mathbf{u}}_{i+1}^{n+1} \\ \bar{\mathbf{p}}_{i+1}^{n+1} \\ \mathbf{u}'_{i+1}{}^{n+1} \\ \mathbf{p}'_{i+1}{}^{n+1} \end{bmatrix} \\
& = \begin{bmatrix} \theta \delta t (\bar{\mathbf{F}} + \bar{\mathbf{N}} - \bar{\mathbf{E}}^M)^{n+1} + \bar{\mathbf{T}}_{NS, M} \\ \theta \delta t (-\bar{\mathbf{E}}^C)^{n+1} + \bar{\mathbf{T}}_{NS, C} \\ \theta \delta t (\mathbf{F}' + \mathbf{N}')^{n+1} + \mathbf{T}'_{NS, M} \\ \mathbf{T}'_{NS, C} \end{bmatrix} \quad (7.24)
\end{aligned}$$

is obtained where $\mathbf{K}_{NS}(\mathbf{u}_i^{n+1})$ denotes the respective linearized submatrices for the convective, viscous and reactive part of the momentum equation, \mathbf{G} the gradient submatrices for the pressure part of the momentum equation and \mathbf{G}^T the divergence submatrices for the continuity equation on the left hand sides of (7.10)-(7.11). \mathbf{F} and \mathbf{N} designate the respective subvectors as well as \mathbf{T}_{NS} the respective entries from the previous time step n on the right hand sides of (7.10)-(7.11). $\bar{\mathbf{E}}$ denotes the entries due to the Dirichlet boundary conditions subject to (7.5). All matrices and vectors are defined according to section 3.3.4.

It is necessary to investigate the stability of this Galerkin approximation. The same problem mentioned for (6.21) in the context of the convection-diffusion-reaction equation for convection-dominated flows emerges here as well. Furthermore, the potential stabilization of the transient term has already been adressed and does not loose its validity here. Additionally, the problem of pressure oscillations due to the non-fulfillment of the inf-sup condition with the chosen equal-order interpolated elements comes into play, consult section 3.4.2. The Taylor-Hood element has been introduced in this section as one sample element known to satisfy the inf-sup condition. If one thinks of the hierarchical counterpart of this element, it looks as follows: linear shape functions for velocity and pressure representing the large-scale approximation and quadratic hierarchical shape functions for the velocity only. This hierarchical basis is identically equal to the original Taylor-Hood element with the only exception that the quadratic hierarchical shape functions have no direct relation to particular nodes as it is the case for the Lagrange-type Taylor-Hood element. As aforementioned, this is a basic feature of hierarchical shape functions and does not matter for the satisfaction of the inf-sup condition. Surely, the same is valid for the 3-D counterpart of the Taylor-Hood element and the related hierarchical basis. Using this simple quadratic-linear hierarchical approximation, the matrix scheme (7.24) simplifies to

$$\begin{bmatrix} \mathbf{K}_{NS}^{\bar{\bar{}}}(\mathbf{u}_i^{n+1}) & \theta \delta t \mathbf{G}^{\bar{\bar{}}} & \mathbf{K}_{NS}^{\bar{\prime}}(\mathbf{u}_i^{n+1}) \\ \theta \delta t \mathbf{G}^{T\bar{\bar{}}} & \mathbf{0} & \theta \delta t \mathbf{G}^{T\bar{\prime}} \\ \mathbf{K}_{NS}^{\bar{}}(\mathbf{u}_i^{n+1}) & \theta \delta t \mathbf{G}^{\bar{\prime}} & \mathbf{K}_{NS}^{\prime}(\mathbf{u}_i^{n+1}) \end{bmatrix} \cdot \begin{bmatrix} \bar{\mathbf{u}}_{i+1}^{n+1} \\ \bar{\mathbf{p}}_{i+1}^{n+1} \\ \mathbf{u}'_{i+1}{}^{n+1} \end{bmatrix}$$

$$= \begin{bmatrix} \theta\delta t(\bar{F} + \bar{N} - \bar{E}^M)^{n+1} + \bar{T}_{NS,M} \\ \theta\delta t(-\bar{E}^C)^{n+1} + \bar{T}_{NS,C} \\ \theta\delta t(F' + N')^{n+1} + T'_{NS,M} \end{bmatrix} \quad (7.25)$$

It may be observed that there is no more small-scale approximation of the pressure at all, i.e. $p' = 0$. As a matter of course, the matrix scheme (7.25) is valid for any approximation enclosing $p' = 0$ beyond the specific example used here. Although it is not dared to carry out a static condensation procedure for (7.25) in reality, it is informative to look at the results to be encountered. By solving the third line of (7.25) for \mathbf{u}'_{i+1} , one obtains

$$\begin{aligned} \mathbf{u}'_{i+1} &= (\mathbf{K}'_{NS}(\mathbf{u}_i^{n+1}))^{-1} \left[\theta\delta t(F' + N')^{n+1} + T'_{NS,M} \right] \\ &\quad - (\mathbf{K}'_{NS}(\mathbf{u}_i^{n+1}))^{-1} \left[\mathbf{K}'_{NS}(\mathbf{u}_i^{n+1}) \bar{\mathbf{u}}_{i+1}^{n+1} + \theta\delta t\mathbf{G}'^- \bar{\mathbf{p}}_{i+1}^{n+1} \right] \end{aligned} \quad (7.26)$$

which by inserting in the first and second line of (7.25) results in the condensed matrix scheme for the large-scale values $\bar{\mathbf{u}}_{i+1}^{n+1}$ and $\bar{\mathbf{p}}_{i+1}^{n+1}$ reading

$$\begin{bmatrix} \mathbf{K}_{NS}^*(\mathbf{u}_i^{n+1}) & \mathbf{G}^*(\mathbf{u}_i^{n+1}) \\ \mathbf{G}^{T*}(\mathbf{u}_i^{n+1}) & \mathbf{H}^*(\mathbf{u}_i^{n+1}) \end{bmatrix} \cdot \begin{bmatrix} \bar{\mathbf{u}}_{i+1}^{n+1} \\ \bar{\mathbf{p}}_{i+1}^{n+1} \end{bmatrix} = \begin{bmatrix} \mathbf{R}_M^*(\mathbf{u}_i^{n+1}) \\ \mathbf{R}_C^*(\mathbf{u}_i^{n+1}) \end{bmatrix} \quad (7.27)$$

where

$$\mathbf{K}_{NS}^*(\mathbf{u}_i^{n+1}) = \mathbf{K}_{NS}^{\bar{-}}(\mathbf{u}_i^{n+1}) - \mathbf{K}_{NS}^{\bar{-}}(\mathbf{u}_i^{n+1}) (\mathbf{K}'_{NS}(\mathbf{u}_i^{n+1}))^{-1} \mathbf{K}'_{NS}(\mathbf{u}_i^{n+1}) \quad (7.28)$$

$$\mathbf{G}^*(\mathbf{u}_i^{n+1}) = \theta\delta t\mathbf{G}^{\bar{-}} - \mathbf{K}_{NS}^{\bar{-}}(\mathbf{u}_i^{n+1}) (\mathbf{K}'_{NS}(\mathbf{u}_i^{n+1}))^{-1} \theta\delta t\mathbf{G}'^- \quad (7.29)$$

$$\mathbf{G}^{T*}(\mathbf{u}_i^{n+1}) = \theta\delta t\mathbf{G}^{T\bar{-}} - \theta\delta t\mathbf{G}^{T-'} (\mathbf{K}'_{NS}(\mathbf{u}_i^{n+1}))^{-1} \mathbf{K}'_{NS}(\mathbf{u}_i^{n+1}) \quad (7.30)$$

$$\mathbf{H}^*(\mathbf{u}_i^{n+1}) = -\theta\delta t\mathbf{G}^{T-'} (\mathbf{K}'_{NS}(\mathbf{u}_i^{n+1}))^{-1} \theta\delta t\mathbf{G}'^- \quad (7.31)$$

and

$$\begin{aligned} \mathbf{R}_M^*(\mathbf{u}_i^{n+1}) &= \theta\delta t(\bar{F} + \bar{N} - \bar{E}^M)^{n+1} + \bar{T}_{NS,M} \\ &\quad - \mathbf{K}_{NS}^{\bar{-}}(\mathbf{u}_i^{n+1}) (\mathbf{K}'_{NS}(\mathbf{u}_i^{n+1}))^{-1} \left[\theta\delta t(F' + N')^{n+1} + T'_{NS,M} \right] \end{aligned} \quad (7.32)$$

$$\begin{aligned} \mathbf{R}_C^*(\mathbf{u}_i^{n+1}) &= \theta\delta t(-\bar{E}^C)^{n+1} + \bar{T}_{NS,C} \\ &\quad - \theta\delta t\mathbf{G}^{T-'} (\mathbf{K}'_{NS}(\mathbf{u}_i^{n+1}))^{-1} \left[\theta\delta t(F' + N')^{n+1} + T'_{NS,M} \right] \end{aligned} \quad (7.33)$$

In reference to the following section, it is even more interesting to have a look at the corresponding continuous-in-space (and still discrete-in-time) problem of (7.17)-(7.18) where (7.18) may be rearranged as an Euler-Lagrange equation with the help of the projection operator \mathcal{P}' projecting onto the small-scale function space \mathcal{V}'_u such that

$$\begin{aligned} & \mathcal{P}' \left[\frac{1}{\delta t} \mathbf{u}' + \mathbf{u}_i \cdot \nabla \mathbf{u}' + \beta (\nabla \cdot \mathbf{u}_i) \mathbf{u}' - \nu \Delta \mathbf{u}' \right] \\ &= - \mathcal{P}' \left[\frac{1}{\delta t} \bar{\mathbf{u}} + \mathbf{u}_i \cdot \nabla \bar{\mathbf{u}} + \beta (\nabla \cdot \mathbf{u}_i) \bar{\mathbf{u}} - \nu \Delta \bar{\mathbf{u}} + \nabla \bar{p} - \left(\mathbf{f} + \frac{\mathbf{u}^n}{\delta t} \right) \right] \quad \text{in } \Omega \end{aligned} \quad (7.34)$$

$$\mathbf{u}' = \mathbf{0} \quad \text{on } \Gamma_g \quad (7.35)$$

$$\mathbf{n} \cdot \nu \nabla \mathbf{u}' = - (\mathbf{n} \cdot (-\bar{p} \mathbf{I} + \nu \nabla \bar{\mathbf{u}}) - \mathbf{h}) \quad \text{on } \Gamma_h \quad (7.36)$$

Please observe five aspects related to (7.34)-(7.36):

- To simplify the notation, it is concentrated on a backward Euler scheme in time, i.e. $\theta = 1$, and the superscripts indicating the respective time step as well as the subscripts denoting the respective iteration step (except the one designating the 'iterative' velocity from the previous iteration step) are omitted here and below. The extension to other variants of the generalized trapezoidal rule appears to be a straightforward matter.
- The viscous term has been altered in (7.34) and (7.36) with respect to the preceding equations in that by setting $\gamma = 0$ in (2.64) the conventional form has been derived. This will be a crucial prerequisite for the following dissection of the residual-free bubbles.
- According to the corresponding discrete example described before, there is no small-scale pressure in (7.34)-(7.36).
- The right hand side of (7.34) and (7.36) is governed by the residual of the large scales projected onto the small-scale space.
- Since one is usually not able to solve this problem (or the corresponding adjoint Green's function problem) on the global domain Ω , the theoretical considerations are brought to a termination here. However, they will be of substantial value for the following inspection of residual-free bubbles.

7.2.2 Local solution by residual-free bubbles

The projection operator \mathcal{P}' will be omitted in the following, since it is not intended to violate the restrictions explained in section 6.2.4. Thus, the strong form of the small-scale equation (7.18) in each element subject to

$$\begin{aligned} & \frac{1}{\delta t} \mathbf{u}' + \mathbf{u}_i \cdot \nabla \mathbf{u}' + \beta (\nabla \cdot \mathbf{u}_i) \mathbf{u}' - \nu \Delta \mathbf{u}' + \nabla p' \\ &= - \left[\frac{1}{\delta t} \bar{\mathbf{u}} + \mathbf{u}_i \cdot \nabla \bar{\mathbf{u}} + \beta (\nabla \cdot \mathbf{u}_i) \bar{\mathbf{u}} - \nu \Delta \bar{\mathbf{u}} + \nabla \bar{p} - \left(\mathbf{f} + \frac{\mathbf{u}^n}{\delta t} \right) \right] \quad \text{in } \Omega_e \end{aligned} \quad (7.37)$$

$$\nabla \cdot \mathbf{u}' = -\nabla \cdot \bar{\mathbf{u}} \quad \text{in } \Omega_e \quad (7.38)$$

$$\mathbf{u}' = \mathbf{0} \quad \text{on } \Gamma_e \quad (7.39)$$

may be formulated. With regard to the global equations (7.34)–(7.36), there is only one extension in that the small-scale part of the pressure is included in (7.37)–(7.39). Please note the usual zero Dirichlet boundary conditions on all element borders. The assigned small-scale continuity equation (7.38) may be replaced by the small-scale pressure Poisson equation (PPE)

$$\begin{aligned} & \Delta p' + \nabla \cdot (\mathbf{u}_i \cdot \nabla \mathbf{u}' - \nu \Delta \mathbf{u}') \\ &= -\nabla \cdot \left[\frac{1}{\delta t} \bar{\mathbf{u}} + \mathbf{u}_i \cdot \nabla \bar{\mathbf{u}} + \beta \bar{\mathbf{u}} (\nabla \cdot \mathbf{u}_i) - \nu \Delta \bar{\mathbf{u}} + \nabla \bar{p} - \left(\mathbf{f} + \frac{\bar{\mathbf{u}}^n}{\delta t} \right) \right] \\ &= -\nabla \cdot \left[\mathfrak{R}_{NS, M}(\bar{\mathbf{u}}, \bar{p}) \right] \quad \text{in } \Omega_e \end{aligned} \quad (7.40)$$

where the consistent PPE (2.69) of Gresho and Sani has been adapted for the small scales. The right hand side of (7.40) has been extended by two terms obviously vanishing in the continuous case due to the continuity condition. This extension clarifies what the right hand side of (7.40) is made of: the negative divergence of the residual of the large-scale momentum equation.

At first, it is concentrated on the small-scale momentum equation (7.37). To the author's knowledge, the first attempt of using residual-free bubbles for the stabilization of a linearized stationary Navier–Stokes problem has to be credited to Russo (1996). The separation of function spaces (merely carried out for the weighting function space here) reads

$$\mathcal{V}_{\mathbf{u}p} \approx \bar{\mathcal{V}}_{\mathbf{u}p} \oplus \mathcal{V}'_{\mathbf{u}, RFB} = \bar{\mathcal{V}}_{\mathbf{u}p} \oplus_{\Omega_e} (B(\Omega_e))^d; \quad e = 1, \dots, n_{el} \quad (7.41)$$

with the usual assumption being $(B(\Omega_e))^d = (H_0^1(\Omega_e))^d$. As may be observed by inspecting the subscripts, the bubble space exclusively enhances the velocity approximation, i.e. $p' = 0$. Remembering the insights into approaches to satisfy the inf-sup condition emphasizes the reasonability of this concept. Therefore, (7.37)–(7.39) is now simplified to

$$\begin{aligned} & \frac{1}{\delta t} \mathbf{u}' + \mathbf{u}_i \cdot \nabla \mathbf{u}' + \beta (\nabla \cdot \mathbf{u}_i) \mathbf{u}' - \nu \Delta \mathbf{u}' \\ &= - \left[\frac{1}{\delta t} \bar{\mathbf{u}} + \mathbf{u}_i \cdot \nabla \bar{\mathbf{u}} + \beta (\nabla \cdot \mathbf{u}_i) \bar{\mathbf{u}} - \nu \Delta \bar{\mathbf{u}} + \nabla \bar{p} - \left(\mathbf{f} + \frac{\bar{\mathbf{u}}^n}{\delta t} \right) \right] \quad \text{in } \Omega_e \end{aligned} \quad (7.42)$$

$$\mathbf{u}' = \mathbf{0} \quad \text{on } \Gamma_e \quad (7.43)$$

If one were able to solve these element-based problems, the overall solution

$$\mathbf{u}' = - \sum_{e=1}^{n_{el}} \left\{ \left(\mathcal{L}_{M, \Omega_e}^{RFB}(\mathbf{u}_i) \right)^{-1} \left(\mathcal{L}_M^{dt, lin}(\mathbf{u}_i)[\bar{\mathbf{u}}, \bar{p}] - \left(\mathbf{f} + \frac{\bar{\mathbf{u}}^n}{\delta t} \right) \right) \right\} \quad (7.44)$$

would be encountered where

$$\mathcal{L}_M^{RFB}(\mathbf{u}_i) = \mathbf{u}_i \cdot \nabla - \nu \Delta + \left(\frac{1}{\delta t} + \beta (\nabla \cdot \mathbf{u}_i) \right) \quad (7.45)$$

The result (7.44) can now be integrated into the large-scale equation in the form (7.17) so as to get

$$\begin{aligned}
& B_{NS}^{dt, lin}(\bar{\mathbf{v}}, \bar{q}, \bar{\mathbf{u}}, \bar{p}) - \sum_{e=1}^{n_{el}} \left(\bar{\mathbf{v}}, \frac{1}{\delta t} \left(\mathcal{L}_{M, \Omega^e}^{RFB}(\mathbf{u}_i) \right)^{-1} \left(\mathcal{L}_M^{dt, lin}(\mathbf{u}_i)[\bar{\mathbf{u}}, \bar{p}] - \left(\mathbf{f} + \frac{\mathbf{u}^n}{\delta t} \right) \right) \right)_{\Omega_e} \\
& - \sum_{e=1}^{n_{el}} \left(\mathcal{L}_M^{*stat}(\mathbf{u}_i)[\bar{\mathbf{v}}, \bar{q}], \left(\mathcal{L}_{M, \Omega^e}^{RFB}(\mathbf{u}_i) \right)^{-1} \left(\mathcal{L}_M^{dt, lin}(\mathbf{u}_i)[\bar{\mathbf{u}}, \bar{p}] - \left(\mathbf{f} + \frac{\mathbf{u}^n}{\delta t} \right) \right) \right)_{\Omega_e} \\
& = \left(\bar{\mathbf{v}}, \frac{\mathbf{u}^n}{\delta t} \right)_{\Omega} + (\bar{\mathbf{v}}, \mathbf{f})_{\Omega} + (\bar{\mathbf{v}}, \mathbf{h})_{\Gamma_h} \quad \forall \{\bar{\mathbf{v}}, \bar{q}\} \in \bar{\mathcal{V}}_{\mathbf{u}p} \tag{7.46}
\end{aligned}$$

where some of the terms in (7.17) vanish due to the assumptions made.

Solving directly for the shape function components of the small-scale solution \mathbf{u}' in the sense already described in chapter 6 is here possible as well, since the underlying problem has been linearized before. It is somewhat more complicated in that it has to be dealt with an additional variable, namely the pressure, on the right hand side in (7.42). The separation of the right hand side described in Franca and Nesliturk (2001) as well as Nesliturk (1999) will be adopted. Starting with the standard elementwise extension of the large-scale velocity and pressure

$$\bar{\mathbf{u}}_e = \sum_{b=1}^{n_{ed}} \sum_{i=1}^{n_{sd}} \bar{N}_b \mathbf{u}_b^i \mathbf{e}_i, \quad \bar{p}_e = \sum_{b=1}^{n_{ed}} \bar{N}_b p_b \tag{7.47}$$

the extension of the small-scale velocity is assumed to be

$$\mathbf{u}'_e = \sum_{b=1}^{n_{ed}} \sum_{i=1}^{n_{sd}} \mathcal{U}_b \mathbf{u}_b^i \mathbf{e}_i + \sum_{b=1}^{n_{ed}} p_b \sum_{i=1}^{n_{sd}} \mathcal{P}_b^i \mathbf{e}_i + \sum_{i=1}^{n_{sd}} \mathcal{F}^i \mathbf{e}_i \tag{7.48}$$

where n_{sd} denotes the number of spatial directions and \mathbf{e}_i the unit vector in the spatial direction i . Furthermore, \mathcal{U} denominates a 'velocity bubble function', \mathcal{P} a 'pressure bubble function' and \mathcal{F} a 'RHS bubble function'. The notation and the choice of the ansatz will hopefully become clear after introducing the equations which have to be solved in order to get these functions. Introducing the extensions in (7.42) and decomposing into the basic components in the fashion of (6.57)-(6.60), n_{ed} equations have to be solved for the velocity bubble functions \mathcal{U}_b subject to

$$\begin{aligned}
& \mathbf{u}_i \cdot \nabla \mathcal{U}_b - \nu \Delta \mathcal{U}_b + \left(\frac{1}{\delta t} + \beta(\nabla \cdot \mathbf{u}_i) \right) \mathcal{U}_b \\
& = - \left(\mathbf{u}_i \cdot \nabla \bar{N}_b - \nu \Delta \bar{N}_b + \left(\frac{1}{\delta t} + \beta(\nabla \cdot \mathbf{u}_i) \right) \bar{N}_b \right) \quad \text{in } \Omega_e \tag{7.49}
\end{aligned}$$

$n_{sd} n_{ed}$ equations for the pressure bubble function \mathcal{P}_b^i subject to

$$\mathbf{u}_i \cdot \nabla \mathcal{P}_b^i - \nu \Delta \mathcal{P}_b^i + \left(\frac{1}{\delta t} + \beta(\nabla \cdot \mathbf{u}_i) \right) \mathcal{P}_b^i = - \frac{\partial \bar{N}_b}{\partial x_i} \quad \text{in } \Omega_e \tag{7.50}$$

and n_{sd} equations for the RHS bubble function \mathcal{F}^i subject to

$$\mathbf{u}_i \cdot \nabla \mathcal{F}^i - \nu \Delta \mathcal{F}^i + \left(\frac{1}{\delta t} + \beta(\nabla \cdot \mathbf{u}_i) \right) \mathcal{F}^i = f_i + \frac{u_i^n}{\delta t} \quad \text{in } \Omega_e \tag{7.51}$$

where all $n_{RFB} = n_{el} (n_{ed} (n_{sd} + 1) + n_{sd})$ entirely independent residual-free bubble equations are subject to zero Dirichlet boundary conditions on the complete element boundary Γ_e . Furthermore, a normalized (w.r.t. the right hand side) equation is introduced reading

$$\mathbf{u}_i \cdot \nabla \mathfrak{B}_1 - \nu \Delta \mathfrak{B}_1 + \left(\frac{1}{\delta t} + \beta (\nabla \cdot \mathbf{u}_i) \right) \mathfrak{B}_1 = 1 \quad \text{in } \Omega_e \quad (7.52)$$

for a normalized bubble function \mathfrak{B}_1 acting as a place holder for all the equations in (7.49)-(7.51) on the one hand and, more importantly, being the object of considerations in the later to be described dynamic modeling process for the subgrid viscosity on the other hand. Please note that in the end a collection of 'pure' scalar convection-diffusion-reaction equations governing the behaviour of the scalar quantity 'bubble function' have been achieved. Hence, the 'circle of description' which started with the model problem of convection-diffusion-reaction equations for a scalar quantity ϕ can be closed now. Thus, additional reasoning is provided for the introduction and investigation of the scalar convection-diffusion-reaction equation throughout this work.

Aside from this, one may think of some furthergoing simplifications. Firstly, the parameter β may be set to zero and the convective iterative velocity \mathbf{u}_i can be approximated by the large-scale part $\bar{\mathbf{u}}_i$. Both assumptions offer some computational convenience. Secondly, one is able to refer back to the concept of quasi-static bubbles (QSB) mentioned in section 6.5. A thorough analysis of Dubois et al. (1999) revealed that the time variations over one time step of small-scale velocity components in multiscale decompositions for turbulent flow calculations are much smaller when compared to the large-scale velocity components. In consequence, they 'freeze' the small-scale components over some time during their simulations while they account for the exact temporal integration of the large-scale components. Therefore, the approximation

$$\mathbf{u}'^{n+1} \approx \mathbf{u}'^n \quad (7.53)$$

seems to be, at least partly, reasonable for such flow regimes. With the just explained simplifications (7.49)-(7.51) read

$$\bar{\mathbf{u}}_i \cdot \nabla \mathfrak{u}_b - \nu \Delta \mathfrak{u}_b = - \left(\bar{\mathbf{u}}_i \cdot \nabla \bar{N}_b - \nu \Delta \bar{N}_b + \frac{1}{\delta t} \bar{N}_b \right) \quad \text{in } \Omega_e \quad (7.54)$$

$$\mathbf{u}_i \cdot \nabla \mathfrak{p}_b^i - \nu \Delta \mathfrak{p}_b^i = - \frac{\partial \bar{N}_b}{\partial x_i} \quad \text{in } \Omega_e \quad (7.55)$$

$$\mathbf{u}_i \cdot \nabla \mathfrak{f}^i - \nu \Delta \mathfrak{f}^i = f_i + \frac{u_i^n}{\delta t} \quad \text{in } \Omega_e \quad (7.56)$$

representing now convection-diffusion equations for the scalar quantity 'bubble function'. In this context, one may again think of restricting the approximation of the original right hand side to the large-scale space (see Codina and Blasco (2002)) resulting in the possibility to omit (7.51) which reduces the overall number of residual-free bubble equations to $n_{RFB} = n_{el} n_{ed} (n_{sd} + 1)$. If one were able to solve the previously described bubble equations analytically, the result might be incorporated into the final matrix system, which will now be described, and everything would be fine with regard to this aspect of the multi-level solution. However, since the achievement of such an analytical solution is impossible in general, an appropriate discrete solution strategy will be presented in the subsequent chapter.

Closing the treatment of the small-scale momentum equation, one more simplification is noted. The decision to solve for shape function components enables to feed the resulting bubble functions into the (not integrated-by-parts) large-scale equation (7.10) being the one and only equation to be solved globally. This leaves us with a matrix scheme similar to (7.27), but now reading

$$\begin{bmatrix} \mathbf{K}_{NS}^{\mathfrak{B}}(\mathbf{u}_i) & \mathbf{G}^{\mathfrak{B}}(\mathbf{u}_i) \\ \mathbf{G}^{T\mathfrak{B}} & \delta t \mathbf{G}^{T\mathfrak{P}} \end{bmatrix} \cdot \begin{bmatrix} \bar{\mathbf{u}}_{i+1} \\ \bar{\mathbf{p}}_{i+1} \end{bmatrix} = \begin{bmatrix} \mathbf{R}_M^{\mathfrak{B}}(\mathbf{u}_i) \\ \mathbf{R}_C^{\mathfrak{B}} \end{bmatrix} \quad (7.57)$$

where the 'bubble-enhanced' matrices read as

$$\mathbf{K}_{NS}^{\mathfrak{B}}(\mathbf{u}_i) = \mathbf{K}_{NS}(\mathbf{u}_i) + \mathbf{K}_{NS}^{\mathfrak{U}}(\mathbf{u}_i) \quad (7.58)$$

$$\mathbf{G}^{\mathfrak{B}}(\mathbf{u}_i) = \delta t \mathbf{G} + \mathbf{K}_{NS}^{\mathfrak{P}}(\mathbf{u}_i) \quad (7.59)$$

$$\mathbf{G}^{T\mathfrak{B}} = \delta t \mathbf{G}^T + \delta t \mathbf{G}^{T\mathfrak{U}} \quad (7.60)$$

and the 'bubble-enhanced' right hand sides as

$$\mathbf{R}_M^{\mathfrak{B}}(\mathbf{u}_i) = \delta t (\bar{\mathbf{F}} + \bar{\mathbf{N}} - \bar{\mathbf{E}}^M) + \bar{\mathbf{M}}\bar{\mathbf{u}}^n - \mathbf{K}_{NS}^{\mathfrak{F}}(\mathbf{u}_i) \quad (7.61)$$

$$\mathbf{R}_C^{\mathfrak{B}} = \delta t (-\bar{\mathbf{E}}^C) - \delta t \mathbf{G}^{T\mathfrak{F}} \quad (7.62)$$

In (7.57)-(7.62), the superscripts \mathfrak{U} or \mathfrak{P} affixed to the various matrices denote the replacement of the standard (large-scale) shape function \bar{N}_b in the evaluation of the respective element matrices (given in section 3.3.4) by the respective velocity bubble function \mathfrak{U}_b or the sum of the respective pressure bubble function \mathfrak{P}_b^i in all spatial directions i . For instance, a sample component of the element gradient matrix with pressure bubble functions replacing the standard (large-scale) shape function \bar{N}_b would be defined as

$$G_{ab}^{\mathfrak{P}e} = - \int_{\Omega_e} \nabla \cdot \bar{N}_a \sum_{i=1}^{n_{sd}} \mathfrak{P}_b^i d\Omega \quad (7.63)$$

The same occurs on the right hand side using the respective RHS bubble function \mathfrak{F}^i . Additional details concerning the calculation of the components of the matrix (7.57) may be found in Franca and Nesliturk (2001) or Nesliturk (1999), respectively.

In the last part of this section, it is returned to the small-scale continuity equation (7.38) left out up to now. Please remember that this equation is actually not needed any more, since there is no small-scale pressure in the small-scale momentum equation to be governed by the small-scale continuity equation. As you will see below however, it may be helpful to revitalize some kind of small-scale pressure being completely independent of the small-scale momentum equation. To be more precise, it will be concentrated on the small-scale PPE (7.40) and tried to find a solution. This should be helpful in fulfilling the continuity condition on the small-scale level, an issue becoming more and more important with increasing Reynolds number, see e.g. Gresho and Sani (1998), Tezduyar and Osawa (2000) or Wall (1999). Therefore, it is supposed to be a crucial ingredient of the solution strategy, since it is aimed at turbulent flows usually linked with high Reynolds numbers.

The residual $\mathfrak{R}_{NS, M}(\bar{\mathbf{u}}, \bar{\mathbf{p}})$ on the right hand side of (7.40) is supposed to be divergence-free or, otherwise, a potential component will be subsumed in a modified small-scale pressure such that

$$\Delta p'_{\text{mod}} = \Delta p' + \nabla \cdot [\mathfrak{R}_{NS, M}(\bar{\mathbf{u}}, \bar{\mathbf{p}})] \quad (7.64)$$

respectively. By using relation (7.38), the following Poisson equation for the modified small-scale pressure may be obtained from (7.40):

$$\Delta p'_{\text{mod}} = - [\mathbf{u}_i \cdot \nabla (\nabla \cdot \bar{\mathbf{u}}) - \nu \Delta (\nabla \cdot \bar{\mathbf{u}})] = - [\mathbf{u}_i \cdot \nabla - \nu \Delta] (\nabla \cdot \bar{\mathbf{u}}) \quad \text{in } \Omega_e \quad (7.65)$$

It is not advisable to solve this differential equation for the small-scale pressure on the element level besides the burden of solving the momentum equation, let alone the difficult question concerning useful pressure boundary conditions for (7.65) on the element boundaries. Here, it is rather intended to incorporate the effect of the small-scale pressure Poisson equation (and, thus, the small-scale continuity equation) into the final (large-scale) equation by way of an additional term in the fashion of a stabilizing term. This leads to an approximation for p' of the form

$$p' \approx - \tau_e^C (\nabla \cdot \bar{\mathbf{u}}) = - \tau_e^C \mathcal{R}_{NS,C}(\bar{\mathbf{u}}) \quad \text{in } \Omega_e \quad (7.66)$$

with an algebraic stabilization parameter τ_e^C and the residual of the large-scale continuity equation $\mathcal{R}_{NS,C}(\bar{\mathbf{u}})$. Recently, Franca and Oliveira (2003) have shown that the derivation of this stabilizing term can be traced back to the potential introduction of something what they call 'pressure bubble'. However, since stabilizing terms are the subject of the next section, this is postponed until then and will be picked up at this point again.

The strategy is summed up now. Residual-free bubbles will be used to solve the small-scale momentum equation. Additionally, the effect of the small-scale continuity equation is incorporated by taking it into account with the aid of a stabilizing term in the final (large-scale) equation. In the end, one is confronted with what may be called a combined residual-free bubble/stabilizing strategy. After all, the main assumption $p' = 0$ in the small-scale momentum equation comes down to the fact that the small-scale velocity is exclusively driven by the residual of the large-scale momentum equation and not by the residual of the continuity equation, confer Codina (2002a). A further interpretation is attempted in the next section.

7.2.3 Interpretation of the local strategy as a local pressure projection method

Starting point of these considerations is the small-scale equation (7.42) in temporally non-discretized form, i.e.

$$\frac{\partial \mathbf{u}'}{\partial t} + \mathbf{u}_i \cdot \nabla \mathbf{u}' - \nu \Delta \mathbf{u}' = - \left[\frac{\partial \bar{\mathbf{u}}}{\partial t} + \mathbf{u}_i \cdot \nabla \bar{\mathbf{u}} - \nu \Delta \bar{\mathbf{u}} + \nabla \bar{p} - \mathbf{f} \right] = - \bar{\mathbf{F}} \quad \text{in } \Omega_e \quad (7.67)$$

where $\beta = 0$ is assumed for simplicity and the right hand side depending on the large scales is summarized within $\bar{\mathbf{F}}$. (7.67) goes along with the zero Dirichlet boundary condition (7.43).

The classical way of performing a pressure projection method according to Chorin (1968) (see also e.g. Gresho (1990) and Gresho and Chan (1990)) may be briefly stated using three steps. Firstly, the momentum equation is solved without the pressure term for an intermediate velocity \mathbf{u}_{int} subject to

$$\frac{\partial \mathbf{u}_{int}}{\partial t} + \mathbf{u}_{int} \cdot \nabla \mathbf{u}_{int} - \nu \Delta \mathbf{u}_{int} = \mathbf{f} \quad (7.68)$$

\mathbf{u}_{int} is not divergence-free in general. Thus, it has to be projected to the space of divergence-free velocities. By using the Navier-Stokes equations system in the form

$$\frac{\partial \mathbf{u}}{\partial t} + \nabla p = \frac{\partial \mathbf{u}_{int}}{\partial t} \quad (7.69)$$

$$\nabla \cdot \mathbf{u} = 0 \quad (7.70)$$

a pressure Poisson equation reading

$$\Delta p = \frac{\partial \mathbf{u}_{int}}{\partial t} \quad (7.71)$$

may be achieved. (7.71) results from the application of the divergence operator to (7.69) and using (7.70). The solution of (7.71) represents the second step. In a third step, the intermediate velocity \mathbf{u}_{int} is 'updated' in order to get a now divergence-free velocity \mathbf{u} subject to

$$\mathbf{u} = \mathbf{u}_{int} - \int_t \nabla p \, dt \quad (7.72)$$

Interpreting (7.67) in the sense of the pressure projection algorithm, it may be stated that (7.67) is solved in the sense of (7.68) for a small-scale velocity \mathbf{u}' with $\bar{\mathbf{F}}$ replacing \mathbf{f} . This 'intermediate' velocity is not divergence-free from the point of view of the pressure projection method. At the same time, it is, however, the 'final' small-scale velocity, since there will be no more equations in the sense of (7.71) and (7.72) to be solved on the small-scale level. As aforementioned, a small-scale pressure will merely be incorporated by a stabilizing term.

How does one achieve some justification for \mathbf{u}' actually being divergence-free? At least, it may be proven that the small-scale velocity is divergence-free in an integral sense within individual element domains Ω_e . This may be done by investigating the zero Dirichlet boundary condition (7.43) which allows to state the following (confer (2.51)):

$$\int_{\Gamma_e} \mathbf{n} \cdot \mathbf{u}' \, d\Gamma = 0 \quad (7.73)$$

i.e. there is no 'small-scale flow' through the element boundaries. This has already been described as being the crucial assumption of residual-free bubbles. Applying Gauss' theorem (2.23) to (7.73) yields the elementwise integrated small-scale continuity equation according to

$$\int_{\Gamma_e} \mathbf{n} \cdot \mathbf{u}' \, d\Gamma = \int_{\Omega_e} \nabla \cdot \mathbf{u}' \, d\Omega = 0 \quad (7.74)$$

i.e. the small-scale velocity is divergence-free in an integral sense and, hence, the small-scale component of the velocity is conservative within the element domain Ω_e . This is an attribute which cannot be extended to the large-scale part of the velocity within the Galerkin finite element method in general. Please consult Hughes et al. (2000b) for a discussion of the missing conservation properties of the Galerkin method - and also for some advice on how this situation can be remedied. Anyway, nothing more can be said concerning local conservation properties of the small-scale equation (7.67) within Ω_e . This is certainly a point eagerly demanding some further investigation.

7.3 Taking into account locally the effect of unresolved scales onto resolved scales

7.3.1 Stabilized methods

Nearly everything what has been said in section 6.3.1 may be transferred to this section in unaltered form. Please remember that the crucial effect of the unresolved scales onto the resolved scales for the convection-diffusion-reaction equation consists in the introduction of an artificial diffusion in the streamline direction - the basic idea of SUPG. However, a second problem has to be dealt with in the context of the Navier-Stokes equations: the fulfillment of the inf-sup condition, either by satisfying it directly or by circumventing it. It may be observed that these two strategies are close together.

An approach for solemnly attacking the last problem was demonstrated by Hughes et al. (1986) for the Stokes equation where this is the only reason for introducing stabilizing terms. This method has been named 'Pressure Stabilizing Petrov-Galerkin' (PSPG) afterwards and the similarity to SUPG is obvious. Combined approaches of SUPG/PSPG are conceivable and have been used, see e.g. Hansbo and Szepessy (1990), Tezduyar et al. (1992) as well as Tezduyar and Osawa (2000). The nontrivial question of the necessary stabilization for elements fulfilling the inf-sup condition addressed in section 3.4.2 is discussed in Gelhard et al. (2003).

For equal-order interpolated elements violating the inf-sup condition, it is, however, more straightforward to use the GLS- and USFEM-type methods being already equipped with everything one needs to overcome both problems. Moreover, due to the inherent switches between differently dominated regimes in the definition of the herein preferred stabilization parameter definition according to Franca and Valentin (6.67)-(6.70), this parameter may be applied for the Navier-Stokes equations as well. Generally, applications of stabilized methods of GLS- and USFEM-type, respectively, to the Navier-Stokes equations are reported, for instance, in Franca and Frey (1992) as well as Codina (2001). Barrenechea and Valentin (2002) have recently analyzed the USFEM-type method for a generalized Stokes problem with a dominating reactive term and shown that it yields good results even in this case. Oñate (2000) has also applied a stabilized method based on the finite increment calculus to the incompressible Navier-Stokes equations. The temporal dependence of the stabilization is particularly investigated in Bochev et al. (2002) for semi-discrete methods applied to the transient Stokes problem. In Jansen et al. (1999), a better consistency for finite element methods with low-order functions is proposed and proven for the Navier-Stokes equations.

Taking into account all these aspects, there is a sufficient 'instrumentation' to stabilize the momentum equation. This means, however, that one is still left with an untreated continuity equation. In (7.66), there has already been a hint how such a stabilizing term may look like from the point of view of a small-scale pressure. It will be stuck to this characteristic form and an appropriate definition merely has to be added for the respective stabilization parameter τ_e^C .

At the beginning of it all, the separation of the function spaces as

$$\mathcal{S}_{up} = \bar{\mathcal{P}}_{up} \oplus \hat{\mathcal{P}}_{up} \quad (7.75)$$

$$\mathcal{V}_{up} = \bar{\mathcal{V}}_{up} \oplus \hat{\mathcal{V}}_{up} \quad (7.76)$$

is introduced with the $(\hat{\cdot})$ -values again indicating unresolved scales in view of the subsequent three-scale separation. The general formulation for the discrete in time (backward Euler) and linearized Navier-Stokes equations looks like

$$B_{NS}^{dt, lin}(\bar{\mathbf{v}}, \bar{q}, \bar{\mathbf{u}}, \bar{p}) + \sum_{e=1}^{n_{el}} \left(\mathcal{L}_M^{stab}(\bar{\mathbf{u}}_i)[\bar{\mathbf{v}}, \bar{q}], \tau_e^M \left(\frac{\bar{\mathbf{u}}}{\delta t} + \mathcal{L}_M^{stat}(\bar{\mathbf{u}}_i)[\bar{\mathbf{u}}, \bar{p}] - \left(\mathbf{f} + \frac{\bar{\mathbf{u}}^n}{\delta t} \right) \right) \right)_{\Omega_e} \\ + \sum_{e=1}^{n_{el}} \left(\nabla \cdot \bar{\mathbf{v}}, \tau_e^C(\nabla \cdot \bar{\mathbf{u}}) \right)_{\Omega_e} = \left(\bar{\mathbf{v}}, \frac{\bar{\mathbf{u}}^n}{\delta t} \right)_{\Omega} + (\bar{\mathbf{v}}, \mathbf{f})_{\Omega} + (\bar{\mathbf{v}}, \mathbf{h})_{\Gamma_h} \quad \forall \{\bar{\mathbf{v}}, \bar{q}\} \in \bar{\mathcal{V}}_{up} \quad (7.77)$$

where the differential operator \mathcal{L}_M^{stab} acting on the weighting functions $\bar{\mathbf{v}}$ and \bar{q} for GLS is defined as

$$\mathcal{L}_M^{stab}(\bar{\mathbf{u}}_i)[\bar{\mathbf{v}}, \bar{q}] = \bar{\mathbf{u}}_i \cdot \nabla \bar{\mathbf{v}} + \beta(\nabla \cdot \bar{\mathbf{u}}_i) \bar{\mathbf{v}} - \nu \Delta \bar{\mathbf{v}} - \nabla \bar{q} \quad (7.78)$$

and for USFEM as

$$\mathcal{L}_M^{stab}(\bar{\mathbf{u}}_i)[\bar{\mathbf{v}}, \bar{q}] = \bar{\mathbf{u}}_i \cdot \nabla \bar{\mathbf{v}} - \beta(\nabla \cdot \bar{\mathbf{u}}_i) \bar{\mathbf{v}} + \nu \Delta \bar{\mathbf{v}} - \nabla \bar{q} \quad (7.79)$$

where the time-dependent term may also be incorporated in order to get

$$\mathcal{L}_M^{stab}(\bar{\mathbf{u}}_i)[\bar{\mathbf{v}}, \bar{q}] = \bar{\mathbf{u}}_i \cdot \nabla \bar{\mathbf{v}} + \left(\frac{1}{\delta t} + \beta(\nabla \cdot \bar{\mathbf{u}}_i) \right) \bar{\mathbf{v}} - \nu \Delta \bar{\mathbf{v}} - \nabla \bar{q} \quad (7.80)$$

and

$$\mathcal{L}_M^{stab}(\bar{\mathbf{u}}_i)[\bar{\mathbf{v}}, \bar{q}] = \bar{\mathbf{u}}_i \cdot \nabla \bar{\mathbf{v}} - \left(\frac{1}{\delta t} + \beta(\nabla \cdot \bar{\mathbf{u}}_i) \right) \bar{\mathbf{v}} + \nu \Delta \bar{\mathbf{v}} - \nabla \bar{q} \quad (7.81)$$

respectively. See also the discussion at the end of section 6.5. Please note that the only fact distinguishing (7.78)-(7.81) from the basic definition of the GLS- and USFEM-type differential operators is basically due to the chosen negative sign in (3.20). τ_e^M in (7.77) is still governed by (6.67)-(6.70) with the appropriate velocity $\bar{\mathbf{u}}_i$, the viscosity ν replacing the diffusion coefficient κ and the appropriate reaction coefficient

$$\sigma = \frac{1}{\delta t} + \beta(\nabla \cdot \bar{\mathbf{u}}_i) \quad (7.82)$$

For τ_e^C , the definition of Codina (2002a) is adopted reading

$$\tau_e^C = \left[\nu^2 + \left(\frac{c_2}{c_1} |\bar{\mathbf{u}}_i| h \right)^2 \right]^{\frac{1}{2}} \quad (7.83)$$

where acceptable choices for c_1 and c_2 are subject to (6.72).

7.3.2 Dissipative effect of unresolved scales: artificial and subgrid viscosity approach

Straightforward adoption of the artificial diffusion approach to the current problem results in an artificial viscosity as follows:

$$\nu_e^{art} = \begin{cases} \frac{|\bar{\mathbf{u}}_i| \bar{h}}{2} \frac{\text{Re}}{3}, & \text{for } \text{Re} < 3 \\ \frac{|\bar{\mathbf{u}}_i| \bar{h}}{2}, & \text{for } \text{Re} \geq 3 \end{cases} \quad (7.84)$$

with the element Reynolds number

$$\text{Re} = \frac{|\bar{\mathbf{u}}_i| \bar{h}}{2\nu} \quad (7.85)$$

In the following, the focus is, however, on an alternative method for introducing artificial viscosity which has been introduced in section 5.2.3 in the context of LES. Despite all its drawbacks, it may be thought of using the Smagorinsky model (5.36) in elementwise form according to

$$\nu_e^T = (C_S \bar{h})^2 |\boldsymbol{\varepsilon}(\bar{\mathbf{u}})| \quad (7.86)$$

with the characteristic element length \bar{h} acting as the analogon of the filter width. Whatever model is applied, (7.84) or (7.86), the final equation to be solved reads

$$\begin{aligned} B_{NS}^{dt, lin}(\bar{\mathbf{v}}, \bar{q}; \bar{\mathbf{u}}, \bar{p}) + \sum_{e=1}^{n_{el}} (\nabla \bar{\mathbf{v}}, \nu_e \nabla \bar{\mathbf{u}})_{\Omega_e} \\ = \left(\bar{\mathbf{v}}, \frac{\bar{\mathbf{u}}^n}{\delta t} \right)_{\Omega} + (\bar{\mathbf{v}}, \mathbf{f})_{\Omega} + (\bar{\mathbf{v}}, \mathbf{h})_{\Gamma_h} \quad \forall \{\bar{\mathbf{v}}, \bar{q}\} \in \bar{\mathcal{V}}_{up} \end{aligned} \quad (7.87)$$

Of course, (7.87) cannot act as a stand-alone method for getting a stable solution of the Navier-Stokes equations. All four points at the end of section 6.3.2 apply here as well and, more importantly, there is nothing looking like an adequate pressure stabilization for equal-order interpolated elements. Therefore, in case no elements passing the inf-sup condition are used, something more has to be added. However, the suitability of this approach will hopefully become clear when such dissipative models are applied 'one level lower' within a three-scale separation. For a recent numerical investigation considering the different amount of numerical viscosity introduced by a stabilized method of SUPG-type and the Smagorinsky model in the context of a particular flow example, namely the 2-D flow past a circular cylinder, it is referred to Akin et al. (2003).

7.4 Separation of three scales

7.4.1 Basic concept and provision for unresolved scales

According to what has been done in the context of the convection-diffusion-reaction equation in section 6.4, the solution and weighting function spaces are separated as follows

$$\mathcal{S}_{up} = \bar{\mathcal{P}}_{up} \oplus \mathcal{S}'_{up} = \bar{\mathcal{P}}_{up} \oplus \mathcal{S}'_{up, h'} \oplus \hat{\mathcal{S}}_{up} \quad (7.88)$$

$$\mathcal{V}_{up} = \bar{\mathcal{V}}_{up} \oplus \mathcal{V}'_{up} = \bar{\mathcal{V}}_{up} \oplus \mathcal{V}'_{up, h'} \oplus \hat{\mathcal{V}}_{up} \quad (7.89)$$

Hence, it has to be dealt with large resolved scales, small resolved scales and unresolved scales. The equation system for the discrete in time, linearized Navier–Stokes equations reads

$$\begin{aligned} & B_{NS}^{dt, lin}(\bar{\mathbf{v}}, \bar{q}; \bar{\mathbf{u}} + \mathbf{u}' + \hat{\mathbf{u}}, \bar{p} + p' + \hat{p}) \\ &= \left(\bar{\mathbf{v}}, \frac{\mathbf{u}^n}{\delta t} \right)_{\Omega} + (\bar{\mathbf{v}}, \mathbf{f}^{n+\theta})_{\Omega} + (\bar{\mathbf{v}}, \mathbf{h}^{n+\theta})_{\Gamma_h} \quad \forall \{\bar{\mathbf{v}}, \bar{q}\} \in \bar{\mathcal{V}}_{u p} \end{aligned} \quad (7.90)$$

$$\begin{aligned} & B_{NS}^{dt, lin}(\mathbf{v}', q'; \bar{\mathbf{u}} + \mathbf{u}' + \hat{\mathbf{u}}, \bar{p} + p' + \hat{p}) \\ &= \left(\mathbf{v}', \frac{\mathbf{u}^n}{\delta t} \right)_{\Omega} + (\mathbf{v}', \mathbf{f}^{n+\theta})_{\Omega} + (\mathbf{v}', \mathbf{h}^{n+\theta})_{\Gamma_h} \quad \forall \{\mathbf{v}', q'\} \in \mathcal{V}'_{u p, h'} \end{aligned} \quad (7.91)$$

$$\begin{aligned} & B_{NS}^{dt, lin}(\hat{\mathbf{v}}, \hat{q}; \bar{\mathbf{u}} + \mathbf{u}' + \hat{\mathbf{u}}, \bar{p} + p' + \hat{p}) \\ &= \left(\hat{\mathbf{v}}, \frac{\mathbf{u}^n}{\delta t} \right)_{\Omega} + (\hat{\mathbf{v}}, \mathbf{f}^{n+\theta})_{\Omega} + (\hat{\mathbf{v}}, \mathbf{h}^{n+\theta})_{\Gamma_h} \quad \forall \{\hat{\mathbf{v}}, \hat{q}\} \in \hat{\mathcal{V}}_{u p} \end{aligned} \quad (7.92)$$

As in section 6.4, it is assumed that

$$B_{NS}^{dt, lin}(\bar{\mathbf{v}}, \bar{q}; \hat{\mathbf{u}}, \hat{p}) \approx 0 \quad (7.93)$$

which relies on a clear separation of the large-scale space and the space of unresolved scales. As indicated by Collis (2001), this amounts to be the first modeling step. Likewise the opposite projection is assumed to be

$$B_{NS}^{dt, lin}(\hat{\mathbf{v}}, \hat{q}; \bar{\mathbf{u}}, \bar{p}) \approx 0 \quad (7.94)$$

leading to a simplified equation system by changing (7.90) to be

$$\begin{aligned} & B_{NS}^{dt, lin}(\bar{\mathbf{v}}, \bar{q}; \bar{\mathbf{u}} + \mathbf{u}', \bar{p} + p') \\ &= \left(\bar{\mathbf{v}}, \frac{\mathbf{u}^n}{\delta t} \right)_{\Omega} + (\bar{\mathbf{v}}, \mathbf{f}^{n+\theta})_{\Omega} + (\bar{\mathbf{v}}, \mathbf{h}^{n+\theta})_{\Gamma_h} \quad \forall \{\bar{\mathbf{v}}, \bar{q}\} \in \bar{\mathcal{V}}_{u p} \end{aligned} \quad (7.95)$$

and (7.92) to be

$$\begin{aligned} & B_{NS}^{dt, lin}(\hat{\mathbf{v}}, \hat{q}; \mathbf{u}' + \hat{\mathbf{u}}, p' + \hat{p}) \\ &= \left(\hat{\mathbf{v}}, \frac{\mathbf{u}^n}{\delta t} \right)_{\Omega} + (\hat{\mathbf{v}}, \mathbf{f}^{n+\theta})_{\Omega} + (\hat{\mathbf{v}}, \mathbf{h}^{n+\theta})_{\Gamma_h} \quad \forall \{\hat{\mathbf{v}}, \hat{q}\} \in \hat{\mathcal{V}}_{u p} \end{aligned} \quad (7.96)$$

whereby (7.91) remains unchanged.

It is now appropriate to reiterate that it is not intended to resolve anything called unresolved a priori. Taking into account the effect of the unresolved scales onto the small scales is the only desire. Therefore, the three possibilities already introduced in section 6.4 are addressed. The main focus will be on the subgrid viscosity approach, since this is the usual and well-established way of taking into account the effect of unresolved scales in 'classical LES' - and, last but not least, the most straightforward approach. The notation is again simplified by focussing on a backward Euler scheme in time, i.e. $\theta = 1$, and omitting the superscript $n + 1$.

Using **stabilizing terms**, for instance, for a global solution approach with hierarchical bases, a new enhanced small-scale equation extending (7.11) and replacing (7.91) may be obtained as

$$\begin{aligned}
& B_{NS}^{dt, lin}(\mathbf{v}', q'; \bar{\mathbf{u}} + \mathbf{u}', \bar{p} + p') \\
& + \sum_{e=1}^{n_{el}} \left(\mathcal{L}_M^{stab}(\mathbf{u}_i)[\mathbf{v}', q'], \tau_e'^M \left(\frac{\mathbf{u}'}{\delta t} + \mathcal{L}_M^{stat}(\mathbf{u}_i)[\mathbf{u}', p'] - \left(\mathbf{f} + \frac{\mathbf{u}^n}{\delta t} \right) \right) \right)_{\Omega_e} \\
& + \sum_{e=1}^{n_{el}} \left(\nabla \cdot \mathbf{v}', \tau_e'^C (\nabla \cdot \mathbf{u}') \right)_{\Omega_e} \\
& = \left(\mathbf{v}', \frac{\mathbf{u}^n}{\delta t} \right)_{\Omega} + (\mathbf{v}', \mathbf{f})_{\Omega} + (\mathbf{v}', \mathbf{h})_{\Gamma_h} \quad \forall \{\mathbf{v}', q'\} \in \mathcal{V}'_{\mathbf{u} p, k-\bar{k}} \quad (7.97)
\end{aligned}$$

where $\tau_e'^M$ and $\tau_e'^C$ differ from the original definition in the parameter m_k , which should be matched to the emerging polynomial orders, or in a modified \bar{h} .

Concerning the idea of using **orthogonal subscales**, the basic thoughts of section 6.4 are still valid. For their application to the Navier-Stokes equations, please consult Codina (2002a).

Only accounting for the **dissipative effect of the unresolved scales** onto the resolved scales will be the result of using a subgrid viscosity approach - the foremost choice here due to its simplicity and its establishment in the 'classical' theory of LES. The small-scale equation then reads

$$\begin{aligned}
& B_{NS}^{dt, lin}(\mathbf{v}', q'; \bar{\mathbf{u}} + \mathbf{u}', \bar{p} + p') + \sum_{e=1}^{n_{el}} \left(\nabla \mathbf{v}', \nu_e' \nabla \mathbf{u}' \right)_{\Omega_e} \\
& = \left(\mathbf{v}', \frac{\mathbf{u}^n}{\delta t} \right)_{\Omega} + (\mathbf{v}', \mathbf{f})_{\Omega} + (\mathbf{v}', \mathbf{h})_{\Gamma_h} \quad \forall \{\mathbf{v}', q'\} \in \mathcal{V}'_{\mathbf{u} p, k-\bar{k}} \quad (7.98)
\end{aligned}$$

where the elementwise subgrid viscosity ν_e' may be represented by three alternative model formulations. The subgrid viscosity due to Guermond reads

$$\nu_e'^G = C_e^G h_e \quad \text{in } \Omega_e \quad (7.99)$$

with a so far unspecified h_e and a bounded constant C_e^G having the dimension of a velocity for consistency of (7.99). Comparing (7.99) to the original proposal of Prandtl (4.20), a striking affinity may be observed. The constant C_e^G is definitely the weak point of Guermond's model as will be for the following approaches. Alternatively, the definition of artificial viscosity in (7.84)-(7.85) either in original form applied to individual elements or modified by the introduction of a here nondimensional constant as

$$\nu_e'^{art} = C_e^{art} |\mathbf{u}_i| h_e \quad \text{in } \Omega_e \quad (7.100)$$

may be used where the only difference to (7.99) lies in the additional introduction of the velocity. Herewith, Prandtl's basic ansatz has been revitalized almost completely. The Smagorinsky model for an elementwise evaluation yields

$$\nu_e'^T = \left(C_e^S h_e \right)^2 |\boldsymbol{\epsilon}(\mathbf{u}_i)| \quad \text{in } \Omega_e \quad (7.101)$$

where the Smagorinsky constant C_e^S is also nondimensional. Using (7.99)-(7.101) to relate C_e^G to C_e^{art} and C_e^S results in

$$C_e^G = C_e^{art} |\mathbf{u}_i| = \left(C_e^S \right)^2 h_e |\boldsymbol{\epsilon}(\mathbf{u}_i)| \quad \text{in } \Omega_e \quad (7.102)$$

Finally, it has to be mentioned that Hughes and co-workers achieved very good results for homogeneous isotropic turbulence in Hughes et al. (2001a) and channel flow in Hughes et al. (2001b) using the Smagorinsky model in the framework of the variational multiscale method. Thus, the behaviour of even such simple models like (7.99)-(7.101) is very much improved by fitting it in this multiscale method.

7.4.2 Interpretation of the three-scale separation in the sense of a DNS/LES

The three-scale separation represents a consequential extension of the two-scale separation. Thus, this section takes up the thoughts of section 7.1.2 and extends them consequentially. In Fig. 7.2, the Kolmogorov energy spectrum is displayed for the situation of a three-scale separation. For ease of comparison, the two-scale separation illustrated in Fig 7.1 is figured again.

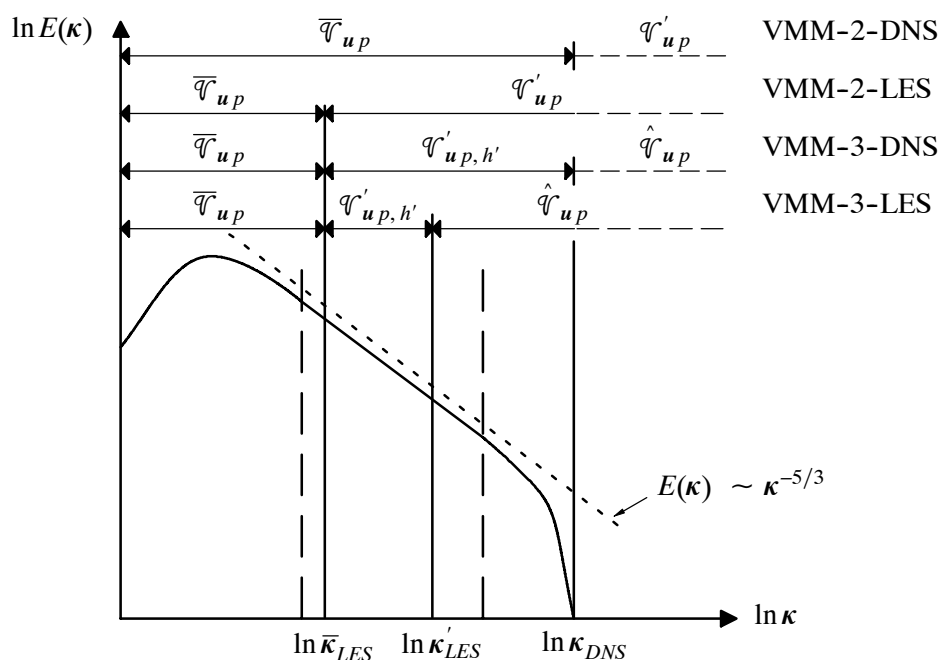


Fig. 7.2: Kolmogorov energy spectrum for 2- and 3-scale separation of VMM

It is observable that there are two ways of performing a DNS or a LES, respectively. A DNS may result from completely resolving all scales necessary therefore by the large-scale space. Alternatively, the same may be done by distributing these scales among a large- and a small-scale space. Whereas this distinction may be more or less of academic nature for a DNS, it is supposed to be a crucial decision for a LES. In contrast to a two-scale LES, a three-scale LES provides one with the opportunity of letting the subgrid-scale model act (directly) only onto the small-scale space. This may be observed by analyzing the equations (7.95)-(7.98). It has been dissected by Hughes and co-workers in Hughes et al. (2000a, 20001a, 2001b) that the crucial advantage of a LES based on the variational multiscale method is caused by the fact that the dissipative model acts (directly) only onto the small scales. Hence, the large scales are treated in a DNS-like manner guaranteeing consistency, if adequate resolution is already achieved by the large-scale space. This last case represents a natural switch to a 'VMM-2-DNS', confer Fig. 7.2. It has to be remarked that the idea of restricting the modeling efforts to the small scales may also be transferred back to the 'classical' procedure, for example, in the context of the dynamic modeling procedure of Ger-

mano et al. (1991). First ideas in this direction have been presented in Vreman (2003) recently. Finally, it is referred to the end of section 8.2 where this discussion is renewed. In particular, a principal comparison to the dynamic modeling procedure of Germano et al. (1991) will be carried out there and some remarks concerning the choice of the absolute and relative size of the large- and small-scale space are given.

7.5 Closure: three-scale separation based on residual-free bubbles and the subgrid viscosity approach

Closing the description of the variational multiscale method for the Navier-Stokes equations, the, for the time being, 'static' three-level approach to be applied to a practical implementation below is pointed out. The steps of this development starting with a two-level finite element method in Wall et al. (2001) and, by including a third level, arriving at a three-level finite element method with dynamic modeling of the effect of the unresolved scales in Gravemeier et al. (2002) and Gravemeier et al. (2003b) have been presented. A detailed overview is provided in Gravemeier et al. (2003a) and some remarks comparing this method with approaches of 'classical' LES have been made in Gravemeier et al. (2003c).

The variational large-scale equation (including the weak form of the large-scale momentum and the large-scale continuity equation) will be treated by a standard Galerkin method. The small-scale momentum equation or their basic constituents in form of bubble shape functions, respectively, will be solved in their basic form with varying right hand sides (7.49)-(7.51) as convection-diffusion-reaction equations. The bubble shape functions enter the final (large-scale) equation by way of the static condensation procedure. Please note that there is no small-scale pressure in the small-scale momentum equation. Therefore, the resulting (large-scale) equation is expected to be solved in a completely stable way. However, the effect of a small-scale pressure will be integrated in the final (large-scale) equation by a stabilizing term like the first term in the second line of (7.77) with (7.83) representing the small-scale continuity equation. Regarding the positive effect of such a term (sometimes called 'bulk viscosity' term) particularly in the range of high Reynolds numbers, please consult e.g. Wall (1999). Finally, the effect of the unresolved scales onto the small scales will be reproduced by a subgrid viscosity approach in the form of (7.99), (7.100) or (7.101). For the time being, it is stuck to a somehow determined constant in either of the formulations. In the following chapter, a dynamic algorithm for determining the subgrid viscosity without any underlying modeling assumption will be proposed. The slightly modified normalized bubble equation representing (7.49)-(7.51) again as a place holder here and in the following chapters now reads

$$\mathbf{u}_i \cdot \nabla \mathcal{B}_1 - (\nu + \nu'_e) \Delta \mathcal{B}_1 + \left(\frac{1}{\delta t} + \beta (\nabla \cdot \mathbf{u}_i) \right) \mathcal{B}_1 = 1 \quad \text{in } \Omega_e \quad (7.103)$$

or in simplified form for the quasi-static case as a convection-diffusion equation

$$\mathbf{u}_i \cdot \nabla \mathcal{B}_1 - (\nu + \nu'_e) \Delta \mathcal{B}_1 = 1 \quad \text{in } \Omega_e \quad (7.104)$$

The convection-diffusion equation (7.104) may be expected to be sufficiently stabilized by the subgrid viscosity. In (7.103), it has to be accounted for a potentially dominating reactive term, particularly due to a small time step δt , by making additional measures.

8 Practical Implementation: a two- and a three-level finite element method

8.1 A two-level finite element method based on the RFB approach

8.1.1 Finite element method on the second level using an elementwise submesh

The idea of using a two-level finite element method for the practical computation of residual-free bubble functions can be traced back to Franca and Macedo (1998), who proposed this methodology for the Helmholtz equation. In the same year, Franca et al. (1998b) published the application of this approach to convection-diffusion equations. Afterwards, Nesliturk and Franca also dealt with the stationary incompressible Navier-Stokes equations in Franca and Nesliturk (2001) as well as Nesliturk (1999). In Gravemeier et al. (2003a), this basic method has been extended in order to use it for the instationary incompressible Navier-Stokes equations being semi-discretized in time. At the same time, this approach exhibits its validity for any kind of convection-diffusion-reaction equation.

Starting point and likewise support for the solution of the large-scale equation of the problem is the basic discretization subject to (3.28)-(3.29). On every individual element domain Ω_e , a submesh will be introduced, see Fig. 8.1.

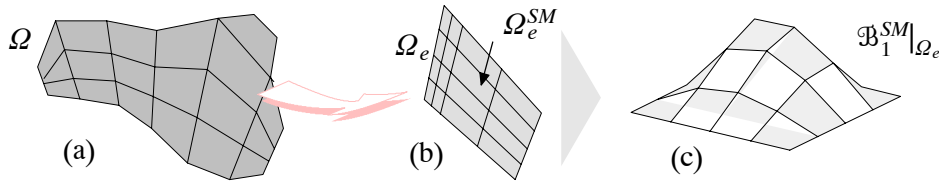


Fig. 8.1: (a) Mesh (first level); (b) submesh (SM - second level); (c) approximated RFB

This discretization on a second level or, more precise, the number of n_{el} discretizations on a second level will now be the support for the solution of the small-scale equations. They are formally identical up to the right hand sides for the convection-diffusion-reaction equation and the Navier-Stokes equations as can be observed by comparing the left hand sides of (6.59)-(6.60) and (7.49)-(7.51). In the following, the discussion is restricted to the normalized equation (7.103) without the addition of a subgrid viscosity or in simplified form as a convection-diffusion equation for the case of quasi-static bubbles (7.104). Please note that omitting the subgrid viscosity ν'_e in (7.103) or (7.104), respectively amounts to eliminating the effect of the unresolved scales onto the small scales and, consequently, going back from a three- to a two-level approach.

Since one is normally unable to find an analytical solution to these equations, the task is clear: Find an approximate residual-free bubble function \mathfrak{B}_1^{SM} in every element of the original discretization with the aid of the elementwise submeshes which then replaces the actually sought-after exact residual-free bubble function \mathfrak{B}_1 . The variational form of (7.103) (omitting ν'_e) with the submesh weighting functions w^{SM} reads

$$\left(w^{SM}, \mathbf{u}_i \cdot \nabla \mathfrak{B}_1^{SM} + \left(\frac{1}{\delta t} + \beta(\nabla \cdot \mathbf{u}_i) \right) \mathfrak{B}_1^{SM} \right)_{\Omega_e} + \left(\nabla w^{SM}, \nu \nabla \mathfrak{B}_1^{SM} \right)_{\Omega_e} = \left(w^{SM}, 1 \right)_{\Omega_e} \quad (8.1)$$

The standard finite element polynomial expansions are introduced as

$$\mathfrak{B}_1^{SM} = \sum_{B=1}^{n_{dofs}^{SM}} N_B^{SM} b_B^{SM}, \quad w^{SM} = \sum_{A=1}^{n_{dofs}^{SM}} N_A^{SM} w_A^{SM} \quad (8.2)$$

where N^{SM} denotes the shape functions belonging to the submesh and b_B^{SM} the degrees of freedom (equivalent to the nodal values for standard Lagrangean bases) of the bubble function. After all, the matrix problem

$$\mathbf{K}^{SM} \mathbf{b}^{SM} = \mathbf{F}^{SM} \quad (8.3)$$

is obtained where one sample component of the element matrices reads

$$K_{ab}^{e, SM} = \int_{\Omega_e^{SM}} N_a^{SM} \left(\mathbf{u}_i \cdot \nabla N_b^{SM} + \left(\frac{1}{\delta t} + \beta(\nabla \cdot \mathbf{u}_i) \right) N_b^{SM} \right) d\Omega + \nu \int_{\Omega_e^{SM}} \nabla N_a^{SM} \cdot \nabla N_b^{SM} d\Omega \quad (8.4)$$

and

$$F_a^{e, SM} = \int_{\Omega_e^{SM}} N_a^{SM} 1 d\Omega \quad (8.5)$$

with a chosen number of n_{el}^{SM} element domains Ω_e^{SM} for the submesh on the respective original element domain Ω_e . After solving (8.3) for the respective equations of (7.49)-(7.51), the exact residual-free bubble functions may then be replaced by the approximate versions in the expansion (7.48) for the Navier-Stokes equations.

Before proceeding to the generation of the submeshes, the choice of elements has to be addressed. As could have already been gathered from previous remarks and the illustration in Fig. 8.1, the use of quadrilateral elements is advocated predominantly in this work. Although the focus is on this type of element in the numerical simulations below, submesh generators for triangular elements, which have proven to be slightly more complicated in their development, have been implemented as well. Aside from some minor problems with the stability of bilinear quadrilaterals under certain circumstances, which seem to be only of technical type according to Brezzi et al. (1998a) (further analyzed in Franca and Tobiska (2002)) though, there is basically no difference in selecting quadrilaterals or triangles for the later algorithm. Therefore, the choice of quadrilateral elements is merely the subjective answer to an optional question.

8.1.2 Uniform and non-uniform Shishkin-type submesh generator

Basically, uniform elementwise submeshes are chosen. This selection goes along with the computational convenience of creating the submeshes once for all during the preprocessing stage. For convection-dominated flow regimes in particular, it is possibly adjuvant to create non-uniform submeshes with the refinement directed towards the outflow boundaries of the elements. Thin boundary layers will have to be resolved at the outflow boundaries wherefore a refined sub-

mesh in the vicinity of these boundaries may be helpful. The major drawback lies in the additional computational effort. Due to the dependence on the velocity distribution, the submesh creation step will possibly have to be repeated at least every time step in rapidly changing flow regimes.

Franca and Hwang (2002) proposed a polynomial-based refinement near the outflow boundaries. A quadratic as well as a cubic version have been implemented and tested. However, a Shishkin-type refinement at the outflow boundaries is proposed here in lieu of these polynomial refinements. See e.g. Hegarty et al. (1995) for the general concept of Shishkin-type meshes. This strategy has the advantage of depending the refinement on the element Reynolds number of the problem (7.103) or (7.104), respectively.

The stabilizing character of Shishkin-type meshes in the case of convection-diffusion equations is well-known. Therefore, in case of quasi-static bubble equations like (7.104), the use of Shishkin-type submeshes might be sufficient to stabilize the small-scale equation (and, thus, incorporate the effects of the unresolved scales redundantly a third level from the point of view of an adequate stabilization). It has to be remarked, however, that the efficient application of refined submeshes in this sense is limited. For very high element Reynolds numbers, extremely thin outflow boundary layers are encountered refusing a reasonable application of this stabilization strategy.

The basic situation for a one-dimensional element establishing also the similar situation for two- and three-dimensional elements in every coordinate direction is depicted in Fig. 8.2(a).



Fig. 8.2: (a) Shishkin-type mesh creation (1-D); (b) velocity vectors at center (2-D)

The convective velocity u is assumed to go from left to right defining the right end of the element as the outflow boundary here. A number of n_{nod}^{SM} submesh nodes is chosen. The distance δ between the 'middle node' and the outflow boundary is defined as

$$\delta = \min \left\{ \frac{h_{\xi_1}}{2}, \frac{\nu}{u} \ln(n_{nod}^{SM}) \right\} \quad (8.6)$$

The remaining nodes will be uniformly distributed on both sides of the 'middle node'. In Fig. 8.2(a) this is shown for $n_{nod}^{SM} = 5$. In two dimensions, the velocity vector at the element center will be determined and projected onto the two element-based coordinate directions u_r and u_s as the relevant velocities replacing u in (8.6), see Fig. 8.2(b). The similar situation in three dimensions for a hexahedral element generates the additional velocity u_t in the third direction.

Algorithm 8.1 displays the general procedure for generating a submesh for an individual element of the basic discretization. The submesh creation takes place on the parent (computational) domain resulting from a transformation of the original (physical) element domain. Confer e.g. Hug-

hes (2000) for further details of this transformation. All steps of the algorithm in bold font are merely necessary for the Shishkin-type non-uniform submesh generator. Please note that the evaluation of the velocity vector at the element center replaces the computationally more expensive determination of the outflow boundaries in the polynomial refinement strategy of Franca and Hwang (2002). The evaluation of the submesh ID- and IEN-arrays is only necessary for one, usually the first, element during the preprocessing stage both for the uniform and for the non-uniform submesh generator. It has to be reiterated that the generation of a uniform submesh has to be done only once during the preprocessing stage whereas the non-uniform generator, in general, has to be called at least every time step if not actually every iteration step.

-
- (i) Input data: number of submesh elements in all coordinate directions and their polynomial order, coordinates of nodes of (large-scale) element on physical and computational domain
 - (ii) **Determine velocity vector at element center**
 - (iii) **Determine unit vectors in r- and s- (and t-)direction**
 - (iv) **Determine projection of velocity vector onto unit vectors**
 - (v) **Calculate distance of middle node from the outflow boundary according to (8.6)**
 - (vi) Determine the number of nodes and the length(s) of the submesh elements in all coordinate directions
 - (vii) Initialize the counter for the number of equations and the number of nodes to zero, respectively
 - (viii) Loop over nodes in first coordinate direction
 - (ix) Loop over nodes in second coordinate direction
(*There has to be a third loop in the 3-D case*)
Increase counter for number of nodes by one
 - (x) Calculate coordinates of node on parent (computational) domain
 - (xi) Calculate (large-scale) shape function values for node in order to determine coordinates on global (physical) domain using the global (physical) coordinates of nodes of (large-scale) element
 - (xii) Determine value of node for submesh ID-array (zero for boundary node)
(*only necessary during the submesh creation for the first (large-scale) element*)
Increase counter for number of equations by one for no-boundary node
 - (xiii) Loop over all submesh elements
 - (xiv) Determine entries of IEN-array for submesh element
(*only necessary during the submesh creation for the first (large-scale) element*)
-

Algorithm 8.1 Uniform and non-uniform submesh generator (**bold font: only non-uniform**)

8.1.3 Computational algorithm for the two-level finite element method

The description of the practical implementation of the two-level finite element method is concluded by providing the reader with an algorithmic outline of the major steps for the calculation. This rough schedule is given by algorithm 8.2.

-
- (i) Read (or compute) initial large-scale velocity field \mathbf{u}^0 and, if necessary, large-scale pressure field p^0 (small-scale values starting with zero for time-dependent residual-free bubbles)
Initialize time counter $n = 0$
 - (ii) Generate uniform submesh
 - (iii) Time loop ($t^{n+1} = t^n + \delta t$)
Initialize iteration counter $i = 0$
 - (iv) Calculate and assemble right hand sides due to body forces, Neumann boundary conditions and values from previous time step ($\rightarrow \bar{\mathbf{F}}, \bar{\mathbf{N}}$ and $\bar{\mathbf{M}}\bar{\mathbf{u}}^n$ in (7.61)) as well as Dirichlet boundary conditions ($\rightarrow \bar{\mathbf{E}}^M$ in (7.61) and $\bar{\mathbf{E}}^C$ in (7.62))
 - (v) Iteration loop ($i \leftarrow i + 1$)
 - (vi) Loop over all large-scale elements
 - (vii) If necessary: non-uniform submesh generator
 - (viii) Loop over all small-scale elements of submesh
 - (ix) Calculate and assemble LHS for small-scale equations (\rightarrow (7.103) or (7.104), in variational form according to (8.1))
 - (x) Calculate and assemble $n_e^{RFB} = n_{ed}(n_{sd} + 1) + n_{sd}$ RHS for small-scale equations (\rightarrow (7.49)-(7.51) or (7.54)-(7.56), respectively)
 - (xi) Solve small-scale equations \rightarrow result: $n_e^{RFB} = n_{ed}(n_{sd} + 1) + n_{sd}$ approximate bubble functions for current large-scale element
 - (xii) Loop over all small-scale elements of submesh
 - (xiii) Calculate and assemble bubble function LHS ($\rightarrow \mathbf{K}_{NS}^{qu}(\mathbf{u}_i)$ in (7.58), $\mathbf{K}_{NS}^p(\mathbf{u}_i)$ in (7.59), \mathbf{G}^{Tqu} in (7.60) and \mathbf{G}^{Tp} in (7.57))
 - (xiv) Calculate and assemble velocity-dependent part of large-scale LHS, if there is no large-scale approximation for the iterative convective velocity \mathbf{u}_i ($\rightarrow \mathbf{K}_{NS}(\mathbf{u}_i)$ in (7.58))
 - (xv) Calculate and assemble bubble function RHS ($\rightarrow \mathbf{K}_{NS}^f(\mathbf{u}_i)$ in (7.61) and \mathbf{G}^{Tf} in (7.62))
 - (xvi) Calculate and assemble velocity-dependent part of large-scale LHS in case of large-scale approximation for the iterative convective velocity $\bar{\mathbf{u}}_i$ ($\rightarrow \mathbf{K}_{NS}(\bar{\mathbf{u}}_i)$ in (7.58))

- (xvii) Calculate and assemble velocity-independent part of large-scale LHS ($\rightarrow \mathbf{G}$ in (7.59) and \mathbf{G}^T in (7.60); add stabilizing term representing small-scale continuity equation ('bulk viscosity' term) to (7.58))
- (xviii) Solve the resulting global system (\rightarrow (7.57))
- (xix) Check convergence: if not converged, go to (v)
- (xx) Check time: if end of simulation not reached, go to (iii)

Algorithm 8.2 Two-level finite element method for Navier-Stokes equations

8.2 Introducing a third level

The objects of investigation in this section are still the normalized residual-free bubble equations (7.103) and (7.104). The primary focus, however, is on the quasi-static case (7.104) which reads in variational form analog to (8.1)

$$\left(w^{SM}, \mathbf{u}_i \cdot \nabla \mathbb{B}_1^{SM} \right)_{\Omega_e} + \left(\nabla w^{SM}, (\nu + \nu'_e) \nabla \mathbb{B}_1^{SM} \right)_{\Omega_e} = \left(w^{SM}, 1 \right)_{\Omega_e} \quad (8.7)$$

The corresponding variational equation for (7.103) is (8.1) with the subgrid viscosity ν'_e added in the same way as in (8.7). At this point, an important statement has to be made. Heretofore, please imagine equation (8.7) without the subgrid viscosity ν'_e . If one were able to solve this basic equation, at least up to the necessary resolution limit for a complete incorporation of all existing scales in the sense of a DNS, a fully satisfying solution for the small scales up to the assumptions, in particular the crucial one that the scales crossing the element boundaries are not taken into account, would be achieved. As attractive this thought may be as unlikely is it, in general, due to limited computer power. However, obtaining at least a good approximation of \mathbb{B}_1 would be the second best choice and, more important, the one which can be afforded in general. To be sure, the quality of the approximation as a whole depends on the quality of the approximation of ν'_e in the original equation.

8.2.1 'Static' modeling of unresolved scales

A 'static' way of modeling the subgrid viscosity is provided, for instance, by the three model formulations (7.99)-(7.101). All of them are handicapped by the obvious drawback of relying on an a priori unknown constant. Here, the only alternative of static modeling without any constant consists in the application of the calculation based on the element Reynolds number in (7.84)-(7.85) to the artificial viscosity approach. This procedure will be used for one example in section 9. For this, the matrix on the left hand side of (8.3) defined in (8.4) has to be enhanced by adding the subgrid viscosity ν'_e to the viscous term.

Secondly, the alternative representation of the effect of the unresolved scales in the small-scale equation by using **stabilizing terms** in lieu of the subgrid viscosity may be revived. Thus, an alternative version of a three-level method with a 'static' third level is encountered. For instance, a stabilizing term in the USFEM-version may be added to the quasi-static analog of the matrix equation (8.3) such that

$$(\mathbf{K}^{SM} + \mathbf{K}^{SM, stab}) \mathbf{b}^{SM} = \mathbf{F}^{SM} + \mathbf{F}^{SM, stab} \quad (8.8)$$

where

$$\mathbf{K}_{ab}^{e, SM, stab} = \int_{\Omega_e^{SM}} (\mathbf{u}_i \cdot \nabla N_a^{SM} + \nu \Delta N_a^{SM}) \tau_e' (\mathbf{u}_i \cdot \nabla N_b^{SM} - \nu \Delta N_b^{SM}) d\Omega \quad (8.9)$$

and

$$\mathbf{F}_a^{e, SM, stab} = \int_{\Omega_e^{SM}} (\mathbf{u}_i \cdot \nabla N_a^{SM} + \nu \Delta N_a^{SM}) \tau_e'(1) d\Omega \quad (8.10)$$

The stabilization parameter due to Franca and Valentin (6.67)-(6.70) is used with the respective reaction coefficient. The characteristic length of the submesh h' replaces \bar{h} .

8.2.2 Dynamic modeling of unresolved scales

Basic concept

Brezzi et al. (2000) suggest a dynamic tune-up for ν_e' from which a reasonably good value should arise. They assume Guermond's approach (7.99) to be the basis of the dynamic algorithm. In contrast to Brezzi et al. (2000), it will be shown that there is no need for any model assumption, since one is able to calculate the subgrid viscosity directly (in an approximate manner at least). For this purpose, a sub-submesh (SSM) has to be chosen being slightly finer than the original submesh (SM) on which the variational equation (8.7) has to be solved as well. Comparing these two solutions, the desired 'good' value for ν_e' will be achieved. However, for this dynamic tune-up to be workable in that an explicit value can be obtained in the end, a criterion has to be established. Motivated by insights from the theory of stabilized methods, Brezzi and co-workers require the average integral of \mathfrak{B}_1 on the large-scale element domain Ω_e (see (6.65)) to be equal to the corresponding value of the adequately resolved bubble for $\nu_e' = 0$ in (8.7) such that

$$\frac{1}{|\Omega_e|} \int_{\Omega_e} \mathfrak{B}_1(\nu_e' = 0) d\Omega_e \approx \frac{1}{|\Omega_e|} \int_{\Omega_e} \mathfrak{B}_1^{SM}(\nu_e') d\Omega_e \approx \frac{1}{|\Omega_e|} \int_{\Omega_e} \mathfrak{B}_1^{SSM}(\nu_e') d\Omega_e \quad (8.11)$$

where the solution on the sub-submesh is indicated by the superscript *SSM*. Criterion (8.11) governs an iterative algorithm amounting to be some kind of extrapolation with the target of this extrapolation (hopefully) being the goal: a 'good' approximation of the analytical residual-free bubble \mathfrak{B}_1 for $\nu_e' = 0$. Variations of the criterion (8.11) potentially better suited for turbulent flow applications are certainly conceivable and it is intended to pursue them in future.

Using the expansion of \mathfrak{B}_1^{SM} in (8.2), the applicability will be extended as compared to Brezzi et al. (2000) where they have merely used an approximation with one degree of freedom on the submesh. This approximation works quite well for convection-diffusion equations, as Brezzi and co-workers were able to prove. However, transferring this strategy to the Navier-Stokes equations does not work any more, at least for quadrilateral elements which are favored herein. This failure is related to the equations for the 'pressure bubble functions' (7.50) or (7.55), respec-

tively. Observing the right hand side of (7.50) and (7.55), one may see that it changes in every coordinate direction. Using one degree of freedom, for instance, in the center of the element permits no distinction between the derivatives in the coordinate directions, i.e. the directional information is lost. The two-dimensional situation for one of the shape functions of a bilinear quadrilateral element is displayed in Fig. 8.3.

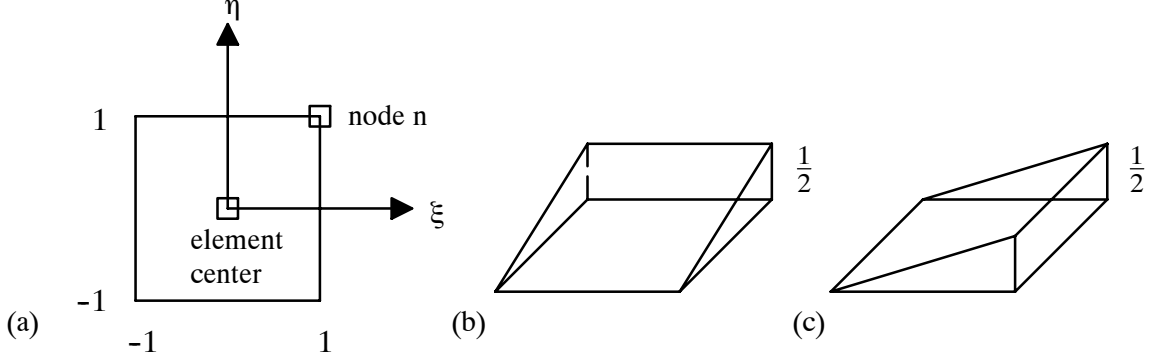


Fig. 8.3: Shape function derivatives for node n : (a) parent domain; (b) ξ -der.; (c) η -der.

However, in order to provide a simpler insight into the following equations, they are formulated for one degree of freedom and extended to more than one afterwards. Thus, inserting (8.2) with one degree of freedom (see Fig. 8.4) in (7.104) yields

$$b_1^{SM} \left[\left(N_1^{SM}, \mathbf{u}_i \cdot \nabla N_1^{SM} \right)_{\Omega_e} + \left(\nabla N_1^{SM}, (\nu + \nu_e') \nabla N_1^{SM} \right)_{\Omega_e} \right] = \left(N_1^{SM}, 1 \right)_{\Omega_e} \quad (8.12)$$

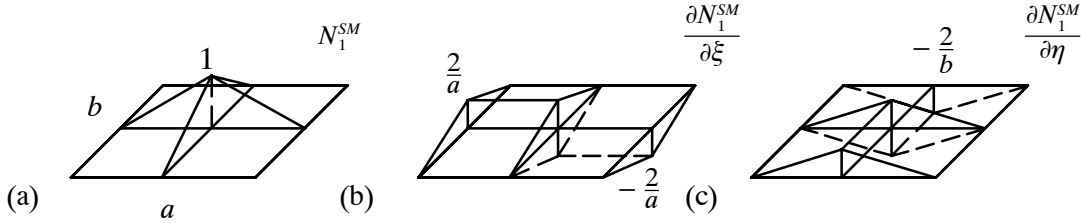


Fig. 8.4: 2×2 submesh: (a) shape function; (b) ξ -derivative; (c) η -derivative

Sufficiently small variations of the velocity field within the large-scale element are assumed. Realizing that the convective term has little effect in (8.12) due to its skew-symmetric character in this case and the zero Dirichlet boundary conditions on the large-scale element boundaries, (8.12) can be simplified to

$$b_1^{SM} \left(\nabla N_1^{SM}, (\nu + \nu_e') \nabla N_1^{SM} \right)_{\Omega_e} = \left(N_1^{SM}, 1 \right)_{\Omega_e} \quad (8.13)$$

A few words concerning the preceding assumption are necessary. This supposition is probably reasonable, if, for instance, the convective iterative velocity \mathbf{u}_i is replaced by the large-scale part $\bar{\mathbf{u}}_i$ as in (7.54)-(7.56). This path will be followed in the numerical examples of laminar flow situations in this study. The fact that this is about to change drastically as soon as turbulent flow regimes are entered has to be emphasized. In this regime, the replacement can be performed no longer and, even more important, the variations of the velocity also within one large-scale element domain become crucial. It is stuck to this procedure here keeping in mind, however, that

it will likely be required to deviate from it for applications in turbulence. The average integral of \mathfrak{B}_1^{SM} may be obtained from (8.13) as

$$\frac{1}{|\Omega_e|} \int_{\Omega_e} \mathfrak{B}_1^{SM} d\Omega_e = \frac{1}{|\Omega_e|} \frac{\left[\int_{\Omega_e} N_1^{SM} d\Omega_e \right]^2}{(\nu + \nu'_e) \int_{\Omega_e} |\nabla N_1^{SM}|^2 d\Omega_e} \quad (8.14)$$

Inserting the solution of the calculation on the sub-submesh according to the approximation (8.11) on the left hand side of (8.14) yields, after some analysis, an equation for the subgrid viscosity reading

$$\nu'_e = \frac{\left[\int_{\Omega_e} N_1^{SM} d\Omega_e \right]^2}{\int_{\Omega_e} |\nabla N_1^{SM}|^2 d\Omega_e \int_{\Omega_e} \mathfrak{B}_1^{SSM} d\Omega_e} - \nu = \frac{f(n_{el, sd}^{SM}, \Omega_e)}{\int_{\Omega_e} \mathfrak{B}_1^{SSM} d\Omega_e} - \nu \quad (8.15)$$

Aside from the physical viscosity, two ingredients for the calculation of the subgrid viscosity remain in the end. The integral of the bubble function \mathfrak{B}_1^{SSM} is obtained by first solving (8.7) for the bubble function on the sub-submesh and then integrating this function over the element domain. Regarding the subgrid viscosity used for the solution, this will be done in iterative manner below. The function $f(n_{el, sd}^{SM}, \Omega_e)$ only depends on the number of submesh elements in every spatial dimension and the geometry of the large-scale element domain. The discussion is confined to uniform submeshes with equal numbers of elements in every spatial dimension for this dynamic algorithm. Fig. 8.4 depicts the shape function and the shape function derivatives for the one-degree-of-freedom approximation.

Starting point of the elementwise iteration is an initial guess for the subgrid viscosity $\nu'_{e,0}$. The core equation of the iteration amounts to be

$$\nu'_{e,i+1} = \frac{f(n_{el, sd}^{SM}, \Omega_e)}{\int_{\Omega_e} \mathfrak{B}_1^{SSM}(\nu'_{e,i}) d\Omega_e} - \nu \quad (8.16)$$

The iteration will be completed, if the convergence criterion

$$|\nu'_{e,i+1} - \nu'_{e,i}| \leq TOL = \frac{\nu}{10} \quad (8.17)$$

is satisfied. The tolerance TOL has been chosen in accordance with Brezzi et al. (2000) to enforce a calculation of ν'_e within an accuracy of one order of magnitude less than the physical viscosity ν . In case of very low physical viscosity (a usual condition for turbulent flows), one might be forced to raise the tolerance level slightly in order to confine the computational effort.

Extension to the Navier-Stokes equations

Paving the ground for approximations of more than one degree of freedom, the following new definition of $f(n_{el, sd}^{SM}, \Omega_e)$ in (8.15) and (8.16) is considered:

$$f(n_{el, sd}^{SM}, \Omega_e) = \sum_{B=1}^{n_{dofs}^{SM}} \left\{ \frac{\left[\int_{\Omega_e} N_B^{SM} d\Omega_e \right]^2}{\int_{\Omega_e} |\nabla N_B^{SM}|^2 d\Omega_e} \right\} \quad (8.18)$$

The underlying assumption of (8.18) is that the off-diagonal entries in the matrix resulting from (8.7) are neglected justified by the predominance of the diagonal entries with respect to the off-diagonal entries. This enables the decoupled calculation of the b_B^{SSM} and, thus, the derivation of the same formula (8.15) with the modified $f(n_{el, sd}^{SM}, \Omega_e)$ in (8.18). Fig. 8.5 displays the situation for 3x3 submesh elements showing the sum of the shape functions and the sum of the shape function derivatives. A general formula for $f(n_{el, sd}^{SM}, \Omega_e)$ can be derived in the case of rectangular elements reading

$$f(n_{el, sd}^{SM}, \Omega_e) = \frac{\left[\left(\frac{n_{el, sd}^{SM} - 1}{n_{el, sd}^{SM}} \right)^2 ab \right]^2}{\frac{4}{3} (n_{el, sd}^{SM} - 1)^2 \left(\frac{a^2 + b^2}{ab} \right)} = \frac{3}{4} \frac{(n_{el, sd}^{SM} - 1)^2}{(n_{el, sd}^{SM})^4} \left(\frac{a^3 b^3}{a^2 + b^2} \right) \quad (8.19)$$

with a and b denoting the side lengths of the rectangle simplifying to

$$f(n_{el, sd}^{SM}, \Omega_e) = \frac{3}{8} \frac{(n_{el, sd}^{SM} - 1)^2}{(n_{el, sd}^{SM})^4} |\Omega_e|^2 \quad (8.20)$$

in the square case. The reader may wish to verify formulas (8.19) and (8.20), for instance, for the 3x3 submesh in Fig. 8.5. Since ν'_e is proportional to $f(n_{el, sd}^{SM}, \Omega_e)$, it may be proven that equation (8.15) for the calculation of the subgrid viscosity shows the right behaviour: if $|\Omega_e| \rightarrow 0$, then $\nu'_e \rightarrow 0$, and if $n_{el, sd}^{SM} \rightarrow \infty$, then likewise $\nu'_e \rightarrow 0$. This is exactly the behaviour such an equation is supposed to show.

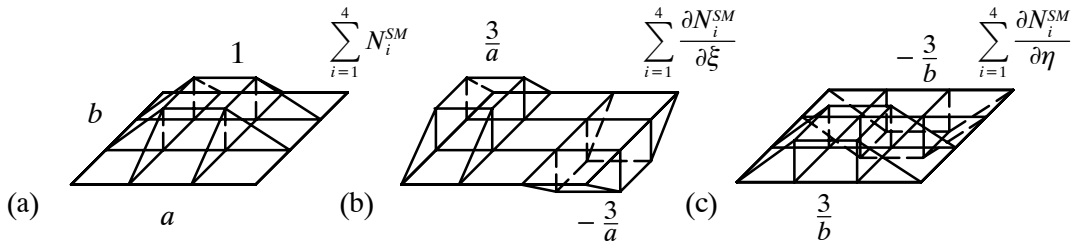


Fig. 8.5: 3x3 submesh: (a) sum of shape functions; (b) sum of ξ -der.; (c) sum of η -der.

It is obvious that assumption (8.18) is a crude one, but after all it is one that works without being forced to bring in immense additional effort for the computation for the third level. Furthermore, please keep in mind that this dynamic algorithm is expected to replace a model based on an a priori fixed constant. For adjudicating what is 'crude' and what is 'fine' in turbulence modeling, one has to bear in mind this starting position. Aside from this, more sophisticated extensions to the multi-degree-of-freedom case are yet to be considered. One idea in this context may refer to the technique of mass lumping, see e.g. Hughes (2000), section 7.3.2. This procedure of diagonalizing matrices by various approaches has been used for mass matrices in solid and structural mechanics as well as heat conduction successfully. Here, the viscous matrix (and the convective as well as the reactive matrix in case they are taken into account additionally) would have to be attacked by this technique. To the author's knowledge, this has not been done for these types of matrices as yet. Moreover, useful adaptations of this dynamic algorithm for higher-order elements have to be considered.

This section is concluded by having a look at the computational algorithm for the dynamic modeling herein after referred to as algorithm 8.3. Algorithm 8.3 may be incorporated into Algorithm 8.2 for the two-level finite element method between step (vi) and (vii) in order to get the final three-level finite element method. Moreover, step (ii) in algorithm 8.2 has to be extended by generating an additional sub-submesh wherefore the same submesh generator (see algorithm 8.1) with a larger number of submesh elements may be used.

-
- (i) Initial guess for the subgrid viscosity $\nu'_{e,0}$ as well as calculation of tolerance TOL (\rightarrow (8.17)) and function f (\rightarrow (8.18))
Initialize iteration counter $i = 0$
 - (ii) Iteration loop ($i \leftarrow i + 1$)
 - (iii) Loop over all elements of sub-submesh
 - (iv) Calculate and assemble LHS for small-scale equation (\rightarrow (8.7))
 - (v) Calculate and assemble normalized RHS for small-scale equation (\rightarrow (8.7))
 - (vi) Solve small-scale equation \rightarrow result: approximate normalized bubble function for current large-scale element based on sub-submesh \mathfrak{B}_1^{SSM}
 - (vii) Calculate integral of \mathfrak{B}_1^{SSM} on current large-scale element domain
 - (viii) Determine updated value of subgrid viscosity $\nu'_{e,i+1}$ (\rightarrow (8.16))
 - (ix) Check convergence (\rightarrow (8.17)): if not converged, go to (ii)
 - (x) Apply converged value of subgrid viscosity to solution process for small-scale equation
-

Algorithm 8.3 Dynamic modeling of subgrid viscosity

A final remark has to be made concerning the equation for the determination of the subgrid viscosity (8.16). It is easy to observe that it allows for negative values of the subgrid viscosity. The permission for negative values might be interpreted as a form of modeling the backward energy

cascade mechanism in turbulent flows described in section 5.2.3. This is a positive feature also attributed to the dynamic model of Germano et al. (1991). The sum of the physical and the sub-grid viscosity is strictly positive in (8.16) however. This is in line with experience from numerical tests of the dynamic model mentioned in section 5.2.3, which have shown that negative values of the overall viscosity are potentially destructive for the stability of the simulation. After all, the artificial condition (5.40) with ν'_e replacing ν^T is already inherent in the just presented dynamic modeling process.

Comparison to the dynamic modeling procedure of Germano et al. (1991) and remarks on space selection

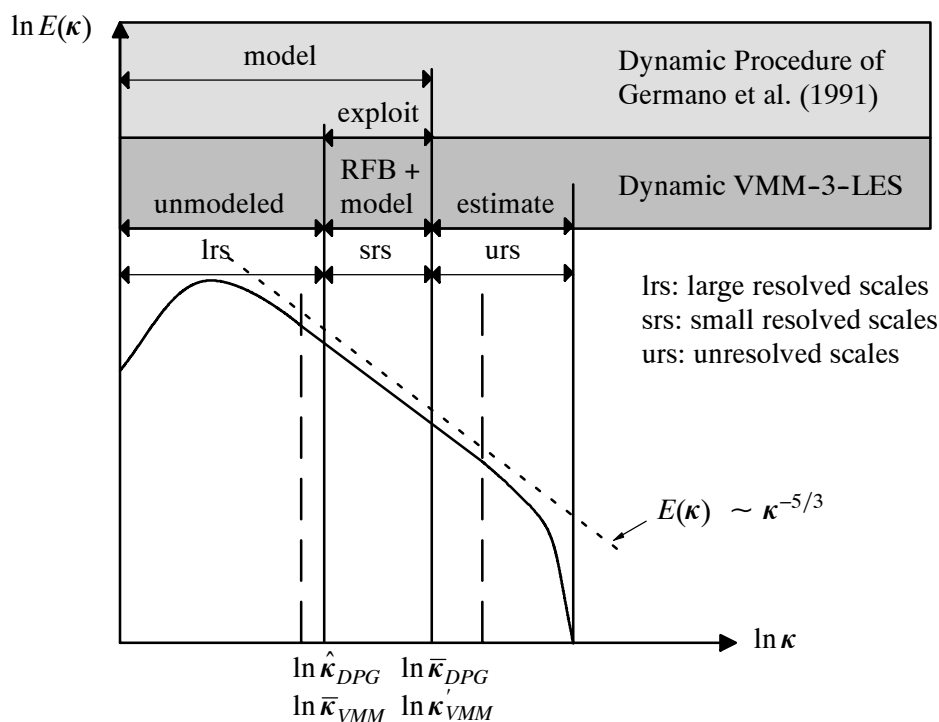


Fig. 8.6: Comparing dynamic procedure of Germano et al. (1991) to proposed procedure

In Fig. 8.6, a principal comparison is drawn between the dynamic modeling procedure of Germano et al. (1991) (DPG) described in section 5.2.3 and the 'VMM-3-LES' with the dynamic modeling procedure just described. Besides the fact that the subgrid-scale model acts on the complete range of scales in 'classical' LES (which is certainly not a specific feature of the dynamic modeling procedure), the crucial difference to be pointed out in Fig. 8.6 refers to the range of scales exploited to fix the undetermined constant in the respective model. In the dynamic modeling procedure, the small resolved scales are exploited and the constant is calculated based on the Germano identity. In the 'VMM-3-LES' with the respective dynamic modeling procedure of this work, the unresolved scales are, admittedly in a crude manner yet, estimated and the resulting model is then applied to the small resolved scales. Furthermore, the approximation of the small resolved scales with the help of the localized residual-free bubble strategy has to be emphasized again.

As pointed out in section 5.2.3, the underlying idea (and certainly the reason for the success) of the dynamic modeling procedure of Germano et al. (1991) has to be found in the hypothesis of

the similarity between the unresolved scales and the small resolved scales. It is, however, assuredly unquestionable that no scales are more similar to the unresolved scales than the unresolved scales themselves. Thus, a dynamic modeling procedure estimating the unresolved scales seems to be promising in the author's point of view, although the actual estimation still occurs in a crude approach.

A final remark in this context surely has to be devoted to the important question of how large the size of the space containing the large as well as the small resolved scales has to be chosen absolutely and in comparison with each other. The combined extension of both spaces is certainly restricted by the amount of computational effort which can be afforded overall. This essential restriction for the size of both spaces in combination still leaves room for deciding on the relative extension of the spaces though. A first basic requirement for the choice of the 'cutoff level' of the large-scale space surely demands it to cover, at least, the range of energy-containing modes, i.e., alternatively expressed, its location is presupposed to be within the inertial subrange. This basic requirement has already been taken into account in the various embodiments of the Kolmogorov energy spectrum in this work starting with Fig. 4.3. Beyond this rather trivial aspect, Sagaut (2002), for instance, mentions that numerical tests for the dynamic modeling procedure of Germano et al. (1991) have revealed an optimal value for the 'cutoff level' associated with the test filter to be about twice as large as the one associated with the basic filter. This may also be accepted as a first hint for an adequate choice of the respective relation of large- and small-scale within the variational multiscale method. It is also referred to the related discussion in Hughes et al. (2000a).

It is without doubt that the just addressed choices strongly affect the impact of a potential subgrid-scale model. On the one hand, the combined size of large- and small-scale space influences the overall impact. For an extensive (large plus small) resolution, there are few unresolved scales left to be modeled. The overall impact of the subgrid-scale model will become crucial however, if the (large plus small) resolution is rather poor. This perception is certainly valid for all ways of performing LES in principle. On the other hand, the relative size of large- and small-scale space influences the specific impact with respect to the variational multiscale method. A dominant large-scale space in comparison with the small-scale space leaves the majority of the scales completely unmodeled. This results in a pure DNS eventually for the extreme case that all scales (with no unresolved scales left) are actually contained in the large-scale space. In opposition to this, a diminutive large-scale space tends towards the classical approach of LES again, since the subgrid-scale model is associated with a substantial margin of the resolved scales. Here, the extreme case with all scales (still leaving unresolved scales however) contained in the small-scale space indeed has to be viewed as being the classical LES procedure again. For further discussion of this, it is referred to Collis (2001).

Concluding this discussion, it may simply be reiterated that the absolute as well as relative choice of the respective spaces influences the overall procedure considerably. In fact, its actual selection is an important parameter of the method. Aside from this, it is undoubtful that the scope of discretion for the particular method based on residual-free bubbles is explicitly limited. The restriction of the small-scale solutions to individual element domains of the basic discretization basically seems to demand a dominant large-scale space in return. Nevertheless, the numerical examples of turbulent flow situations to be described in chapter 10 are executed with rather coarse large-scale spaces, in order to gain some impression concerning the performance of this particular method under these less comfortable circumstances. After all, this is also the only aspect the author's

availability of computational resources allows to pursue. The investigation of dominant large-scale spaces inescapably associated with extremely fine basic discretizations poses a challenge being far beyond the author's prospects at this stage.

8.3 Future topics

8.3.1 Advanced boundary conditions for the residual-free bubble equations

May we believe in paradise?

In the first two sections of this chapter, efforts have been focussed on getting an approximate solution for the residual-free bubble equation (7.103) or (7.104), respectively, as close to the analytical solution as possible. With the help of the dynamic subgrid viscosity approach, there may be hope that one will in fact succeed in achieving this goal. In order to pursue this computationally attractive strategy of localization for the small-scale solution and static condensation subsequently, a potentially high prize had to be paid however. Artificial zero Dirichlet boundary conditions for the small-scale part of the solution on Γ_e have to be accepted being undoubtedly incorrect in general. It is intended to go beyond this 'zero-strategy' now.

At first, let us think of the 'ideal' residual-free bubble equation in every element for just a moment, i.e. the one with the correct Dirichlet and/or Neumann boundary conditions on Γ_e . This would in fact be a situation of paramount attraction - 'paradise' for the three-level approach from the point of view of the second level. The correct boundary conditions will not be accessible, however, and even a slight deviation from them will potentially leave us behind with an ill-posed problem, let alone that the right problem is not solved any more. Due to its great attraction, this 'ideal' solution is worth being kept in mind for the future yet.

A further idea in this context concerns the use of non-conforming bubbles. Farhat et al. (2001) (see also Farhat et al. (2003)) have done this by introducing interelement Lagrange multipliers and developing herewith a discontinuous enrichment method. Their enrichment contains free-space solutions of the underlying homogeneous differential equation that are not represented by the basic polynomial approximation. For the main goal, the Navier-Stokes equations the search for such free-space solutions is certainly kind of ambitious and mostly impossible. The Lagrange multipliers represent the means for approximating the flow over the element boundaries Γ_e and, thus, what has to be considered as the correct Neumann boundary conditions for the enrichment. Consequently, some approximate boundary conditions are obtained, but it has to be paid for them in that additional degrees of freedom related to the Lagrange multipliers appear in the final equation system. The elementwise solution process of the residual-free bubble equation is replaced by an actual elementwise static condensation process. Comparing this approach to the residual-free bubble approach, it may be stated that better boundary conditions (which in fact never appear as boundary conditions in the method) have to be expected. Furthermore, the user gets rid of the elementwise solutions. For this purpose, it has to be paid with an elementwise static condensation (with potentially expensive matrix inversions), a larger final equation system and the necessity to provide a framework for dealing computationally with the Lagrange multipliers.

The idea to be pointed out briefly in the following section is somewhat different to the ones addressed before. Here, the element edges in the 2-D case (and, likewise, the element faces and

edges in the 3-D case) will be occupied by additional functions. Brezzi (2002) already suggested the addition of, at least some (in fact not too many), edge functions with special shape. This should be done in an iterative manner using information from previous solution steps. The main drawback is that, similar to the discontinuous enrichment method, all these additional functions will appear in the final equation system, since they do not go away during the static condensation process. In this context, it is further referred to Brezzi and Marini (2002) providing the reader with a very general framework related to augmented spaces and two-level methods.

Due to the aforementioned drawback of a larger equation system, the attention is now turned to a different approach ensuring the final equation system to remain of the same size. Such an idea was already pursued by Hughes et al. (1998). They add residual-free edge functions in 2-D as a furthergoing means to resolve the remaining residual on the elements. It is straightforward to think of a 3-D counterpart including also residual-free face functions. The problem of all these edge functions being globally coupled is overcome by concentrating on one respective edge which is linked to two elements. This is certainly a severe approximation, but they hope to get some improvement with respect to the exclusive use of residual-free bubbles. However, this approach seems to be uninviting for the ultimate goal, the numerical simulation of turbulent flows usually linked with very small physical viscosities. As you may observe by inspecting (6.13) and (7.16), the jump terms on the element boundaries which have been omitted in the wake of the residual-free bubble approximation are both diffusive or viscous terms, respectively. For the Navier-Stokes equations, this is only the case for continuous pressure interpolations as a matter of course. This means that by approaching very small diffusion or viscosity, respectively, the influence of these terms vanishes more and more. Therefore, it makes no sense to put extra effort in taking into account these edge functions unless a diffusion-dominated problem has to be solved. For exactly this kind of problem, namely the Stokes problem, the benefit of these edge-functions (here on a macro-element) was demonstrated by Franca and Russo (1996). The idea of using such macro-elements for improving the solution quality was picked up by Sangalli (2003) for elliptic problems with rapidly varying coefficients recently.

Finally, it is concentrated on the approach which was recently proposed by Franca et al. (2002, 2003). They call the resulting functions multiscale functions which are based on additional residual-free functions on the element edges (or element faces and edges in 3-D) determined in a different procedure in comparison to the one just mentioned. The main drawback lies in the necessity to solve for these additional functions separately as will be seen below. The stimulation for the formulation of the edge functions in the 2-D case goes back to Hou and co-workers who have applied this to elliptic problems e.g. in Hou and Wu (1997) as well as Hou et al. (1999). The concept is outlined in the following. The basic idea of Franca et al. (2002, 2003) will be extended to convection-diffusion-reaction equations as well as to the 3-D case in a straightforward manner. This procedure has been implemented and the respective algorithms will be given below. However, it has not been tested for numerical examples yet. Hence, nothing can be said about its actual performance. According to this, the description of this procedure has been subsumed under the label 'future topics'. Some early results of Franca et al. (2002, 2003) have shown a superior performance of this procedure with respect to stabilized methods and approaches based on residual-free bubbles with zero Dirichlet boundary conditions for reaction-dominated diffusion-reaction problems. However, there remain serious doubts in the author's point of view that this superior performance can be transferred in an equivalent form to convection-dominated convection-diffusion-reaction problems.

Lower-dimensional residual-free functions

The goal is still the solution of the 'normalized' small-scale bubble equation (7.103) or (7.104), respectively. Now, the concept of Franca and co-workers extending the basic residual-free bubble procedure by residual-free edge functions is followed. Referring to the residual-free bubble approach for convection-diffusion-reaction equations, it is stuck to the separation of the weighting function space in (6.48), but a different separation for the solution function space is defined as

$$\mathcal{P}_\phi \approx \bar{\mathcal{P}}_\phi \oplus \mathcal{P}'_{MF} = \bar{\mathcal{P}}_\phi \oplus_{\Omega_e} E(\Omega_e); \quad e = 1, \dots, n_{el} \quad (8.21)$$

where $E(\Omega_e)$ is the new infinite-dimensional multiscale function space in the element Ω_e . Due to the fact that the definition of the weighting function space has been kept alive, the elementwise projected equation (6.49)-(6.50) and, likewise, the elementwise strong form (6.51) are still valid. Thus, it is allowed to walk along the same path already followed before with the multiscale functions now taking the place formerly held by the bubble functions.

The idea is illustrated for the 2-D case adding some comments to the more involved 3-D case. The small-scale equation (6.51) with zero Dirichlet boundary condition (6.50) now reads

$$\mathcal{L}_{cdr}\phi'_e = - (\mathcal{L}_{cdr}\bar{\phi} - f) \quad \text{in } \Omega_e \quad (8.22)$$

$$\mathcal{L}_{cdr}^{1-D}\phi'_e = \mathfrak{R}[- (\mathcal{L}_{cdr}\bar{\phi} - f)] \quad \text{on } \Gamma_e \quad (8.23)$$

$$\phi'_e = 0 \quad \text{on } \partial\Gamma_e \quad (8.24)$$

where ϕ'_e denotes the new enriched small-scale function, $\partial\Gamma_e$ in fact the nodes of the element domain Ω_e , \mathfrak{R} the trace operator acting on the right hand side here and

$$\mathcal{L}_{cdr}^{1-D}\phi = \mathcal{L}_c^{1-D}\phi + \mathcal{L}_d^{1-D}\phi + \mathcal{L}_r^{1-D}\phi = a_r\partial_r\phi - \kappa\partial_{rr}\phi + \sigma_{(mod)}\phi \quad (8.25)$$

represents for the convection-diffusion-reaction equation the lower-(here one-)dimensional differential operator. r indicates the direction aligned with the respective edge of the element at this juncture and, thus, a_r the projection of the convective velocity vector \mathbf{a} onto this direction. At this point, the strategy becomes clear. Starting with condition (8.24) assuming that the small-scale value at the element nodes is zero representing the necessary boundary conditions, (8.23) is solved on every edge of Ω_e . Please note that this amounts to be the solution of an ordinary differential equation on each edge. The solution of (8.23) provides us with the sought-after boundary conditions for the elementwise problem (8.22). With the aid of the zero conditions on the nodes of the element being the harborage of the only (large-scale) nodal function values, it is still allowed to apply the static condensation procedure.

In the 3-D case, this approach is substantially extended. Starting with zero Dirichlet boundary conditions at each node of the element, 1-D ordinary differential equations have to be solved on every edge of the element. This gives rise to boundary conditions for 2-D partial differential equations restricted to the respective faces of the element which have to be solved afterwards. Not until then, the actual 3-D elementwise problem (8.22) may be tackled. Perhaps, this short outline of the 3-D case already gives an impression of the effort being necessary for doing this in practice. Moreover, the extension to higher-order Lagrange elements seems to be difficult, let alone the extension to higher-order hierarchical elements (values no longer nodal-based!), which seems to be an undissolved mystery to the author for the time being.

Nevertheless, this promising approach will be specified for 2-D applications of the Navier-Stokes equations. For this purpose, the enhanced versions of (7.103) and (7.104) omitting the zero-condition at the nodes read

$$\mathbf{u}_i \cdot \nabla \mathfrak{B}_1 - (\nu + \nu'_e) \Delta \mathfrak{B}_1 + \left(\frac{1}{\delta t} + \beta(\nabla \cdot \mathbf{u}_i) \right) \mathfrak{B}_1 = 1 \quad \text{in } \Omega_e \quad (8.26)$$

$$u_{i,r} \partial_r \mathfrak{B}_1 - (\nu + \nu'_e) \partial_{rr} \mathfrak{B}_1 + \frac{1}{\delta t} \mathfrak{B}_1 = 1 \quad \text{on } \Gamma_e \quad (8.27)$$

and

$$\mathbf{u}_i \cdot \nabla \mathfrak{B}_1 - (\nu + \nu'_e) \Delta \mathfrak{B}_1 = 1 \quad \text{in } \Omega_e \quad (8.28)$$

$$u_{i,r} \partial_r \mathfrak{B}_1 - (\nu + \nu'_e) \partial_{rr} \mathfrak{B}_1 = 1 \quad \text{on } \Gamma_e \quad (8.29)$$

where the normalized right hand side has to be replaced by the trace operators applied to the right hand sides of (7.49)-(7.51) or (7.54)-(7.56) for the actual solution of the 1-D equations (8.27) or (8.29), respectively. Of course, there is no term in the 1-D equation (8.27) being adequate to the term in (8.26) containing the divergence of the velocity vector \mathbf{u} .

Computational algorithms

The reader is now provided with the algorithms for this approach as well. Within the preprocessing stage, algorithm 8.1 for the (uniform) submesh generation in 2-D shall be replaced by algorithm 8.4, if residual-free edge functions are included in the calculation. The main algorithm 8.5 for the computation of the residual-free edge functions may be integrated into the overall solution algorithm 8.2 for the Navier-Stokes equations between step (vii) and step (viii). If the dynamic algorithm for the evaluation of the subgrid viscosity is used additionally, algorithm 8.4 will have to be placed into algorithm 8.3 between step (ii) and step (iii). Please note that in the subsequent calculations of the bubble functions Dirichlet boundary values representing the resulting approximate residual-free edge functions have to be considered in the assembly of the right hand sides.

-
- (i) Input data: number of submesh elements in all coordinate directions and their polynomial order, coordinates of nodes of (large-scale) element on physical and computational domain
 - (ii) Determine the number of nodes and the length of the submesh elements in all coordinate directions
 - (iii) Loop over edges of large-scale element
 - (iv) Determine values of nodes for submesh edge ID-array (zero for boundary node) *(only necessary during the submesh creation for the first (large-scale) element)*
 - (v) Initialize the counter for the number of equations and the number of nodes to zero, respectively, as well as the counter for the number of supported equations to the overall number of equations
 - (vi) Loop over nodes in first coordinate direction

- (vii) Loop over nodes in second coordinate direction
Increase counter for number of nodes by one
- (viii) Calculate coordinates of node on parent (computational) domain
- (ix) Calculate (large-scale) shape function values for node in order to determine coordinates on global (physical) domain using the global (physical) coordinates of nodes of (large-scale) element
- (x) Determine value of node for submesh ID-array: zero for node of large-scale element; otherwise, distinguish supported and non-supported node
(only necessary during the submesh creation for the first (large-scale) element)
Increase counter for number of equations by one for non-supp. node
Increase counter for number of supported equations by one for supp. node
- (xi) Determine edge-element-correlation array identifying for every edge-related node number the respective submesh node number
(only necessary during the submesh creation for the first (large-scale) element)
- (xii) Loop over all edge-submesh elements
 - (xiii) Determine entries of IEN-array for edge-submesh element
(only necessary during the submesh creation for the first (large-scale) element)
- (xiv) Loop over all submesh elements
 - (xv) Determine entries of IEN-array for submesh element
(only necessary during the submesh creation for the first (large-scale) element)

Algorithm 8.4 Uniform submesh generator including edge-submeshes

- (xvi) Loop over all edges of large-scale element
 - (xvii) Loop over all elements of edge-submesh
 - (xviii) Calculate and assemble LHS for s.-s. edge equation (\rightarrow (8.27) or (8.29))
 - (xix) Calculate and assemble $n_e^{RFB} = n_{ed}(n_{sd} + 1)$ RHS for s.-s. edge equation (\rightarrow trace operator acting on RHS of (7.49)-(7.51) or (7.54)- (7.56), resp.)
 - (xx) Solve small-scale edge equation and evaluate for the $n_e^{RFB} = n_{ed}(n_{sd} + 1) + n_{sd}$ RHS
 \rightarrow result: approximate residual-free edge functions for current edge of large-s. element
 - (xxi) Copy solution in array for boundary values for following computation of bubble function in current large-scale element

Algorithm 8.5 Computation of residual-free edge functions

8.3.2 Alternative strategies

In this last section of chapter 8, two alternative strategies will be presented. Besides the favoured local strategy of this work based on the use of residual-free bubbles and the also introduced global concept based on the use of hierarchical bases (sections 6.2.1 and 7.2.1), two alternative approaches are proposed here, which may in future serve as a way to implement the variational multiscale method practically into a finite element method. On the one hand, another type of hierarchical bases is exemplified and, on the other hand, the (at this time highly adored) concept of discontinuous Galerkin methods (DGM) is brought into play. As will be seen below, both methods, however, suffer from the same drawback having forced the author to refrain from a practical implementation up to now.

Hierarchical finite element method based on the partition of unity method (PUM)

The hierarchical bases to be presented briefly in the following predicate on the idea of the partition of unity method (PUM) presented in Melenk and Babuska (1996) as well as Babuska and Melenk (1997). Taylor et al. (1998) developed a finite element method based on this general framework. The key point is the structure of the finite element function which Taylor et al. (1998) propose to look like

$$\phi^h = \sum_{B=1}^{n_{dofs}} N_B^k [\phi_B + \mathbf{P}_B^k \mathbf{b}_B] = \sum_{B=1}^{n_{dofs}} N_B^k \phi_B + N_B^k \mathbf{P}_B^k \mathbf{b}_B \quad (8.30)$$

compared to the usual finite element functions (3.32), for instance, for the scalar quantity ϕ subject to a convection-diffusion-reaction equation. The superscript k denotes the polynomial order of the basic element interpolation. The first term on the right hand side of (8.30) constitutes the large-scale approximation being completely similar to (6.19) within the basic hierarchical concept. The second term on the right hand side of (8.30) represents the small-scale approximation, which is an additional polynomial term of one order higher associated with the (large-scale) degrees of freedom (usually nodes in this concept exclusively) being the only number of degrees of freedom eventually. The reader may ascertain a striking affinity with the residual-free bubbles concept in this respect. The chosen polynomial orders may vary from one degree of freedom to the other in this approach. Two forms of the additional polynomials in the 1-D case reading in row vector representation as

$$\mathbf{P}_B^k(x) = \left[(x - x_B)^{k+1} \quad (x - x_B)^{k+2} \quad \dots \right] \quad (8.31)$$

and

$$\mathbf{P}_B^k(x) = \left[(x^{k+1} - x_B^{k+1}) \quad (x^{k+2} - x_B^{k+2}) \quad \dots \right] \quad (8.32)$$

respectively, were proposed by Taylor et al. (1998). The quadratic polynomial addition in the 2-D case, for example, according to form (8.31) looks like

$$\mathbf{P}_B^k(\mathbf{x}) = \left[(x_1 - x_{1B})^2 \quad (x_1 - x_{1B})(x_2 - x_{2B}) \quad (x_2 - x_{2B})^2 \right] \quad (8.33)$$

According to this, the column vector of the respective parameters reads

$$\mathbf{b}_B = \begin{bmatrix} b_B^{x_1 x_1} \\ b_B^{x_1 x_2} \\ b_B^{x_2 x_2} \end{bmatrix} \quad (8.34)$$

The drawback of this approach and, likewise, the reason for not applying it yet lies in the notably increased number of functions for higher-order approximations with respect to the basic hierarchical concept. Analyzing the number of functions for linear to quartic interpolated triangles and quadrilaterals in 2-D, i.e. based on the highest polynomial order appearing, the results for the basic hierarchical concept (HBFEM) and the just presented concept (PUFEM) reported in Table 8.1 are obtained. The enormous increase related to the PUFEM-concept for higher polynomial orders may easily be observed. In the context of the Navier-Stokes equations, this problem becomes considerably worse, since it has to be dealt with 'scalar' velocity variables in every coordinate direction, i.e. up to 3, and the additional scalar pressure variable. Hence, the trouble will be quadrupled. After all, this drawback has to be judged as a vital handicap for the time being, since the limitation of the already huge number of degrees of freedom for the problems of this work forms a crucial objective. Nevertheless, this concept should be kept in mind in the author's point of view.

	HBFEM-tri.	PUFEM-tri.	HBFEM-quad.	PUFEM-quad.
linear	3	3	4	4
quadratic	6	12	8	16
cubic	10	21	12	28
quartic	15	30	17	40

Table 8.1 Number of degrees of freedom related to hierarchical concepts for 2-D elements

Discontinuous (in space) Galerkin methods (DGM)

It is definitely impossible to present the complete concept of discontinuous Galerkin methods in a short section. Consequently, it is refrained from trying out to do this here and, thus, it is focused on the basic idea, some references providing the details as well as the two major advantages and the crucial drawback of these methods for the underlying problems. The basic idea of these methods consists in a somewhat more 'autonomous' treatment of each element of the discretization. More precisely spoken, a polynomial approximation within each element is enforced, but these approximations are allowed to be discontinuous between adjoining elements. The resulting gap between values on either side of an element boundary is tried to be 'closed' by enforcing continuity weakly in the discontinuous Galerkin formulation.

Concerning the details of discontinuous Galerkin methods, it is referred to the respective literature. In particular, the compilation of Cockburn et al. (2000) containing, among others, a description concerning the history and state of the art of these methods is surely worth mentioning. Besides this, it is referred to e.g. Baumann and Oden (1999a, 1999b) for work related to convection-diffusion problems as well as the Euler and Navier-Stokes equations and Engel et al. (2002) for an exhaustive comparison of continuous and discontinuous Galerkin methods combined with stabilized methods. Concerning the last reference, the reader should not be distracted by the title of the publication related mainly to problems being actually far besides the problems of this

work. The comparing part of this paper relates to convection–diffusion problems as well. First steps towards an application of discontinuous Galerkin methods for the numerical simulation of turbulence within the framework of the variational multiscale method have recently been presented in Collis (2002) as well as Collis et al. (2003).

Two major advantages may be ascribed to the discontinuous Galerkin method in the context of fluid mechanics. On the one hand, potential velocity oscillations described in section 3.4.1 may be precluded by avoiding to prescribe Dirichlet boundary conditions at the outflow boundary. Nevertheless, instabilities can be exhibited for certain problems requiring, for instance, the introduction of stabilizing techniques in order to overcome these shortcomings, confer e.g. Engel et al. (2002). On the other hand, the discontinuous Galerkin method provides a formulation being conservative within each element. This aspect of local conservation is emphasized in Hughes et al. (2000a) to be an attribute for methods used for LES. However, the continuous Galerkin method may also be qualified in a straightforward manner to be an elementwise conserving scheme. This can be done by adding a postprocessing procedure proposed in Hughes et al. (2000b) or Hughes (2000), p. 107, respectively. In section 7.2.3, it has already been indicated that the treatment of the small scales in the primary method of this work guarantees elementwise conservation due to chosen approach based on residual-free bubbles. Within a thought experiment, one may slightly alter the presented three-level method by just using a discontinuous Galerkin method on the first level in lieu of the continuous Galerkin method without any further changes on the second and third level. This small change would guarantee the method to be completely conserving in an elementwise form. As already indicated, the same goal may also be achieved in an even simpler approach by adding the aforementioned postprocessing procedure to the presented continuous method.

The serious drawback is the same as before in the context of the hierarchical bases related to the partition of unity method. The number of degrees of freedom is substantially increased, since every element ‘meeting’ at a certain node of the discretization brings in its particular degree of freedom due to the concept. An analysis similar to what has been done in Table 8.1 was performed in Engel et al. (2002) for 1-D, 2-D and 3-D elements. The crucial difference with respect to the PUFEM-concept is that here the ratio relating the number of degrees of freedom for the discontinuous Galerkin method to the one for the continuous Galerkin method reading e.g. for 2-D quadrilaterals

$$\frac{n_{dofs}(DGM)}{n_{dofs}(CGM)} = \left(\frac{k+1}{k}\right)^2 \quad (8.35)$$

aims at unit value for increasing polynomial order k . For the practical polynomial orders indicated in Table 8.1, however, (8.35) results in a ratio of 4, 2.25, 1.78 and 1.56 for linear, quadratic, cubic and quartic interpolations, respectively. For the mostly used linear and quadratic interpolations, these ratios are even worse than the ones for the PUFEM-concept (1 and 2, respectively), confer Table 8.1. For linear interpolations, the discontinuous Galerkin may simply be categorized as being ‘horrible’ from the point of view of required effort to the author’s mind.

9 Numerical examples of laminar flow situations

This chapter presents numerical simulations of laminar flow situations using the two- and three-level finite element methods as well as the stabilized method of USFEM-type described above. Additionally, some hints will be given for the interpretation of the results of one of these examples with regard to turbulent flow simulations. The only restriction to be dealt with in the following examples consists in focussing on the preferred choice of quadrilateral elements. Apart from this, the influence of a variety of parameters on the results will be tested. For the submesh of the two-level method, a uniform 4x4-element discretization in 2-D and a uniform 4x4x4-element discretization in 3-D is usually chosen, respectively. For the three-level method, the aforementioned submesh discretization is usually employed on the sub-submesh level and a 3x3-(or 3x3x3-)element discretization is used for the submesh level. Five flow situations have been selected covering a variety of demands on the numerical methods. Some remarks concerning the computational tools used for these sample calculations are provided in appendix C.

First of all, the 2-D stationary problem of an impinging fluid flow is demonstrated, for which a closed-form analytical solution is known. The second example is the famous lid-driven cavity. In this 2-D flow situation, a stationary solution is searched for achieved by using a stationary solver for lower Reynolds numbers and an instationary solver for higher Reynolds numbers. The description of this lid-driven cavity flow will be augmented by adding some remarks with regard to turbulent regimes. The geometric situation of the cavity is also the origin of the third example where an oscillating lid is introduced distinguishing it from the former classical version of the lid-driven cavity. This example should serve as a challenging instationary flow problem. A classical instationary example is represented by the 2-D flow past a circular cylinder constituting the fourth numerical test here. It is concluded with a 3-D example, the so-called Beltrami flow. This example combines three attractive features which cannot be met elsewhere in this unification according to Ethier and Steinman (1994). It describes a fully three-dimensional instationary flow situation, all terms in the Navier-Stokes equations play a crucial role, i.e. no degeneration in the sense that one or more terms are identically zero, and a closed-form analytical solution exists.

9.1 Impinging fluid flow (2-D)

This problem consists of a jet impinging upon a wall with a controlled body force on a domain $\Omega = [0, 1] \times [0, 1]$ and can be found e.g. in Hendriana and Bathe (2000). The situation is depicted in Fig. 9.1(a). A slip boundary condition is assumed on the surface of the left wall.

The body force functions are

$$f_1 = 5x_1x_2^8 + 10x_1x_2^3 + 60\nu x_1x_2^2 \quad (9.1)$$

$$f_2 = 0 \quad (9.2)$$

where the kinematic viscosity ν is assumed to be equal to the dynamic viscosity μ , i.e. the fluid density is $\rho = 1$. The analytical solution of the problem then reads

$$u_1 = -5x_1x_2^4 \quad (9.3)$$

$$u_2 = -\frac{1}{2} + x_2^5 \quad (9.4)$$

$$p = \frac{1}{2}x_2^5 - \frac{1}{2}x_2^{10} + 5\nu x_2^4 \quad (9.5)$$

Two quite different flow regimes are considered, a diffusion-dominated flow with $\nu = 10$ and a convection-dominated flow with $\nu = 0.001$. The Reynolds number based on the chosen viscosity, the length of the domain and the maximum velocity is $\text{Re} = 0.5025$ and $\text{Re} = 5025$, respectively. Uniform discretizations with 4×4 , 8×8 and 16×16 elements are used. The results in terms of the velocity vectors and the pressure distribution for the diffusion-dominated as well as the convection-dominated flow obtained by using the finest mesh with 16×16 hierarchical quadratic elements are displayed in Fig. 9.1(b) and Fig. 9.2, respectively.

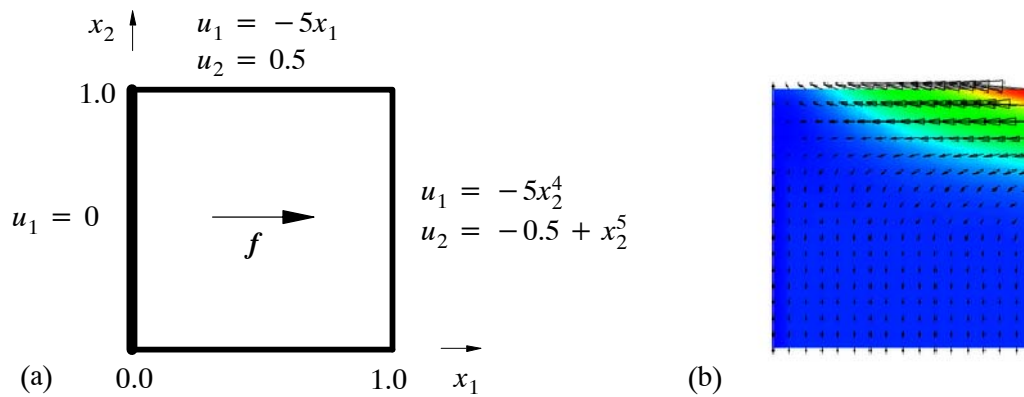


Fig. 9.1: *Impinging fluid flow: (a) geometry, boundary conditions and body force; (b) velocity vectors on colored velocity distribution obtained by using 16×16 hierarchical quadratic elements*

The purpose of this numerical example is manifold. First of all, it is intended to test the performance of higher-order elements, namely quadratic and cubic elements. Deviating from the preponderant use of higher-order elements based on Lagrange shape functions, higher-order elements based on hierarchical shape functions are preferred in this example as described in the preceding chapters. Aside from the type of elements used, this numerical example seems to be 'well-suited' for testing higher-order elements, since the use of linear elements leads to bad results for the pressure in a diffusion-dominated flow regime, confer Fig. 9.3. In Fig. 9.3(a) (corresponding to Fig. 9.2(a)), the situation is depicted for the stabilized method with linear elements. Of course, using the two- and three-level method bears exactly the same phenomenon. This wrong behaviour of the pressure results from the inability of linear elements to represent the viscous part of the stabilizing term in the sense of PSPG. In the end, the effect may be blamed to be a virtual natural boundary condition for the pressure enforced in a weak sense. For elaboration of this topic, please consult e.g. Wall (1999). Besides this particular problem for flow situations with high viscosities, the pressure solution using linear elements in case of low viscosities (see Fig. 9.3(b)) is obviously also a good deal worse than the one in Fig. 9.2(c) obtained with hierarchical quadratic elements.

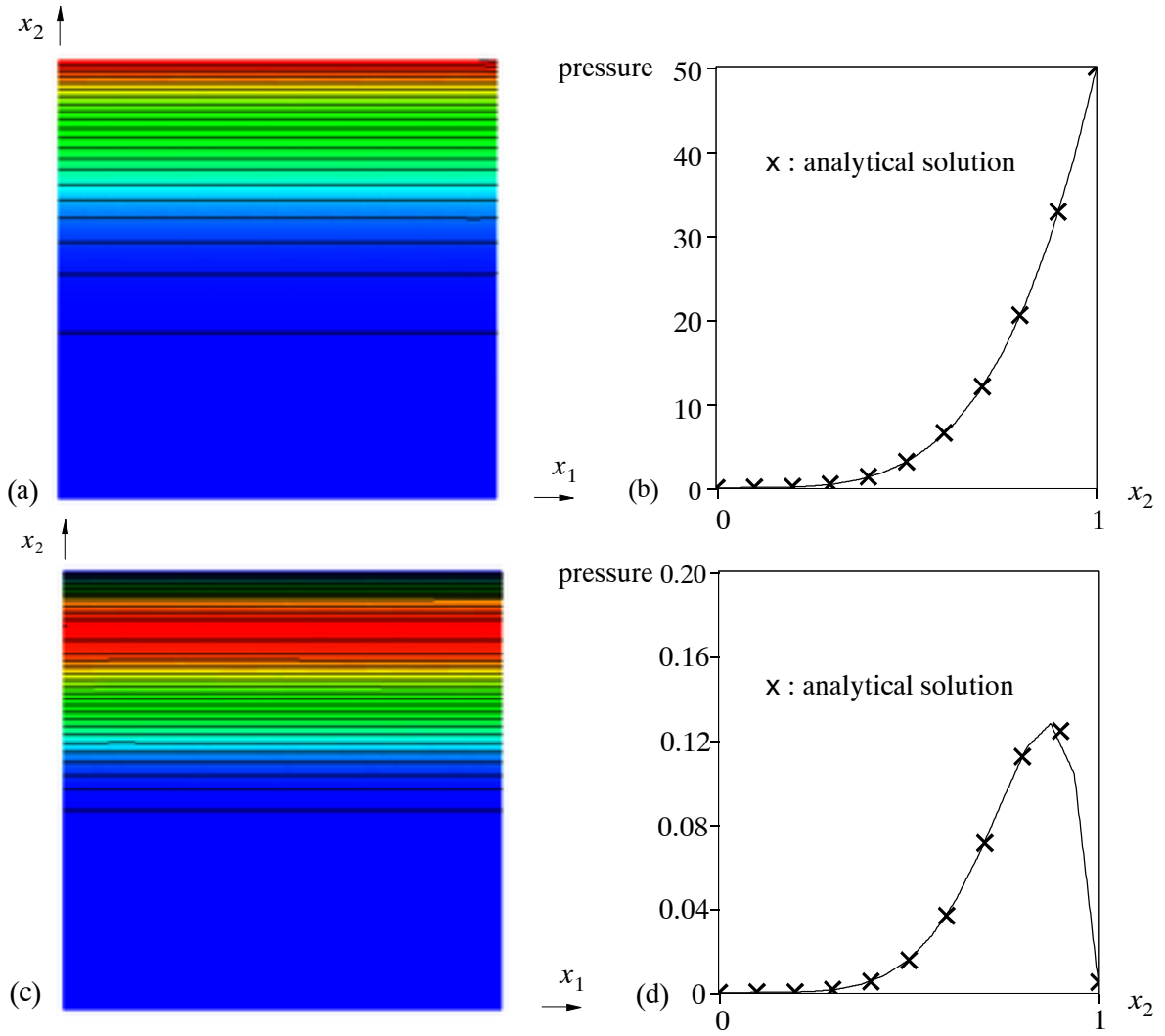


Fig. 9.2: Pressure solution obtained by using 16x16 hierarchical quadratic elements: (a) pressure isolines on colored pressure distribution for diffusion-dominated flow; (b) pressure distribution along x_2 -axis for diffusion-dominated flow; (c) pressure isolines on colored pressure distribution for convection-dominated flow; (d) pressure distribution along x_2 -axis for convection-dominated flow

Despite the spoiled pressure results, the solutions obtained with the help of linear elements are included in the convergence diagrams (see Figs. 9.4-9.6). The main focus is on quadratic and cubic elements, however. The error of the velocity solution is measured using the L_2 -norm subject to

$$e_0^u = \frac{\| \mathbf{u} - \mathbf{u}^h \|_0}{\| \mathbf{u} \|_0} = \left[\frac{\int_{\Omega} (\mathbf{u} - \mathbf{u}^h)^2 d\Omega}{\int_{\Omega} \mathbf{u}^2 d\Omega} \right]^{\frac{1}{2}} \quad (9.6)$$

the error of the velocity solution using the H^1 -norm subject to

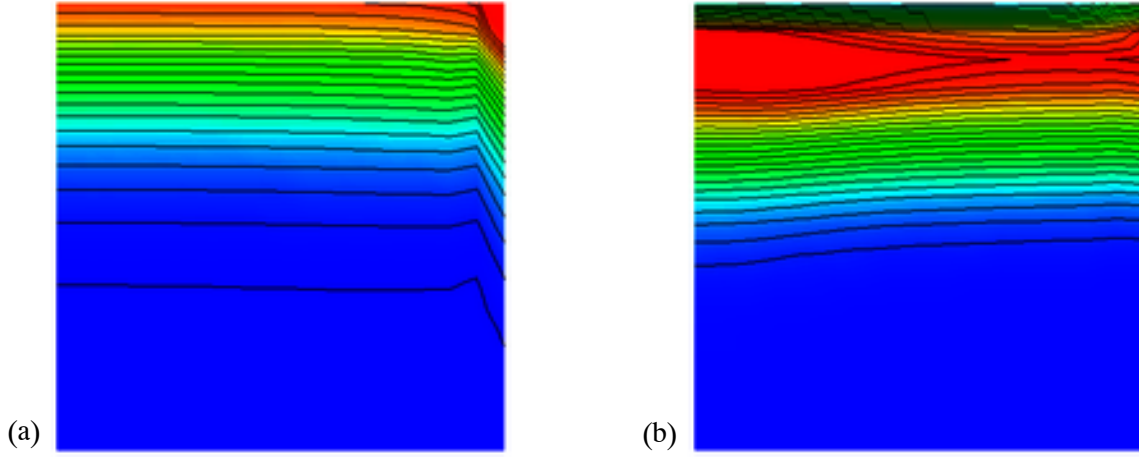


Fig. 9.3: Pressure isolines and colored pressure distribution on 16x16 mesh with linear elements: (a) diffusion- dominated flow; (b) convection-dominated flow

$$e_1^u = \frac{\| \mathbf{u} - \mathbf{u}^h \|_1}{\| \mathbf{u} \|_1} = \left[\frac{\int_{\Omega} (\mathbf{u} - \mathbf{u}^h)^2 + (\nabla \mathbf{u} - \nabla \mathbf{u}^h)^2 d\Omega}{\int_{\Omega} \mathbf{u}^2 + (\nabla \mathbf{u})^2 d\Omega} \right]^{\frac{1}{2}} \quad (9.7)$$

and the error of the pressure solution in the L_2 -norm subject to

$$e_0^p = \frac{\| p - p^h \|_0}{\| p \|_0} = \left[\frac{\int_{\Omega} (p - p^h)^2 d\Omega}{\int_{\Omega} p^2 d\Omega} \right]^{\frac{1}{2}} \quad (9.8)$$

For the stabilized methods, $\mathbf{u}^h = \bar{\mathbf{u}}$ and $p^h = \bar{p}$, since there are no explicit small-scale parts of the velocity and the pressure. For the two- and three-level methods, the small-scale part of the velocity is incorporated into the error calculation for the velocity by using $\mathbf{u}^h = \bar{\mathbf{u}} + \mathbf{u}'^h$ where the small-scale part depends on the characteristic length h' of the chosen submesh discretization. For this example, a 'static' version of the three-level method according to section 8.2.1 is applied by adding an artificial viscosity to the second level. Since it is not possible to use the dynamic algorithm of section 8.2.2 for higher-order elements as yet, the 'static' way of modeling the unresolved scales is currently the only opportunity for treating all element types (linear and higher-order) alike in the context of a three-level method.

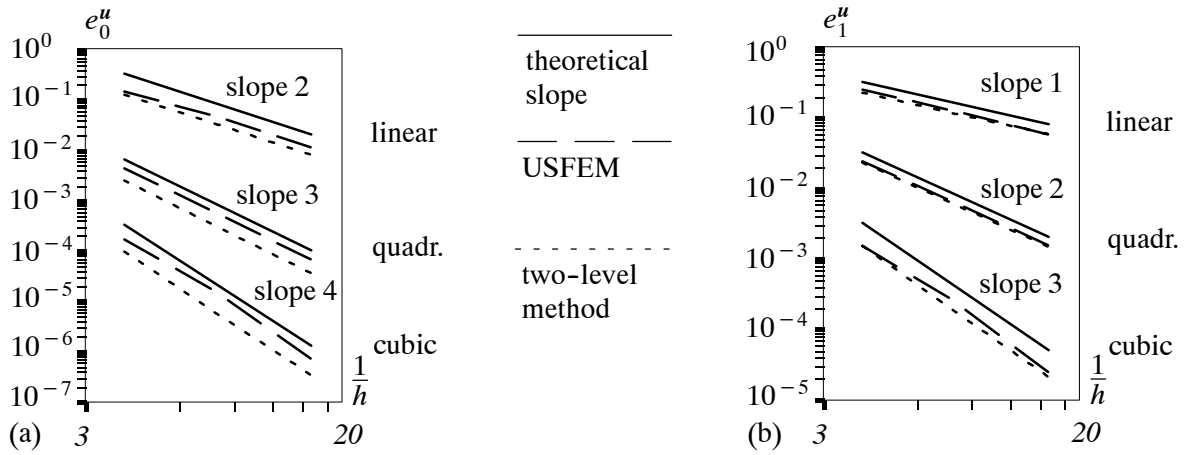


Fig. 9.4: Velocity error for diffusion-dominated flow: (a) L^2 -norm; (b) H^1 -norm

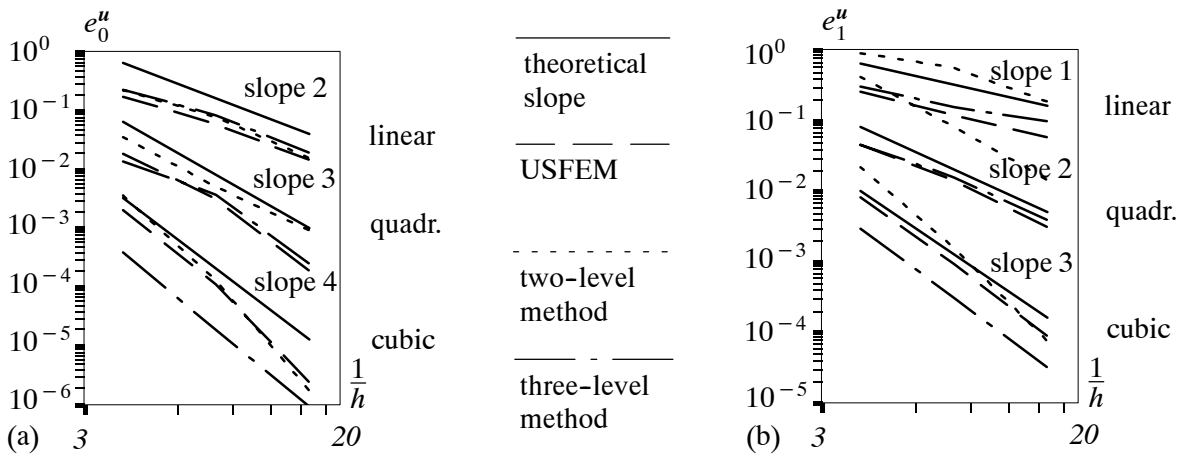


Fig. 9.5: Velocity error for convection-dominated flow: (a) L^2 -norm; (b) H^1 -norm

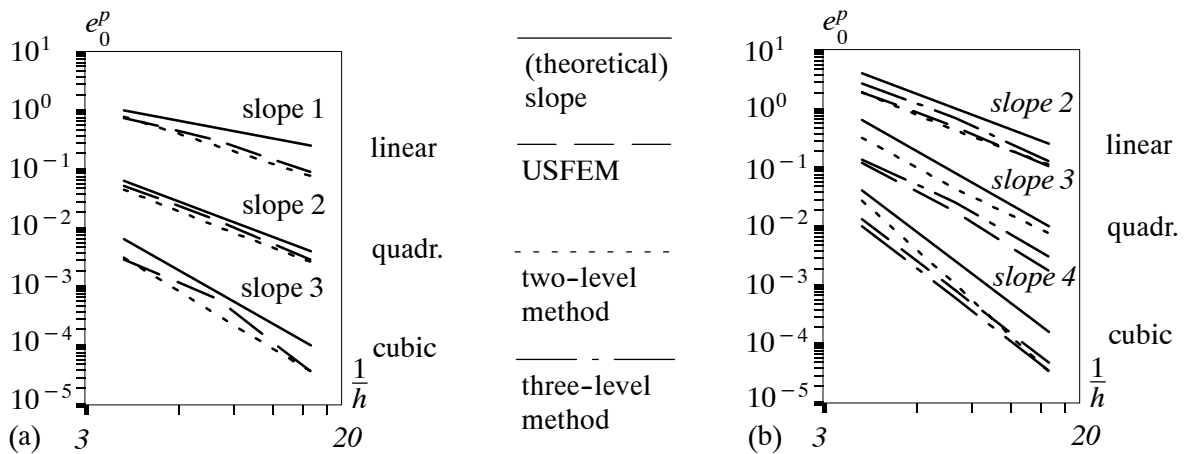


Fig. 9.6: Pressure error in L^2 -norm: (a) diffusion-dom. flow; (b) convection-dom. flow

Fig. 9.4 and Fig. 9.5 display the velocity error in the L_2 -norm and in the H^1 -norm. For the diffusion-dominated flow (Fig. 9.4), the convergence rates which have to be expected from theoretical error analysis are accurately matched by both the two-level method and the stabilized method. The two-level method exhibits a slightly smaller error in this context. The use of the

three-level method is certainly useless for a diffusion-dominated flow, since no gain can be expected with regard to the two-level method here. This changes drastically within the convection-dominated flow, see Fig. 9.5. The actual error can be reduced significantly by using the three-level method. Particularly, the two-level method is no longer able to guarantee an acceptable error in the H^1 -norm. This deficiency is amplified for higher-order elements. This point is picked up again after discussing the pressure error. Apart from this, the stabilized method of USFEM-type works fine most of the time for both regimes as anticipated, and the three-level method shows superior performance especially for the hierarchical cubic element.

The convergence rate of the pressure error for the diffusion-dominated case matches the theoretically expected value of suboptimal rate analyzed by Hughes et al. (1986) for the Stokes equation (the rate for the linear elements being even higher, however), see Fig. 9.6(a). In Fig. 9.6(b), it may be observed that in the convection-dominated regime the error converges at about one order higher, i.e. actually at an optimal rate. Furthermore, it may be gathered from both diagrams in Fig. 9.6 that there is virtually no difference between the pressure results using any of the methods.

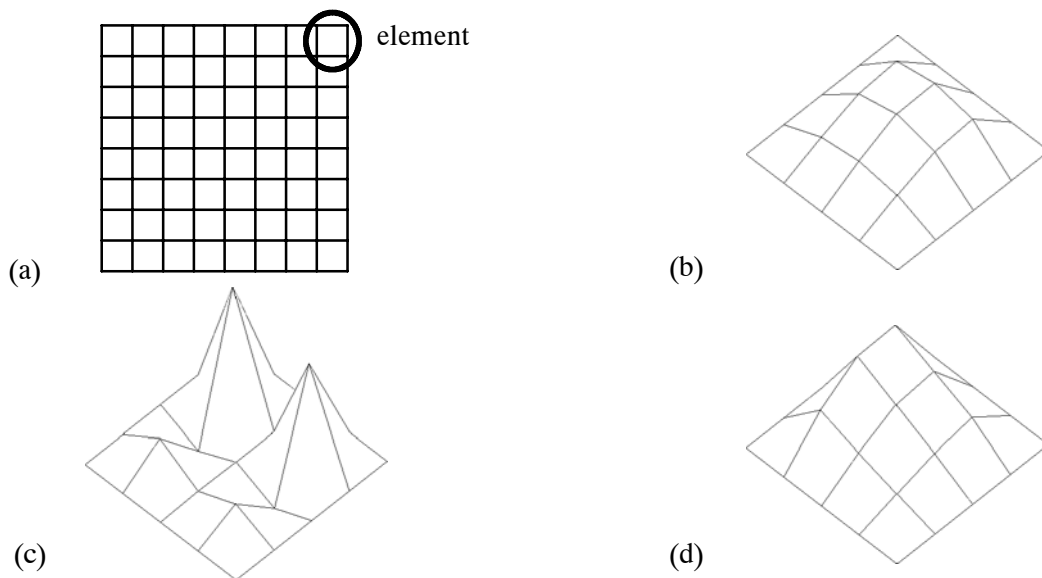


Fig. 9.7: Exemplary velocity bubble function for element in the upper right corner of 8x8 linear elements: (a) element identification; (b) two-level method for diffusion-dominated flow (factor 1000); (c) two-level method for convection-dominated flow (factor 1); (d) three-level method with artificial subgrid viscosity for convection-dominated flow (factor 10)

The reason for the failure of the two-level method in solving the velocity for convection-dominated flows (see Fig. 9.5(b)) is clearly due to the fact that the chosen 4x4 submesh is not able to resolve all the small scales beyond the basic discretization level. This can be observed in Fig. 9.7 showing an exemplary approximated residual-free (velocity) bubble for the diffusion-dominated case as well as for the convection-dominated case with and without the introduction of a third level. Please note the respective amplification factors within the illustration, in order to categorize accurately the respective bubble functions. It is obvious that the bubble function resulting from the application of the two-level method in the convection-dominated case is not stable

(see Fig. 9.7(c)). This problem is overcome by the introduction of the third level in form of an artificial viscosity on the second level (see Fig. 9.7(d)).

Finally, the influence exerted by changes of various parameters for the two- and three-level method has been investigated. To be sure, this represents nothing more than a spot check. It may, however, give some hints or confirm some speculations. The results for the diffusion-dominated regime are summarized in Table 9.1 as well as the results for the convection-dominated regime in Table 9.2. Expectedly, the inclusion of the small-scale continuity equation is as irrelevant for the solution of a diffusion-dominated flow as the use of a Shishkin-type non-uniform submesh. Some improvement may be reached by using a more refined submesh either by increasing the number of elements or enhancing the polynomial order of the existing elements. For a convection-dominated flow, there is in fact a significant impact which has to be credited to the small-scale continuity equation. As already anticipated during the course of section 8.1.2, neither the use of a Shishkin-type submesh nor the refinement of the submesh is helpful in improving the solution quality due to the very thin boundary layers which have to be resolved within the elements. Some gain in solution quality is merely achieved by the use of the three-level finite element method with an artificial subgrid viscosity.

standard case with 4x4 subm.	1.0475 e-02	2.8195 e-04	5.7233 e-03
change of parameters	L_2 -error pressure	L_2 -error velocity	H^1 -error velocity
without s.-s. continuity equat.	1.0475 e-02	2.8195 e-04	5.7233 e-03
4x4 Shishkin-type submesh	1.0475 e-02	2.8195 e-04	5.7233 e-03
8x8 submesh	5.9532 e-03	2.2538 e-04	4.4482 e-03
4x4 quadratic submesh	4.9094 e-03	2.0863 e-04	4.1095 e-03

Table 9.1 Error investigation for parameter changes for two-level method with 8x8 hierarchical quadratic elements and 4x4 submesh - diffusion-dominated flow

two-level with 4x4 submesh	4.2724 e-02	4.9094 e-03	8.0184 e-02
change of parameters	L_2 -error pressure	L_2 -error velocity	H^1 -error velocity
without s.-s. continuity equat.	7.8976 e-02	9.4986 e-03	9.7626 e-02
4x4 Shishkin-type submesh	4.2037 e-02	6.3121 e-03	7.6307 e-02
8x8 submesh	3.6441 e-02	4.2804 e-03	7.4143 e-02
8x8 Shishkin-type submesh	4.3320 e-02	4.9786 e-03	7.8460 e-02
4x4 quadratic submesh	3.3957 e-02	3.9835 e-03	9.1148 e-02
4x4 + artif. viscosity (three-l.)	2.5325 e-02	3.6829 e-03	1.5475 e-02
4x4 + USFEM (three-level)	4.1586 e-02	4.6269 e-03	3.6964 e-02

Table 9.2 Error investigation for parameter changes for two-level method with 8x8 hierarchical quadratic elements and 4x4 submesh - convection-dominated flow

9.2 Lid-driven cavity flow (2-D)

9.2.1 Description and results for flow example

This standard benchmark problem is considered on a domain $\Omega = [0, 1] \times [0, 1]$ where a horizontal velocity of unit value was prescribed along the lid at $x_2 = 1$. The situation is depicted in Fig. 9.8(a). The pressure is prescribed to be zero at the midpoint of the cavity bottom in order to fix the constant the pressure is determined up to through the formulation. The more challenging non-leaky boundary conditions are assumed, i.e. the left and the right wall were closed up to the lid. The prescribed velocity distribution is confined by the so-called 'ramp condition' permitting the velocity to go down from unit value at the next to last corner node to zero at the last corner node. As a result of the prescribed flow at the top of the cavity, a recirculation region is set up bearing a primary vortex in the middle of the cavity. Depending on the Reynolds number (and this is actually the interesting and important phenomenon), a number of further secondary vortices in the corners of the cavity may be observed. The highest number of vortices to be achieved in case of a Reynolds number up to 10000 is six with one additional vortex in the lower right corner being hardly observable. See Fig. 9.8(b) for a sketch of these vortices. Due to the character of the cavity problem, it is a well-suited test for the introduction of artificial numerical viscosity and the accurate prediction of vortex development.

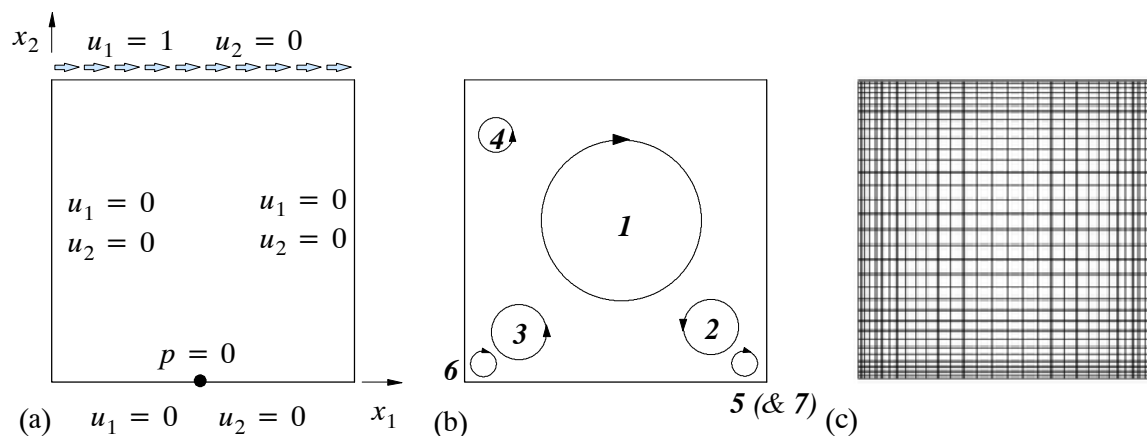


Fig. 9.8: Lid-driven cavity flow: (a) geometry and boundary conditions; (b) sketch of vortices; (c) mesh 32x32

Within the sample calculations, a wide range of Reynolds numbers, namely 400, 1000, 5000 and 10000, is covered. With increasing Reynolds number, the basic discretization is refined leaving the submesh parameters constant yet. Starting with a 32x32 mesh for Reynolds numbers 400 and 1000, a 50x50 mesh for Reynolds number 5000 and two discretizations (64x64 and 80x80) for Reynolds number 10000 are used. All of these meshes consist of linear elements and are similarly refined towards the walls with a proportion of 1:5 for the largest element in the middle and the smallest element at the wall. This is equally done in both spatial directions (see Fig. 9.8(c)). The calculations for Reynolds numbers 400 and 1000 are performed using a stationary solver whereby an instationary solver served for the solution of the problems with higher Reynolds numbers. The achievement of a stationary solution is stated, if the normalized velocity and pressure deviations within one time step are lower than a chosen tolerance of 10^{-6} . To compare some of the results, those of Ghia et al. (1982), which have become a standard reference in the mean-

time, are considered. They have been obtained from a very fine grid of 129x129 and 257x257, respectively, applying a second-order accurate finite difference method.

Deviating from the frequent practice of comparing the velocity profiles of Ghia et al. (1982), the focus is on two other interesting aspects of the cavity flow, the pressure and the vortex formation. First of all, the pressure results are analyzed. In Fig. 9.9, the pressure isolines obtained by using the USFEM as well as the two- and the dynamic three-level method of chapter 8 are depicted for every Reynolds number. The minimum and maximum values are extracted in Table 9.3. It may be observed that the two-level method mostly introduces less numerical viscosity allowing the extreme pressure values in the top left (negative) and right (positive) corner to develop without excessive damping. This phenomenon has also been observed by Franca and Nesliturk (2001) as well as Nesliturk (1999) and can be confirmed here.

	two-level method	three-level meth.	USFEM
Re=400, mesh 32x32	-1.7686 / 2.9723	-1.1974 / 2.4579	-0.5004 / 1.6748
Re=1000, mesh 32x32	-0.6070 / 1.7204	-0.3839 / 1.5537	-0.1916 / 1.1138
Re=5000, mesh 50x50	-0.1297 / 1.1504	-0.1095 / 1.1732	-0.1107 / 0.9174
Re=10000, mesh 64x64	-0.0730 / 1.0465	-0.0904 / 1.1278	-0.0975 / 0.8774
Re=10000, mesh 80x80	-0.1156 / 1.1336	-0.3153 / 1.2038	-0.1170 / 0.9377

Table 9.3 Minimum and maximum values of pressure for various Reynolds numbers and discretization

The most interesting feature is the genesis of a varying number of vortices inside the cavity. Fig. 9.10 shows the streamlines displayed on the colored vorticity distribution for Reynolds numbers 1000, 5000 and 10000. Please compare them with the sketch in Fig. 9.8(b). A nice quantitative comparison consists in determining the location of the respective vortex centers. This is executed in Table 9.4 for the stabilized method, the two-level and the three-level method. For comparison reasons, the aforementioned data from Ghia et al. (1982) as well as results from Wall (1999) obtained unexceptionally on the very fine 80x80 mesh with a GLS-type stabilization are included. The stabilized method in Wall (1999) differs from the USFEM-type stabilized method used here merely in partial sign changes within the differential operator acting on the weighting function which have already been mentioned in section 7.3.1. Moreover, there are slight differences in the definition of the stability parameters. The (hardly recognizable) seventh vortex in the lower right corner is omitted, although it is resolved by every method with the help of a 80x80 discretization. As a measure for the accuracy of the respective methods, the total deviation including all resolved vortices as well as the deviation per resolved vortex with regard to the data of Ghia et al. (1982) is determined in Table 9.5. Please note the high accuracy of the two- and three-level method in predicting the correct vortex centers in spite of the partly very much coarser basic discretizations with respect to Wall (1999). Both methods give better predictions than the USFEM throughout using the same basic discretization. Furthermore, it can be observed that there is in fact no gain in this case using the three-level method.

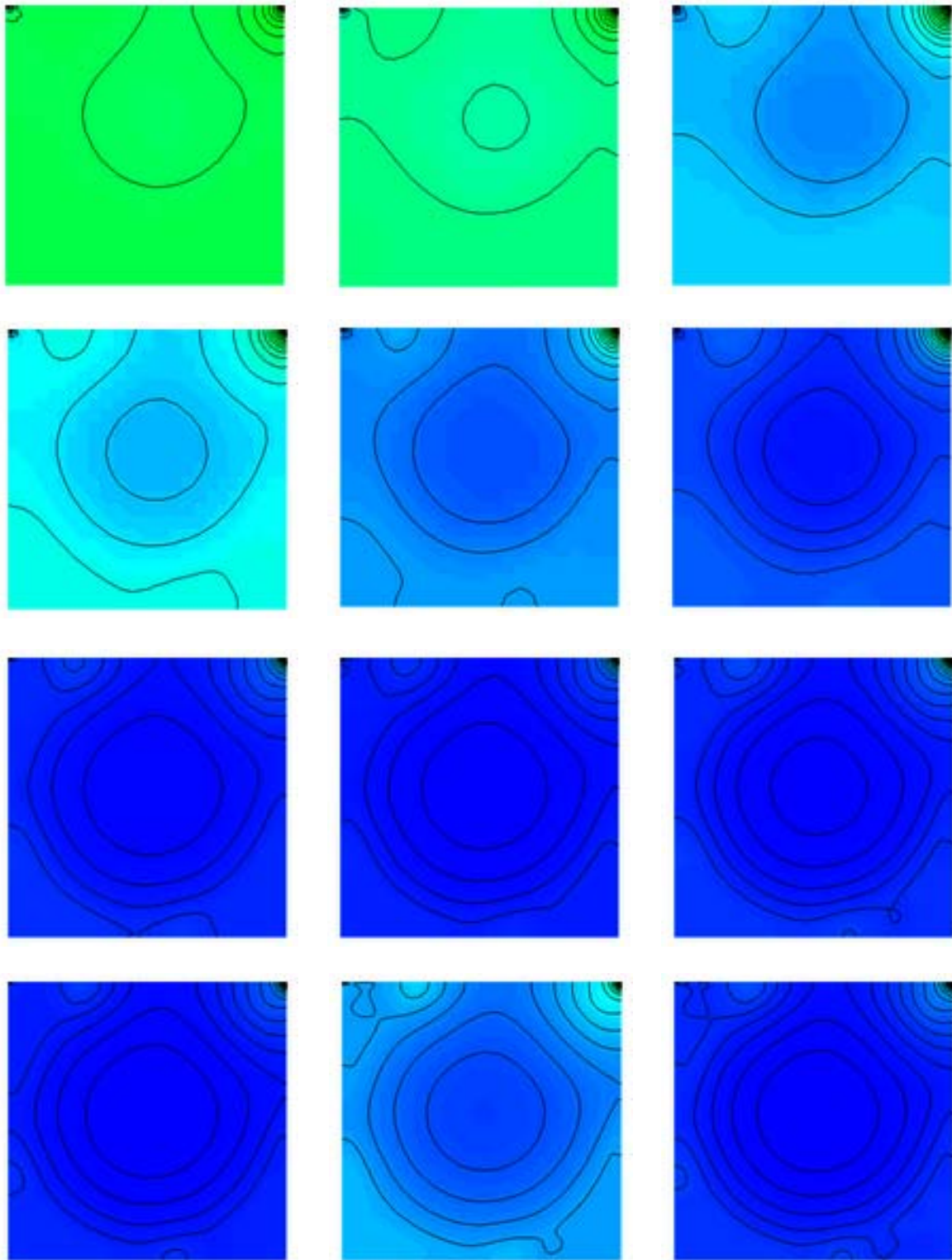


Fig. 9.9: Pressure isolines (50 lines between minimum and maximum value) on colored pressure distribution: left: two-level method; middle: three-level method; right: USFEM; from top to bottom: $Re=400$ with 32×32 mesh, $Re=1000$ with 32×32 mesh, $Re=5000$ with 50×50 mesh, $Re=10000$ with 80×80 mesh

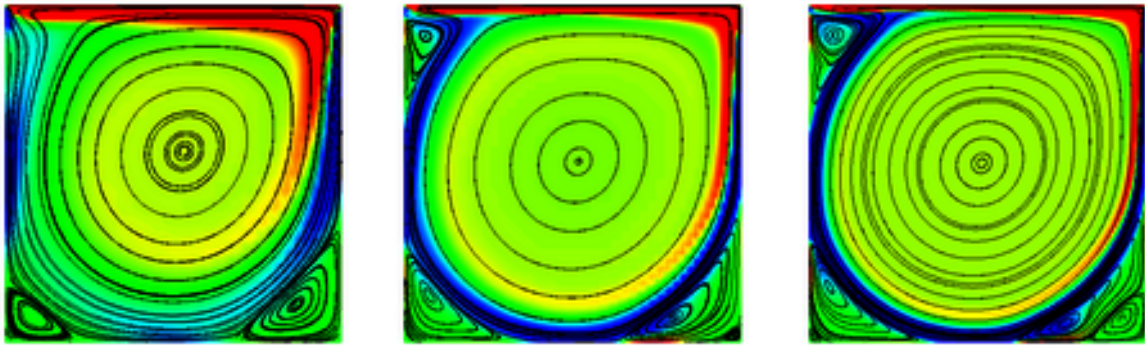


Fig. 9.10: Streamlines on colored vorticity distribution (ranging from -5 (blue) to +5 (red)) obtained by using the two-level method: left: $Re=1000$ with 32×32 mesh; middle: $Re=5000$ with 50×50 mesh; right: $Re=10000$ with 80×80 mesh

	Vortex 1	Vortex 2	Vortex 3	Vortex 4	Vortex 5	Vortex 6
--	----------	----------	----------	----------	----------	----------

$Re = 1000$

two-level 32x32	0.5312 / 0.5664	0.8638 / 0.1112	0.0838 / 0.0776			
three-level 32x32	0.5310 / 0.5668	0.8631 / 0.1113	0.0835 / 0.0774			
USFEM 32x32	0.5317 / 0.5680	0.8623 / 0.1107	0.0803 / 0.0768			
Wall (99) 80x80	0.5308 / 0.5660	0.8643 / 0.1115	0.0832 / 0.0775	0.9941 / 0.0066		
Ghia et al. (1982)	0.5313 / 0.5625	0.8594 / 0.1094	0.0859 / 0.0781	0.9922 / 0.0078		

$Re = 5000$

two-level 50x50	0.5154 / 0.5358	0.7941 / 0.0683	0.0725 / 0.1387	0.0618 / 0.9087	0.9748 / 0.0209	
three-level 50x50	0.5152 / 0.5360	0.7923 / 0.0683	0.0724 / 0.1385	0.0618 / 0.9083	0.9725 / 0.0222	
USFEM 50x50	0.5156 / 0.5373	0.7922 / 0.0683	0.0705 / 0.1407	0.0613 / 0.9068	0.9659 / 0.0281	
Wall (99) 80x80	0.5148 / 0.5362	0.7959 / 0.0706	0.0728 / 0.1365	0.0624 / 0.9076	0.9728 / 0.0223	0.0070 / 0.0073
Ghia et al. (1982)	0.5117 / 0.5352	0.8086 / 0.0742	0.0703 / 0.1367	0.0625 / 0.9102	0.9805 / 0.0195	0.0117 / 0.0078

Re = 10000

two-level 64x64	0.5126 / 0.5299	0.7688 / 0.0546	0.0571 / 0.1702	0.0671 / 0.9115	0.9302 / 0.0736	0.0168 / 0.0203
two-level 80x80	0.5119 / 0.5306	0.7608 / 0.0549	0.0582 / 0.1651	0.0697 / 0.9102	0.9293 / 0.0717	0.0164 / 0.0188
three-level 64x64	0.5124 / 0.5301	0.7660 / 0.0543	0.0570 / 0.1702	0.0672 / 0.9111	0.9287 / 0.0765	0.0170 / 0.0206
three-level 80x80	0.5117 / 0.5308	0.7572 / 0.0545	0.0582 / 0.1646	0.0700 / 0.9099	0.9279 / 0.0732	0.0165 / 0.0189
USFEM 64x64	0.5127 / 0.5314	0.7662 / 0.0555	0.0557 / 0.1727	0.0665 / 0.9112	0.9266 / 0.0837	0.0170 / 0.0201
USFEM 80x80	0.5118 / 0.5317	0.7558 / 0.0547	0.0573 / 0.1660	0.0692 / 0.9099	0.9244 / 0.0802	0.0163 / 0.0184
Wall (99) 80x80	0.5064 / 0.5284	0.7548 / 0.0555	0.0578 / 0.1659	0.0709 / 0.9092	0.9266 / 0.0791	0.0138 / 0.0163
Ghia et al. (1982)	0.5117 / 0.5333	0.7656 / 0.0586	0.0586 / 0.1641	0.0703 / 0.9141	0.9336 / 0.0625	0.0156 / 0.0195

Table 9.4 Locations of vortex centers (coordinate x_1 / coordinate x_2)

	number of re- solved vortices	total deviation [10 ⁻³]	dev. per resolved vortex [10 ⁻³]
--	----------------------------------	--	---

Re = 1000

two-level meth., mesh 32x32	3	10.8	3.6
three-level meth., mesh 32x32	3	11.6	3.9
USFEM, mesh 32x32	3	14.4	4.8
Wall (99) - GLS, mesh 80x80	4	18.2	4.6

Re = 5000

two-level meth., mesh 50x50	5	29.9	6.0
three-level meth., mesh 50x50	5	34.7	6.9
USFEM, mesh 50x50	5	46.4	9.3
Wall (99) - GLS, mesh 80x80	6	34.5	5.8

Re = 10000

two-level meth., mesh 64x64	6	32.1	5.4
three-level meth., mesh 64x64	6	34.8	5.8
USFEM, mesh 64x64	6	43.0	7.2
two-level meth., mesh 80x80	6(7)	25.0	4.2
three-level meth., mesh 80x80	6(7)	29.9	5.0

USFEM, mesh 80x80	6(7)	40.0	6.7
Wall (99) - GLS, mesh 80x80	6(7)	47.0	7.8

Table 9.5 Deviation of locations of vortex centers with respect to data of Ghia et al. (1982)

Closing this example, the reader should be provided with a visual impression of how much 'stabilization' is introduced by a stabilized method and by the residual-free bubble based multilevel methods presented here. It has been observed by several authors that residual-free bubble methods introduce less 'stabilization' (at least for triangular elements in the convection-dominated case), see e.g. Brezzi and Russo (1994), Nesliturk (1999) and Russo (1996). First considerations for quadrilateral elements may be found in Brezzi et al. (1998). Here, the situation is investigated with bilinear quadrilateral elements in case of a moderate overall Reynolds number of 400. For the depiction in Fig. 9.11, the element integrals of bubble functions governed by (7.49)-(7.51) have been calculated for every element of the 32x32 mesh in this case. The absolute value of them is merely considered and the corresponding integral in the sense of (6.65) within the stabilized method of USFEM-type paying no attention to the respective signs and display them as a column on the respective element. The presentation is restricted to one sample velocity bubble function, \mathcal{U}_2 , and one sample pressure bubble function, \mathcal{P}_4^1 . The remaining velocity and pressure bubble functions provide a quite similar impression, however. It is clearly visible by inspecting Fig. 9.11 that the residual-free bubble method indeed introduces less 'stabilization' with both the velocity and the pressure bubble function in comparison to the corresponding terms of the USFEM in this sample case.

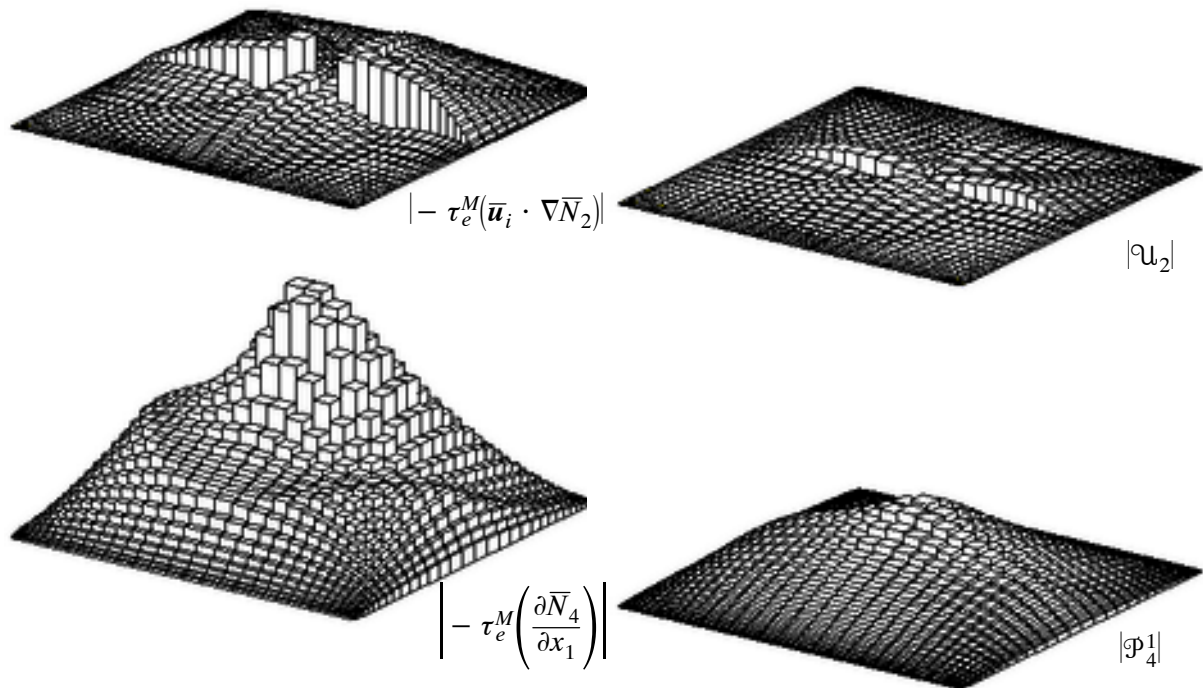


Fig. 9.11: Two sample element integrals of velocity and pressure bubble functions and corresponding element integrals in stabilized method for $Re=400$ on 32x32 mesh: left: 'stabilizing integral'; right: 'bubble integral'

9.2.2 Interpretation of the results with regard to turbulent flow simulations

For the 3-D counterpart of the 2-D lid-driven cavity flow presented in the preceding section, the occurrence of Taylor-Görtler-type vortices formed as a result of the curvature of the streamlines due to the first vortex were observed experimentally. According to this, the 3-D version of the lid-driven cavity flow will be investigated in the context of the numerical simulation of turbulent flow situations in section 10.2. The 3-D lid-driven cavity problem has also recently been picked up by Iliescu et al. (2003). They report the temporal evolution of the total kinetic energy for a calculation at a Reynolds number of 10000 applying $8 \times 8 \times 8$ elements with biquadratic velocity interpolation and discontinuous bilinear pressure interpolation. This element is known to fulfill the inf-sup condition and, moreover, considered to be the most stable and best performing element for finite element discretizations of the Navier-Stokes equations fulfilling the inf-sup condition according to e.g. Fortin (1993) as well as Gresho and Sani (1998). More importantly for the context of this section, Iliescu et al. (2003) spend most of their numerical investigations on the 2-D case studied in the previous section. Their primary goal in this numerical study is aimed at the analysis of two necessary conditions required for a reasonable LES. Firstly, the LES should replicate laminar flows and, secondly, the total kinetic energy should be bounded for high Reynolds number flows. Obviously, the violation of one of the two conditions leads inescapably to the conclusion that the applied method exhibits serious deficiencies.

Iliescu et al. (2003) take three subgrid-scale models into account, namely the simple Smagorinsky model (see section 5.2.3), a traditional Taylor LES model of Clark et al. (1979) and two variants of a new rational LES model developed in Galdi and Layton (2000). Discretizations with 16×16 , 32×32 and 64×64 elements with equidistant meshes applying the aforementioned biquadratic/discontinuous-bilinear type of element were used. These discretizations are comparable (exactly from the point of view of velocity and roughly from the point of view of pressure degrees of freedom) to 32×32 -, 64×64 - and 128×128 -element discretizations of the equal-order interpolated linear type used above. Calculations are reported for Reynolds numbers of 400 and 10000 both also used in the calculations at hand. Besides the perception that there are no problems related to the total kinetic energy for $Re = 400$ as expected, it is shown that the Taylor LES model produces an energy blow-up in finite time for $Re = 10000$. This corresponds with results reported, for instance, by Cantekin et al. (1994). Thus, this model is considered by Iliescu et al. (2003) as not being suited to model turbulent flows. The other models did not cause an energy blow-up and exhibited reasonable results with the Smagorinsky model (Smagorinsky constant $C_S = 0.1$) being notably more diffusive as expected. Based on these considerations, the following three final statements concerning the results of the previous section with regard to turbulent flow calculations can be made:

- The first basic requirement that any method used for turbulent flow calculations must replicate laminar flow situations as well can be ascertained for the two- and three-level method as well as the stabilized method for this flow example (and, as you will see, for all other examples of this chapter).
- The second basic requirement that the total kinetic energy must remain bounded during the complete simulation time can also be established for all methods, since no energy blow-up in any calculation up to the highest Reynolds number of 10000 chosen here.

- Beyond these basic requirements, the two- and three-level method, in particular, have demonstrated their ability to predict specific flow phenomena like the spatially correct occurrence of vortices in this example.

9.3 Cavity flow with oscillating lid (2-D)

The situation of the preceding example depicted in Fig. 9.8(a) is preserved. Instead of the constant velocity $u_1 = 1$, a time-dependent function is now prescribed for the development of the velocity at $x_2 = 1$ reading

$$u_1(t) = 1 - \cos\left(\frac{2\pi t}{T}\right); \quad 0 \leq t \leq \frac{T}{2} \quad (9.9)$$

$$u_1(t) = 2 \cos\left(\frac{2\pi}{T}\left(t - \frac{T}{2}\right)\right); \quad \frac{T}{2} < t \leq T \quad (9.10)$$

with a period of $T = 7.5$ time units. The calculation is run for 4 periods, i.e. an overall duration of 30 time units. A time step of $\delta t = 0.1$ has been chosen and two iterations within each time step have been performed. Furthermore, the non-leaky boundary conditions from the preceding example are withdrawn by leaving open the range $x_2 = [0.9375, 1]$ of both side walls for the velocity u_1 . Flow situations with Reynolds numbers 1000 and 10000 are considered applying the 32x32 discretization and the 64x64 discretization from the previous example, respectively. Additionally, a very coarse mesh of 16x16 linear elements is investigated for the problem with the lower Reynolds number as well. Fig. 9.12 may help to exhibit the flow situation at different points in time by showing the velocity vectors depicted on the colored velocity distribution.

The interesting aspect to be observed is the temporal evolution of the velocities u_1 and u_2 as well as the pressure p . Thus, four representative nodes have been chosen within the cavity. The respective nodes are displayed in Fig. 9.13 with the coordinates and the gathered values. The nodes for gathering data in case of the higher Reynolds number certainly have to be located closer to the lid, since the sphere of influence of the prescribed velocity inside the cavity is substantially smaller due to the lower viscosity. Within the generalized trapezoidal rule, two different values for the parameter θ are tested in order to check the performance of the two-level method in combination with a semi-discrete time-stepping algorithm. Particularly, the backward Euler method (BE - $\theta = 1$) and the Crank-Nicolson method (CN - $\theta = 1/2$), the two prominent representatives of implicit methods within the generalized trapezoidal rule, are employed. The use of the three-level method provides no gain in this example similar to the previous one. For reasons of clarity, the results for the three-level method are omitted in the following diagrams, since they are virtually indistinguishable from the corresponding two-level results.

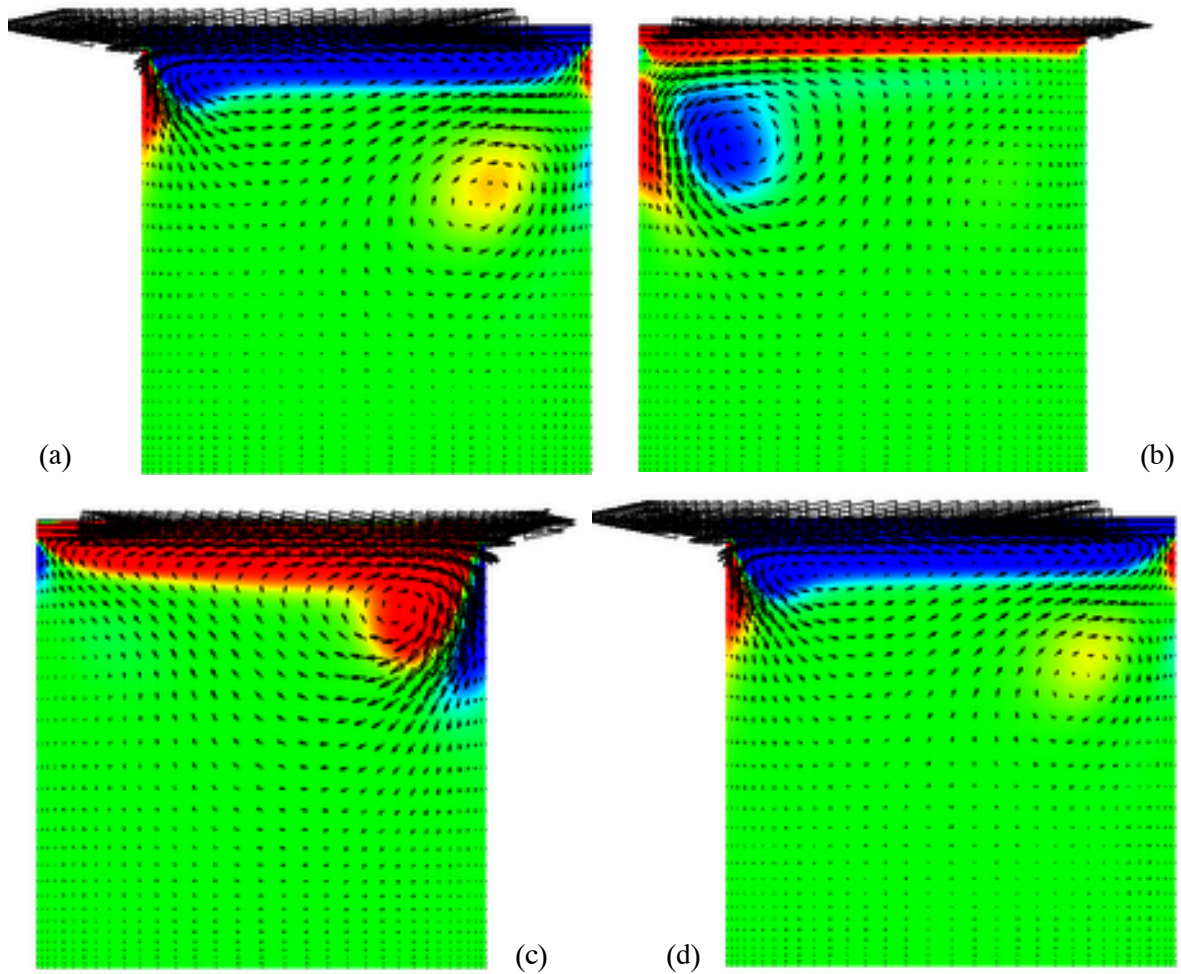


Fig. 9.12: Cavity flow with oscillating top ($Re = 1000$) over one time period: velocity vectors on colored vorticity distribution (ranging from -5 (blue) to $+5$ (red)) obtained by using the two-level method on a 32×32 mesh for (a) $T = 7.5$; (b) $T = 10.0$; (c) $T = 12.5$; (d) $T = 15.0$

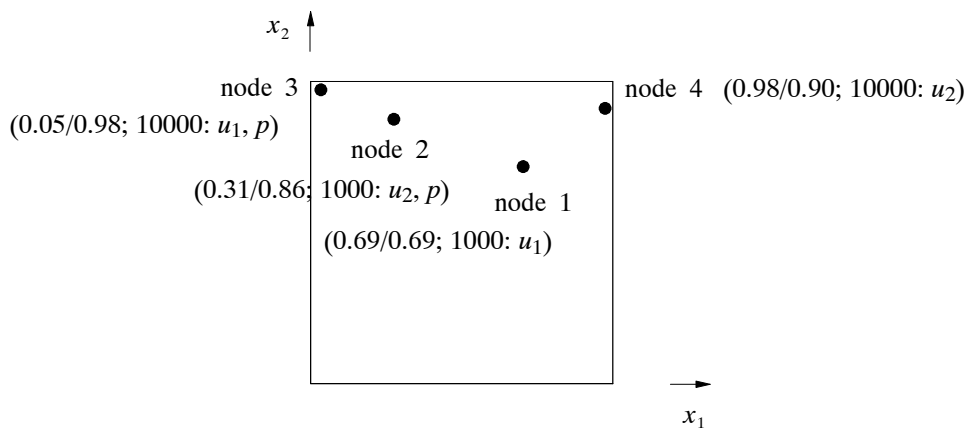


Fig. 9.13: Identification of nodes: node (coordinate x_1 /coordinate x_2 ; Reynolds number: gathered variable(s))

Fig. 9.14 shows the temporal evolution for a Reynolds number of 1000 obtained on a 32x32 mesh. One may observe the obvious impact of the chosen time-stepping scheme. The results obtained by the stabilized method of USFEM-type and the two-level method with the assumption of quasi-static bubbles using a backward Euler scheme in both cases can hardly be distinguished. Without the quasi-static bubbles, the backward Euler scheme is less diffusive. This is explicitly recognizable due to the higher amplitudes in the oscillation. This process is considerably amplified for the Crank-Nicolson scheme.

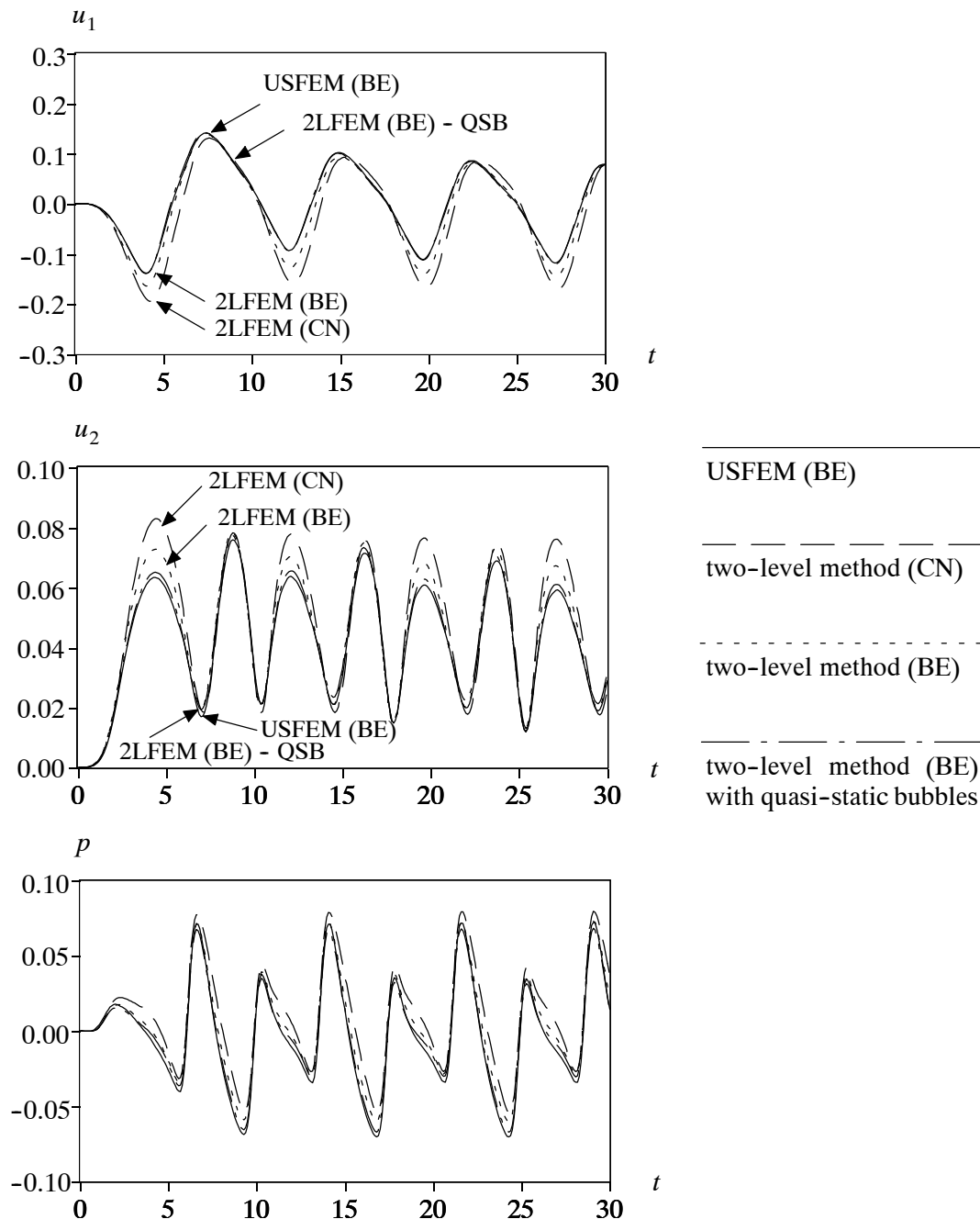


Fig. 9.14: Temporal evolution of velocity and pressure for $Re = 1000$ on 32x32 mesh: (a) u_1 at node 1; (b) u_2 at node 2; (c) p at node 2

In Fig. 9.15, the situation for a Reynolds number of 10000 surveyed on a 64x64 discretization is depicted. Here, equal tendencies in comparison to the previous case with the lower Reynolds number may be noted.

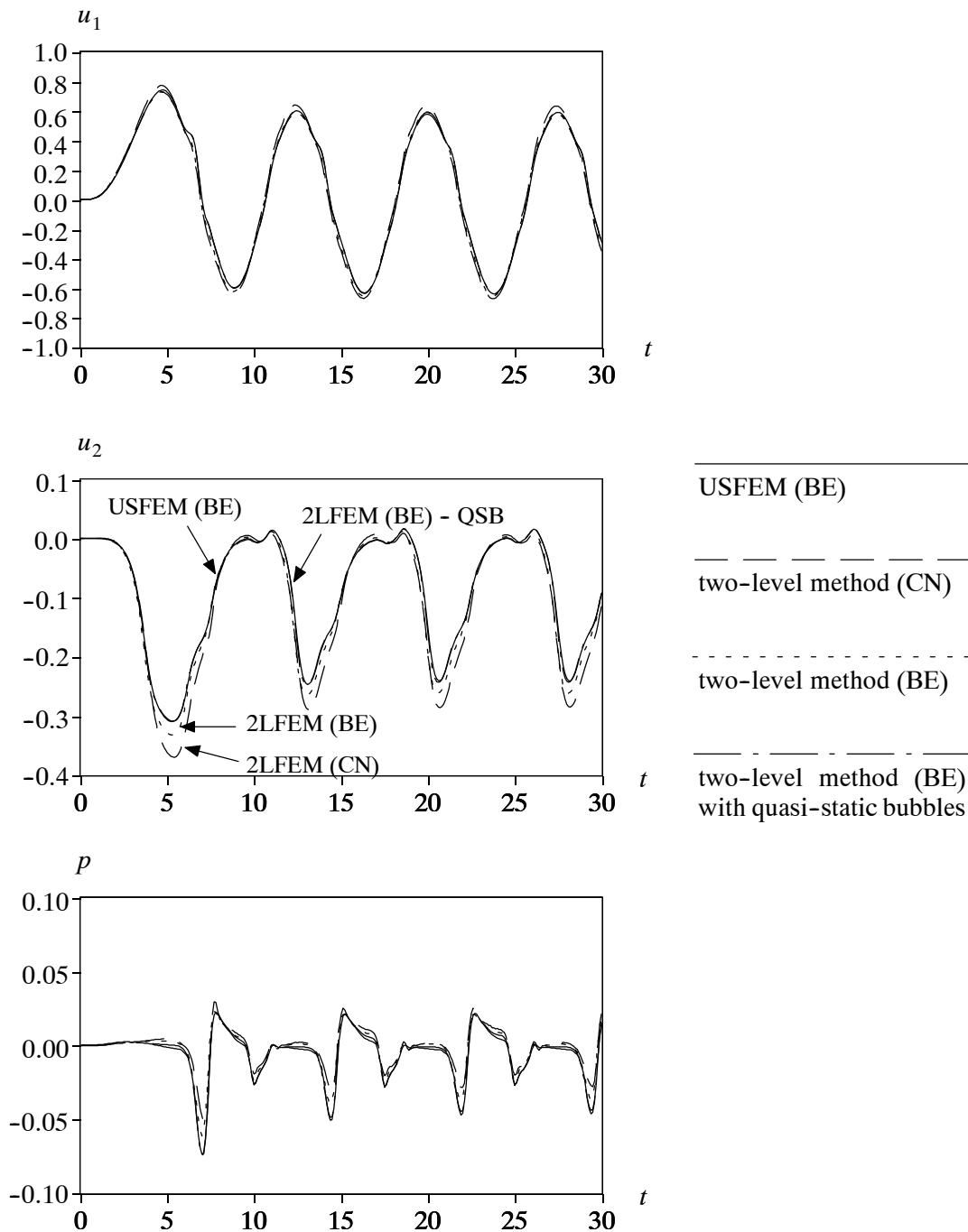


Fig. 9.15: Temporal evolution of velocity and pressure for $Re = 10000$ on 64×64 mesh: (a) u_1 at node 3; (b) u_2 at node 4; (c) p at node 3

In Fig. 9.16 finally, one velocity result for the same flow using the coarser 16×16 mesh is reported. For orientation to some degree, the corresponding results from Fig. 9.14 are also displayed in the background. The amplitudes are even higher for the backward Euler and the Crank-Nicol-

son scheme. The stabilized method and the two-level method with quasi-static bubbles remain nearly identically. Among others, this example shows that the assumption of quasi-static bubbles provokes another diffusive effect independent of the time-stepping scheme.

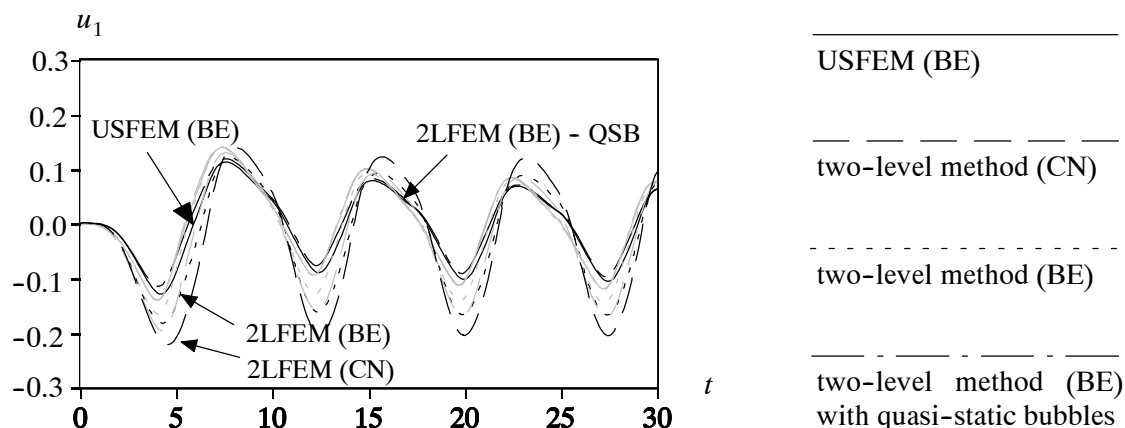


Fig. 9.16: Temporal evolution of u_1 at node 1 for $Re = 1000$ on 16×16 mesh; results from 32×32 mesh displayed in the background with pallid color

9.4 Flow past a circular cylinder (2-D)

The next example describes a widely solved benchmark problem. Apart from the specific object (a cylinder here) being passed, it is of basic engineering interest, since the flow past some solid body is one of the major areas of engineering applications. By choosing a Reynolds number of 100 based on the cylinder diameter and the inflow velocity, a range of Reynolds numbers is entered where the occurrence of the famous Karman vortex street may be expected. This vortex shedding phenomenon consists of an alternate separation of a vortex at both the upper and the lower side of the cylinder. This takes place with a certain frequency. Limit ranges depending on the Reynolds number and governing the occurrence of different flow characteristics can be found, for example, in Schlichting (1979). Experimental investigations concerning this flow have been reported, for instance, by Norberg (1994) and Williamson (1996). The numerical solution of this problem was, among others, the subject of benchmarking efforts in Schäfer and Turek (1996). Furthermore, Brooks and Hughes (1982) have used this example for the validation of their SUPG-method in the context of the Navier-Stokes equations.

The flow situation is depicted in Fig. 9.17(a). The inflow velocity is predefined as $u_1^{in} = 1$, the cylinder diameter as $D = 0.16$ and the kinematic viscosity as $\nu = 0.0016$ for unit density, in order to achieve a Reynolds number of 100. Two basic discretizations have been chosen which are referred to as 'coarse' and 'fine' in the following. The coarse mesh comprised 2986 bilinear quadrilateral elements (3091 nodes) whereas the fine mesh contained 7298 elements (7461 nodes) both being refined while approaching the cylinder. The fine mesh is shown in Fig. 9.17(b). The time step is chosen to be 0.032 time units and the calculation is run for 1000 time steps resulting in an overall simulation time of 32 time units. Within each time step, only a single iteration is performed. The simulation is started with a zero initial velocity field and the inflow velocity is allowed to evolve to full extent within one time unit governed by a trigonometrical function keeping it constant afterwards.

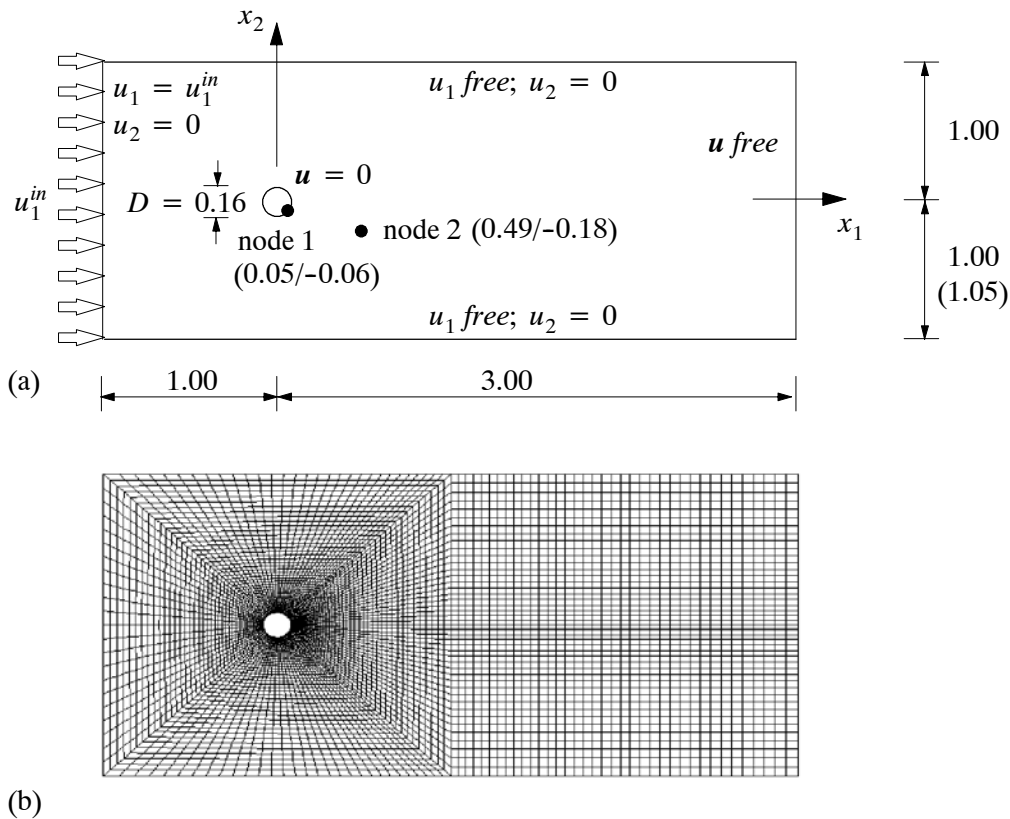


Fig. 9.17: Flow past a circular cylinder: (a) geometry and boundary conditions plus identification of nodes (node (coordinate x_1 /coordinate x_2)); (b) fine mesh (7298 elements)

The major quantitative point of interest is the so-called Strouhal number St here defined as

$$St = \frac{u_1^{in} D}{t_0} \quad (9.11)$$

which can be used as some kind of quantification for the periodic solution of the vortex street. t_0 denotes the period of one oscillation. The temporal evolution of the pressure is gathered in Figs. 9.18–9.20 at two points, one directly located on the surface of the cylinder and the other somewhat further away in the wake of the cylinder (see Fig. 9.17(a)). On the one hand, these graphs may report basic differences between the results obtained by using variants of the generalized trapezoidal rule. On the other hand, the Strouhal numbers for these test calculations can be determined and compared among themselves as well as with results from selected literature. Since spurious oscillations from one time step to the next are obtained for the Crank–Nicolson method ($\theta = 1/2$), it is followed the suggestion of Heywood and Rannacher (1990), mentioned in section 3.3.2, to slightly shift the CN-scheme in form of an increase of the parameter, in order to avoid such spurious oscillations. After all, $\theta = 0.6$ is chosen to be the parameter of the second scheme besides the backward Euler (BE) algorithm.

For reasons of brevity, pictures of the various stages of the flow development are left out. However, the flow past a cylinder is a well documented example from the standpoint of visualization. Pictures stemming from numerical simulations of this setup may be found, for instance, in the literature quoted in this section. Moreover, the album of van Dyke (1982) provides us with nice

photographs of experiments for this flow situation, among others. Because of this comprehensive selection of visual impressions, it is focussed on the, admittedly less spectacular, data below.

Four results for each case are reported in Figs. 9.18-9.20, respectively: the backward Euler scheme and the scheme with $\theta = 0.6$ for both the stabilized method of USFEM-type and the two-level method. Fig. 9.18 depicts the temporal evolution of the pressure at nodes 1 and 2 for the coarse mesh. It may be observed that for the $\theta = 0.6$ -scheme the stabilized method reaches the state of vortex shedding at about 6 to 7 time units and, thus, considerably earlier than the two-level method where this takes place at about 23 time units after the start of the simulation. This is contrary for the backward Euler algorithm. As anticipated, backward Euler schemes introduce considerably more numerical viscosity preventing the vortex shedding from being started. At the end of the diagram in Fig. 9.18, one may (hardly) see, however, that the oscillations are about to start for the two-level method at around 31 time units whereas the stabilized method remains without oscillations throughout the simulation time of 32 time units. Test calculations reaching beyond this global simulation time limit reveal that the stabilized method admits the start of the vortex shedding at about 36 time units and even a backward-Euler-based calculation with the quasi-static bubble assumption allows for this phenomenon at ca. 49 time units. Fig. 9.19 shows the same flow situation calculated with the fine mesh. Here, the starting points in time for the two-level method with backward Euler and the $\theta = 0.6$ -scheme are both moved forward by about 3 to 4 time units and also the BE-stabilized method initiates oscillations within the depicted simulation time.

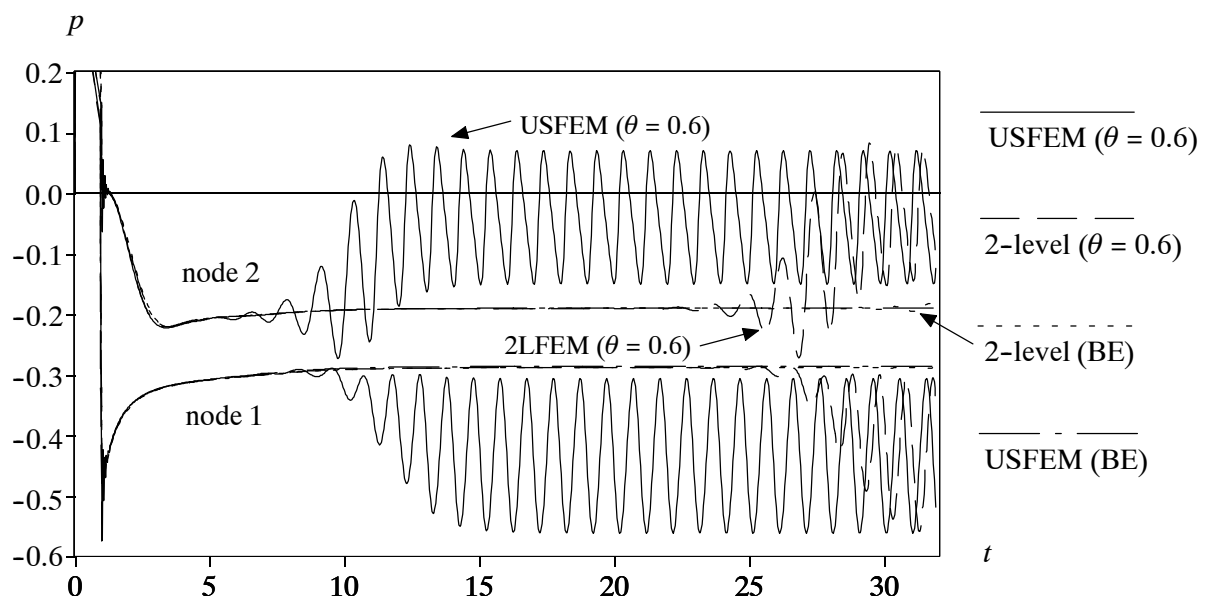


Fig. 9.18: Temporal evolution of p at nodes 1 and 2 ($Re = 100$) for coarse mesh

After all, the underlying conditions of perfect geometric symmetry basically provide no support for the timely evolution of the vortex street. For instance, Brooks and Hughes (1982) tried to hasten the vortex shedding by adding a perturbation in form of small forces added to the nodes of the boundary layer at the cylinder. This showed but little noticeable effect. Here, a somewhat different perturbation is introduced by cancelling the symmetry of the domain, i.e. in particular enlarging the lower part of the domain with regard to the cylinder location (see Fig. 9.17(a)). As a result, all methods are now forced to start oscillating at about the same time as may be observed

in Fig. 9.20. Henceforth, the expected consequence has to be noticed conspicuously that the backward Euler scheme merely admits substantially smaller amplitudes, regardless of the specific method used.

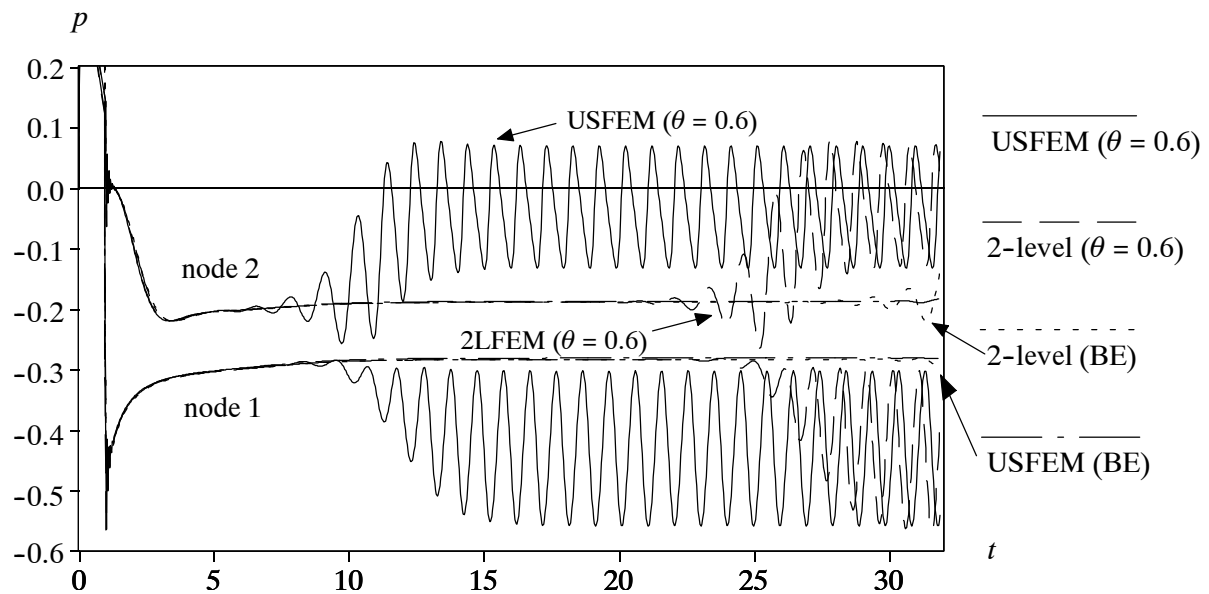


Fig. 9.19: Temporal evolution of p at nodes 1 and 2 ($Re = 100$) for fine mesh

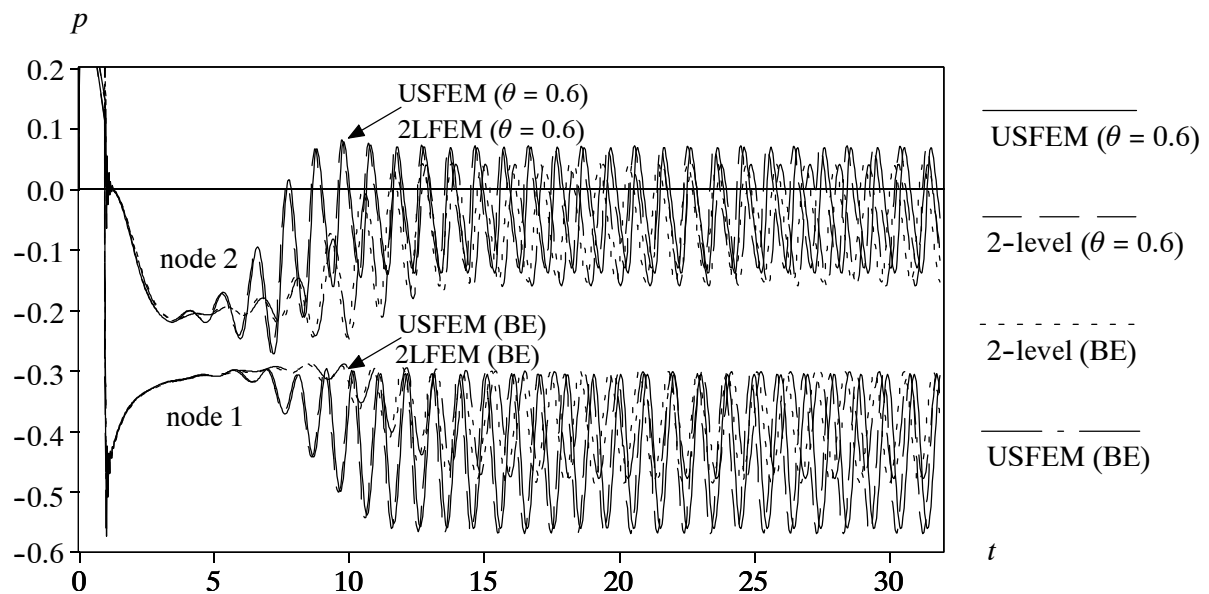


Fig. 9.20: Temporal evolution of p at nodes 1 and 2 ($Re = 100$) for coarse mesh on an unsymmetric domain

Evaluating the respective Strouhal numbers reveals identical values for the stabilized method and the two-level method. To give some orientation concerning 'correct' values for the Strouhal number, it is referred to the empirical formula of Norberg (1994) derived from the results of a multitude of experiments which reads

$$St = \frac{A}{Re} + B + C Re \quad (9.12)$$

with the empirical constants $A = -3.458$, $B = 0.1835$ and $C = 1.51 \times 10^{-4}$ (valid in the Reynolds number range from around 47 up to around 165). For the problem with Reynolds number 100, the formula yields 0.164 as the 'correct' Strouhal number. This value is matched more or less exactly by both methods on both discretizations for the modified Crank–Nicolson scheme. Using the backward Euler scheme yields a Strouhal number of approximately 0.147. The additional assumption of quasi-static bubble functions lowers the number to about 0.138 notably pointing out the problem with the introduction of too much numerical viscosity in the course of these variants thus. A few exemplary values for Strouhal numbers obtained by other authors with comparable finite element methods are: 0.167 by Brooks and Hughes (1982) with a stabilized method of SUPG-type and a predictor-multicorrector algorithm in time, 0.164 by Wall (1999) with a stabilized method of GLS-type and $\theta = 0.6$ on the fine mesh described above, 0.174 by Codina (2002a) with an algebraic subgrid scale (ASGS) method which is similar to the GLS-type method as well as 0.175 with the method of orthogonal subscales (adumbrated in sections 6.4 and 7.4.1, respectively). Codina (2002a) employed a Crank–Nicolson scheme in time. The results of Brooks and Hughes (1982) are gained on a good deal smaller domain with regard to the cylinder diameter. The domain in Codina (2002a) is even smaller. The crucial aspect in this context references to the distance between the cylinder center and the lateral boundary which is about $6.25 D$ in the example of this work. Brooks and Hughes (1982) have chosen $4.50 D$ and Codina (2002) $4.00 D$. Thus, an unequal influence of the lateral boundaries on the results has obviously to be expected within the various domains, which may serve as one explanation for the differences between the results on varying domains. Behr et al. (1995) have shown that $8.00 D$ should be guaranteed at least, in order to minimize the impact of the lateral boundaries on the prediction of the global parameters like, for instance, the Strouhal number. For the three-dimensional version of the flow past a cylinder, Lei et al. (2001) have shown the effect of this geometrical distance on the simulation.

9.5 Beltrami flow (3-D)

The special features have already been indicated in the introduction of this chapter making this flow example a unique one. It was developed by Ethier and Steinman (1994) for benchmarking purposes, although it is unlikely to be physically realized eventually. Possibly more familiar to the reader is the 2-D counterpart of this flow, the Taylor problem (see Taylor (1923)), which was used by Kim and Moin (1985) for 2-D calculations.

The problem is solved on a domain $\Omega = [-1, 1] \times [-1, 1] \times [-1, 1]$. The exact solutions for the velocity and the pressure read as follows:

$$u_1 = -a \left[e^{ax_1} \sin(ax_2 \pm dx_3) + e^{ax_3} \cos(ax_1 \pm dx_2) \right] e^{-vd^2t} \quad (9.13)$$

$$u_2 = -a \left[e^{ax_2} \sin(ax_3 \pm dx_1) + e^{ax_1} \cos(ax_2 \pm dx_3) \right] e^{-vd^2t} \quad (9.14)$$

$$u_3 = -a \left[e^{ax_3} \sin(ax_1 \pm dx_2) + e^{ax_2} \cos(ax_3 \pm dx_1) \right] e^{-vd^2t} \quad (9.15)$$

$$p = -\frac{a^2}{2} \left[e^{2ax_1} + e^{2ax_2} + e^{2ax_3} + 2 \sin(ax_1 \pm dx_2) \cos(ax_3 \pm dx_1) \right] e^{a(x_2 + x_3)}$$

$$\begin{aligned}
& + 2 \sin(ax_2 \pm dx_3) \cos(ax_1 \pm dx_2) e^{a(x_3+x_1)} \\
& + 2 \sin(ax_3 \pm dx_1) \cos(ax_2 \pm dx_3) e^{a(x_1+x_2)}] e^{-2vd^2t}
\end{aligned} \tag{9.16}$$

where a and d are open parameters separating a family of solutions. They will be fixed according to Ethier and Steinman (1994) with the values $a = \pi/4$ and $d = \pi/2$. The characteristic feature of this flow is a series of counter-rotating vortices intersecting one another at oblique angles. The time-dependent terms in (9.13)-(9.16) indicate the exponential decay in time of the initial flow configuration.

Similar to the first example, two quite different flow regimes are considered, a diffusion-dominated flow with $\nu = 1$ and a convection-dominated flow with $\nu = 0.001$. The Reynolds number based on the chosen viscosity, the length of the domain and the maximum velocity is $Re = 6.62$ and $Re = 6620$, respectively. Uniform discretizations with $4 \times 4 \times 4$, $8 \times 8 \times 8$ and $16 \times 16 \times 16$ elements are used. Due to the negative imbalance between the substantial computational demands of higher-order elements in 3-D and the limited computational resources being at the author's disposal at the time of calculating this flow example, linear elements are merely applied. Fig. 9.21 presents the fully three-dimensional situation by displaying the initial pressure distribution. Furthermore, the $8 \times 8 \times 8$ discretization is included. Fig. 9.22 depicts the initial state regarding the velocity vectors on various velocity distributions in the three orthogonal cutting planes $x_1 = 0$, $x_2 = 0$ and $x_3 = 0$. The initial state is the same for both the diffusion- and the convection-dominated flow regime, since the viscosity has no effect for $t = 0$. The reader may confirm this by studying (9.13)-(9.16).

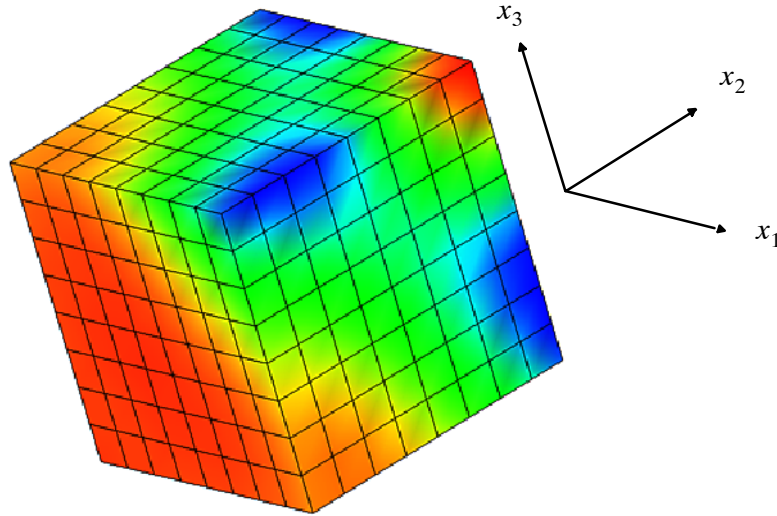


Fig. 9.21: Beltrami flow: colored initial pressure distribution with mesh $8 \times 8 \times 8$

A backward Euler time scheme is used for the calculation. For the two- and three-level method, the bubble functions were assumed to be quasi-static. In addition, the dynamic algorithm described in section 8.2.2 is employed for obtaining the dissipative effect of the unresolved scales within the three-level method. The simulation is started with the initial field governed by (9.13)-(9.16). Thereafter, Dirichlet boundary conditions likewise based on (9.13)-(9.16) are applied on all boundaries. The calculation is run 16 time steps with $\delta t = 0.00625$ and then stopped at $t = 0.1$, in order to quantify the current errors in the velocity and pressure calculation. The error

measures in (9.6)-(9.8) still keep their validity including the subsequent remark concerning the incorporation of the small-scale velocity.

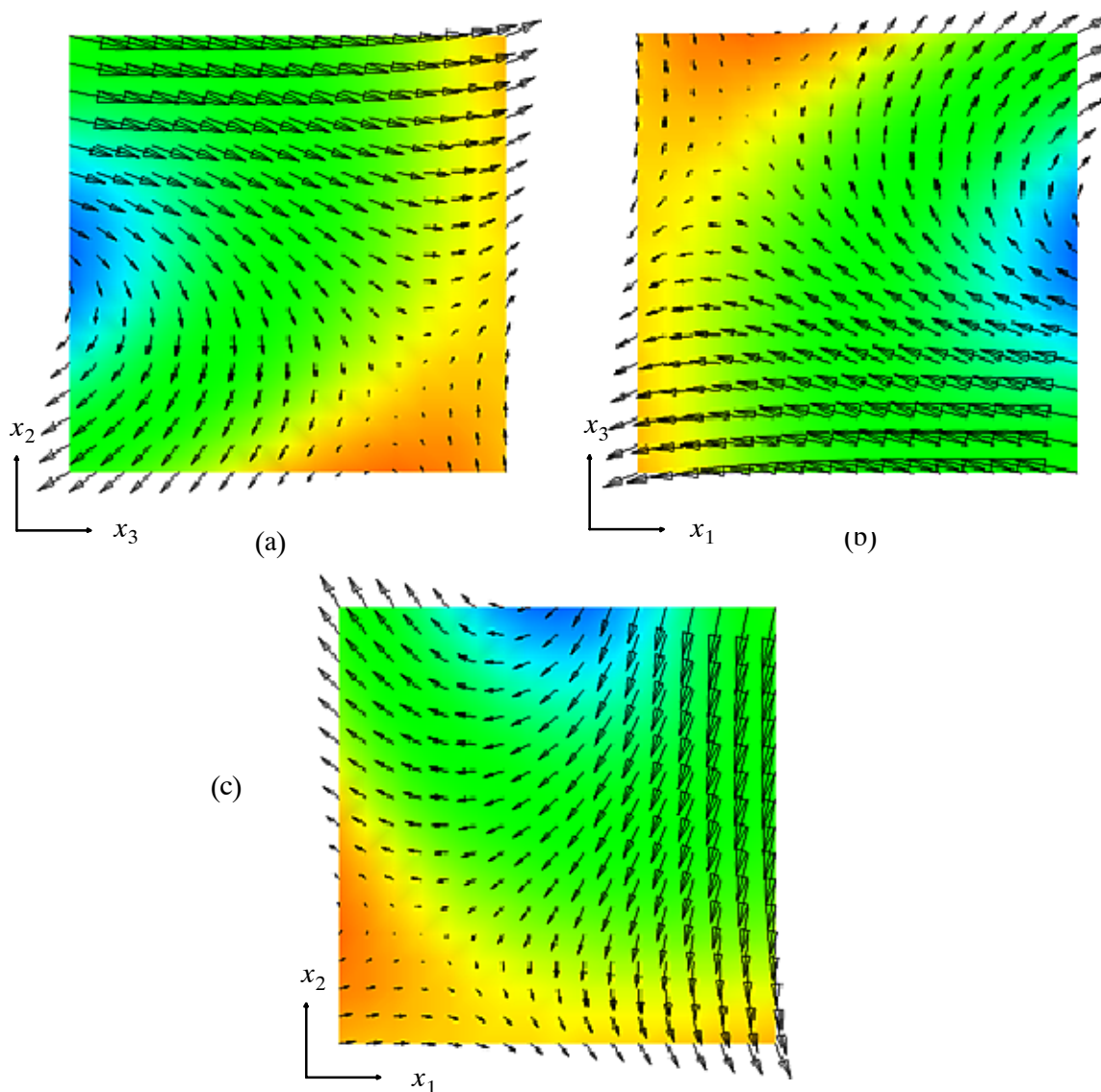


Fig. 9.22: Velocity vectors on colored velocity distribution (initial state for velocity): (a) u_1 in plane $x_1 = 0$; (b) u_2 in plane $x_2 = 0$; (c) u_3 in plane $x_3 = 0$

Fig. 9.23 and Fig. 9.24 depict the velocity error in the L_2 -norm and in the H^1 -norm, respectively. For the diffusion-dominated flow, the convergence rates which have to be expected from theoretical error analysis are accurately matched by all methods, and, moreover, they can not be distinguished from one another in terms of the absolute error. This is obviously quite different for the convection-dominated flow. The stabilized method and the three-level method still work fine, although the absolute velocity error in the H^1 -norm for the three-level method is not as good as for the stabilized method. However, this tendency could be observed for linear elements in the 2-D example of impinging fluid flow as well and may supposedly be blamed to the negative effect of the stringent zero Dirichlet boundary conditions (being even stronger in 3-D) within the residual-free bubble method especially with regard to the H^1 -error. This performance is, ho-

wever, then reversed for higher-order elements in favor of the three-level method there. Similar behaviour might be expected in 3-D. The crucial surveillance is that the two-level method is no longer able to guarantee an acceptable error in both the L_2 -norm and the H^1 -norm. Tendencies already observed in 2-D are particularly amplified concerning the error in the H^1 -norm. As in 2-D, the crucial deficiency described in the 2-D-case (confer also the illustration in Fig. 9.7) is removed with the discretization becoming finer.

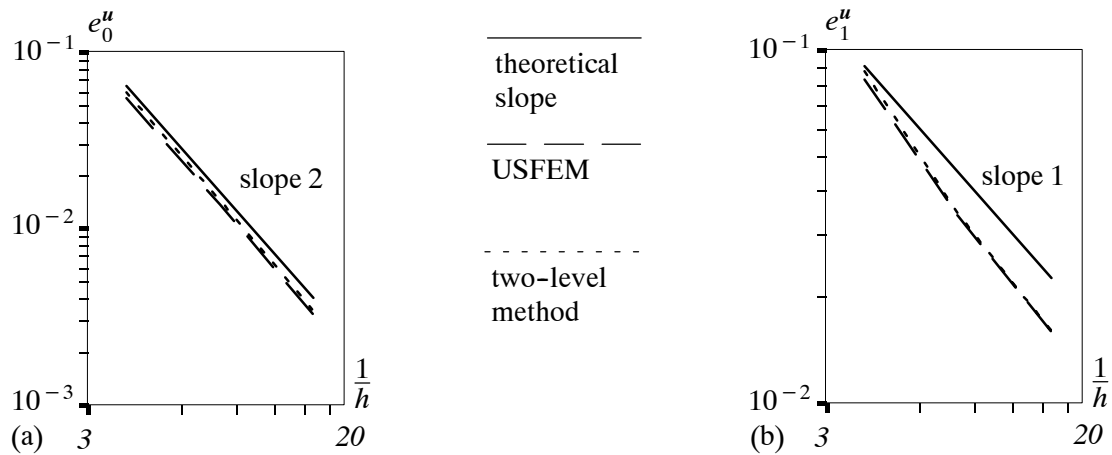


Fig. 9.23: Velocity error for diffusion-dominated flow: (a) L^2 -norm; (b) H^1 -norm

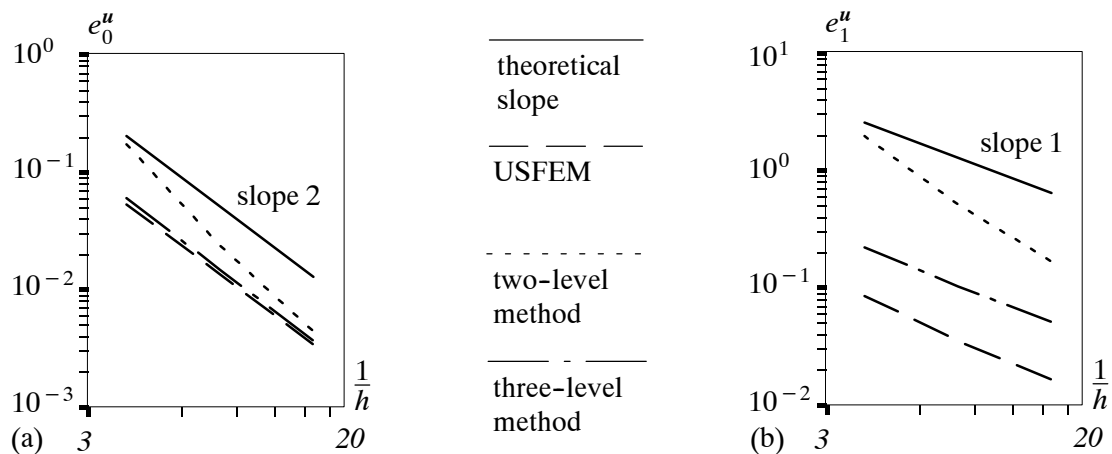


Fig. 9.24: Velocity error for convection-dominated flow: (a) L^2 -norm; (b) H^1 -norm

In Fig. 9.25, the pressure error is reported including in both diagrams lines displaying the slopes of suboptimal (slope 1) and optimal (slope 2) rate. It may be observed that all three methods match the optimal rate in both the diffusion- and the convection-dominated case. The stabilized method shows but a slight deviation from this behaviour in the diffusion-dominated flow regime in negative direction as well as the two- and three-level method in positive direction.

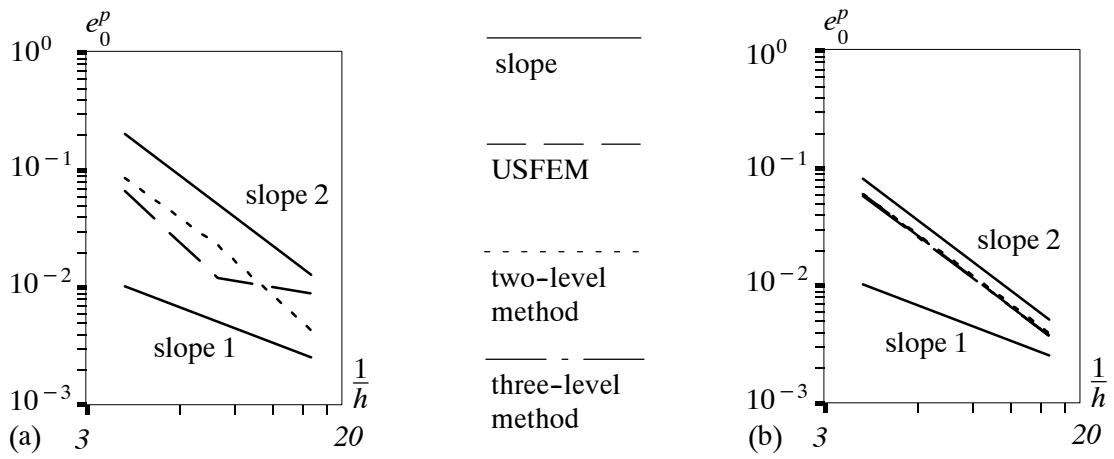


Fig. 9.25: Pressure error in L^2 -norm: (a) diffusion-dom. flow; (b) convection-dom. flow

10 Numerical examples of turbulent flow situations

10.1 The choice of turbulent flow examples

Turbulent flow examples may be distinguished in view of the number of directions of inhomogeneity according to Sagaut (2002), chapter 13. Fig. 10.1 depicts the classification in general.

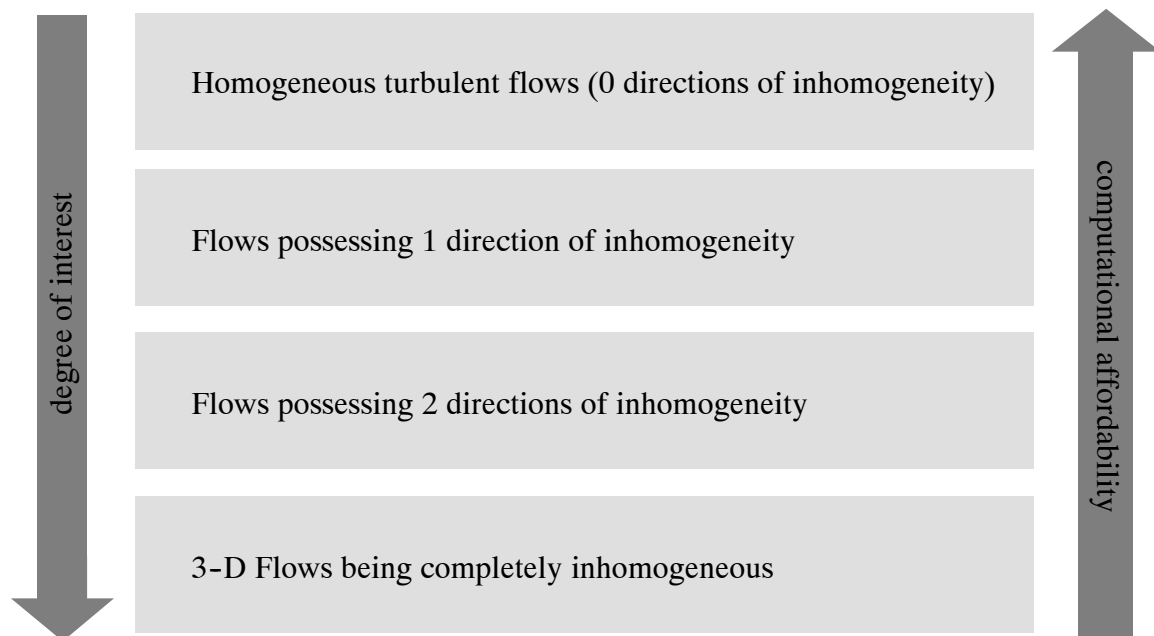


Fig. 10.1: General classification of turbulent flows

The computer resources needed for an adequate resolution usually increase with every additional direction of inhomogeneity. On the one hand, completely homogeneous turbulence, either isotropic or anisotropic, is not of major interest for the long-term goals of this work. On the other hand, interesting 3-D flows being completely inhomogeneous surely pose a challenge which cannot be taken with the computer resources available to the author currently. Due to the intention of providing a proper DNS data basis (or, more precisely spoken, a data basis being as close to DNS as possible), even flows with two directions of inhomogeneity will not be within reach. Just to give two examples, the flow over a backward facing step and the flow past a square-section or circular cylinder are certainly two of the most important examples of wall-bounded flows fitting into this category. A DNS of a flow over a backward facing step has been performed by Le et al. (1997). For this purpose, an overall number of about 9.5 million computational cells resulting in about 38.5 million degrees of freedom have been applied. This is far beyond the available capacity, even if it is aimed at a slightly coarser resolution. The same has to be stated for the case of the flow past a square-section cylinder after studying, for instance, the results of a workshop considering LES for this type of flow summarized in Rodi et al. (1997).

As a result of these preliminary considerations, the focus has to be on flows possessing one direction of inhomogeneity. According to this, the numerical realization of a non-wall-bounded flow

in form of a completely two-dimensional plane mixing layer is performed belonging to the group of flows with one direction of inhomogeneity. In particular, the opportunity to go back to a purely two-dimensional calculation allows the numerical simulation up to a certain level of resolution with the available computer resources. This flow example is described in detail in section 10.3.

Previously, the 3-D lid-driven cavity is investigated as already announced in the wake of the description of the 2-D lid-driven cavity in section 9.2. This represents an example for turbulent recirculating flows. Although this is a flow being bounded by walls in all coordinate directions, numerical realizations with discretizations of relatively low and moderate refinement have been performed and yielded good results in comparison to experimental data.

10.2 Lid-driven cavity flow (3-D)

10.2.1 Some reports of earlier experimental and numerical investigations

The turbulent recirculating flow in a 3-D lid-driven cavity will now be presented. As already indicated in section 9.2.2, this flow exhibits the occurrence of Taylor-Görtler-type vortices formed as a result of the curvature of the streamlines due to the first vortex. Please consult, for instance, Schlichting (1979) for a description of these particular vortices. Experimental data are reported for flows with Reynolds numbers 3200, 5000, 7500 and 10000 inside cavities with varying spanwise aspect ratio (SAR) in Prasad and Koseff (1989). The SAR is defined to be the ratio of the length of the cavity in x_3 -direction and the length of the cavity in x_1 -direction. Kim and Moin (1985) picked up an earlier report of an experimental study by Koseff and co-workers and tried to verify the appearance of these vortices in a numerical simulation using a fractional-step method. They were able to show weak vortical structures for a calculation at Reynolds number 1000.

Zang et al. (1992) and Zang et al. (1993) performed an LES in a finite volume method using the dynamic procedure of Germano et al. (1991), which they named DSM, and a dynamic mixed model (DMM), where they, additionally, took into account the scale similarity model of Bardina for this. The last combined structural/functional model has already been mentioned as an attractive modeling approach in section 5.3.3. In Zang et al. (1993), three cases are reported: a flow at a Reynolds number 3200 and SAR of the cavity being 1.0 on a $32 \times 32 \times 32$ grid as well as flows at Reynolds number 7500 and 10000, respectively, with SAR of the cavity being 0.5 on a $64 \times 64 \times 32$ grid. The grid points are clustered near the walls in x_1 -direction and x_2 -direction with minimum grid length in these directions being 0.01 for Reynolds numbers 3200 and 7500 as well as 0.005 for Reynolds number 10000. Based on experimental experience in Prasad and Koseff (1989), they describe the flow at Reynolds number 3200 to be essentially laminar, although an inherent unsteadiness may occur. For Reynolds number 7500, a transitional stage is reached, since the flow becomes unstable near the downstream eddy at Reynolds numbers higher than about 6000. With even higher Reynolds number at about 10000, the flow becomes fully turbulent. Thus, laminar, transitional, and turbulent regimes have been covered by the choice of these three cases in Zang et al. (1993).

Further numerical results are reported, for instance, in Ding and Tsang (2001) as well as Iliescu et al. (2003). With an LES based on a least-squares finite element method, Ding and Tsang (2001) simulate a flow at Reynolds number 3200 inside a cavity with SAR 1.0 and compare the

velocity profiles to the experimental data of Prasad and Koseff (1989). They use a relatively fine discretization of $60 \times 60 \times 60$ trilinear hexaeder elements with minimum element size being 0.005. As already mentioned in section 9.2.2, Iliescu et al. (2003) report the temporal evolution of the total kinetic energy for a calculation at a Reynolds number of 10000 in a cavity with SAR 1.0 applying $8 \times 8 \times 8$ elements with biquadratic velocity interpolation and discontinuous bilinear pressure interpolation. From the point of view of velocity degrees of freedom, this discretization is equivalent to $16 \times 16 \times 16$ trilinear hexaeder elements. The number of pressure degrees of freedom, however, is less than half with respect to the mesh employing $16 \times 16 \times 16$ trilinear hexaeder elements.

10.2.2 Setup for numerical simulations

Following the guidelines of Zang et al. (1993), the three Reynolds numbers 3200, 7500, and 10000 will be studied here as well. However, all three flows will be considered in a cavity with SAR 1.0, i.e. the 2-D cavity displayed in Fig. 9.8(a) will be stretched to unit length in the third coordinate direction. The no-slip boundary conditions for the velocity in x_2 -direction will be transferred to the velocity in x_3 -direction in a straightforward manner, and the pressure prescription will be put on at the same node as in the 2-D case. A relatively coarse basic discretization with $16 \times 16 \times 16$ trilinear hexaeder elements is chosen for all flow situations exhibiting linear refinement towards the walls in x_1 -direction and x_2 -direction with minimum element length of 0.02 in these directions. For the second and third level in the two- and three-level method, respectively, the same types of sub- and sub-submeshes already described in the introductory part of chapter 9 are applied. This overall choice of coarse discretizations on all three levels goes along with the predominant goal of investigating the performance of the considered methods with relatively coarse resolution provided by the chosen meshes.

Analog to what is done in Zang et al. (1993) and Iliescu et al. (2003), an impulsive start is performed, i.e. the initial condition is a zero velocity field. The Crank-Nicolson scheme, i.e. $\theta = 0.5$, is used for the temporal discretization with a time step $\delta t = 0.1$. A time scale T_{cav} is defined in Zang et al. (1993) to be the estimated time for a particle at the edge of the top boundary layer to travel back to its starting position in the cavity. This time scale is roughly estimated to be about 10 time units for the current calculations. Initially, the simulation is run for five time scales T_{cav} , i.e. 50 time units or 500 time steps. Within this time period, the flow is expected to develop to full extent including a subsequent relaxation time. Afterwards, statistics are collected for another five time scales T_{cav} .

10.2.3 Results

All results are compared to the experimental data of Prasad and Koseff (1989). Unfortunately, the experimental data for the flow at Reynolds number 7500 has only been evaluated for half of the cavity. The numerical simulations in Zang et al. (1993) have merely been performed for a cavity SAR of 0.5 for Reynolds numbers 7500 and 10000. Thus, a direct comparison with this numerical data is not feasible. The mean velocities $\langle u_1 \rangle$ and $\langle u_2 \rangle$ as a discrete time average according to (A.2) (see appendix A) are analyzed on the centerlines of the midplane at $x_3 = 0.5$. Furthermore, the root-mean-square values (square-root of the variance subject to (A.15)) for the velocities u_1 and u_2 as well as the component $\langle \tilde{u}_1 \tilde{u}_2 \rangle$ of the Reynolds stress tensor (4.12) are charted. The rms-values and the Reynolds stress components are multiplied by the amplification fac-

tors 10 and 500, respectively, in order to guarantee a reasonable visual impression of these values within the respective graphs. Additionally, the temporal evolution of the total kinetic energy subject to

$$E_{kin}(\mathbf{u}^h) = \frac{1}{2} \int_{\Omega} \mathbf{u}^h \cdot \mathbf{u}^h \, d\Omega \quad (10.1)$$

is depicted. Various methods are investigated. Firstly, a stabilized method of USFEM-type is applied. Secondly, the Smagorinsky model in the elementwise form (7.86) is employed on a PSPG finite element method. The Smagorinsky constant is fixed to be $C_S = 0.1$ and the element length \bar{h} is defined to be cubic root of the element volume, i.e. for the discretization at hand $\bar{h} = 1/16$. Thirdly, the two-level method and the three-level method with dynamic as well as 'static' modeling are utilized. For Reynolds numbers 3200 and 7500, the dynamic modeling procedure is applied, and the Smagorinsky model again with $C_S = 0.1$ as a 'static' way of modeling is applied for the flow at Reynolds number 10000. This last case may clearly exhibit differences between the application of the Smagorinsky model on level 2 and the application one level 'lower' on level 3.

Fig. 10.2 displays the temporal evolution of the total kinetic energy for all three cases. The introduction of various amounts of numerical viscosity bears an interesting consequence for the results in this example. It is physically well-known that the higher the physical viscosity of the flow the larger is the zone of influence of the prescribed velocity at the top boundary of cavity. Simply spoken, the higher the physical viscosity the larger the extensions of the layers at the respective boundaries of the cavity towards the center of the cavity. Here, this leads to the fact that the method which is supposed to introduce the highest amount of numerical viscosity also exhibits the highest values of the total kinetic energy throughout the simulation. This is to be observed for all three Reynolds numbers in Fig. 10.2. The three-level method and the USFEM bear about the same amount of numerical viscosity for Reynolds numbers 7500 and 10000 with the USFEM being more viscous in the case with the lowest Reynolds number 3200. The two-level method introduces the least numerical viscosity for every case under consideration. The discrepancy in this respect becomes quite substantial for higher Reynolds numbers.

Sample calculations variegating the Smagorinsky constant to higher and lower values have yielded higher and lower values of the total kinetic energy, respectively, as expected. Another simulation using the artificial viscosity (7.84) along with (7.85) yielded a stationary solution at a very high energy level after about 17 time units proving the enormous amount of numerical viscosity introduced by this approach. Furthermore, a test calculation with another definition of the element length \bar{h} , namely the streamlength, i.e. the length of the element in streamline direction, has led to substantially higher values of the total kinetic energy. These results for this element length definition, which is often used for the stability parameter calculation within stabilized methods, has to be expected, since it usually results in a larger element length \bar{h} than the one obtained as the cubic root of the element volume. This emphasizes the sensitivity of the results to the choice of the Smagorinsky constant as well as the element length definition. This has been analyzed by Zang et al. (1993) where they display the progression of the Smagorinsky constant obtai-

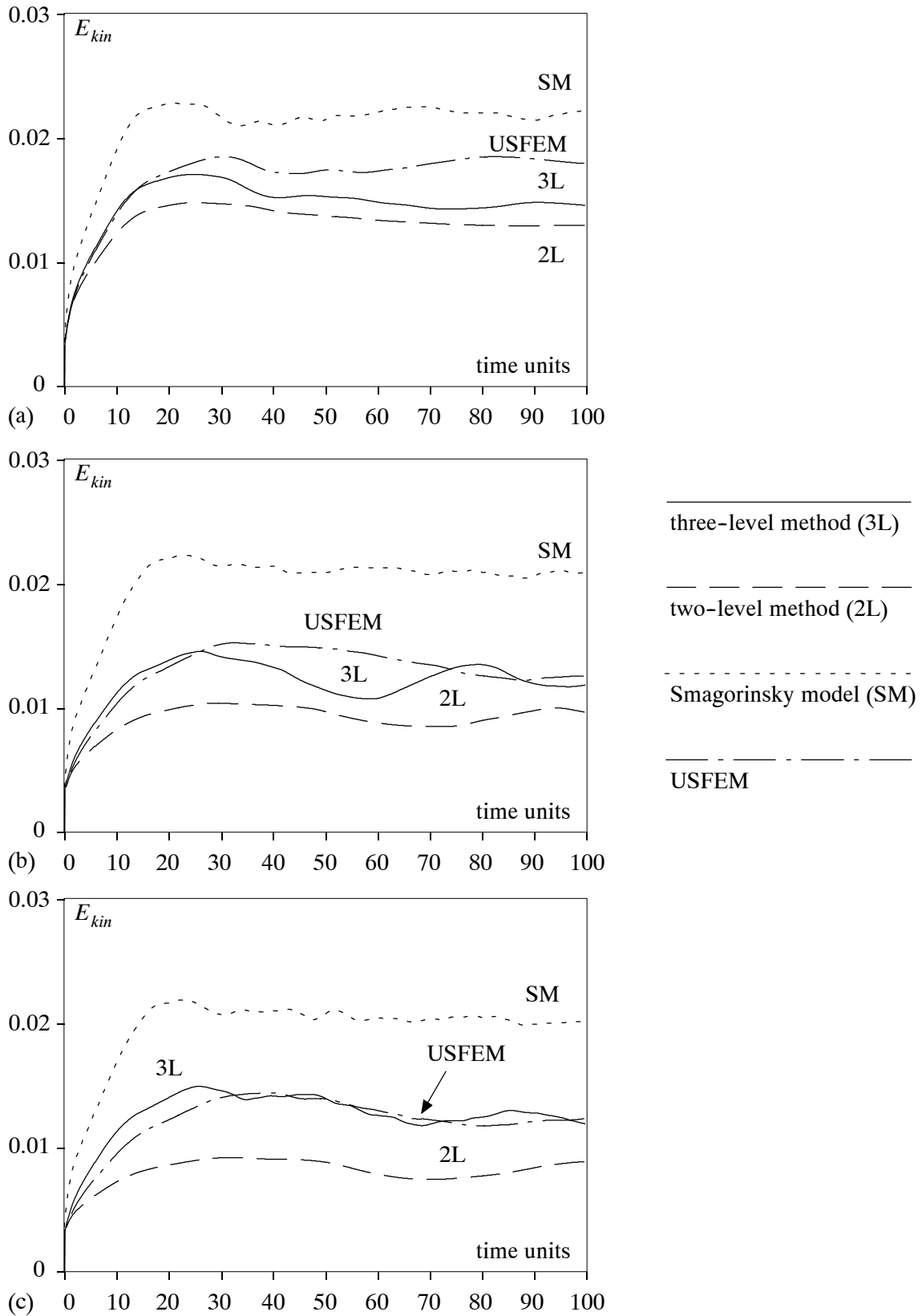


Fig. 10.2: Temporal evolution of total kinetic energy for: (a) $Re = 3200$; (b) $Re = 7500$; (c) $Re = 10000$

ned by the dynamic procedures DSM and DMM throughout the centerlines in the midplane. They have been able to show that C_S from DMM is nearly everywhere (except from from a few peaks) substantially smaller than 0.1. In comparison, DSM bears explicitly larger values.

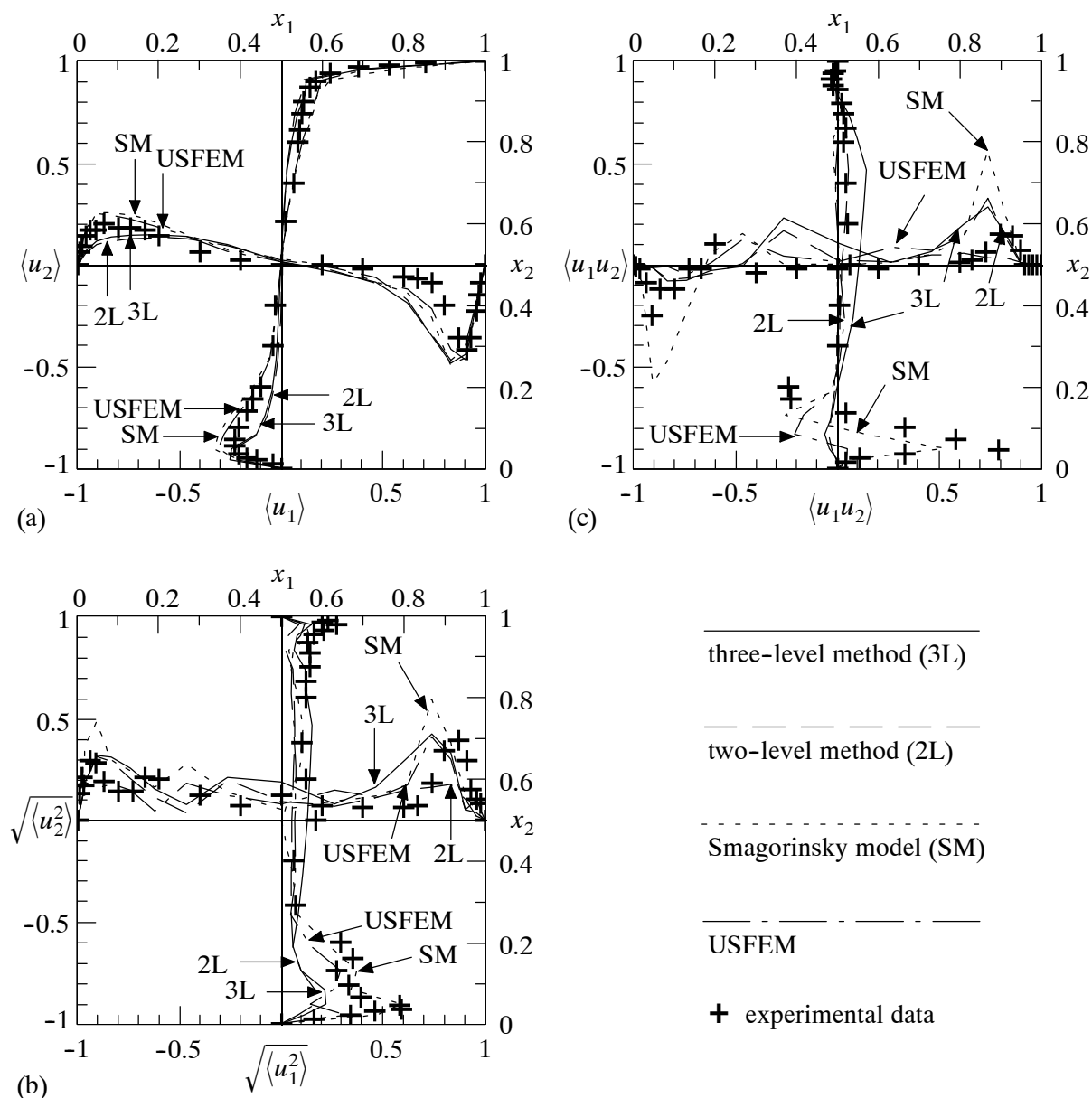


Fig. 10.3: Quantities on the centerlines in the midplane for $Re = 3200$ and SAR 1.0: (a) mean velocities; (b) rms velocities (factor 10); (c) Reynolds stress (factor 500)

Analyzing the profiles of the mean velocities $\langle u_1 \rangle$ and $\langle u_2 \rangle$ for the various cases in Figs. 10.3(a), 10.4(a), and 10.5(a), it may be stated that the USFEM as well as, in particular, the Galerkin method with the Smagorinsky model overpredict the velocity values and the two- as well as three-level method underestimates them (with one exception for $\langle u_2 \rangle$ at the right boundary) for Reynolds number 3200. For Reynolds numbers 7500 and 10000, the two- and, in particular, the three-level method show very good agreement with the experimental data even with the coarse basic discretization at hand. The Smagorinsky model as well as the USFEM still overestimate.

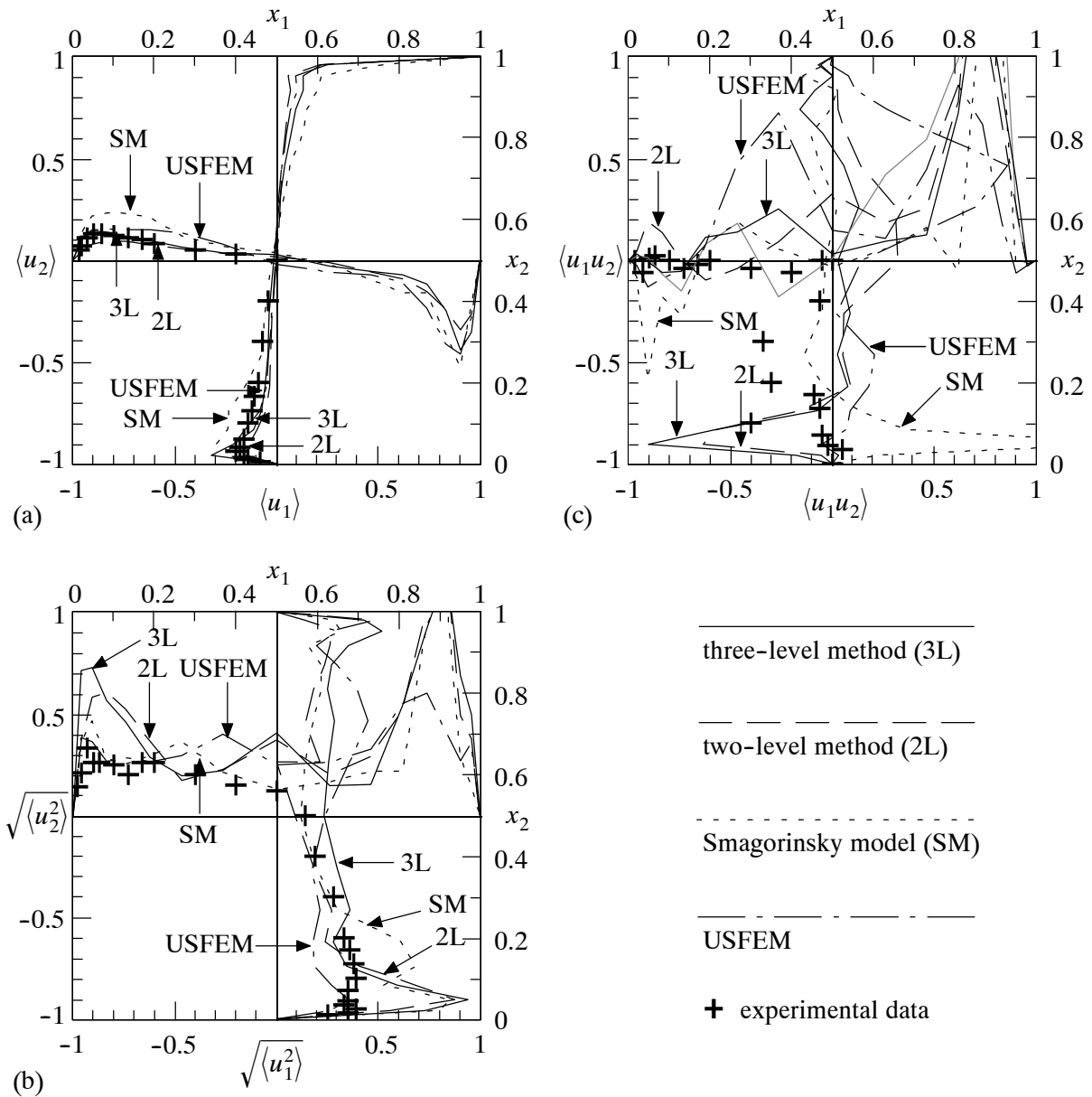


Fig. 10.4: Quantities on the centerlines in the midplane for $Re = 7500$ and SAR 1.0: (a) mean velocities; (b) rms velocities (factor 10); (c) Reynolds stress (factor 500)

This relatively good agreement cannot be maintained for the root-mean-square values and the components of the Reynolds stress particularly. The general tendency of the experimental curve for the root-mean-square values at Reynolds number 3200 in Fig. 10.3(b) can be reproduced by the various methods with the Smagorinsky model being the only method which, on the one hand, correctly predicts the lower peak of the vertical curve and, on the other hand, overpredicts both peaks of the horizontal curve. Similar observations, in a more distinct manner however, may be made for the Reynolds stresses in Fig. 10.3(c). It has to be emphasized that mispredictions of various peaks of these curves (although in a less distinct manner admittedly) may also be found in the numerical results of Zang et al. (1993) achieved with a two times finer discretization in every coordinate direction and even some slight deviations in the numerical results of Ding and Tsang (2001) obtained with the help of an almost four times finer discretization in every coordi-

nate direction. This underlines the difficulty in predicting these values. Aside from this, experimental uncertainties cannot be ruled out completely in this context either. In accordance with this, it has to be stated that the root-mean-square values in Figs. 10.4(b) and 10.5(b) partly as well as the Reynolds stresses in Figs. 10.4(c) and 10.5(c) for the most part, respectively, are not acceptable for all applied methods compared with the experimental data at hand. Probably, the basic discretization chosen here simply has to be viewed as being insufficient for a correct prediction of these extremely sensitive values. A finer discretization, possibly about two times in every direction at least, may be sufficient to obtain reasonable results also for the root-mean-square values and the Reynolds stresses.

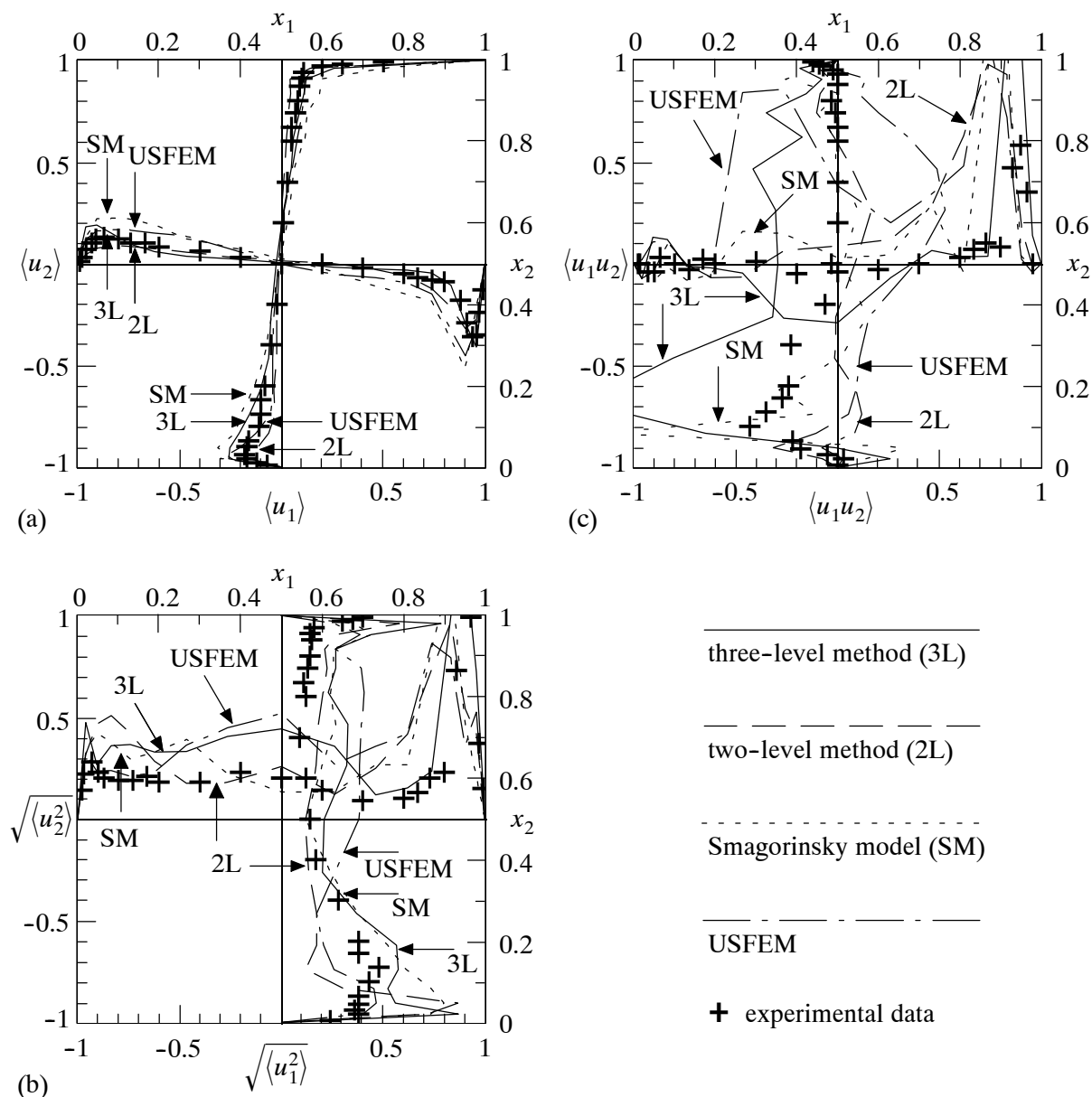


Fig. 10.5: Quantities on the centerlines in the midplane for $Re = 10000$ and $SAR = 1.0$: (a) mean velocities; (b) rms velocities (factor 10); (c) Reynolds stress (factor 500)

10.3 Plane mixing layer (2-D)

10.3.1 Problem description

The domain of the problem is defined to be $\Omega = [0, 1] \times [0, 1]$, see Fig. 10.6(a). No, i.e. free-slip, boundary conditions are applied at the boundaries $x_2 = 0$ as well as $x_2 = 1$ and periodic boundary conditions at the boundaries $x_1 = 0$ as well as $x_1 = 1$. The initial velocity field is given by a hyperbolic tangent profile reading

$$u_1(x_2) = u_{1,\max} \tanh\left(\frac{2x_2 - 1}{\delta_0}\right) \quad (10.2)$$

where δ_0 denotes the initial vorticity thickness, which will be defined in section 10.3.4. According to Boersma et al. (1997), δ_0 is chosen to be $1/28$. The velocity component u_2 is assumed to be zero initially. The initial velocity distribution (10.2) is displayed in Fig. 10.6(b).

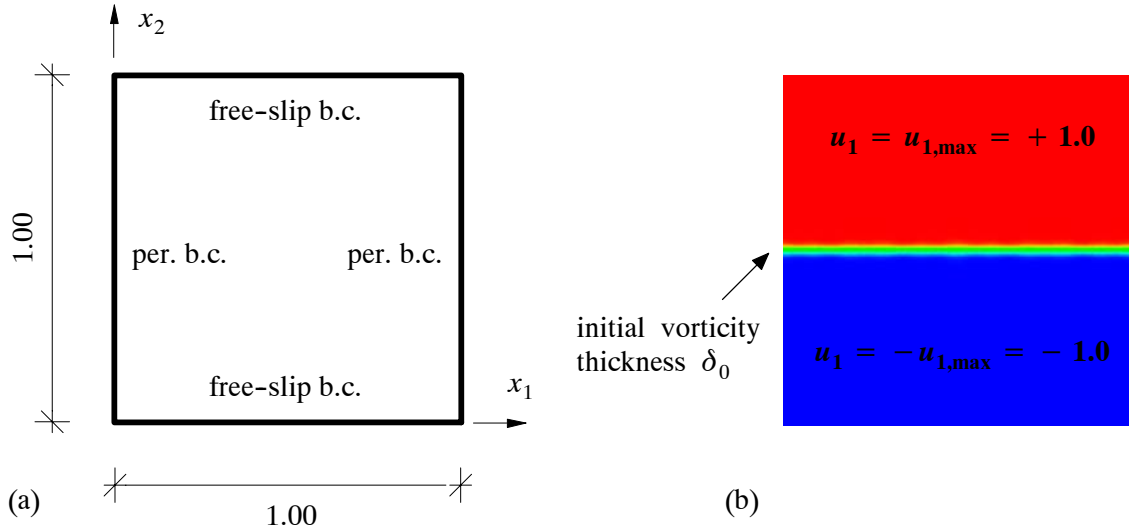


Fig. 10.6: Plane mixing layer: (a) domain with boundary conditions; (b) colored initial velocity distribution

A white-noise perturbation of small amplitude is imposed on the initial velocity field expressed in a streamfunction formulation as

$$\psi_{per} = c_{noise} u_{1,\max} e^{-\left(\frac{x_2 - 0.5}{\delta_0}\right)^2} \cos(\alpha x_1) \quad (10.3)$$

It may be proven by the reader that this perturbation is divergence-free. The corresponding wavenumber is $\alpha = 2\pi/\lambda$ with a wavelength λ . This random perturbation injects energy into all longitudinal spatial modes according to Lesieur et al. (1988) and should, therefore, reasonably approximate the case of a real mixing layer that is naturally submitted to a residual turbulence having a broadband spectrum. The small perturbation in the initial condition is expected to be amplified by so-called Kelvin-Helmholtz instabilities during the evolution of the flow. According to Michalke (1964), the most unstable wavelength λ_a is given by $\lambda_a = 7\delta_0$, i.e. $\lambda_a = 1/4$ in this case. The most amplified wavenumber is

$$\alpha_a = \frac{2\pi}{\lambda_a} = \frac{2\pi}{7\delta_0} = 8\pi \quad (10.4)$$

Thus, a number of n_{vort} Kelvin-Helmholtz vortices is expected to develop in the streamwise direction for a domain with length $l_s = 7\delta_0 n_{vort}$ in this direction. With unit length chosen here, 4 vortices will appear. As can be observed in (10.3), a deterministic sine perturbation is also imposed. This results in fixing the position of the Kelvin-Helmholtz vortices on the x_1 -axis. Otherwise, the vortices would take a randomly distributed position from one run to another, confer Lesieur et al. (1988). The sum of two waves with wavelength $\lambda_a = 1/4$ and a smaller wavelength $\lambda_a = 1/10$ are chosen according to Boersma et al. (1997). Consequently, the final velocity components including the perturbation are

$$u_{1,per}(x_2) = u_{1,max} \left[\tanh\left(\frac{2x_2 - 1}{\delta_0}\right) + c_{noise} \frac{\partial\psi_{per}}{\partial x_2} \right] \quad (10.5)$$

and

$$u_{2,per}(x_2) = -u_{1,max} c_{noise} \frac{\partial\psi_{per}}{\partial x_1} \quad (10.6)$$

where $u_{1,max}$ and c_{noise} are specified to be 1 and 10^{-3} , respectively. With these parameter specifications and a viscosity of $\nu = 3.571 \times 10^{-6}$ at hand, the Reynolds number of the problem amounts to be

$$Re = \frac{u_{1,max}\delta_0}{\nu} = 10000 \quad (10.7)$$

Furthermore, a non-dimensional time unit to be used later on is defined to be the actual time scaled by $\delta_0/u_{1,max} = 1/28$.

10.3.2 Relevance and earlier investigations

Mixing layers are encountered in aerodynamics, in the atmosphere or the ocean (e.g. in the wake of mountains, in the Gulf stream or in the Mediterranean sea), as well as in the atmospheres of Jupiter and Saturn (at the interface between neighboring zonal jets), confer Lesieur et al. (1988). It is actually a flow developing far away from boundaries, and the influence of boundaries is eliminated in this example thus. As an answer to potential objections that a two-dimensional flow will not lead to what is usually perceived as 'turbulence', the following features of the flow considering it to be 'turbulent in a certain sense' have to be returned (consult Lesieur et al. (1988)):

- The flow is extremely sensitive to the initial condition. In fact, it would be completely unpredictable in an infinite domain. This has been proven by investigating two flows which were very close in the relevant parameters initially. In an infinite domain, they would show a complete decorrelation. Only the finite domain, which has to be chosen for the simulation being viable, 'prevents' the flow from being completely unpredictable.
- After a first pairing (to be described in the subsequent section), a broadband energy spectrum of slope intermediate between k^{-4} and k^{-3} is developed. The interaction between two- and three-dimensional turbulence related to this flow situation has been elaborated in Lesieur et al. (1988), section 4.

The mixing layer has been investigated experimentally, for instance, in Brown and Roshko (1974) as well as Winant and Browand (1974). A review of this type of flows is given in Ho and Huerre (1984). Numerically, it has been thoroughly analyzed in a quasi-DNS applying a second-order finite difference method on a 256x256 grid by Lesieur et al. (1988). Further numerical studies may be found in Boersma et al. (1997), Griebel and Koster (2000), John (2002a, 2002c), and Nägele and Wittum (2002). The corresponding three-dimensional case has been analyzed numerically by Balaras et al. (2001) as well as Rogers and Moser (1994).

10.3.3 Physical evolution of the flow

The physical evolution of the flow will be explained with the help of Fig. 10.7. This picture series has been obtained from a simulation using the basic method, which will be described in section 10.3.6, with 160x160 elements. The flow situations at non-dimensional time 10, 20, 30, 40, 70, 100, 110, 120 and 200 are displayed. Four different stages of this flow may be distinguished:

- **Development of four primary eddies:** The distinct appearance of the four primary eddies can be observed at about 15 time units. This corresponds to the time also observed by Lesieur et al. (1988) for the development to occur. John (2002a, 2002c) found a later development at 30 time units.
- **First pairing:** The first pairing takes place at about 35 time units. Again, this compares exactly to the point in time noticed by Lesieur et al. (1988). The later pairing in the simulation of John (2002a, 2002c) at about 80 time units went on in a non-symmetric procedure, i.e. one pairing started earlier than the other. Here, both pairings occur at the same time.
- **Second pairing:** The second pairing is finished at about 115 time units. This is a later point in time in comparison to Lesieur et al. (1988) (75 time units) as well as an earlier one in comparison to John (2002a, 2002c) (140 time units).
- **Rotation of the final vortex:** After the end of the second pairing the final vortex rotates at a fixed position. The value of the vorticity thickness oscillates during this stage due to the elliptic shape of this vortex, confer Fig. 10.8.

10.3.4 Measured values

Four aspects of the flow are recorded quantitatively: the mean velocity $\langle u_1 \rangle$, the root-mean-square value of the velocity u_1 , the total kinetic energy and the vorticity thickness. The mean velocity $\langle u_1 \rangle$ at every node is evaluated as a discrete time average according to (A.2) over the complete simulation time. In addition, these nodal values are spatially averaged along the periodic x_1 -direction, in order to achieve a final velocity profile along the x_2 -direction. The respective root-mean-square value is evaluated during this averaging procedure. The total kinetic energy has already been defined in (10.1), and this definition is applied here again for the quantification of the temporal evolution of the energy. In principal, an evolution exhibiting a somehow decaying total amount of kinetic energy has to be expected, since the initial velocity distribution is subject to a non-zero viscosity, and no additional energy input is provided.

According to the general definition of the vorticity vector (2.8), the scalar vorticity in the 2-D case reads

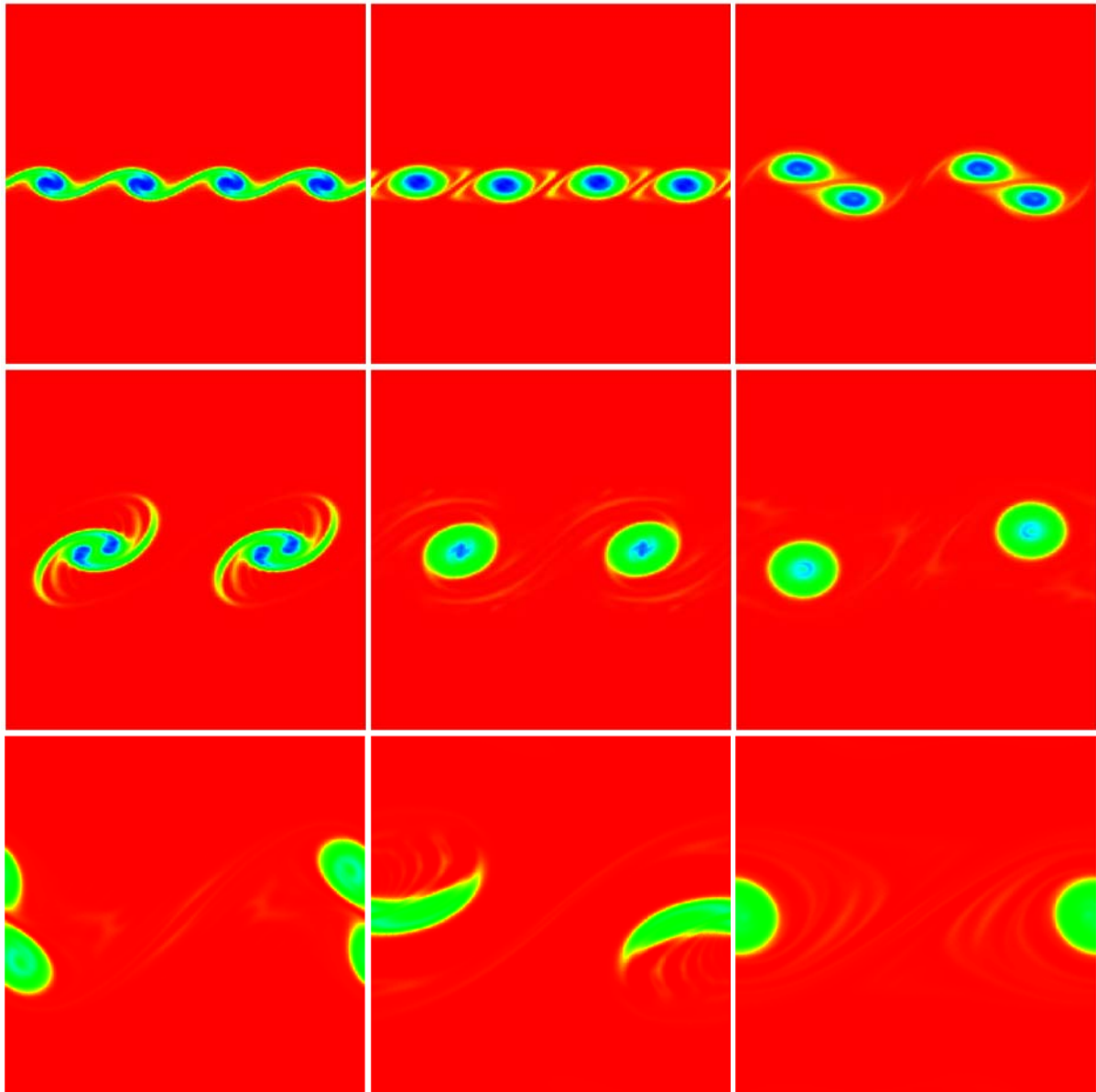


Fig. 10.7: Colored vorticity field (blue: intense vorticity, red: irrotational outer flow) at time units 10, 20, 30, 40, 70, 100, 110, 120, 200 (left to right, top to bottom)

$$\omega = \frac{1}{2} \left(\frac{\partial u_2}{\partial x_1} - \frac{\partial u_1}{\partial x_2} \right) \quad (10.8)$$

Nägele and Wittum (2002) define the maximum value of ω as

$$\omega_{\max}(t) = \sup_{x_2 \in [0,1]} | \langle \omega \rangle (x_2, t) | \quad (10.9)$$

where $\langle \omega \rangle (x_2, t)$ denotes the integral mean in the periodic x_1 -direction reading

$$\langle \omega \rangle (x_2, t) = \frac{\int_0^1 \omega(x_1, x_2, t) dx_1}{\int_0^1 dx_1} = \int_0^1 \omega(x_1, x_2, t) dx_1 \quad (10.10)$$

In the practical computation, this integral is evaluated discretely for all mesh lines parallel to the x_1 -axis (confer John (2002a, 2002c)) and the maximum of these results is employed for ω_{\max} . With this maximum value of ω at hand, the vorticity thickness δ is defined to be

$$\delta(t) = \frac{\Delta u_{ml}}{\omega_{\max}(t)} = \frac{2u_{1,\max}}{\omega_{\max}(t)} \quad (10.11)$$

with Δu_{ml} indicating the velocity jump across the mixing layer. The initial value for the vorticity thickness corresponding to the undisturbed velocity distribution has already been chosen to be $\delta(t = 0) = \delta_0 = 1/28$. All values $t > 0$ are scaled by this initial value δ_0 . A principal sketch of the temporal evolution is displayed in Fig. 10.8 related to the calculation displayed in Fig. 10.7. The particular stages of the respective flow characterized in the preceding section may be discovered in this course. The maximum values of the vorticity thickness at the first and second pairing are slightly higher than the comparable values in Lesieur et al. (1988) and John (2002a, 2002c).

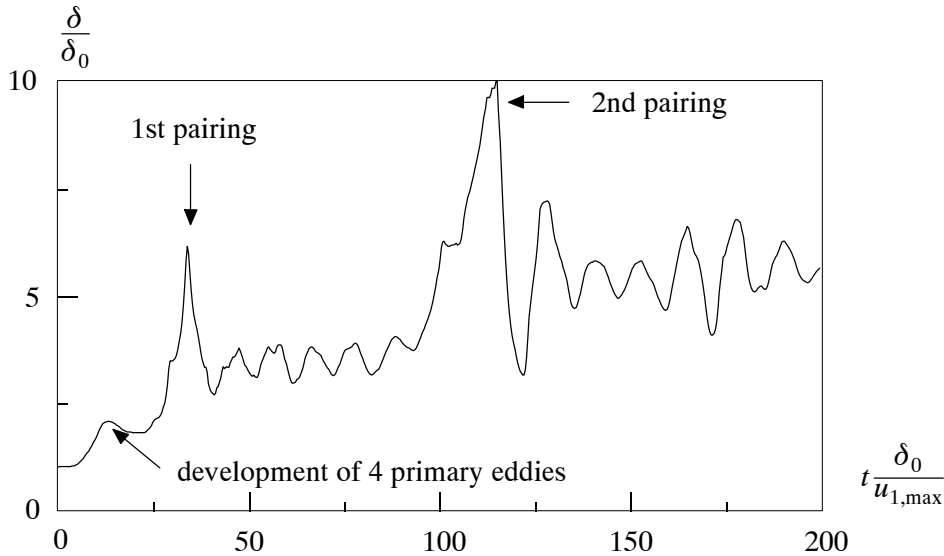


Fig. 10.8: Principal sketch of temporal evolution of vorticity thickness (cf. Fig. 10.7)

10.3.5 Spatial and temporal discretization

For the previously described flow at Reynolds number 10000, basic discretizations with 40x40, 80x80, 160x160, and 240x240 bilinear quadrilateral elements of uniform length have been chosen, respectively. The sub- and sub-submeshes are created as in the previous examples. With the 240x240 mesh, the resolution level of the quasi-DNS by Lesieur et al. (1988) is almost re-

ached. Boersma et al. (1997), among other things, have applied local grid refinement up to this level only in the middle part of the flow domain starting from an initial 80×80 discretization. John (2002a, 2002c) reached even further than Lesieur et al. (1988) by using elements employing bi-quadratic velocity interpolation and discontinuous bilinear pressure interpolation for his DNS. The resolution level is comparable up to 1024×1024 purely bilinear elements with respect to the number of velocity degrees of freedom (about 2 million). The number of pressure degrees of freedom is considerably lower for this type of elements and resolution level in comparison to equal-order interpolated bilinear quadrilaterals.

Starting with the perturbed initial velocity field (10.5)-(10.6), the Crank-Nicolson scheme with $\theta = 0.5$ is used for the temporal discretization with a time step $\delta t = 0.35\delta_0/u_{1,\max} = 0.0125$. 570 time steps are performed resulting in an overall simulation time of approximately 200 non-dimensional time units. Statistics are collected during the complete simulation time.

10.3.6 Results

Various methods are investigated. Firstly, a basic method will be defined. Secondly, the Smagorinsky model already used for the previous example is applied, i.e. the Smagorinsky constant is again chosen to be $C_S = 0.1$. Thirdly, the two-level method as well as the three-level method with dynamic modeling are utilized.

A first attempt to define a 'pure' PSPG finite element method to be the basic method for the following investigations failed even for the finest discretization (240×240). An immediate energy blow-up has been observed for this method with every discretization. This concurs with impressions received by studying the aforementioned literature dealing with this flow example. Even Lesieur et al. (1988) added a biharmonic dissipative term to their formulation applied to a 256×256 grid. (By the way, this explains the here used marking 'quasi-DNS' for this simulation.) Boersma et al. (1997) incorporated a Smagorinsky term with $C_S = 0.1$ in the method applied on their finest grid with 240×240 grid points. John (2002a, 2002c) mentions explicitly an energy blow-up for a simulation without any additional dissipative term on a discretization level roughly comparable to a 128×128 mesh. According to the conclusion that it is not possible to perform a DNS with the underlying discretizations, an additional dissipative term has to be incorporated into the PSPG finite element method. Deviating from the frequent use of the Smagorinsky model, an alternative in form of the bulk viscosity term is employed here. The obvious analogy of this term in comparison to the Smagorinsky term may be identified by analyzing them (The reader may just compare the first term in the second line of (7.77) with the second term in first line of (7.87)). With this supplementary term at hand, a reasonable basic method can be defined.

In Fig. 10.9, the results for simulations with this basic method on the various discretization levels are displayed. Fig. 10.9(a) shows that the mean velocity profiles achieved with the help of the different discretizations are fairly close together. The curves for the root-mean-values displayed in Fig. 10.9(b) uncover the expected differences for the various resolution levels more distinctly. Concerning the temporal evolution of the total kinetic energy depicted in Fig. 10.9(c), it may simply be stated that the lower the resolution level the higher the overall energy loss, i.e. the more dissipative is the method. An interesting observation may be made by analyzing the temporal evolution of the vorticity thickness in Fig. 10.9(d). The results for the 240×240 mesh and the 160×160 mesh almost coincide. However, the character of the curve is substantially mo-

dified for the coarser discretizations. In particular, it may be observed that the coarser the discretization the later the point in time indicating the first pairing and, simultaneously, the sooner the second pairing. Furthermore, the actual values of the various amplitudes also show up quite differently. It may be concluded that the chosen discretization level has a considerable influence on the temporal development of the vorticity thickness and, hence, on the character of the flow.

The same conclusion may be drawn, if various methods on the same resolution level are investigated instead of one method on various discretizations. Fig. 10.10(d) shows the temporal evolution of the vorticity thickness for the aforementioned four methods applied to a basic discretization with 40×40 elements. The basic method and the Smagorinsky model are fairly close together which may be justified by their inherent similarity. Despite the small difference in the method however, both curves may be distinguished precisely. The difference to the two- and three-level method is evident, and even the one between both multi-level methods. In particular, the last episode of the simulated flow exhibits interesting varieties. Whereas the final vortex in the simulation using the basic method reveals a slightly elliptic character (confer e.g. the last picture of the series in Fig. 10.7), the two-level method, on the one hand, produces an almost circularly shaped final vortex and the three-level method, on the other hand, bears a more distinctly elliptic vortex at the end of the simulation. This is indicated by the amplitude of the oscillations in the temporal evolution of the vorticity thickness during the final stage of the flow. It has been possible to verify by suitable calculations that the specified general tendency is not changed by using, for instance, a two-level method with a finer 8×8 submesh or a three-level method with various 'static' ways of modeling. By observing the velocity profiles in Figs. 10.10(a) and 10.10(b), it may be concluded that the two-level method fails to produce reasonable results at this Reynolds number. Particularly, the overshoots in the left as well as the right section of the curve for the mean velocity in Fig. 10.10(a) produce evidence for this conclusion. Finally, the temporal evolution of the energy depicted in Fig. 10.10(c) indicates that the two- and three-level method are less dissipative than the basic method and the Smagorinsky model is (not surprisingly) the most dissipative method of all.

A final remark has to be made concerning the stabilized method of USFEM-type for this particular flow example. The reader might have wondered at the neglect of this method during the report of the results. There is a definite and fatal reason for this disregard, see Fig. 10.11. For every discretization, an energy blow-up has been observed approximately around the occurrence of the second pairing. Comparing the USFEM-type method to the basic method introduced before, it may be concluded that for the employed bilinear elements the only major difference between these two methods consists in the convective stabilization term, i.e., alternatively expressed, the classical SUPG-term introducing a certain amount of dissipation in the streamline direction. Further investigations have revealed that the zone of influence where this energy blow-up emerges can be restricted to the vicinity of the upper and lower (free-slip) boundary. In particular, a sinusoidal perturbation with small amplitude on top of the actually constant velocity distribution of (absolute) unit value along the upper and lower boundary arises around the time of the second pairing. The amplitude is quickly amplified provoking the drastic energy blow-up in Fig. 10.11 and causing the simulation to break down finally. This issue is not pursued further, since the main focus of this work is not on improving stabilized methods, and, thus, it is also refrained from disturbing the reader by putting the author's speculative point of view. It is, however, interesting to note that this problem has not been observed for the two- and three-level method despite the close affinity between the USFEM and the multi-level finite element methods.

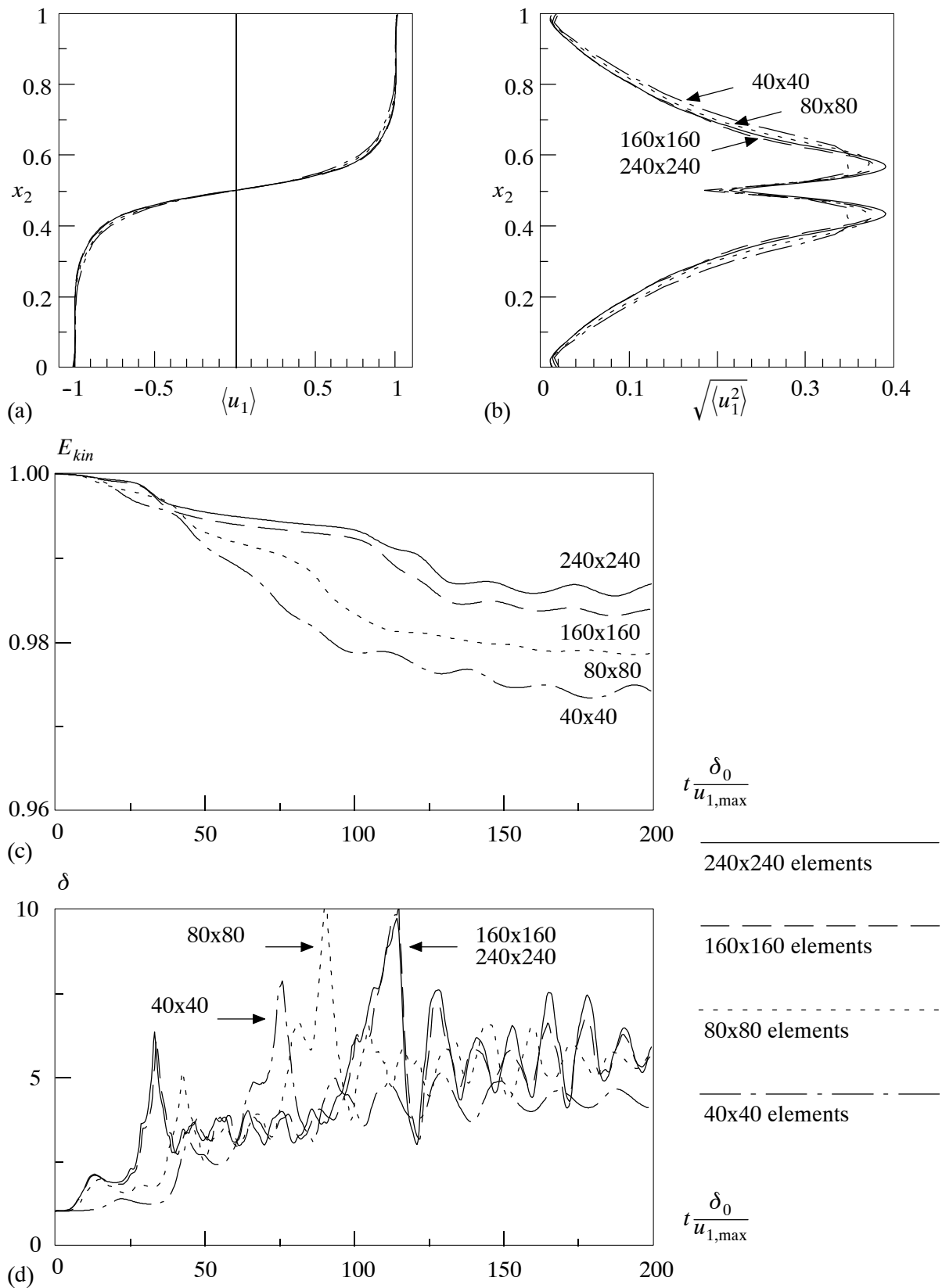


Fig. 10.9: Various discretizations for the basic method: (a) mean velocities; (b) rms velocities; (c) total kinetic energy; (d) vorticity thickness

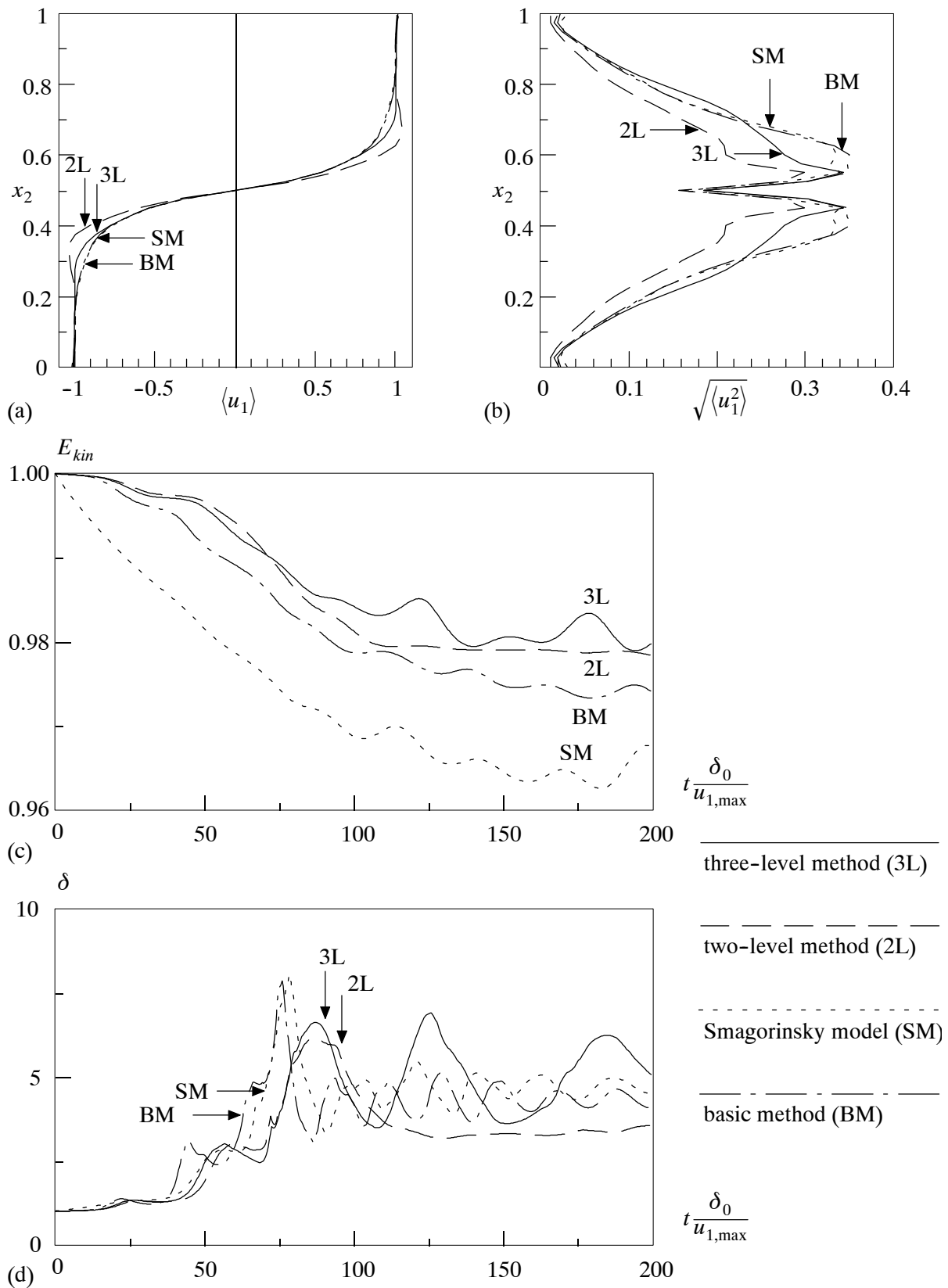


Fig. 10.10: Various methods on a basic discretization with 40x40 elements: (a) mean velocities; (b) rms velocities; (c) total kinetic energy; (d) vorticity thickness

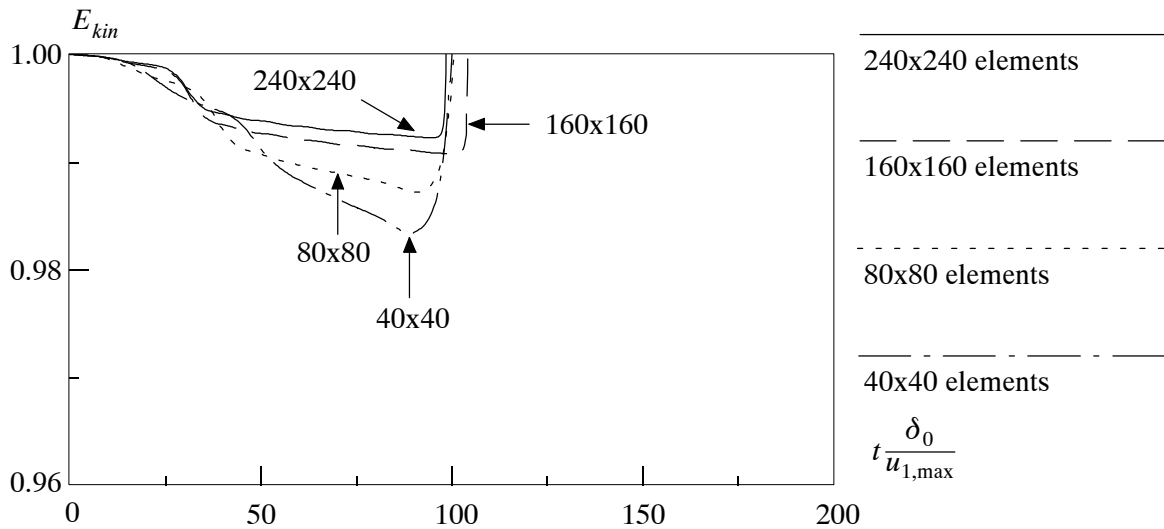


Fig. 10.11: Evolution of the total kinetic energy for the USFEM on various discretizations

10.4 Remark concerning computational cost of the applied methods

An important last remark has to be made concerning the computational cost of the two- and the three-level method on the one hand and the stabilized method of USFEM-type on the other hand. This can be dealt with in few words. It is unambiguous that the two- as well as the three-level method are by no means on a competitive basis with the stabilized method from the point of view of computational cost. Depending on the respective example, it roughly comes down to a factor of 5 up to about 10 for the 2-D flow examples (and a considerably higher factor for the 3-D flow examples) which the cost for the two- and three-level method can be set in proportion to the cost of the stabilized method on one processor. Definitely, this depends on a lot of parameters of the multi-level methods, in particular the chosen submesh and sub-submesh, respectively, on every element domain. Furthermore, the choice of quasi-static bubble functions, for example, diminishes the computational expenses considerably. Comparing the two-level method to the three-level method in the versions used in the numerical examples in chapters 9 and 10, it may be stated that the three-level method with $3 \times 3(x3)$ submesh and $4 \times 4(x4)$ sub-submesh requires less computational effort than the two-level method with $4 \times 4(x4)$ submesh. The savings become substantial for the 3-D examples in particular. Of course, the 'end of the road' for the multi-level methods is not reached yet, since there is still some room for increasing computational efficiency with regard to all major parts of the method. In particular, the use of multi-processor machines is extremely favorable for the calculations on the second and third level of the multi-level finite element methods. The procedure on these lower levels is almost completely parallel. Thus, substantial gain may be achieved by using a high number of processors. Unambiguous in almost the same manner however, it is essential to admit that the multi-level methods will probably not ever overtake the stabilized methods in matters of computational cost.

11 Summary and Outlook

11.1 The past (of this work) ...

The contents of this work have aimed at three issues: the development of a general framework, the specific implementation of a method based on the preceding general development, and an extensive test program for this method in form of numerical examples for laminar and turbulent flow situations.

The variational multiscale method has been utilized for the purpose of providing the methodological background for the general framework. For the linear model problem of a scalar convection-diffusion-reaction equation, the enormous potential of the variational multiscale method as a starting point for various solution strategies has been exposed and some solution strategies have been suggested. The transition to the more complicated problem of the nonlinear set of incompressible Navier-Stokes equations has been performed and two of the solution strategies, a global and a local one, have been picked up again seeming to be reasonable approaches for the Navier-Stokes problem as well. These considerations are valid for the incompressible Navier-Stokes equations in general. However, additional considerations have to be taken into account as soon as the challenging phenomenon of turbulent flow regimes is encountered. As a starting point for these particular considerations, the classical procedures of Direct Numerical Simulation (DNS) and Large Eddy Simulation (LES) have been adapted to the numerical method of choice in this work, the Galerkin finite element method, in a straightforward manner. Afterwards, particular attention has been paid to the retrospective interpretation of the basic DNS and LES procedures within the framework of the variational multiscale method. It was, in fact, possible to identify these classical approach as special cases of the variational multiscale method. Moreover, the variational multiscale method gives rise to further approaches going beyond this. In particular, the core version of the variational multiscale method consisting in a separation of two scales has been extended to a separation of three scales. This three-scale separation represents the general framework matching the first goal of this work.

In order to meet the second claim of this work, i.e. a practical method based on this general framework, a three-level finite element method has been developed. The major focus of this practical method had to be on computational efficiency due to the limitations with respect to available computer resources. Therefore, the local approximation in form of residual-free bubbles has been exploited as a first approach. The name of the method especially accounts for three different types of discretizations linked with the respective levels. Starting with a basic discretization (level 1), submeshes (level 2) are introduced on each element of this basic mesh. These two levels constitute a two-level finite element method for the time being, which has been tested in numerical examples. With the help of these submeshes, approximate solutions for residual-free bubbles on these elements are pursued. Particular attention has also been paid to the adequate consideration of the continuity condition on level 2. The proposed three-level method is not achieved until a third level is introduced. The simple introduction of stabilizing terms or dissipative models on the second level has been identified as a 'static' way of exhibiting a third level. Beyond this simple approach, a dynamic way of modeling the still unresolved scales of the problem is proposed as the manifestation of third level. According to this, a third type of discretization, namely ele-

mentwise sub-submeshes, i.e. slightly refined submeshes with regard to the submeshes on the second level, is employed into the method.

The previously described two- and three-level finite element method as well as a well-established and inherently linked stabilized method (USFEM) were tested for several flow situations. It was possible to show that these methods work in various arrangements, i.e., for example, with element interpolations of lower and higher order on the first and second level as well as with various models on each level. Analyzing the performance of these methods for the sample flows chosen in this work, some final conclusions may be drawn. The two-level method may be judged as being a reasonable method for flows at low and moderate Reynolds number, but it mostly fails for higher Reynolds number flows. Thus, it does not seem to be well-suited for turbulent flows in particular. As soon as the Reynolds number becomes higher, the introduction of a third level is inevitable. The three-level method with dynamic modeling on the third level has yielded excellent results for laminar flows even at high Reynolds number. A final judgement concerning the performance of this method for turbulent flows is not advisable based on the two examples in this work in the author's point of view. These two sample flows have been investigated here with very coarse basic discretizations, i.e. up to a factor of about 6 in comparison with analog calculations reported in the literature. Nevertheless, this 'coarse' modus operandi has already brought to light the limitations for these methods based on residual-free bubbles. In the author's opinion, the severe assumption of 'cutting' all inter-element connections by using elementwise solutions on levels 2 and 3 clearly limits the applicability to turbulent flows. This issue will be further addressed in the next section. The stabilized method of USFEM-type has also yielded good results for laminar flows at low and high Reynolds number with some minor deficits in view of accuracy compared to the multi-level methods. However, the stabilized methods are certainly equipped with the crucial advantage of providing substantial computational savings in comparison to the multi-level methods. In the context of turbulent flows, the results of the sample flows in this work seem to indicate that the limitations of the stabilized methods outcrop even more distinct casting a reasonable application of these methods into doubt for the time being. This is not surprising, since stabilized methods suffer from the same 'localization problem' as the residual-free bubbles in even stronger occurrence due to the crucial additional approximation expressing itself in the notorious algebraic parameter.

11.2 ... and the future (beyond this work)?

The variational multiscale method basically offers an enormous potential for providing a methodological framework for the numerical simulation of turbulent flows from the author's point of view. Nevertheless, the main object of concern linked with the particular implementation in form of the proposed methods of this work, the two- and three-level finite element method, has already been activated in the preceding section. The use of residual-free bubbles with assumed zero Dirichlet boundary conditions on the element boundaries most likely has to be 'credited' for most of the shortcomings of the multi-level methods. Aside from this, the multi-level methods are still open to improvements in various places. In particular, the dynamic procedure on the third level which is initially based on some crude approximations still invites to some further considerations. Even with substantial improvements, the aforementioned main drawback of the multi-level methods in the chosen characteristic remains and needs some further investigation, especially for the application to turbulent flow situations. Apart from this, a somehow localized

approach on the second level seems to be adequate for turbulent flow simulations in the author's opinion. This is mainly due to the perceptions of section 4.3 where it has been shown that the addressed two-point correlations show, in principal, substantial significance only over a finite sector of the domain. The crucial measure in this context is the integral length scale and its relation to the length of the domain both depending on the respective flow situation. The very tough localization procedure used here for the time being and resulting in a restriction to individual elements surely exceeds the tolerable degree of localization by far. However, a strategy ranging between this 'extreme' localization on the one hand and a completely global concept potentially demanding enormous computer resources on the other hand seems to be a very attractive approach to the author's mind.

Some potential alternatives which may be pursued in the future have already been pointed out in section 8.4. It remains to be proven if the addressed improvement of the residual-free bubble strategy may extend its success in the context of diffusion-reaction equations also to problems with dominating convective terms. Casting doubts on this is probably not completely devious. Aside from this, two alternative implementations for the complete procedure, i.e. also concerning the large-scale solution, have also been proposed. First results with one of these two approaches, namely the discontinuous Galerkin method, have already been reported by another author (Scott Collis). Aside from the particular choice of the method from the point of view of approximation strategy, the important topic addressing the absolute and relative choice of large- and small-scale spaces discussed at the end of section 8.2 is named here again for emphasis. Being a crucial parameter of the method, this selection demands careful and intensive future study from the author's point of view. Further improvements are surely necessary from the point of view of subgrid-scale modeling as well. Here, it may be reverted to the achievements which have already been made for the 'classical' ways of performing LES.

Altogether, it may be stated that the 'field' in form of the variational mutiscale method is existing; it has to be 'cultivated' now. For this purpose, the 'agricultural implements' in form of further reasonable practical methods have to be developed. It is safe to say that this will not be an easy exercise. As in the beginning, Peter Bradshaw, whom the author admires as a valuable source of quotable statements, is granted to articulate a word of caution marking the termination of this work: "*The user of a turbulence model is more like a test pilot than a sunny Sunday Cessna flier*" (Bradshaw (1998)). The author thinks that nothing remains to be added at this point to this statement in principle; it may rather be extended to any kind of modeling process performed afore and in the future - and, thus, **this** work has reached its very end. Contemporaneously, it opens the stage to successive endeavors.

Appendix A Some measures for the statistical description of turbulence

At first, three different ways of averaging are presented. It is important to keep in mind that either way of averaging provides us with an estimation of the mean value $\langle v \rangle$ of some variable v . It cannot be measured with certainty. Afterwards, the alternative definition of the mean value $\langle v \rangle$ by using its probability density function (PDF) is introduced. Given an underlying theoretical analysis of the respective PDF, the mean value $\langle v \rangle$ may be estimated with some level of confidence, but also not with certainty. The introduction of the PDF will also be exploited to define important higher-order moments of statistics besides the first-order moment 'mean value'. Furthergoing studies of basics of statistics may be done in special literature dealing with this topic or in the respective chapters in most of the books on turbulence mentioned in the introductory part of chapter 4.

A.1 Reynolds averaging

In order to get a mean value of, for instance, the velocity in the first coordinate direction u_1 three different ways of averaging are conceivable. First of all, the most general way of averaging is **ensemble averaging** by taking into account the measurements from N identical experiments or numerical simulations. With the n^{th} result for the velocity denoted u_1^n , the ensemble average $\langle u_1 \rangle^E(\mathbf{x}, t)$ is obtained as

$$\langle u_1 \rangle^E(\mathbf{x}, t) = \lim_{N \rightarrow \infty} \frac{1}{N} \sum_{n=1}^N u_1^n(\mathbf{x}, t) \quad (\text{A.1})$$

For stationary turbulence, **time averaging** is an appropriate procedure. The time average $\langle u_1 \rangle^T(\mathbf{x})$ starting at some time t is defined as

$$\langle u_1 \rangle^T(\mathbf{x}) = \lim_{T \rightarrow \infty} \frac{1}{T} \int_t^{t+T} u_1(\mathbf{x}, t) dt \quad (\text{A.2})$$

For discrete methods in time, the integral may be replaced by a summation over the discrete time steps. Strictly speaking, time averaging is only valid for stationary turbulence leaving behind a mean value $\langle u_1 \rangle^T(\mathbf{x})$ depending only on the spatial location. Stationary turbulence in this context means

$$\frac{\partial \langle u_1^T \rangle(\mathbf{x})}{\partial t} = 0 \quad (\text{A.3})$$

For slowly varying mean flow, one may, more generally, consider the temporal dependence in $\langle u_1 \rangle^T(\mathbf{x}, t)$, if the time scale of the mean flow does not interact with the time scale of the fluctuations. For problems with this procedure, please confer Wilcox (1998). Most turbulent flows being of engineering interest, in particular the ones considered in this work, fulfill condition (A.3) approximately.

Independently of this, **spatial averaging** may be performed over one or more homogeneous directions if there are any. A completely homogeneous flow, for example, allows for spatial avera-

ging over all coordinate directions representing a volume V yielding the spatial average $\langle u_1 \rangle^S(t)$ as

$$\langle u_1 \rangle^S(t) = \lim_{V \rightarrow \infty} \frac{1}{V} \int \int \int_V u_1(\mathbf{x}, t) dV \quad (\text{A.4})$$

According to the ergodic hypothesis, all three averages $\langle u_1 \rangle^E$, $\langle u_1 \rangle^T$ and $\langle u_1 \rangle^S$ are equal for flows being stationary and homogeneous in all spatial directions.

A.2 Probability density function

The probability of an event E assuming, for example, the velocity u_1 being smaller than a defined velocity, say, $u_a = 5$ m/s reads

$$p = P(E) = P\{u_1 < u_a\} \quad (\text{A.5})$$

Here, p is a real number in the range between 0 and 1. The cumulative distribution function defined as

$$CDF(u_a) = P\{u_1 < u_a\} \quad (\text{A.6})$$

determines the probability of any event with the limits $CDF(-\infty) = 0$ and $CDF(+\infty) = 1$ as well as the important property of non-decrease subject to

$$CDF(u_b) \geq CDF(u_a) \quad (\text{A.7})$$

for $u_b \geq u_a$. The probability density function is defined to be the derivative of the CDF subject to

$$PDF(u) = \frac{dCDF(u)}{du} \quad (\text{A.8})$$

satisfying the conditions

$$\int_{-\infty}^{+\infty} PDF(u) du = 1 \quad (\text{A.9})$$

and $PDF(-\infty) = PDF(+\infty) = 0$. This function defines the probability of u_1 having its value between two defined velocities u_a and u_b as

$$P\{u_a \leq u_1 < u_b\} = CDF(u_b) - CDF(u_a) = \int_{u_a}^{u_b} PDF(u_1) du \quad (\text{A.10})$$

Using the PDF , the mean value of u_1 now reads

$$\langle u_1 \rangle = \int_{-\infty}^{+\infty} u_1 PDF(u_1) du \quad (\text{A.11})$$

This mean value may be interpreted as the probability-weighted average of all possible values of u_1 .

A.3 Higher-order moments of statistics

Applying the Reynolds decomposition to the variable u_1 subject to

$$u_1 = \langle u_1 \rangle + \tilde{u}_1 \quad (\text{A.12})$$

the fluctuating part \tilde{u}_1 may be extracted with

$$\langle \tilde{u}_1 \rangle = 0 \quad (\text{A.13})$$

By shifting the *PDF* of u_1 over the distance of the mean value $\langle u_1 \rangle$ along the u_1 -axis, the *PDF* of the fluctuating part \tilde{u}_1 is created. The moments formed with the fluctuating part and its *PDF* are termed central moments. To be sure, the first central moment of \tilde{u}_1 analog to (A.11) is zero. The n^{th} -order central moment in general form reads

$$\langle \tilde{u}_1^n \rangle = \int_{-\infty}^{+\infty} \tilde{u}_1 \text{PDF}^n(\tilde{u}_1) du \quad (\text{A.14})$$

The second-order central moment is called variance, and its square root is termed standard deviation or root mean square of \tilde{u}_1 , respectively. The third-order central moment normalized by the standard deviation is called skewness and the equivalently normalized fourth-order central moment kurtosis or flatness.

To be sure, all these higher-order moments of statistics may also be achieved by collecting values in the sense of Reynolds averaging. Here, the variance ($n = 2$) reads

$$\langle \tilde{u}_1^2 \rangle = \langle \tilde{u}_1 \tilde{u}_1 \rangle = \langle u_1 u_1 \rangle - \langle u_1 \rangle \langle u_1 \rangle \quad (\text{A.15})$$

with the standard deviation (root mean square) defined as $\sqrt{\langle \tilde{u}_1^2 \rangle}$. The skewness ($n = 3$) normalized by the standard deviation may be written as

$$\langle \tilde{u}_1^3 \rangle = \frac{\langle \tilde{u}_1 \tilde{u}_1 \tilde{u}_1 \rangle}{\left(\sqrt{\langle \tilde{u}_1^2 \rangle} \right)^3} \quad (\text{A.16})$$

and the flatness ($n = 4$) is defined as

$$\langle \tilde{u}_1^4 \rangle = \frac{\langle \tilde{u}_1 \tilde{u}_1 \tilde{u}_1 \tilde{u}_1 \rangle}{\left(\sqrt{\langle \tilde{u}_1^2 \rangle} \right)^4} \quad (\text{A.17})$$

Appendix B A hierarchy of functional spaces

A hierarchy of functional spaces may be displayed as in Fig. B.1.

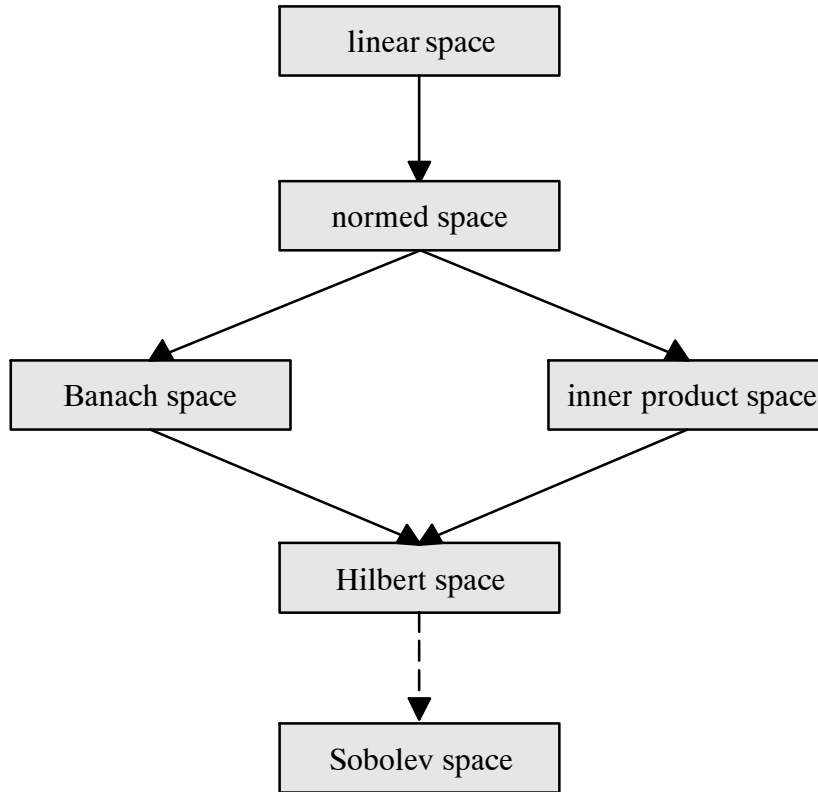


Fig. B.1: Sketch of a hierarchy of functional spaces

In Fig. B.1, $X \rightarrow Y$ means that all properties of the functional space X are also exhibited by the functional space Y . This is not the case in opposite direction however. A **linear space** is a collection which is closed under the operations of addition and scalar multiplication, i.e. for a linear space X , it is assumed

$$(L1) \quad x + y \in X \quad \forall x, y \in X \quad (B.1)$$

$$(L2) \quad \lambda x \in X \quad \forall x \in X \quad (B.2)$$

for a scalar λ . Within a **normed space**, there exists a norm $\|x\|$ with the properties

$$(N1) \quad \|x\| \geq 0, \text{ and } \|x\| = 0 \text{ if and only if } x = 0 \quad (B.3)$$

$$(N2) \quad \|\lambda x\| = |\lambda| \|x\|, \text{ where } |\lambda| \text{ is the absolute value of } \lambda \quad (B.4)$$

$$(N3) \quad \|x + y\| \leq \|x\| + \|y\| \quad (B.5)$$

$\forall x, y \in X$ and a scalar λ . A **Banach space** X is a completely normed space in the sense that every Cauchy-convergent sequence in X converges to a member of X . For an **inner product space**, an inner product $(x, y) \forall x, y \in X$ is defined with the properties

$$(I1) \quad (x, y) = (y, x) \quad (B.6)$$

$$(I2) \quad (\lambda_1 x + \lambda_2 y, z) = \lambda_1 (x, z) + \lambda_2 (y, z) \quad (B.7)$$

$$(I3) \quad (x, x) \geq 0; \quad (x, x) = 0 \text{ if and only if } x = 0 \quad (B.8)$$

(I1)-(I3) are the properties of symmetry, bilinearity and positive-definiteness, respectively. Herewith, a natural norm defined as

$$\|x\| := (x, x)^{\frac{1}{2}} \quad \forall x \in X \quad (B.9)$$

exists for every inner product space. A **Hilbert space** unifies the properties of the Banach space and the inner product space and, finally, a **Sobolev space** is a particular case of the Hilbert space with respect to the inner product.

The two main Sobolev spaces used throughout this work are now being addressed. The space L_2 (being essentially equal to H^0) is the space of square-integrable functions with the particular L_2 -inner product

$$(x, y)_0 = \int_{\Omega} xy \, d\Omega \quad (B.10)$$

and the corresponding natural norm

$$\|x\|_0 = \left[\int_{\Omega} x^2 \, d\Omega \right]^{\frac{1}{2}} \quad (B.11)$$

$\forall x, y \in L_2$. Furthermore, the space H^1 is the space of square-integrable functions with square-integrable generalized derivatives. The H^1 -inner product

$$(x, y)_1 = \int_{\Omega} xy + \nabla x \nabla y \, d\Omega \quad (B.12)$$

corresponds to the natural norm

$$\|x\|_1 = \left[\int_{\Omega} x^2 + |\nabla x|^2 \, d\Omega \right]^{\frac{1}{2}} \quad (B.13)$$

It is obvious that H^1 is a subspace of L_2 . In general, $H^{k+1} \subset H^k$.

The last question to be answered concerns the relationship between the Sobolev spaces and the classical spaces of bounded differentiable functions C_b^k . Sobolev's imbedding theorem states, among others, that $H^{k+1} \subset C_b^k$ in one dimension. In the multidimensional case with n indicating the number of dimensions, it may be stated that $H^s \subset C_b^k$ where $s > n/2 + k$, i.e., for instance, H^1 is not a subset of C_b^0 and, hence, H^1 contains functions which are not in C_b^0 . Thus, H^1 may be viewed as the largest functional space in which a variational formulation is reasonable for the finite elements with C^0 -shape functions used throughout this work.

Appendix C A brief survey of used computational tools

C.1 Preprocessing stage

The problem data necessary for the initiation of the simulation process put into execution with the help of the research code(s) (see below) is provided by an ASCII input file. This data file contains information related to the chosen algorithm, the generated mesh data (including the respective submeshes if necessary), the specification of the chosen type of elements and the boundary conditions of the problem. For the new generation of the research code, the program GID (see GID (2003)) is available as a helpful assistance within the pre- and postprocessing stage. However, this opportunity has merely been used for the preprocessing stages of the examples in chapter 10 to a limited extent, since the geometric domains of the numerical examples in this work do not require sophisticated mesh generation techniques.

C.2 Research code - The next generation

During this work, the author has been blessed with the 'delight' of observing a change of generations with respect to the research code used at the Institute of Structural Mechanics. Starting this work in 2000, the 'old' research code CARAT ('Computer Aided Research Analysis Tool') represented the platform for most of the programming efforts at the Institute. CARAT is based on the programming language FORTRAN. All sample calculations exhibited in chapter 9 have been performed using CARAT. In the course of the year 2002, however, the 'wind of change' blew through the Institute of Structural Mechanics and, finally, the next generation was born: CCA-RAT. Although the change might seem to be miniscule (just another 'C' in front of the name), the old one is hoped to 'pale' in comparison though. The two most important advances in CCA-RAT with regard to CARAT are as follows: The development of CCA-RAT has explicitly been oriented towards multifield problems, in particular problems of fluid-structure-interaction. Moreover, CCA-RAT can be run as a sequential as well as a parallel code where the parallelization is based on Message Passing Interface (MPI). Please consult e.g. Gropp et al. (1998) for the complete reference and Pacheco (1997) for an introduction to MPI. The change in language directly observable in the title, i.e. from FORTRAN to C, as well as the new environment implicated the joyful task of programming the two- and three-level finite element method again - practice makes perfect. Consequently, the numerical examples of chapter 10 have been computed using the new code CCA-RAT.

C.3 Solver

Four different solver packages have been attached to CARAT and/or CCA-RAT, respectively, and used for the solution of the various linear systems of equations arising within the two- and three-level finite element methods:

- The direct solver package LAPACK has been applied to the solution of all linear systems of equations on the second and third level, i.e. the ones based on the elementwise submeshes and sub-submeshes. More precisely, the module DGENV (see GAMS (2003) for a comprehensive description of the respective modules) for

the solution of a general linear system of equations has been attached to CARAT and CCARAT. This simple direct solver showed a satisfactory performance due to the relatively small number of unknowns of these equation systems.

- For the solution of the final (large-scale) linear systems of equations in the sample calculations of chapter 9, the direct solver package UMFPACK (see Davis (2002) for product details) based on the unsymmetric multifrontal method and direct sparse LU factorization has been attached to CARAT. Please consult also Davis and Duff (1997) for elaboration of the basic solution procedure. The performance of this powerful direct solver has been sufficient for the respective problem sizes of these numerical examples.
- More efficient solvers have been required for the solution of the final (large-scale) linear systems of equations in the sample calculations of chapter 10. A high-capacity object-oriented direct solver package for sparse linear systems of equations named SPOOLES (see Ashcraft et al. (1999) for product details) as well as the iterative solver package AZTEC (see Tuminaro et al. (1999) for product details) have been available for these linear equations systems with substantially larger number of unknowns. More precisely, a stabilized biconjugate gradient (BiCGSTAB) method along with a symmetric Gauss-Seidel preconditioner or an incomplete LU preconditioner has been chosen from the extensive range of potential solution procedures offered within the AZTEC-package.

C.4 Postprocessing stage

The most important aspect of the postprocessing stage consists in the visual presentation of the achieved data. For this purpose, the visualization tools *Visual2* (see Haimes and Giles (1992)) for the 2-D examples and *Visual3* (see Haimes (1998)) for the 3-D examples have been used throughout this work exclusively. These visualizations tools have been available for all examples, i.e. the ones computed with the old as well as the new research code, by adding an appropriate interface to the respective code.

References

- Akin, J.E., Tezduyar, T., Ungor, M. and Mittal, S. (2003):** ‘Stabilization Parameters and Smagorinsky Turbulence Model’, *ASME Journal of Applied Mechanics*, **70**, 2-9.
- Ashcraft, C., Pierce, D., Wah, D.K. and Wu, J. (1999):** ‘The Reference Manual for SPOOLES, Release 2.2: An Object Oriented Software Library for Solving Sparse Linear Systems of Equations’, *Report*, Boeing Shared Services Group, Seattle.
- Babuska, I. and Melenk, J.M. (1997):** ‘The Partition of Unity Method’, *International Journal for Numerical Methods in Engineering*, **40**, 727-758.
- Baiocchi, C., Brezzi, F. and Franca, L.P. (1993):** ‘Virtual Bubbles and Galerkin-Least-Squares Type Methods (Ga.L.S.)’, *Computer Methods in Applied Mechanics and Engineering*, **105**, 125-141.
- Balaras, E., Piomelli, U. and Wallace, J.W. (2001):** ‘Self-similar states in turbulent mixing layers’, *Journal of Fluid Mechanics*, **446**, 1-24.
- Barbone, P.E. and Harari, I. (2001):** ‘Nearly H^1 -optimal finite element methods’, *Computer Methods in Applied Mechanics and Engineering*, **190**, 5679-5690.
- Bardina, J., Ferziger, J.H. and Reynolds, W.C. (1980):** ‘Improved subgrid scale models for large eddy simulation’, *AIAA Paper 80-1357*.
- Bardina, J., Ferziger, J.H. and Reynolds, W.C. (1983):** ‘Improved turbulence models based on large eddy simulation of homogeneous, incompressible, turbulent flows’, *Report TF-19*, Thermosciences Division, Department of Mechanical Engineering, Stanford University.
- Barrenechea, G.P. and Valentin, F. (2002):** ‘An unusual stabilized finite element method for a generalized Stokes problem’, *Numerische Mathematik*, **92**, 653-677.
- Basol, I. (2003):** *Projection methods and pressure treatment for the instationary incompressible Navier-Stokes equations*. Master Thesis, Institut für Baustatik, Universität Stuttgart.
- Batchelor, G.K. (1953):** *The Theory of Homogeneous Turbulence*. Cambridge University Press, Cambridge.
- Batchelor, G.K. (1967):** *An Introduction to Fluid Dynamics*. Cambridge University Press, Cambridge.
- Bathe, K.-J. (1996):** *Finite Element Procedures*. Prentice-Hall, Englewood Cliffs.
- Baumann, C.E. and Oden, J.T. (1999a):** ‘A discontinuous hp finite element method for convection-diffusion problems’, *Computer Methods in Applied Mechanics and Engineering*, **175**, 311-341.
- Baumann, C.E. and Oden, J.T. (1999b):** ‘A discontinuous hp finite element method for the Euler and Navier-Stokes equations’, *International Journal for Numerical Methods in Fluids*, **31**, 79-95.
- Behr, M., Hastreiter, D., Mittal, S. and Tezduyar, T.E. (1995):** ‘Incompressible Flow past a Circular Cylinder: Dependence of the Computed Flow Field on the Location of the Lateral Boundaries’, *Computer Methods in Applied Mechanics and Engineering*, **123**, 309-316.
- Bochev, P.B., Shadid, J.N. and Gunzburger, M.D. (2002):** ‘On stabilized finite element methods for transient problems with varying time scales’ In: Mang, H.A., Rammerstorfer, F.G. and Eberhardsteiner, J. (eds.), *Proceedings of the Fifth World Congress on Computational Mechanics (WCCM V)*, Publisher: Vienna University of Technology, ISBN 3-9501554-0-6, <http://wccm.tuwien.ac.at>.
- Boersma, B.J., Kooper, M.N., Nieuwstadt, F.T.M. and Wesseling, P. (1997):** ‘Local grid refinement in large-eddy simulations’, *Journal of Engineering Mathematics*, **32**, 161-175.
- Boussinesq, J. (1877):** ‘Théorie de l’Écoulement Tourbillant’, *Mem. Présentés par Divers Savants Acad. Sci. Inst. Fr.*, **23**, 46-50.
- Bradshaw, P. (1971):** *An Introduction to Turbulence and its Measurement*. Pergamon Press, New York.
- Bradshaw, P. (1994):** ‘Turbulence: the chief outstanding difficulty of our subject’, *Experiments in Fluids*, **16**, 203-216.

- Bradshaw, P. (1998):**, 'Highlights of Turbulence Modeling ... Or, You Don't Get What You Don't Pay For', Lecture at the ASME "ME '98" Meeting, Anaheim, CA.
- Brenner, S.C. and Scott, L.R. (1994):** *The Mathematical Theory of Finite Element Methods*. Springer, New York.
- Breuer, M. (2000):**, 'Large Eddy Simulation of Turbulent Flows', Lecture at the Institute of Structural Mechanics, Universität Stuttgart, Germany, Jan. 31.
- Brezzi, F. and Fortin, M. (1991):** *Mixed and Hybrid Finite Element Methods*. Springer, New York.
- Brezzi, F., Bristeau, M.-O., Franca, L.P., Mallet, M. and Rogé, G. (1992):** 'A Relationship between Stabilized Finite Element Methods and the Galerkin Method with Bubble Functions', *Computer Methods in Applied Mechanics and Engineering*, **96**, 117-129.
- Brezzi, F. and Russo, A. (1994):** 'Choosing Bubbles for Advection-Diffusion Problems', *Mathematical Models and Methods in Applied Science*, **4**, 571-587.
- Brezzi, F., Franca, L.P., Hughes, T.J.R. and Russo, A. (1996):** 'Stabilization Techniques and Subgrid Scales Capturing'. *Preprint - Istituto di Analisi Numerica*, Pavia, Pubb. 1011.
- Brezzi, F., Franca, L.P., Hughes, T.J.R. and Russo, A. (1997):** 'b= $\int g$ ', *Computer Methods in Applied Mechanics and Engineering*, **145**, 329-339.
- Brezzi, F., Franca, L.P. and Russo, A. (1998a):** 'Further considerations on residual-free bubbles for advective-diffusive equations', *Computer Methods in Applied Mechanics and Engineering*, **166**, 25-33.
- Brezzi, F., Marini, D. and Russo, A. (1998b):** 'Applications of the pseudo residual-free bubbles to the stabilization of convection-diffusion problems', *Computer Methods in Applied Mechanics and Engineering*, **166**, 51-63.
- Brezzi, F. (2000):**, 'Interacting with the subgrid world' In: Griffiths, D.F. and Watson, G.A. (eds.), *Numerical Analysis 1999*, Chapman & Hall/CRC, Boca Raton, 69-82.
- Brezzi, F., Houston, P., Marini, D. and Süli, E. (2000):** 'Modeling subgrid viscosity for advection-diffusion problems', *Computer Methods in Applied Mechanics and Engineering*, **190**, 1601-1610.
- Brezzi, F. (2002):**, 'Recent results in the treatment of subgrid scales' In: Blouza, A., Danaila, I., Joly, P., Kaber, S.M., Lucquin, B., Murat, F. and Postel, M. (eds.), *Editeurs ESAIM: Proceedings Volume 11*, 61-84.
- Brezzi, F. and Marini, L.D. (2002):** 'Augmented spaces, two-level methods and stabilizing subgrids', *International Journal for Numerical Methods in Fluids*, **40**, 31-46.
- Brezzi, F., Hauke, G., Marini, L.D. and Sangalli, G. (2003):** 'Link-Cutting Bubbles for the Stabilization of Convection-Diffusion-Reaction Problems', *Mathematical Models and Methods in Applied Science*, **13(3)**, 445-461.
- Bronstein, I.N. and Semendjajew, K.A. (1991):** *Taschenbuch der Mathematik*, 25. Auflage. B.G. Teubner, Stuttgart (in German).
- Brooks, A.N. and Hughes, T.J.R. (1982):** 'Streamline Upwind/Petrov-Galerkin Formulations for Convection Dominated Flows with Particular Emphasis on the Incompressible Navier-Stokes Equations', *Computer Methods in Applied Mechanics and Engineering*, **32**, 199-259.
- Brown, G.L. and Roshko, A. (1974):** 'On density effects and large structure in turbulent mixing layers', *Journal of Fluid Mechanics*, **64**, 775-816.
- Camarri, S., Salvetti, M.V., Koobus, B. and Dervieux, A. (2002):** 'Large-eddy simulation of a bluff-body flow on unstructured grids', *International Journal for Numerical Methods in Fluids*, **40**, 1431-1460.
- Cantekin, M.E., Westerink, J.J. and Luetlich Jr., R.A. (1994):** 'Low and moderate Reynolds number transient flow simulations using space filtered Navier-Stokes equations', *Numerical Methods for Partial Differential Equations*, **10**, 491-524.
- Canuto, C., Hussaini, M.Y., Quarteroni, A. and Zang, T.A. (1988):** *Spectral Methods in Fluid Dynamics*. Springer, Berlin.
- Carati, D., Ghosal, S. and Moin, P. (1995):** 'On the representation of backscatter in dynamic localization models', *Physics of Fluids*, **7(3)**, 606-616.

- Carnevali, P., Morris, R.B., Tsuji, Y. and Taylor, G. (1993):** ‘New Basis Functions and Computational Procedures for p-version Finite Element Analysis’, *International Journal for Numerical Methods in Engineering*, **36**, 3759-3779.
- Chalot, F., Marquez, B., Ravachol, M., Ducros, F., Nicoud, F. and Poinso, T. (1998):** ‘A Consistent Finite Element Approach to Large Eddy Simulation’, *AIAA Paper 98-2652*.
- Chen, M. and Temam, R. (1991):** ‘Incremental unknowns for solving partial differential equations’, *Numerische Mathematik*, **59**, 255-271.
- Chorin, A.J. (1968):** ‘Numerical Solution of the Navier-Stokes Equations’, *Mathematics of Computation*, **22**, 745-762.
- Clark, R.A., Ferziger, J.H. and Reynolds, W.C. (1979):** ‘Evaluation of subgrid-scale models using an accurately simulated turbulent flow’, *Journal of Fluid Mechanics*, **91**, 1-16.
- Cockburn, B., Karniadakis, G.E. and Shu, C.-W. (eds.) (2000):** *Discontinuous Galerkin Methods - Theory, Computation and Applications*. Lecture Notes in Computational Science and Engineering, **11**, Springer, Berlin.
- Codina, R. (1998):** ‘Comparison of some finite element methods for solving the diffusion-convection-reaction equation’, *Computer Methods in Applied Mechanics and Engineering*, **156**, 185-210.
- Codina, R. (2000a):** ‘A nodal-based implementation of a stabilized finite element method for incompressible flow problems’, *International Journal for Numerical Methods in Fluids*, **33**, 737-766.
- Codina, R. (2000b):** ‘On stabilized finite element methods for linear systems of convection-diffusion-reaction equations’, *Computer Methods in Applied Mechanics and Engineering*, **188**, 61-82.
- Codina, R. (2000c):** ‘Stabilization of incompressibility and convection through orthogonal sub-scales in finite element methods’, *Computer Methods in Applied Mechanics and Engineering*, **190**, 1579-1599.
- Codina, R. (2001):** ‘A stabilized finite element method for generalized stationary incompressible flows’, *Computer Methods in Applied Mechanics and Engineering*, **190**, 2681-2706.
- Codina, R. (2002a):** ‘Stabilized finite element approximation of transient incompressible flows using orthogonal subscales’, *Computer Methods in Applied Mechanics and Engineering*, **191**, 4295-4321.
- Codina, R. (2002b):** ‘Analysis of a stabilized finite element approximation of the Oseen equations using orthogonal subscales’, Preprint.
- Codina, R. and Blasco, J. (2002):** ‘Analysis of a stabilized finite element approximation of the transient convection-diffusion-reaction equation using orthogonal subscales’, *Computing and Visualization in Science*, **4**, 167-174.
- Collis, S.S. (2001):** ‘Monitoring unresolved scales in multiscale turbulence modeling’, *Physics of Fluids*, **13(6)**, 1800-1806.
- Collis, S.S. (2002):** ‘Discontinuous Galerkin methods for turbulence simulation’, In: *Proceedings of the Summer Program*, Center for Turbulence Research, Stanford, 155-167.
- Collis, S.S., Ghayour, K. and Ramakrishnan, S. (2003):** ‘Multiscale Turbulence Modeling in the Discontinuous Galerkin Method’, *Abstracts of the Seventh U.S. National Congress on Computational Mechanics (USNCCM 7)*, Albuquerque.
- Cuvelier, C., Segal, A. and Steenhoven, A.A. van (1986),** *Finite Element Methods and Navier-Stokes Equations*. D. Reidel Publishing Company, Dordrecht.
- Davis, T.A. and Duff, I.S. (1997):** ‘A Combined Unifrontal / Multifrontal Method for Unsymmetric Sparse Matrices’, *Technical Report TR-97-016*, Department of Computer and Information Science and Engineering, University of Florida.
- Davis, T.A. (2002):** ‘UMFPACK Version 4.0 User Guide’, *Report*, Department of Computer and Information Science and Engineering, University of Florida, Gainesville, <http://www.cise.ufl.edu/research/sparse/umfpack>.
- Debussche, A., Dubois, T. and Temam, R. (1995):** ‘The nonlinear Galerkin method: a multiscale method applied to simulation of homogeneous turbulent flows’, *Theoretical and Computational Fluid Dynamics*, **7**, 279-315.

- Dettmer, W. and Peric, D. (2003):** ‘An analysis of the time integration algorithms for the finite element solutions of incompressible Navier–Stokes equations based on a stabilised formulation’, *Computer Methods in Applied Mechanics and Engineering*, **192**, 1177–1226.
- Ding, X. and Tsang, T.T.H. (2001):** ‘Large eddy simulation of turbulent flows by a least-squares finite element method’, *International Journal for Numerical Methods in Fluids*, **37**, 297–319.
- Domaradzki, J.A. and Loh, K.C. (1999):** ‘The subgrid-scale estimation model in the physical space representation’, *Physics of Fluids*, **11(8)**, 2330–2342.
- Domaradzki, J.A. and Yee, P.P. (2000):** ‘The subgrid-scale estimation model for high Reynolds number turbulence’, *Physics of Fluids*, **12(1)**, 193–196.
- Domaradzki, J.A., Loh K.C. and Yee, P.P. (2002):** ‘Large Eddy Simulations Using the Subgrid-Scale Estimation Model and Truncated Navier-Stokes Dynamics’, *Theoretical and Computational Fluid Dynamics*, **15**, 421–450.
- Donea, J. and Huerta, A. (2003):** *Finite Element Methods for Flow Problems*. John Wiley & Sons, Chichester.
- Dubois, T. and Bouchon, F. (1998):** ‘Subgrid-scale models based on incremental unknowns for large eddy simulations’, In: *Annual Research Briefs*, Center for Turbulence Research, Stanford, 221–236.
- Dubois, T., Jauberteau, F. and Temam, R. (1998):** ‘Incremental unknowns, multilevel methods and the numerical simulation of turbulence’, *Computer Methods in Applied Mechanics and Engineering*, **159**, 123–189.
- Dubois, T., Jauberteau, F. and Temam, R. (1999):** *Dynamic Multilevel Methods and the Numerical Simulation of Turbulence*. Cambridge University Press, Cambridge.
- Duffy, D.G. (2001):** *Green’s Functions with Applications*. Chapman & Hall/CRC, Boca Raton.
- Dyke, M. van (1982):** *An Album of Fluid Motion*. Parabolic Press, California.
- Engel, G., Garikipati, K., Hughes, T.J.R., Larson, M.G., Mazzei, L. and Taylor, R.L. (2002):** ‘Continuous/discontinuous finite element approximations of fourth-order elliptic problems in structural and continuum mechanics with applications to thin beams and plates, and strain gradient elasticity’, *Computer Methods in Applied Mechanics and Engineering*, **191**, 3669–3750.
- Eriksson, K., Estep, D., Hansbo, P. and Johnson, C. (1996):** *Computational Differential Equations*. Cambridge University Press, Cambridge.
- Ethier, C.R. and Steinman, D.A. (1994):** ‘Exact fully 3D Navier-Stokes solution for benchmarking’, *International Journal for Numerical Methods in Fluids*, **19**, 369–375.
- Farhat, C., Harari, I. and Franca, L.P. (2001):** ‘The discontinuous enrichment method’, *Computer Methods in Applied Mechanics and Engineering*, **190**, 6455–6479.
- Farhat, C., Harari, I. and Hetmaniuk, U. (2003):** ‘The discontinuous enrichment method for multiscale analysis’, *Computer Methods in Applied Mechanics and Engineering*, **192**, 3195–3209.
- Ferziger, J.H. and Peric, M. (1999):** *Computational Methods for Fluid Dynamics, 2nd Edition*. Springer, Berlin.
- Fletcher, C.A.J. (1991):** *Computational Techniques for Fluid Dynamics, Volume II*. Springer, Berlin.
- Fortin, M. (1993):** ‘Finite element solution of the Navier–Stokes equations’, *Acta Numerica*, 239–284.
- Franca, L.P. and Hughes, T.J.R. (1988):** ‘Two Classes of Mixed Finite Element Methods’, *Computer Methods in Applied Mechanics and Engineering*, **69**, 89–129.
- Franca, L.P., Frey, S.L. and Hughes, T.J.R. (1992):** ‘Stabilized Finite Element Methods: I. Application to the Advective–Diffusive Model’, *Computer Methods in Applied Mechanics and Engineering*, **95**, 253–276.
- Franca, L.P. and Frey, S.L. (1992):** ‘Stabilized Finite Element Methods: II. The incompressible Navier–Stokes equations’, *Computer Methods in Applied Mechanics and Engineering*, **99**, 209–233.
- Franca, L.P. and Farhat, C. (1995):** ‘Bubble functions prompt unusual stabilized Finite Element Methods’, *Computer Methods in Applied Mechanics and Engineering*, **123**, 299–308.

- Franca, L.P. and Russo, A. (1996):** ‘Approximation of the Stokes problem by residual-free macro bubbles’, *East-West Journal of Numerical Mathematics*, **4**, 265-278.
- Franca, L.P. and Macedo, A.P. (1998):** ‘A Two-Level Finite Element Method and its Application to the Helmholtz equation’, *International Journal for Numerical Methods in Engineering*, **43**, 23-32.
- Franca, L.P., Farhat, C., Lesoinne, M. and Russo, A. (1998a):** ‘Unusual Stabilized Finite Element Methods and Residual-Free-Bubbles’, *International Journal for Numerical Methods in Fluids*, **27**, 159-168.
- Franca, L.P., Nesliturk, A. and Stynes, M. (1998b):** ‘On the stability of residual-free bubbles for convection-diffusion problems and their approximation by a two-level finite element method’, *Computer Methods in Applied Mechanics and Engineering*, **166**, 35-49.
- Franca, L.P. and Valentin, F. (2000):** ‘On an improved unusual stabilized finite element method for the advective-reactive-diffusive equation’, *Computer Methods in Applied Mechanics and Engineering*, **190**, 1785-1800.
- Franca, L.P. and Nesliturk, A. (2001):** ‘On a two-level finite element method for the incompressible Navier-Stokes equation’, *International Journal for Numerical Methods in Engineering*, **52**, 433-453.
- Franca, L.P. and Hwang, F.-N. (2002):** ‘Refining the submesh strategy in the two-level finite element method: application to the advection-diffusion equation’, *International Journal for Numerical Methods in Fluids*, **39**, 161-187.
- Franca, L.P. and Tobiska, L. (2002):** ‘Stability of the residual free bubble method for bilinear finite elements on rectangular grids’, *IMA Journal of Numerical Analysis*, **22**, 73-87.
- Franca, L.P., Madueira, A.L. and Valentin, F. (2002):**, ‘Modeling Multiscale Phenomena via Finite Element Methods’ In: Mang, H.A., Rammerstorfer, F.G. and Eberhardsteiner, J. (eds.), *Proceedings of the Fifth World Congress on Computational Mechanics (WCCM V)*, Publisher: Vienna University of Technology, ISBN 3-9501554-0-6, <http://wccm.tuwien.ac.at>.
- Franca, L.P. and Oliveira, S.P. (2003):** ‘Pressure bubbles stabilization features in the Stokes problem’, *Computer Methods in Applied Mechanics and Engineering*, **192**, 1929-1937.
- Franca, L.P., Madueira, A.L., Valentin, F. and Tobiska, L. (2003):** ‘Modeling Multiscale Phenomena by a Finite Element Method’, *Abstracts of the Seventh U.S. National Congress on Computational Mechanics (USNCCM 7)*, Albuquerque.
- Frisch, U. (1995):** *Turbulence*. Cambridge University Press, Cambridge.
- Fröhlich, J. and Rodi, W. (2000):** ‘Introduction to Large Eddy Simulation of Turbulent Flows’, Preprint, appeared in: Launder, B.E. and Sandham, N.D. (eds.), *Closure Strategies for Turbulent and Transitional Flows*, Cambridge University Press, Cambridge.
- Fung, L.E. (1977):** *A First Course in Continuum Mechanics, 2nd Edition*. Prentice-Hall, Englewood Cliffs.
- Galdi, G.P. and Layton, W.J. (2000):** ‘Approximation of the larger eddies in fluid motion II: a model for space-filtered flow’, *Mathematical Models and Methods in Applied Sciences*, **10(3)**, 343-350.
- GAMS (2003):** ‘Modules in LAPACK’, <http://gams.nist.gov/serve.cgi/PackageModules/LAPACK>, Guide to Available Mathematical Software (GAMS), National Institute of Standards and Technology, Gaithersburg.
- Garikipati, K. and Hughes, T.J.R. (1998):** ‘A study of strain localization in a multiple scale framework - The one-dimensional problem’, *Computer Methods in Applied Mechanics and Engineering*, **159**, 193-222.
- Garikipati, K. and Hughes, T.J.R. (2000):** ‘A variational multiscale approach to strain localization - formulation for multidimensional problems’, *Computer Methods in Applied Mechanics and Engineering*, **188**, 39-60.
- Garikipati, K. and Hughes, T.J.R. (2000):** ‘Embedding a Micromechanical Law in the Continuum Formulation: A Multiscale Approach Applied to Discontinuous Solutions’, *International Journal for Computational Civil and Structural Engineering*, **1**, 64-78.
- Gelhard, T., Lube, G. and Olshanskii, M. (2003):** ‘Stabilized finite element schemes with LBB-stable elements for incompressible flows’, Preprint.

- Gellert, M. and Harbord, R. (1987):** ‘Symmetric forms for finite element analysis of the Navier-Stokes problem’, *Computers & Fluids*, **15(4)**, 379-389.
- Germano, M. (1986):** ‘A proposal for a redefinition of the turbulent stresses in the filtered Navier-Stokes equations’, *Physics of Fluids*, **29(7)**, 2323-2324.
- Germano, M., Piomelli, U., Moin, P. and Cabot, W.H. (1991):** ‘A dynamic subgrid-scale eddy viscosity model’, *Physics of Fluids A*, **3(7)**, 1760-1765.
- Germano, M. (1992):** ‘Turbulence: The filtering approach’, *Journal of Fluid Mechanics*, **238**, 325-336.
- Germano, M. (1999):** ‘From RANS to DNS: towards a bridging model’ In: Voke, P.R., Sandham, N.D. and Kleiser, L. (eds.), *Direct and Large Eddy Simulation III*, Kluwer, Dordrecht, 225-236.
- Ghia, U., Ghia, K.N. and Shin, C.T. (1982):** ‘High-Re Solutions for Incompressible Flow Using the Navier-Stokes Equations and a Multigrid Method’, *Journal of Computational Physics*, **48**, 387-411.
- Ghosal, S. and Moin, P. (1995):** ‘The basic equations for the large-eddy simulation of turbulent flows in complex geometry’, *Journal of Computational Physics*, **118**, 24-37.
- Ghosal, S., Lund, T.S., Moin, P. and Akselvoll, K. (1995):** ‘A dynamic localization model for large-eddy simulation of turbulent flows’, *Journal of Fluid Mechanics*, **286**, 229-255.
- GID (2003):** ‘GID 7 - The personal pre and post processor’, <http://gid.cimne.upc.es>, CIMNE, Barcelona.
- Girault, V. and Raviart, P.-A. (1986):** *Finite Element Methods for Navier-Stokes Equations - Theory and Algorithms*. Springer, Berlin.
- Girault, V. and Lions, J.-L. (2001):** ‘Two-grid finite-element schemes for the transient Navier-Stokes problem’, *Mathematical Modelling and Numerical Analysis*, **35(5)**, 945-980.
- Gravemeier, V., Wall, W.A. and Ramm, E. (2002):**, ‘A three-level approach for incompressible Navier-Stokes’ In: Mang, H.A., Rammerstorfer, F.G. and Eberhardsteiner, J. (eds.), *Proceedings of the Fifth World Congress on Computational Mechanics (WCCM V)*, Publisher: Vienna University of Technology, ISBN 3-9501554-0-6, <http://wccm.tuwien.ac.at>.
- Gravemeier, V., Wall, W.A. and Ramm, E. (2003a):** ‘A three-level finite element method for the instationary incompressible Navier-Stokes equations’, Preprint, *SFB 404-Report 2003/26*, accepted for publication in: *Computer Methods in Applied Mechanics and Engineering*.
- Gravemeier, V., Wall, W.A. and Ramm, E. (2003b):**, ‘Numerical Solution of the Incompressible Navier-Stokes Equations by a Three-Level Finite Element Method’ In: Bathe, K.J. (ed.), *Proceedings of the Second MIT Conference on Computational Fluid and Solid Mechanics*, Elsevier, Amsterdam, 915-918.
- Gravemeier, V., Wall, W.A. and Ramm, E. (2003c):** ‘Tackling turbulent flows with a three-level finite element method’, *Abstracts of the Seventh U.S. National Congress on Computational Mechanics (USNCCM 7)*, Albuquerque.
- Gresho, P.M. (1990):** ‘On the Theory of Semi-Implicit Projection Methods for Viscous Incompressible Flow and its Implementation via a Finite Element Method that also introduces a Nearly Consistent Mass Matrix. Part 1: Theory’, *International Journal for Numerical Methods in Fluids*, **11**, 587-620.
- Gresho, P.M. and Chan, S.T. (1990):** ‘On the Theory of Semi-Implicit Projection Methods for Viscous Incompressible Flow and its Implementation via a Finite Element Method that also introduces a Nearly Consistent Mass Matrix. Part 2: Implementation’, *International Journal for Numerical Methods in Fluids*, **11**, 621- 659.
- Gresho, P.M. (1991a):** ‘Incompressible Fluid Dynamics: Some Fundamental Formulation Issues’, *Annual Review of Fluid Mechanics*, **23**, 413-453.
- Gresho, P.M. (1991b):** ‘Some Current CFD Issues Relevant to the Incompressible Navier-Stokes Equations’, *Computer Methods in Applied Mechanics and Engineering*, **87**, 201-252.
- Gresho, P.M. (1992):** ‘Some Interesting Issues in Incompressible Fluid Dynamics, Both in the Continuum and in Numerical Simulation’, *Advances in Applied Mechanics*, **28**, 45-140.
- Gresho, P.M. and Sani, R.L. (1998):** *Incompressible Flow and the Finite Element Method*. John Wiley & Sons, Chichester.

- Griebel, M. and Koster, F. (2000):** 'Adaptive wavelet solvers for the unsteady incompressible Navier-Stokes equations' In: Malek, J., Necas, J. and Rokyta, M. (eds.), *Advances in Mathematical Fluid Mechanics*, Springer, Berlin, 67-118.
- Gropp, W., Huss-Lederman, S., Lumsdaine, A., Lusk, E., Nitzberg, B., Saphir, W. and Snir, M. (1998):** *MPI: The Complete Reference, Volume 1 and 2*. MIT Press, Cambridge.
- Guermont, J.-L. (1999):** 'Stabilization of Galerkin approximations of transport equations by subgrid modeling', *Mathematical Modelling and Numerical Analysis*, **33**, 1293-1316.
- Guermont, J.-L. (2001):** 'Subgrid stabilization of Galerkin approximations of linear monotone operators', *IMA Journal of Numerical Analysis*, **21**, 165-197.
- Guermont, J.-L., Oden, J.T. and Prudhomme, S. (2002):** 'Mathematical perspectives on large eddy simulation models for turbulent flows', Preprint.
- Gunzburger, M.D. (1989):** *Finite Element Methods for Viscous Incompressible Flows - A Guide to Theory, Practice and Algorithms*. Academic Press, San Diego.
- Haimes, B. and Giles, M. (1992):** 'VISUAL2 User's & Programmer's Manual', *Report*, Massachusetts Institute of Technology, Cambridge, <http://raphael.mit.edu/visual2/visual2.html>.
- Haimes, B. (1998):** 'VISUAL3 User's & Programmer's Manual' and 'VISUAL3 Advanced Programmer's Guide', *Reports*, Massachusetts Institute of Technology, Cambridge, <http://raphael.mit.edu/visual3/visual3.html>.
- Hansbo, P. and Szepessy, A. (1990):** 'A Velocity-Pressure Streamline Diffusion Finite Element Method for the Incompressible Navier-Stokes Equations', *Computer Methods in Applied Mechanics and Engineering*, **84**, 175-192.
- Harari, I. and Hughes, T.J.R. (1992):** 'What are C and h ?: Inequalities for the Analysis and Design of Finite Element Methods', *Computer Methods in Applied Mechanics and Engineering*, **97**, 157-192.
- Harari, I., Franca, L.P. and Oliveira, S.P. (2001):** 'Streamline Design of Stability Parameters for Advection-Diffusion Problems', *Journal of Computational Physics*, **171(1)**, 115-131.
- Harbord, R. and Gellert, M. (1990):** 'Progress in symmetric formulation of the incompressible Navier-Stokes equations', *Computer Methods in Applied Mechanics and Engineering*, **83**, 201-209.
- Hauke, G. and Garcia-Olivares, A. (2001):** 'Variational subgrid scale formulations for the advection-diffusion-reaction equation', *Computer Methods in Applied Mechanics and Engineering*, **190**, 6847-6865.
- Hauke, G. (2002):** 'A simple subgrid scale stabilized method for the advection-diffusion-reaction equation', *Computer Methods in Applied Mechanics and Engineering*, **191**, 2925-2947.
- Hegarty, A.F., Miller, J.J.H., O'Riordan, E. and Shishkin, G.I. (1995):** 'Special Meshes for Finite Difference Approximations to an Advection-Diffusion Equation with Parabolic Layers', *Journal of Computational Physics*, **117**, 47-54.
- Hendriana, D. and Bathe, K.-J. (2000):** 'On upwind methods for parabolic finite elements in incompressible flows', *International Journal for Numerical Methods in Engineering*, **47**, 317-340.
- Heywood, J.G. and Rannacher, R. (1990):** 'Finite Element Approximation of the Nonstationary Navier-Stokes Problem, Part IV: Error Analysis for Second-Order Time Discretization', *SIAM Journal on Numerical Analysis*, **27(2)**, 353-384.
- Heywood, J.G., Rannacher, R. and Turek, S. (1996):** 'Artificial Boundaries and Flux and Pressure Conditions for the Incompressible Navier-Stokes Equations', *International Journal for Numerical Methods in Fluids*, **22**, 325-352.
- Hinze, J.O. (1959):** *Turbulence: An Introduction to its Mechanisms and Theory*. McGraw-Hill, New York.
- Hirsch, C. (1988):** *Numerical Computation of Internal and External Flows, Volume I: Fundamentals of Numerical Discretization*. John Wiley & Sons, New York.
- Hirsch, C. (1990):** *Numerical Computation of Internal and External Flows, Volume II: Computational Methods for Inviscid and Viscous Flows*. John Wiley & Sons, New York.

- Ho, C.M. and Huerre, L.S. (1984):** ‘Perturbed free shear layers’, *Annual Review of Fluid Mechanics*, **16**, 365-424.
- Homsy, G.M., Aref, H., Breuer, K.S., Hochgreb, S., Koseff, J.R., Munson, B.R., Powell, K.G., Robertson, C.R. and Thoroddsen, S.T. (2000):** *Multimedia Fluid Mechanics – CD-ROM Teaching Tool*. Cambridge University Press, Cambridge.
- Horiuti, K. (1997):** ‘A new dynamic two-parameter mixed model for large-eddy simulation’, *Physics of Fluids*, **9(11)**, 3443-3464.
- Hou, T.Y. and Wu, X.-H. (1997):** ‘A multiscale finite element method for elliptic problems in composite materials and porous media’, *Journal of Computational Physics*, **134**, 169-189.
- Hou, T.Y., Wu, X.-H. and Cai, Z. (1999):** ‘Convergence of a multiscale finite element method for elliptic problems with rapidly oscillating coefficients’, *Mathematics of Computation*, **68**, 913-943.
- Huerta, A. and Donea, J. (2002):** ‘Time-accurate solution of stabilized convection-diffusion-reaction equations: I-time and space discretization’, *Communications in Numerical Methods in Engineering*, **18**, 565-573.
- Hughes, T.J.R., Franca, L.P. and Balestra, M. (1986):** ‘A New Finite Element Formulation for Computational Fluid Dynamics: V. Circumventing the Babuska-Brezzi Condition: A Stable Petrov-Galerkin Formulation of the Stokes Problem accommodating equal-order Interpolation’, *Computer Methods in Applied Mechanics and Engineering*, **59**, 85-99.
- Hughes, T.J.R. (1987):** ‘Recent Progress in the Development and Understanding of SUPG Methods with Special Reference to the Compressible Euler and Navier-Stokes Equations’, *International Journal for Numerical Methods in Fluids*, **7**, 1261-1275.
- Hughes, T.J.R., Franca, L.P. and Hulbert, M. (1989):** ‘A New Finite Element Formulation for Computational Fluid Dynamics: VIII. The Galerkin/Least-squares method for advective-diffusive equations’, *Computer Methods in Applied Mechanics and Engineering*, **73**, 173-189.
- Hughes, T.J.R., Franca, L.P., Chalot, F. and Johan, Z. (1994a):** *Stabilized Finite Element Methods in Fluid Mechanics*. Course notes, Department of Mechanical Engineering, Stanford University.
- Hughes, T.J.R., Hauke, G., Jansen, K. and Johan, Z. (1994b):** ‘Stabilized Finite Element Methods in Fluids: Inspirations, Origins, Status and Recent Developments’ In: Hughes, T.J.R., Oñate, E. and Zienkiewicz, O.C. (eds.), *Recent Developments in Finite Element Methods*, CIMNE, Barcelona, 272-292.
- Hughes, T.J.R. (1995):** ‘Multiscale Phenomena: Green’s Functions, The Dirichlet-to-Neumann Formulation, Subgrid Scale Models, Bubbles and the Origins of Stabilized Methods’, *Computer Methods in Applied Mechanics and Engineering*, **127**, 387-401.
- Hughes, T.J.R. and Stewart, J.R. (1996):** ‘A space-time formulation for multiscale phenomena’, *Journal of Computational and Applied Mathematics*, **74**, 217-229.
- Hughes, T.J.R., Feijóo, G., Mazzei, L. and Quincy, J.-B. (1998):** ‘The variational multiscale method - a paradigm for computational mechanics’, *Computer Methods in Applied Mechanics and Engineering*, **166**, 3-24.
- Hughes, T.J.R. (2000):** *The Finite Element Method, Linear Static and Dynamic Finite Element Analysis*. Dover Publications, Mineola.
- Hughes, T.J.R., Mazzei, L. and Jansen, K.E. (2000a):** ‘Large eddy simulation and the variational multiscale method’, *Computing and Visualization in Science*, **3**, 47-59.
- Hughes, T.J.R., Engel, G., Mazzei, L. and Larson, M.G. (2000b):** ‘The continuous Galerkin method is locally conservative’, *Journal of Computational Physics*, **163**, 467-488.
- Hughes, T.J.R., Mazzei, L., Oberai, A.A. and Wray, A.A. (2001a):** ‘The multiscale formulation of large eddy simulation: Decay of homogeneous isotropic turbulence’, *Physics of Fluids*, **13(2)**, 505-512.
- Hughes, T.J.R., Oberai, A.A. and Mazzei, L. (2001b):** ‘Large eddy simulation of turbulent channel flows by the variational multiscale method’, *Physics of Fluids*, **13(6)**, 1784-1799.

- Iliescu, T., John, V. and Layton, W.J. (2002):** ‘Convergence of finite element approximations of large eddy motion’, *Numerical Methods for Partial Differential Equations*, **18(6)**, 689-710.
- Iliescu, T., John, V., Layton, W.J., Matthies, G. and Tobiska, L. (2003):** ‘A numerical study of a class of LES models’, *International Journal of Computational Fluid Dynamics*, **17**, 75-85.
- Jansen, K. (1993):** ‘Unstructured grid large eddy simulation of wall bounded turbulent flows’, In: *Annual Research Briefs*, Center for Turbulence Research, Stanford, 1-7.
- Jansen, K. (1994):** ‘Unstructured grid large-eddy simulation of flow over an airfoil’, In: *Annual Research Briefs*, Center for Turbulence Research, Stanford, 161-175.
- Jansen, K. (1995):** ‘Preliminary large-eddy simulation of flow around a NACA 4412 airfoil using unstructured meshes’, In: *Annual Research Briefs*, Center for Turbulence Research, Stanford, 61-72.
- Jansen, K. (1996):** ‘Large-eddy simulation of flow around a NACA 4412 airfoil using unstructured grids’, In: *Annual Research Briefs*, Center for Turbulence Research, Stanford, 225-232.
- Jansen, K. (1999):** ‘A stabilized finite element method for computing turbulence’, *Computer Methods in Applied Mechanics and Engineering*, **174**, 299-317.
- Jansen, K.E., Collis, S.S., Whiting, C. and Shakib, F. (1999):** ‘A better consistency for low-order stabilized finite element methods’, *Computer Methods in Applied Mechanics and Engineering*, **174**, 153-170.
- Jansen, K., Whiting, C.H. and Hulbert, G. (2000):** ‘A generalized α -method for integrating the filtered Navier-Stokes equations with a stabilized finite element method’, *Computer Methods in Applied Mechanics and Engineering*, **190**, 305-319.
- Jansen, K.E. (2001a):** ‘Stabilized FEM Using a Hierarchical Basis’, Lecture at: *C.I.M.E. Summer Course on Multiscale Problems and Methods in Numerical Simulations*, Martina Franca, Italy, Sept. 9-15.
- Jansen, K.E. (2001b):** ‘A variational multiscale model (VMM) for large-eddy simulation (LES)’, Lecture at: *C.I.M.E. Summer Course on Multiscale Problems and Methods in Numerical Simulations*, Martina Franca, Italy, Sept. 9-15.
- Jansen, K.E. and Tejada-Martinez, A.E. (2002):** ‘An Evaluation of the Hierarchical Basis in Variational Multiscale LES’ In: Mang, H.A., Rammerstorfer, F.G. and Eberhardsteiner, J. (eds.), *Proceedings of the Fifth World Congress on Computational Mechanics (WCCM V)*, Publisher: Vienna University of Technology, ISBN 3-9501554-0-6, <http://wccm.tuwien.ac.at>.
- John, V. (2001):** ‘Residual a posteriori error estimates for two-level finite element methods for the Navier-Stokes equations’, *Applied Numerical Mathematics*, **37**, 503-518.
- John, V. (2002a):** *Large Eddy Simulation of Turbulent Incompressible Flows. Analytical and Numerical Results for a Class of LES Models*. Habilitation Thesis, Fakultät für Mathematik, Otto-von-Guericke-Universität Magdeburg.
- John, V. (2002b):** ‘Slip with friction and penetration with resistance boundary conditions for the Navier-Stokes equations - numerical tests and aspects of the implementation’, *Journal of Computational and Applied Mathematics*, **147**, 287-300.
- John, V. (2002c):** ‘The behaviour of the rational LES model in a two-dimensional mixing layer problem’, Preprint 28/02, Fakultät für Mathematik, Otto-von-Guericke-Universität Magdeburg.
- John, V. and Layton, W.J. (2002):** ‘Analysis of numerical errors in large eddy simulation’, *SIAM Journal of Numerical Analysis*, **40(3)**, 995-1020.
- Johnson, C., Nävert, U. and Pitkäranta, J. (1984):** ‘Finite Element Methods for Linear Hyperbolic Problems’, *Computer Methods in Applied Mechanics and Engineering*, **45**, 285-312.
- Johnson, C. and Saranen, J. (1986):** ‘Streamline Diffusion Methods for the Incompressible Euler and Navier-Stokes Equations’, *Mathematics of Computation*, **47(175)**, 1-18.
- Johnson, C. (1987):** *Numerical Solution of Partial Differential Equations by the Finite Element Method*. Cambridge University Press, Cambridge.
- Karamanos, G.S. and Karniadakis, G.E. (2000):** ‘A Spectral Vanishing Viscosity Method for Large-Eddy Simulations’, *Journal of Computational Physics*, **163**, 22-50.

- Kaya, S. (2003):** ‘Numerical Analysis of a Subgrid Scale Eddy Viscosity Method for Higher Reynolds Number Flow Problems’, *Technical Report TR-MATH 03-04*, Department of Mathematics, University of Pittsburgh.
- Kaya, S. and Layton, W.J. (2003):** ‘Subgrid-Scale Eddy Viscosity Methods are Variational Multiscale Methods’, *Technical Report TR-MATH 03-05*, Department of Mathematics, University of Pittsburgh.
- Kim, J. and Moin, P. (1985):** ‘Application of a fractional-step method to incompressible Navier–Stokes equations’, *Journal of Computational Physics*, **21**, 308–323.
- Kollmann, W., McCallen, R.C. and Leone Jr., J.M. (2002):** ‘An examination of LES filtering within the finite element method’, *Communications in Numerical Methods in Engineering*, **18**, 513–528.
- Kolmogorov, A.N. (1941):** ‘The local structure of turbulence in incompressible viscous fluid for very large Reynolds numbers’, *Dokl. Akad. Nauk SSSR*, **30**, 299–303 (in Russian).
- Kolmogorov, A.N. (1991):** ‘The local structure of turbulence in incompressible viscous fluid for very large Reynolds numbers’, *Proceedings of the Royal Society London A*, **434**, 9–13.
- Lai, W.M., Rubin, D. and Krempl, E. (1993):** *Introduction to Continuum Mechanics, 3rd Edition*. Butterworth–Heinemann, Woburn.
- Landahl, M.T. and Mollo-Christensen, E. (1986):** *Turbulence and Random Processes in Fluid Mechanics*. Cambridge University Press, Cambridge.
- Launder, B.E. and Spalding, D.B. (1972):** *Mathematical Models of Turbulence*. Academic Press, London.
- Layton, W.J. (1993):** ‘A two-level discretization method for the Navier–Stokes equations’, *Computers and Mathematics with Applications*, **26(2)**, 33–38.
- Layton, W.J. (2000):** ‘Approximation of the larger eddies in fluid motion V: kinetic energy balance of scale similarity models’, *Mathematical and Computer Modelling*, **31(8-9)**, 1–7.
- Layton, W.J. (2002):** ‘A connection between subgrid scale eddy viscosity and mixed methods’, *Applied Mathematics and Computation*, **133**, 147–157.
- Layton, W.J. (2003):** ‘A Mathematical Introduction to Large Eddy Simulation’, *Technical Report TR-MATH 03-03*, Department of Mathematics, University of Pittsburgh.
- Le, H., Moin, P. and Kim, J. (1997):** ‘Direct numerical simulation of turbulent flow over a backward-facing step’, *Journal of Fluid Mechanics*, **330**, 349–374.
- Lei, C., Cheng, K. and Kavanagh, K. (2001):** ‘Spanwise length effects on three-dimensional modelling of flow over a circular cylinder’, *Computer Methods in Applied Mechanics and Engineering*, **190**, 2909–2923.
- Leonard, A. (1974):** ‘Energy cascade in large eddy simulation of turbulent fluid flow’, *Advances in Geophysics A*, **18**, 237–248.
- Lesieur, M., Staquet, C., LeRoy, P. and Comte, P. (1988):** ‘The mixing layer and its coherence examined from the point of view of two-dimensional turbulence’, *Journal of Fluid Mechanics*, **192**, 511–534.
- Lesieur, M. (1990):** *Turbulence in Fluids - Stochastic and Numerical Modelling*. Kluwer, Dordrecht.
- Lesieur, M. and Metais, O. (1996):** ‘New Trends in Large-eddy Simulations of Turbulence’, *Annual Review of Fluid Mechanics*, **28**, 45–82.
- Leslie, D.C. (1973):** *Developments in the Theory of Turbulence*. Clarendon Press, Oxford.
- Lilly, D.K. (1967):** ‘The representation of small-scale turbulence in numerical simulation experiments’ In: *Proceedings of the IBM Scientific Computing Symposium on Environmental Sciences*, Yorktown Heights.
- Lilly, D.K. (1992):** ‘A proposed modification of the Germano subgrid-scale closure method’, *Physics of Fluids A*, **4(3)**, 633–635.
- Löhner, R. (2001):** *Applied CFD Techniques: An Introduction based on Finite Element Methods*. John Wiley & Sons, Chichester.
- Malvern, L.E. (1969):** *Introduction to the mechanics of a continuous medium*. Prentice–Hall, Englewood Cliffs.

- Marion, M. and Temam, R. (1990):** ‘Nonlinear Galerkin methods: the finite elements case’, *Numerische Mathematik*, **57**, 205-226.
- Marion, M. and Temam, R. (1998):**, ‘Navier-Stokes Equations: Theory and Approximation’ In: Ciarlet, P.G. and Lions, J.L. (eds.), *Handbook of Numerical Analysis Volume VI*, Elsevier, Amsterdam.
- Marsden, A.L., Vasilyev, O. and Moin, P. (2002):** ‘Construction of Commutative Filters for LES on Unstructured Meshes’, *Journal of Computational Physics*, **175**, 584-603.
- Mathieu, J. and Scott, J. (2000):** *An Introduction to Turbulent Flow*. Cambridge University Press, Cambridge.
- McComb, W.D. (1990):** *The physics of fluid turbulence*. Clarendon Press, Oxford.
- McDonough, J.M., Bywater, R.J. and Buell, J.C. (1984):** ‘An investigation of strange attractor theory and small-scale turbulence’, *AIAA Paper 84-1674*.
- McDonough, J.M. and Bywater, R.J. (1985):** ‘Effects of local large-scale parameters on the small-scale chaotic solutions to Burgers equations’, *AIAA Paper 85-1653*
- Melenk, J.M. and Babuska, I. (1996):** ‘The partition of unity finite element method: basic theory and applications’, *Computer Methods in Applied Mechanics and Engineering*, **139**, 289-314.
- Meneveau, C., Lund, T.S. and Cabot, W.H. (1996):** ‘A Lagrangian dynamic subgrid-scale model of turbulence’, *Journal of Fluid Mechanics*, **319**, 353-385.
- Meneveau, C. and Katz, J. (2000):** ‘Scale-Invariance and Turbulence Models for Large-Eddy Simulation’, *Annual Review of Fluid Mechanics*, **32**, 1-32.
- Michalke, A. (1964):** ‘On the inviscid instability of the hyperbolic tangent velocity profile’, *Journal of Fluid Mechanics*, **19**, 543-556.
- Moin, P. and Mahesh, K. (1998):** ‘Direct Numerical Simulation: A Tool in Turbulence Research’, *Annual Review of Fluid Mechanics*, **30**, 539-578.
- Moin, P. (2002):** ‘Advances in large eddy simulation methodology for complex flows’, *International Journal of Heat and Fluid Flow*, **23**, 710-720.
- Mok, D.P. (2001):** *Partitionierte Lösungsansätze in der Strukturmechanik und der Fluid-Struktur-Interaktion*. Ph.D.-Dissertation, Report No. 36, Institut für Baustatik, Universität Stuttgart (in German).
- Monin, A.S. and Yaglom, A.M. (1971):** *Statistical Fluid Mechanics, Volume 1*. MIT Press, Cambridge.
- Monin, A.S. and Yaglom, A.M. (1975):** *Statistical Fluid Mechanics, Volume 2*. MIT Press, Cambridge.
- Nägele, S. and Wittum, G. (2002):** ‘Large-eddy simulation and multigrid methods’, Preprint.
- Nesliturk, A.I. (1999):** *Approximating the incompressible Navier Stokes equations using a Two Level Finite Element Method*. Ph.D. Thesis, Department of Mathematic, University of Colorado at Denver.
- Nesliturk, A. and Harari, I. (2003):** ‘The nearly-optimal Petrov-Galerkin method for convection-diffusion problems’, *Computer Methods in Applied Mechanics and Engineering*, **192**, 2501-2519.
- Norberg, C. (1994):** ‘An Experimental Investigation of the Flow around a Circular Cylinder: Influence of Aspect Ratio’, *Journal of Fluid Mechanics*, **258**, 287-316.
- Oberai, A.A. and Pinsky, P.M. (1998):** ‘A multiscale finite element method for the Helmholtz equation’, *Computer Methods in Applied Mechanics and Engineering*, **154**, 281-297.
- Oden, J.T., Belytschko, T., Babuska, I. and Hughes, T.J.R. (2003):** ‘Research directions in computational mechanics’, *Computer Methods in Applied Mechanics and Engineering*, **192**, 913-922.
- Oñate, E., Garcia, J. and Idelsohn, S. (1997):** ‘Computation of the stabilization parameter for the finite element solution of advective-diffusive problems’, *International Journal for Numerical Methods in Fluids*, **25**, 1385-1407.
- Oñate, E. (1998):** ‘Derivation of stabilized equations for numerical solution of advective-diffusive transport and fluid flow problems’, *Computer Methods in Applied Mechanics and Engineering*, **151**, 233-265.
- Oñate, E. (2000):** ‘A stabilized finite element method for incompressible viscous flows using a finite increment calculus formulation’, *Computer Methods in Applied Mechanics and Engineering*, **182**, 355-370.

- Pacheco, P.S. (1997):** *Parallel Programming with MPI*. Morgan Kaufmann, San Francisco.
- Panchev, S. (1971):** *Random Functions and Turbulence*. Pergamon Press, Oxford.
- Piomelli, U. (1994):** 'Large-eddy simulation of turbulent flows', *TAM Report No. 767*.
- Piomelli, U. (1999):** 'Large-eddy simulation: achievements and challenges', *Progress in Aerospace Science*, **35**, 335-362.
- Pironneau, O. (1989):** *Finite Element Methods for Fluids*. John Wiley & Sons / Masson, Paris.
- Pope, S.B. (2000):** *Turbulent Flows*. Cambridge University Press, Cambridge.
- Prandtl, L. (1904):** 'Über Flüssigkeitsbewegung bei sehr kleiner Reibung', *Verhandlg. III. Intern. Math. Kongr.*, Heidelberg, 484-491 (in German).
- Prandtl, L. (1925):** 'Bericht über Untersuchungen zur ausgebildeten Turbulenz', *Zeitschrift für angewandte Mathematik und Mechanik*, **5**, 136-139 (in German).
- Prasad, A.K. and Koseff, J.R. (1989):** 'Reynolds number and end-wall effects on a lid-driven cavity flow', *Physics of Fluids A*, **1(2)**, 208-218.
- Quarteroni, A. and Valli, A. (1994):** *Numerical Approximation of Partial Differential Equations*. Springer, Berlin.
- Quéméré, P. and Sagaut, P. (2002):** 'Zonal multi-domain RANS/LES simulations of turbulent flows', *International Journal for Numerical Methods in Fluids*, **40**, 903-925.
- Ramakrishnan, S. and Collis, S.S. (2002):** 'Planar Variational Multi-Scale Modeling', *MEMS Preprint 2002-007*, Mechanical Engineering and Materials Science, Rice University.
- Reddy, J.N. and Gartling, D.K. (2001):** *The Finite Element Methods in Heat Transfer and Fluid Dynamics, 2nd Edition*. CRC Press, Boca Raton.
- Richardson, L.F. (1922):** *Weather Prediction by Numerical Process*. Cambridge University Press, Cambridge.
- Rodi, W., Ferziger, J.H., Breuer, M. and Pourquié, M. (1997):** 'Status of Large Eddy Simulation: Results of a Workshop', *ASME Journal of Fluids Engineering*, **119(2)**, 248-262.
- Rogallo, R.S. and Moin, P. (1984):** 'Numerical simulation of turbulent flows', *Annual Review of Fluid Mechanics*, **16**, 99-137.
- Rogers, M. and Moser, R.D. (1994):** 'Direct simulation of a self-similar turbulent mixing layer', *Physics of Fluids*, **6(2)**, 903-923.
- Rollet-Miet, P., Laurence, D. and Ferziger, J. (1999):** 'LES and RANS of turbulent flow in tube bundles', *International Journal of Heat and Fluid Flow*, **20**, 241-254.
- Rotta, C. (1972):** *Turbulente Strömungen*. B.G. Teubner, Stuttgart (in German).
- Russo, A. (1996):** 'Bubble Stabilization of Finite Element Methods for the Linearized Incompressible Navier-Stokes Equations', *Computer Methods in Applied Mechanics and Engineering*, **132**, 335-343.
- Sagaut, P. (2002):** *Large Eddy Simulation for Incompressible Flows, 2nd Edition*. Springer, Berlin.
- Sangalli, G. (2003):** 'Capturing small scales in elliptic problems using a residual-free bubbles finite element method', *Multiscale Modeling and Simulation*, **1(3)**, 485-503.
- Sarghini, F., Piomelli, U. and Balaras, E. (1999):** 'Scale-similar models for large-eddy simulations', *Physics of Fluids*, **11(6)**, 1596-1607.
- Schäfer, M. and Turek, S. (1996):** 'Benchmark Computations of Laminar Flow Around a Cylinder' In: Hirschel, E.H. (ed.), *Flow Simulation with High-Performance Computers II*, Notes on Numerical Fluid Mechanics, **52**, Vieweg, 547-566.
- Schlichting, H. (1979):** *Boundary-Layer Theory, 7th Edition*. McGraw-Hill, New York.
- Schumann, U. (1975):** 'Subgrid scale model for finite difference simulations of turbulent flows in plane channels and annuli', *Journal of Computational Physics*, **18**, 376-404.

- Shakib, F. (1988):** *Finite Element Analysis of the Compressible Euler and Navier-Stokes Equations*. Ph.D. Thesis, Department of Mechanical Engineering, Stanford University.
- Shephard, M.S., Dey, S. and Flaherty, J.E. (1997):** ‘A straightforward structure to construct shape functions for variable p-order meshes’, *Computer Methods in Applied Mechanics and Engineering*, **147**, 209-233.
- Simo, J.C. and Armero, F. (1994):** ‘Unconditional Stability and Long-Term Behavior of Transient Algorithms for the Incompressible Navier-Stokes and Euler Equations’, *Computer Methods in Applied Mechanics and Engineering*, **111**, 11-154.
- Simo, J.C., Armero, F. and Taylor, C.A. (1995):** ‘Stable and Time-Dissipative Finite Element Methods for the Incompressible Navier-Stokes Equations in Advection Dominated Flows’, *International Journal for Numerical Methods in Engineering*, **38**, 1475-1506.
- Smagorinsky, J. (1963):** ‘General Circulation Experiments with the Primitive Equations. I. The Basic Experiment’, *Monthly Weather Review*, **91(3)**, 99-164.
- Spalart, P.R., Jou, W.H., Strelets, M. and Allmaras, S.R. (1997):**, ‘Comments on the feasibility of LES for wings, and on a hybrid RANS/LES approach’ In: Liu, C. and Liu, Z. (eds.), *Advances in DNS/LES*, Greyden Press, 137-147.
- Spalart, P.R. (2002):**, ‘Detached-eddy simulation, 1997-2000’ In: Friedrich, R. and Rodi, W. (eds.), *Advances in LES of Complex Flows*, Kluwer, Dordrecht, 235-237.
- Stakgold, I. (1998):** *Green’s Functions and Boundary Value Problems, 2nd Edition*. John Wiley & Sons, New York.
- Strang, G. and Fix, G.J. (1973):** *An Analysis of the Finite Element Method*. Prentice-Hall, Englewood Cliffs.
- Strauss, W.A. (1992):** *Partial Differential Equations: An Introduction*. John Wiley & Sons, New York.
- Strelets, M. (2001):** ‘Detached eddy simulation of massively separated flows’, *AIAA Paper 2001-0879*.
- Szabo, B. and Babuska, I. (1991):** *Finite Element Analysis*. John Wiley & Sons, New York.
- Taylor, C. and Hood, P. (1973):** ‘A numerical solution of the Navier-Stokes equations using the finite element technique’, *Computers & Fluids*, **1**, 73-100.
- Taylor, G.I. (1923):** ‘On the decay of vortices in a viscous fluid’, *Philosophical Magazine*, **46**, 671-674.
- Taylor, G.I. (1935):** ‘Statistical Theory of Turbulence’, *Proceedings of the Royal Society London A*, **151**, 421.
- Taylor, R.L., Zienkiewicz, O.C. and Oñate, E. (1998):** ‘A hierarchical finite element method based on the partition of unity’, *Computer Methods in Applied Mechanics and Engineering*, **152**, 73-84.
- Tejada-Martinez, A.E. and Jansen, K. (2003):** ‘Spatial test filters for dynamic model large-eddy simulation with finite elements’, *Communications in Numerical Methods in Engineering*, **19**, 205-213.
- Temam, R. (1979):** *Navier-Stokes - Theory and Numerical Analysis*. North-Holland, Amsterdam.
- Temam, R. (1991):** ‘Approximation of attractors, large eddy simulations and multiscale methods’, *Proceedings of the Royal Society London A*, **434**, 23-39.
- Tennekes, H. and Lumley, J.L. (1972):** *A First Course in Turbulence*. MIT Press, Cambridge.
- Terracol, M., Sagaut, P. and Basdevant, C. (2001):** ‘A multilevel algorithm for large-eddy simulation of turbulent incompressible flows’, *Journal of Computational Physics*, **167**, 439-474.
- Terracol, M., Sagaut, P. and Basdevant, C. (2003):** ‘A time self-adaptive multilevel algorithm for large-eddy simulation’, *Journal of Computational Physics*, **184(2)**, 339-365.
- Tezduyar, T.E., Mittal, S., Ray, S.E. and Shih, R. (1992):** ‘Incompressible flow computations with stabilized bilinear and linear equal-order-interpolation velocity-pressure elements’, *Computer Methods in Applied Mechanics and Engineering*, **95**, 221-242.
- Tezduyar, T.E. and Osawa, Y. (2000):** ‘Finite element stabilization parameters computed from element matrices and vectors’, *Computer Methods in Applied Mechanics and Engineering*, **190**, 411-430.
- Townsend, A.A. (1956):** *The Structure of Turbulent Shear Flow*. Cambridge University Press, Cambridge.

- Travin, A., Shur, M., Strelets, M. and Spalart, P. (1999):** ‘Detached-Eddy Simulations Past a Circular Cylinder’, *Flow, Turbulence and Combustion*, **63**, 293-313.
- Tuminaro, R.S., Heroux, M., Hutchinson, S.A. and Shadid, J.N. (1999):** ‘Official Aztec User’s Guide Version 2.1’, *Report SAND99-8801J*, Massively Parallel Computing Research Laboratory, Sandia National Laboratories, Albuquerque.
- Vasilyev, O., Lund, T.S. and Moin, P. (1998):** ‘A general class of commutative filters for LES in complex geometries’, *Journal of Computational Physics*, **146**, 82-104.
- Vreman, A.W. (2003):** ‘The filtering analog of the variational multiscale method in large-eddy simulation’, *Physics of Fluids*, **15(8)**, L61-L64.
- Wagner, G.J. and Liu, W.K. (2000):** ‘Turbulence simulation and multiple scale subgrid models’, *Computational Mechanics*, **25**, 117-136.
- Wall, W.A. (1999):** *Fluid-Struktur-Interaktion mit stabilisierten Finiten Elementen*. Ph.D.-Dissertation, Report No. 31, Institut für Baustatik, Universität Stuttgart (in German).
- Wall, W.A., Gravemeier, V. and Ramm, E. (2001):** ‘On a Two-Level Finite Element Method for instationary, incompressible flows’, *Abstracts of the Sixth U.S. National Congress on Computational Mechanics (USNCCM 6)*, Dearborn.
- Wesseling, P. (2001):** *Principles of Computational Fluid Dynamics*. Springer, Berlin.
- Whiting, C.H. (1999):** *Stabilized finite element methods for fluid dynamics using a hierarchical basis*. Ph.D. Thesis, Department of Mechanical Engineering, Rensselaer Polytechnic Institute.
- Whiting, C.H., Jansen, K.E. and Dey (2000):** ‘Hierarchical basis for stabilized finite element methods for compressible flows’, *SCOREC Report 11-2000*, Scientific Computation Research Center, Rensselaer Polytechnic Institute.
- Whiting, C.H. and Jansen, K.E. (2001):** ‘A stabilized finite element method for the incompressible Navier-Stokes equations using a hierarchical basis’, *International Journal for Numerical Methods in Fluids*, **35**, 93-116.
- Wilcox, D.C. (1998):** *Turbulence Modeling for CFD, 2nd Edition*. DCW Industries, La Canada.
- Williamson, C.H.K. (1996):** ‘Vortex Dynamics in the Cylinder Wake’, *Annual Review of Fluid Mechanics*, **28**, 477-539.
- Winant, C.D. and Browand, F.K. (1974):** ‘Vortex pairing: the mechanism of turbulent mixing layers’, *Journal of Fluid Mechanics*, **63**, 237-255.
- Winckelmans, G.S., Lund, T.S., Carati, D. and Wray, A.A. (1996):** ‘A priori testing of subgrid-scale models for the velocity-pressure and vorticity-velocity formulations’, In: *Proceedings of the Summer Program*, Center for Turbulence Research, Stanford, 309-329.
- Zang, Y., Street, R.L. and Koseff, J.R. (1992):** ‘Application of a dynamic subgrid-scale model to turbulent recirculating flows’, In: *Annual Research Briefs*, Center for Turbulence Research, Stanford, 85.
- Zang, Y., Street, R.L. and Koseff, J.R. (1993):** ‘A dynamic mixed subgrid-scale model and its application to turbulent recirculating flows’, *Physics of Fluids A*, **5(12)**, 3186-3196.
- Zienkiewicz, O.C., Gago, J.P. de S.R. and Kelly, D.W. (1983):** ‘The Hierarchical Concept in Finite Element Analysis’, *Computers & Structures*, **16**, 53-65.
- Zienkiewicz, O.C. and Taylor, R.L. (2000a):** *The Finite Element Method, Volume 1: The Basis*. Butterworth-Heinemann, Oxford.
- Zienkiewicz, O.C. and Taylor, R.L. (2000b):** *The Finite Element Method, Volume 3: Fluid Dynamics*. Butterworth-Heinemann, Oxford.

Curriculum Vitae

Name: Volker Reiner Gravemeier

Geburtsdatum: 19. Juli 1974

Geburtsort: Neuwied/Rhein

Eltern: Dieter Gravemeier, Architekt
Hannelore Gravemeier, geb. Stein, Bilanzbuchhalterin

Nationalität: Deutschland

Familienstand: ledig, keine Kinder

1980 - 1984: Grundschule St. Martin in Andernach

1984 - 1993: Kurfürst-Salentin-Gymnasium in Andernach

Juni 1993: Zeugnis der allgemeinen Hochschulreife

1993 - 1994: Zivildienst im St. Nikolaus Stiftshospital in Andernach

1994 - 1999: Studium der Fachrichtung Bauingenieurwesen im Fachbereich Architektur /
Raum- und Umweltplanung / Bauingenieurwesen (ARUBI) an der
Universität Kaiserslautern

Februar 1998: Aufnahme in die 'Studienstiftung des deutschen Volkes'

Oktober 1999: Abschluss als Diplom-Ingenieur

Oktober 2000: Auszeichnung für den besten Abschluss in der Fachrichtung
Bauingenieurwesen an der Universität Kaiserslautern im Jahrgang
1999/2000

2000 - 2003: Wissenschaftlicher Mitarbeiter am Institut für Baustatik der Universität
Stuttgart

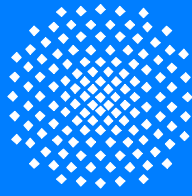
seit Jan. 2004: Postdoctoral Fellow am Center for Turbulence Research, Stanford
University, Stanford, CA, und NASA Ames Research Center, Moffet Field,
CA, USA

Berichte des Instituts für Baustatik der Universität Stuttgart

- 1 (1983) P. Osterrieder:**
Traglastberechnung von räumlichen Stabwerken bei großen Verformungen mit finiten Elementen.
- 2 (1983) T. A. Kompfner:**
Ein finites Elementmodell für die geometrisch und physikalisch nichtlineare Berechnung von Stahlbetonschalen.
- 3 (1983) A. Diack:**
Beitrag zur Stabilität diskret längsversteifter Kreiszyinderschalen unter Axialdruck.
- 4 (1984) A. Burmeister, F. W. Bornscheuer, E. Ramm:**
Traglasten von Kugelbehältern mit Stützen und Formabweichungen unter Innendruck und Stützenlängskraft.
- 5 (1985) H. Stegmüller:**
Grenzlastberechnungen flüssigkeitsgefüllter Schalen mit „degenerierten“ Schalenelementen.
- 6 (1987) A. Burmeister:**
Dynamische Stabilität nach der Methode der finiten Elemente mit Anwendungen auf Kugelschalen.
- 7 (1987) G. Kammler:**
Ein finites Elementmodell zur Berechnung von Trägern und Stützen mit offenem, dünnwandigem Querschnitt unter Berücksichtigung der Interaktion zwischen globalem und lokalem Versagen.
- 8 (1988) A. Matzenmiller:**
Ein rationales Lösungskonzept für geometrisch und physikalisch nichtlineare Strukturberechnungen.
- 9 (1989) D. Tao:**
Die Technik der reduzierten Basis bei nichtlinearen finiten Element-Berechnungen.
- 10 (1989) K. Weimar:**
Ein nichtlineares Balkenelement mit Anwendung als Längsstreifen axialbelasteter Kreiszyylinder.
- 11 (1990) K.-U. Bletzinger:**
Formoptimierung von Flächentragwerken.
- 12 (1990) S. Kimmich:**
Strukturoptimierung und Sensibilitätsanalyse mit finiten Elementen.
- 13 (1991) U. Andelfinger:**
Untersuchungen zur Zuverlässigkeit hybrid-gemischter finiter Elemente für Flächentragwerke.

- 14 (1992) N. Büchter:**
Zusammenführung von Degenerationskonzept und Schalentheorie bei endlichen Rotationen.
- 15 (1992) Th. J. Hofmann:**
Beitrag zur verfeinerten Balkentheorie.
- 16 (1994) D. Roehl:**
Zur Berechnung von großen elastoplastischen Deformationen bei Flächentragwerken und Kontinua.
- 17 (1994) R. Reitinger:**
Stabilität und Optimierung imperfektionsempfindlicher Tragwerke.
- 18 (1995) R. Suanno:**
Ein dreidimensionales Simulationsmodell für Stahlbeton mit Plastizität und Schädigung.
- 19 (1995) M. Braun:**
Nichtlineare Analysen von geschichteten, elastischen Flächentragwerken.
- 20 (1996) N. Rehle:**
Adaptive Finite Element Verfahren bei der Analyse von Flächentragwerken.
- 21 (1996) C. Haußer:**
Effiziente Dreieckselemente für Flächentragwerke.
- 22 (1996) D. Kuhl:**
Stabile Zeitintegrationsalgorithmen in der nichtlinearen Elastodynamik dünnwandiger Tragwerke.
- 23 (1998) H. Schmidts:**
Zur effizienten Modellierung und Analyse von Hochhaustragwerken.
- 24 (1998) H. Wang:**
Interaktion des lokalen und globalen Stabilitätsverhaltens dünnwandiger Stäbe.
- 25 (1998) K. Maute:**
Topologie- und Formoptimierung von dünnwandigen Flächentragwerken.
- 26 (1998) B. Maurer:**
Karl Culmann und die graphische Statik.
- 27 (1998) F. Çirak:**
Adaptive Finite-Element-Methoden bei der nichtlinearen Analyse von Flächentragwerken.
- 28 (1998) M. Trautz:**
Zur Entwicklung von Form und Struktur historischer Gewölbe aus der Sicht der Statik.

- 29 (1999) H. Menrath:**
Numerische Simulation des nichtlinearen Tragverhaltens von Stahlverbundträgern.
- 30 (1999) M. Bischoff:**
Theorie und Numerik einer dreidimensionalen Schalenformulierung.
- 31 (1999) W. A. Wall:**
Fluid-Struktur-Interaktion mit stabilisierten finiten Elementen.
- 32 (2000) E. Kuhl:**
Numerische Modelle für kohäsive Reibungsmaterialien.
- 33 (2001) A. Maute:**
Adaptive Finite-Element-Methoden in der Strukturdynamik.
- 34 (2001) S. Schwarz:**
Sensitivitätsanalyse und Optimierung bei nichtlinearem Strukturverhalten.
- 35 (2001) A. Haufe:**
Dreidimensionale Simulation bewehrter Flächentragwerke aus Beton mit der Plastizitätstheorie.
- 36 (2002) D.P. Mok:**
Partitionierte Lösungsverfahren in der Strukturdynamik und der Fluid-Struktur-Interaktion.
- 37 (2002) H. Steeb:**
Fehlerschätzer für FE-Berechnungen bei entfestigenden Materialien.
- 38 (2002) K. Krausz:**
Tragverhalten gemauerter Tonnengewölbe mit Stichkappen.
- 39 (2002) M. Hörmann:**
Nichtlineare Versagensanalyse von Faserverbundstrukturen.



Universität Stuttgart

ISBN 3-00-013034-9

